DOE/ID/13235--1
(DE95017709)

Energy CONSERVATION

CASTING DIMENSIONAL CONTROL AND FATIGUE LIFE PREDICTION FOR PERMANENT MOLD CASTING DIES

Technical Progress Report for the Period
September 29, 1993 - September 30, 1994

By
The Pennsylvania State University

November 1994

Work Performed Under Contract No. FC07-93ID13235

For
U.S. Department of Energy
Assistant Secretary for
Energy Efficiency and Renewable Energy
Washington, D.C.

DISCLAIMER

DOE/ID/13235--1
(DE95017709)
Distribution Category UC-1400

CASTING DIMENSIONAL CONTROL AND FATIGUE LIFE PREDICTION FOR PERMANENT MOLD CASTING DIES

Technical Progress Report for the Period
September 29, 1993–September 30, 1994

By
The Pennsylvania State University
University Park, Pennsylvania

November 1, 1994

Work Performed
Under Contract No. DE-FC07-93ID13235

Work prepared for
U.S. Department of Energy

Number of pages in this report: 231

This report has been reproduced from the best available copy. Available in paper copy and microfiche.

DOE and DOE contractors can obtain copies of this report from: Office of Scientific and Technical Information, P.O.Box 62 Oak Ridge, TN 37831 (615)576-8401

This report is publicly available from the Department of Commerce; National Technical Information Service, 5285 Port Royal Road, Springfield, VA 22161 (703)487-4650

ABSTRACT

First year efforts as part of a three year program to address metal casting dimensional control and fatigue life prediction for permanent mold casting dies are described.

Procedures have been developed and implemented to collect dimensional variability data from production steel castings. The influence of process variation and casting geometry variables on dimensional tolerances have been investigated. Preliminary results have shown that these factors have a significant influence on dimensional variability, although this variability is considerably less than the variability indicated in current tolerance standards. Gage repeatability and reproducibility testing must precede dimensional studies to insure that measurement system errors are acceptably small.

Also initial efforts leading to the development and validation of a CAD/CAE model to predict the thermal fatigue life of permanent molds for aluminum castings are described. An appropriate thermomechanical property database for metal, mold and coating materials has been constructed. A finite element model has been developed to simulate the mold temperature distribution during repeated casting cycles. Initial validation trials have indicated the validity of the temperature distribution model developed.

PROJECT OBJECTIVES

The objectives of the three-year dimensional control efforts are, together with industry partners, to identify factors contributing to the dimensional variability in production steel castings and to formulate guidelines for producing close-tolerance castings. This will also lead to the development of improved dimensional tolerance specifications for users of steel castings. The objectives of the three-year permanent mold casting effort are, together with industry partners, to develop and validate a CAD/CAE model to predict the thermal fatigue life of molds used for aluminum permanent mold casting. This includes the development of a robust mold crack initiation and propagation model. In both of these efforts timely deployment of research results is assured by the direct participation of a large network of industrial partners.

PROGRESS SUMMARY

The dimensional control effort is directed by Dr. Robert C. Voigt at Penn State University (PSU). Year one efforts have included the direct participation of six steel foundries. Dimensional characterization of 57 casting designs have been completed. This effort included the measurement of 498 casting features on 1475 individual castings for a total of 12,587 dimensional measurements on production steel castings at foundry sites across the country. Dimensional control tasks, all of which continue into the second and third year of effort are substantially on schedule. Initial subtask efforts to develop improved shrinkage allowance guidelines, scheduled for year one completion, are still ongoing.

The permanent mold effort is being administered as a subcontract to the University of Missouri - Rolla (UMR) under the direction of Dr. Kofi Nyamekye. Year one efforts have included the installation and startup of a permanent mold casting machine from Stahl Specialty Co. and the direct participation of the American Foundryman's Society Permanent Mold Committee. Most experimental and modeling activities are substantially on schedule: model development subtasks have been delayed somewhat by delays in equipment and instrumentation acquisition.

Industry support and direct participation for both of these continuing efforts is very strong. The outline of research tasks developed at the beginning of the research program remains sound and continues to have industry endorsement. . . . . .

TABLE OF CONTENTS

LIST OF FIGURES

LIST OF TABLES

Chapter 1

DIMENSIONAL CAPABILITY ASSESSMENTS OF METAL CASTINGS

The casting customer is demanding increasingly tighter dimensional tolerances for cast components. The first step in meeting these demands is for the foundry to know its present dimensional capabilities. With an accurate dimensional capability assessment, a foundry can more effectively communicate with a customer about achievable casting tolerances. Furthermore, improved dimensional control will allow the foundry to take fuller advantage of the near net shape capabilities of the casting process. However, an accurate dimensional capability assessment is difficult to obtain. The overall casting dimensional variability is due to variations from many intermediate processes.

Dimensional errors can be classified into two groups. Random errors are caused by controllable and uncontrollable variations of all of the intermediate casting production processes. Examples of the intermediate production processes include core making, mold making, mold and core assembly, cleaning of castings, and heat treatment. Random errors are typically quantified by the standard deviation or variance; measures of the spread of dimensions about the mean.

Systematic errors are the second type of casting errors. A systematic error is the difference between the mean, or average value, and the desired dimension. These errors could be caused by inaccurate or worn patterns. Long term changes in the sand system or molding method are also classified as systematic errors.

Figure 1 displays the major categories of random and systematic variables which affect the overall dimensional variability of steel castings.

The steel casting industry is competing against many other industries, including aluminum and iron casting, machining, and fabrication, for market share. To be able to most effectively compete against these industries, as well as other steel foundries, an accurate dimensional capability assessment and improved dimensional control are required. The American Foundrymen's Society has identified dimensional control as a major need for the metal casting industry.[1] Improved dimensional control will allow the foundry to design castings with more features cast to size, or closer to size, which will reduce or eliminate the need for subsequent machining operations. With an accurate knowledge of the dimensional capability, castings can also be designed to reduce the casting weight. These improvements will reduce the overall customer cost for a particular component.

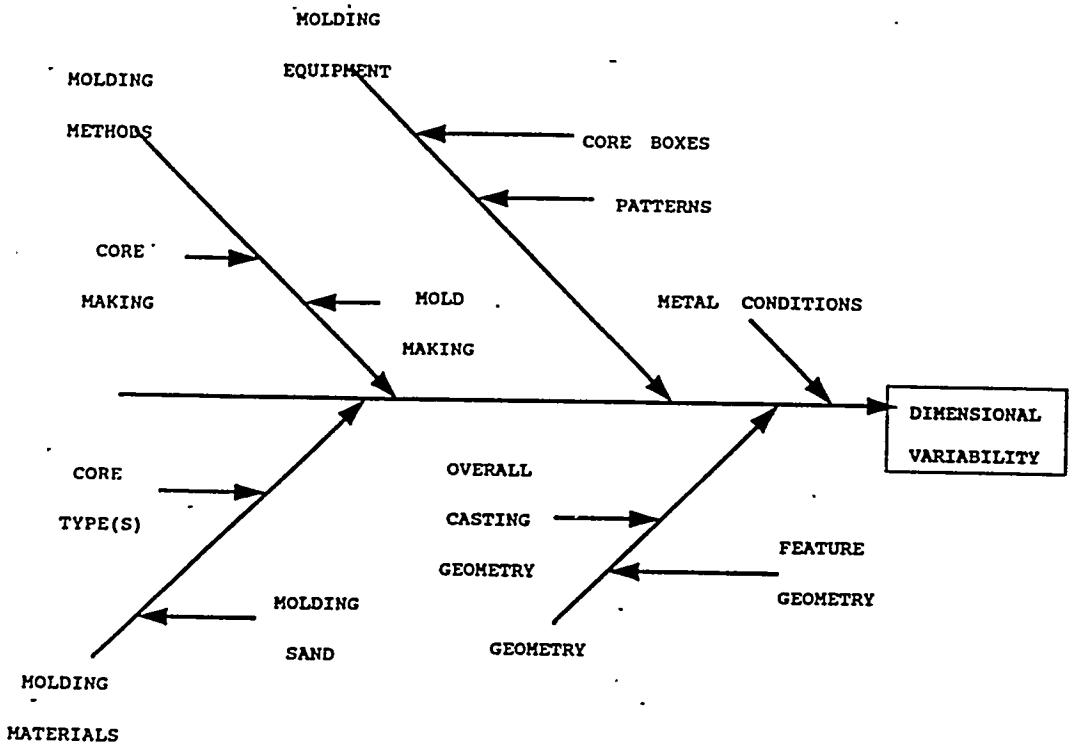

Figure 1: Major categories of variables which affect dimensional variability
Source: Peters, F.E. and R.C. Voigt

Because of the nature of steel castings and steel casting methods, the dimensional challenges for this segment of the metal casting industry are the most severe. Steel castings are often dimensionally complex, and can range in size from 1 to 100,000 pounds. The inherently high pouring temperature of steel, relative to other commonly cast metals, is an additional problem. The higher temperature metal will cause dimensional changes in the sand molds during casting. Steel castings also require an additional post-casting heat treatment to improve mechanical properties, which may also contribute to dimensional variability.

Due to the large number of process variables, laboratory trials are generally not sufficient to assess the dimensional capabilities of a foundry. Dimensional capability is unique to a foundry, and can only be obtained by measuring production steel castings.

This report will review previous dimensional capability studies of metal casting processes and existing standards. The inability of past studies to differentiate between measurement system variability and actual casting dimensional variability will be highlighted. Procedures have been developed to determine the dimensional variability of production steel castings. These procedures have been carried out at steel foundries to collect dimensional data from production castings. The data were analyzed to determine the foundries dimensional capabilities for the range of castings studied. Designed experiments were also conducted to study the specific influence of key casting production variables on dimensional variability. The dimensional variability observed will be compared to existing dimensional standards for steel castings.

Chapter 2

REVIEW OF CAPABILITY STUDIES AND TOLERANCE STANDARDS

Several studies have been conducted to examine the dimensional variability of metal castings. Some studies have focused on a particular casting process; others were comprehensive studies that examined a wide spectrum of metals and molding methods. This chapter reviews the significant studies conducted during the last thirty years and current dimensional standards for steel castings.. Table 1 provides an overview of the major dimensional capability studies that have been performed. Most of the studies investigated the effect of mold relationship on the dimensional variability of a feature. Figure 2 displays the common mold relationships.

The Institute of British Foundrymen (IBF) established a technical subcommittee in 1966 to evaluate the dimensional variability of normal casting production for iron, steel and non-ferrous castings. The first committee report discussed the difference between random errors and systematic errors (errors caused by pattern equipment).[5] The report noted a lack of general knowledge about casting contraction and the problem of measurement accuracy. Linear regression techniques were shown to be an effective method of analyzing data from production castings.

IBF continued to collect dimensional data from several thousand castings. Included in the second report[6] was an extensive discussion of the importance of core accuracy, core setting and core prints. The use of core locating jigs was shown to eliminate the need for wider tolerances for mold-to-core type dimensions. The dimensional variability of casting features was greater after heat treatment than before. This study also suggested that foundries do not adequately specify their needs to the patternmaker and that casting shrinkage (which controls nominal dimensions) cannot be accurately predicted for complex casting shapes. Decisions to modify patterns should be based on measurements of at least 25 castings. Foundries should spend more time collecting data on casting shrinkage to develop a better understanding.

Using multiple linear regression analysis, the IBF committee developed an updated linear regression model to predict the dimensional variability that can be expected from iron, steel, and aluminum castings.

Table 1: Major dimensional capability studies of metal casting processes and tolerance standards

1971 Institute of British Foundrymen (IBF)
most alloys, sand molding[5,6]

1977 American Foundrymen's Society (AFS)
grey iron, sand molding[4]

1977 Steel Founders' Society of America (SFSA)
steel, sand molding[2]

1978 Steel Casting Research and Trade Association (SCRATA)
steel, sand molding[8]

1984 International Standards Organization (ISO)
many alloys, many molding methods[7]

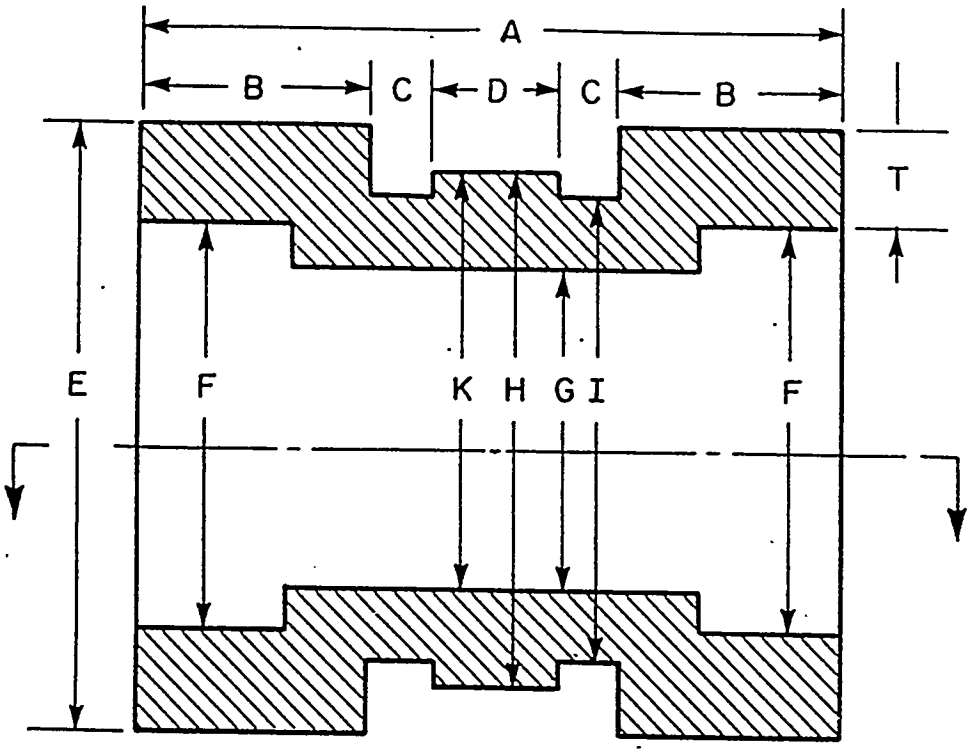

A,B,C,D	=	Mold to Mold
T	=	Mold to Core
E,H,I	=	Mold to Mold Across the Parting Line
K	=	Mold to Core Across the Parting Line
F,G	=	Wholly on One Core

Figure 2: Dimension types of a casting classified by the mold components which control them
Source: Wieser, P.F.

St.Dev. = + 0.86 X Drawing dimension (inches)
(.001 ") + 0.05 X Projected core area (inches^2)
+ 8.02 X General wall thickness (inches)
- 8.6 if dimension is made wholly by mold
+ 1.7 if the dimension crosses mold joint
- 9.9 if the dimension is made in one core
- 0.5 if the dimension is from a part of the mold to a core set by a print
- 10.5 if the dimension is from a part of the mold to a core set by a jig
- 2.9 if the dimension is between 2 cores
+ 6.2 if the alloy is grey iron
+ 8.7 if the alloy is white iron
+ 12.8 if the alloy is malleable iron
+ 27.4 if the alloy is steel
+ 12.7 if the alloy is aluminum

The final two quantities should be treated with great reserve, since relatively few results were obtained for steel and aluminum castings. This equation had a residual error of 0.01155 and a multiple correlation coefficient of 0.813.

Villner described a general system of tolerances for castings based on the International Standards Organization (ISO) system for machined pieces.[16] Casting dimensional data were collected from production castings. The data were used to establish the fundamental shape and spacing of the tolerance curves based on the existing ISO tolerance format. The following equation was developed:

$$T = 0.6(10^{1/7})^{n-16} D^a$$

where T = total dimensional tolerance
D = basic feature dimension
a = constant
0.33 for grey iron, steel and non-ferrous
0.45 for malleable and ductile iron
n = tolerance grade (9 to 21).

Figure 3 displays the tolerance width versus the basic dimension. Grey iron, steel and non-ferrous castings are defined as GTA grade. GTB grade is defined for malleable and ductile iron castings. Villner suggests that an additional tolerance should be added for dimensions that cross a mold joint or are subject to mold mismatch.

Further research was conducted in Sweden to establish tolerance guidelines for castings based on the tolerance system described by Villner.[15] Measurements were taken from 328 different parts; typically, four features per part were measured. The mean and statistical spread were calculated for each feature from a sample size of ten castings. A tolerance grade number was assigned to each feature based on the measured variability. The

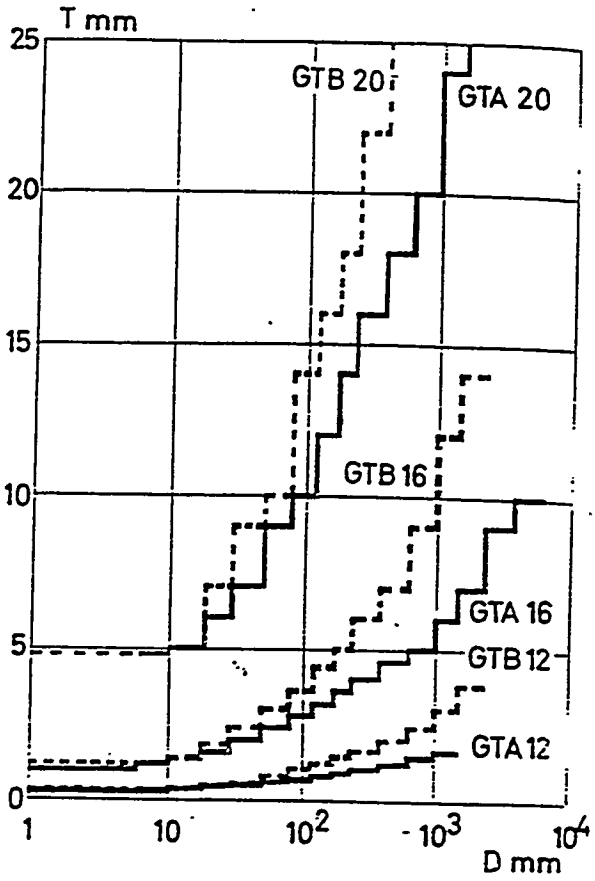

Figure 3: Tolerance width T as a function of basic dimension D for tolerance grades GTA and GTB 12, 16 and 20
Source: Villner, L.

features were then grouped by their respective casting variables, such as metal type, mold type, and production quantity. For each group, the assigned tolerance grade numbers were averaged. The average value for each group was established as the low (best) specified tolerance. To account for such variables as pattern condition and casting complexity, a range of tolerance grades was established in the following manner. The average was established as the lowest or best specified tolerance for the particular group of casting variables, and the next two higher grades were also selected. The average values were defined as the best specified tolerance grade, because the castings measured were generally from "bigger well-managed foundries."[15]

Svensson and Villner also commented on random and systematic dimensional deviations. Random errors are caused by the normal process variables in molding, core making, mold assembly, etc. Systematic errors were divided into permanent errors, typically pattern equipment errors, and semi-permanent errors. Semi-permanent systematic errors are errors caused by the sand system or long term molding method changes. Since the castings measured in this study were made over a short time period, the authors felt the tolerance guidelines developed only represented the random errors. Surface roughness was recognized as potentially dominating the actual feature variability, especially for small features. The amount of variability caused by certain specific variables, such as measurement error, mold coatings and flask pin alignment was assigned a corresponding tolerance grade. For instance, the deviation caused by the alignment pin and bushing clearance could cause variance equal to GTA 11.

The Steel Casting Research and Trade Association (SCRATA) sponsored research to determine the dimensional capabilities of normal production steel castings.[8] The study measured 520 features on 120 parts. The linear regression approach used by the IBF[5] was used in this study to develop dimensional variability guidelines. The following expression describes the variability observed for dimensions less than 10 inches.

St.Dev. = + 25.2
(.001 ") + 0.004 X Volume of Casting (inches^3)
+ 2 X Drawing Dimension (inches)
+ 11 if steel is austenitic manganese
+ 4 if casting is stress relieved
+ 4 X the number of mold joints crossing the dimension
- 7 if a core is involved in the dimension
- 9 if molding process is either shell molded or a core assembly

The equation had a residual error of 0.012 inches. A second equation was developed to express the variability observed for dimensions greater than 10 inches.

St.Dev. = + 22.7
(.001 ") + 0.025 X Volume of Casting (inches^3)
+ 45 if molding is green sand slinging
+ 10.6 if a wood pattern is involved

The residual error term was 0.0125 inches.

Research by Aubrey for the Steel Founders' Society of America (SFSA) resulted in the establishment of dimensional tolerance guidelines specifically for steel castings.[2] Dimensional data were collected from 1370 production castings which represented 57 different parts. A total of 295 features was measured. Multiple regression was used to determine a relationship between process variables and dimensional deviation. The following equation was developed based on data from castings weighing up to 131,000 pounds.

Natural Tolerance = + 0.064
(inches) + 0.00027 X Length X Weight$^{1/3}$
+ 0.239 if dry sand was used

Natural tolerance was defined as ± three standard deviations of the measurements. The weight and length were given in pounds and inches, respectively. Since a majority of the data were collected from castings weighing less than 2000 pounds, another regression equation was developed to describe the natural tolerance for those castings.

Natural Tolerance = - 0.00138
(inches) + 0.01296 X Weight$^{1/3}$ (pounds)
+ 0.0221 X Length$^{1/3}$ (inches)
- 0.04128 if no bake molding
- 0.04224 if shell molding
- 0.03165 if dimension is across one core
+ 0.03336 if the dimension is between a mold wall and a core and crosses a parting line

These linear regression equations were based on the means of the data. Six tolerance grades were established by multiplying the tolerance obtained from the second equation by the following constants: 0.75, 1, 1.25, 1.5, 1.75, and 2. These tolerances were later published in the *Steel Castings Handbook*[18] and have become the basis of the widely used U.S. dimensional tolerance guidelines for steel castings, Appendix A.

Pattern measurements were also obtained for 202 of the 295 features measured. The calculated shrinkage allowances based on the mean of the data and the pattern measurements ranged from -13.5% to 10.8%. The shrinkage amount is represented in different

formats in Table 2. The average shrinkage amount for all features was 1.78%. All of the 'extreme' shrinkage values were obtained for dimensions less than ten inches; most were from dimensions less than three inches. Although not stated, measurement errors and surface irregularities were likely causes of the extreme shrinkage values. The apparent shrinkage amount was found to be less for dimensions on a core than for mold-to-mold dimensions. Also, the apparent shrinkage of castings made in shell molds was greater than those made in green sand.

The International Standards Organization (ISO) published ISO 8062,[7] which is a system of dimensional tolerance for castings, Appendix B. Sixteen grades of casting tolerances are defined. The tolerance is only a function of feature length. The appropriate tolerance grades for non-ferrous, iron and steel castings were then identified for a variety of different molding processes.

The American Foundrymen's Society studied the dimensional capabilities of iron castings made by high pressure green sand molding. Initial data were collected from production castings; however, difficulties in establishing practical dimensional tolerances from the data were encountered.[4] Therefore, follow-up laboratory experiments were conducted using a standard T-bar shape, Figure 4.[4] Fifteen foundries produced two lots of fifteen castings. Grey iron castings were made using high density green sand molding. Each foundry created their own gating system for the test part. There was no single predominant distribution of measurements within a single lot of fifteen castings. A significant difference in the mean dimension and the variability of dimensions was observed among the participating foundries.

A dimensional tolerance system for castings has also been described by Reddy et al.[11] The system was based on measurements of production castings. In this study, the measurements were grouped by the following variables:

- dimension direction (horizontal or vertical),
- dimension formed or not formed by cores,
- dimensions made by one or two mold halves.

The tolerance system was based on the following equation:

$$\text{Tolerance} = K_i D^{.33}$$

For this equation, K_i determines the tolerance grade, and the quotient value is $10^{1/10}$.

Law made comparisons between his equation,[8] relationships developed by IBF TS71,[6] the then unpublished SFSA tolerances,[2] the tolerance grades developed by Svensson and Villner[15] and recommendations from the Steel Castings Development Committee.[14]

Table 2: Different representations of shrinkage allowances

percentage	mm/m	in/ft
0.5%	5	1/4
1.0	10	1/8
1.6	16	3/16
2.1	21	1/4
2.6	26	5/16
3.1	31	3/8

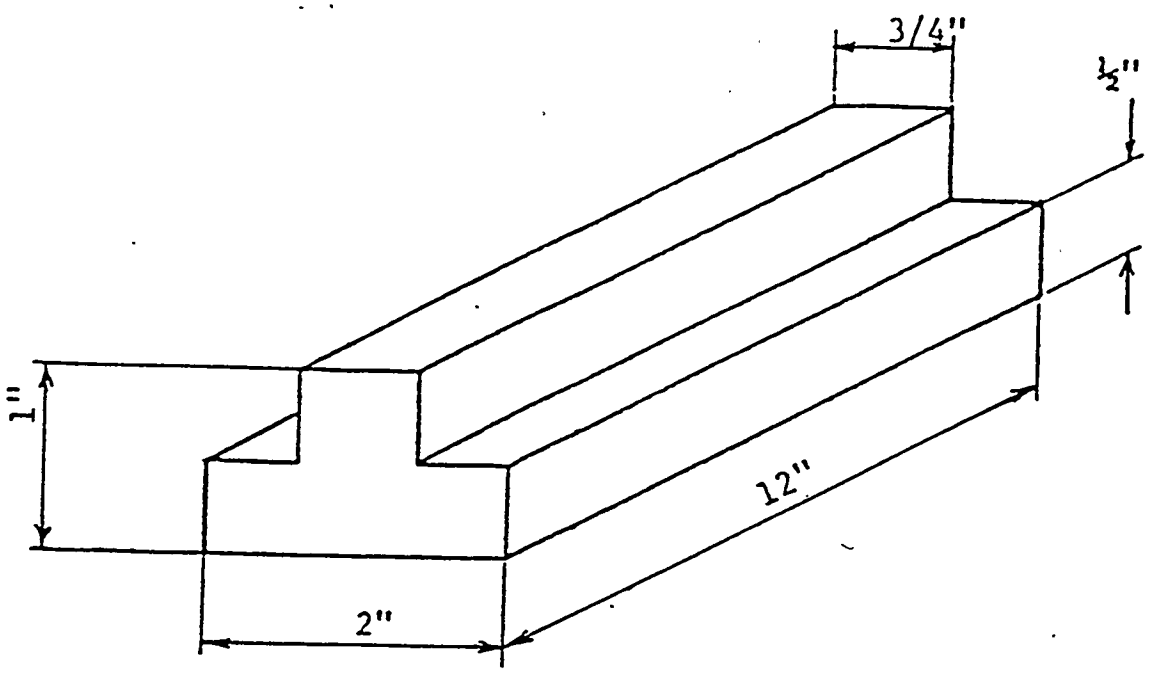

Figure 4: AFS Committee standard T bar for determining dimensional tolerances for production castings
Source: Draper, A.B.

The comparisons were limited to tolerance guidelines identified for steel castings. This comparison is shown in Table 3.

Voigt and Peters compared tolerance guidelines developed and used by several high tonnage users of steel castings.[17,10] Many assumptions had to be made to compare the guidelines because of the various formats. However, the casting guidelines were, in general, tighter than both the SFSA and ISO 8062 standards.[18,7]

An important part of any dimensional capability assessment should be an assessment of the measurement system. In the studies reviewed here, there were only a few brief references to measurement system errors. None of the previous studies included a measurement system analysis to verify that the measurement systems used were sensitive enough to detect casting dimensional variability. Ross recently conducted gage repeatability and reproducibility (gage R & R) tests on the measurement systems used by some U.S. steel foundries to measure castings as well as patterns.[12,13] In many instances, the variability of the measurement system was unacceptable with respect to the tolerance allowed for the particular features measured. This indicates that previous studies of casting variability and the resultant guidelines may be seriously flawed.

Major dimensional variability studies of the sand casting processes were reviewed. However, there has not been any work conducted recently on the tolerance capabilities of steel foundries using contemporary production practices. Therefore, any dimensional improvements made by the industry are not represented in the current standards. In addition, measurement system errors were not measured and were likely reported as casting process variability in the present standards. Work is needed to accurately characterize the tolerance capabilities of steel foundries.

Table 3: Comparison of dimensional tolerance systems

Mean cast dimension (in)	Casting volume (in^3)	Core projected area (in^2)	Material (steel type)	Moulding process	Wall thickness (in)	Heat treated	Type of dimension	Wood pattern	Mould joint crossed	SCRATA A	SCRATA B	IBF[4]	Villner[7]	SCDC[2]	SFSA[12]	Actual standard deviation (in)
2.002	3229	320	Non aust	CO_2 compaction	1.16	Yes	Mould/mould	No	No	0.037	–	0.045	0.021-0.043	0.015-0.042	0.014	0.0231
6.762	3229	320	Non aust	CO_2 compaction	1.16	Yes	Across one core	No	No	0.039	–	0.043	0.032-0.063	0.022-0.047	0.014	0.0353
3.250	213	16	Non aust	Green sand jolt-squeeze	2.90	Yes	Across one core	Yes	No	0.029	–	0.044	0.028-0.056	0.018-0.042	0.030	0.0203
3.000	213	16	Non aust	Green sand jolt-squeeze	2.90	Yes	Mould/mould	Yes	No	0.036	–	0.045	0.028-0.056	0.018-0.042	0.032	0.0318
18.534	661	145	Non aust	Green sand jolt-squeeze	0.50	Yes	Mould/mould	No	No	–	0.039	0.046	0.047-0.094	0.035-0.060	0.072	0.0210
20.669	5622	400	Non aust	CO_2 compaction	1.50	Yes	Mould/core	Yes	No	–	0.049	0.076	0.047-0.094	0.040-0.070	N.A.	0.0402
7.673	5622	400	Non aust	CO_2 compaction	1.50	Yes	Mould/core	Yes	No	0.051	–	0.065	0.035-0.070	0.021-0.047	N.A.	0.0443
2.250	220	12	Aust mang	CO_2 sand	1.88	No	Mould/mould	Yes	No	0.033	–	0.065	0.024-0.048	0.021-0.042	N.A.	0.0443
1.750	265	43	Non aust	Green sand jolt-squeeze	0.75	Yes	One core	Yes	No	0.027	–	0.021	0.0125-0.0250	0.016-0.041	0.030	0.0321
2.250	226	36	Non aust	Green sand jolt-squeeze	0.63	Yes	Mould/core	No	Yes	0.246	–	0.036	0.024-0.048	0.017-0.042	0.038	0.0299
12.000	252	37	Non aust	Green sand jolt-squeeze	0.75	Yes	Mould/mould	Yes	No	–	0.085	0.037	0.039-0.078	0.027-0.052	0.072	0.0502
1.500	220	12	Aust mang	CO_2 sand	1.88	No	Mould/core	Yes	No	0.024	–	0.044	0.0125-0.0250	0.015-0.041	0.014	0.0177

Source: Law, T.D.

Chapter 3

PROCEDURES

Initial year one efforts have been directed at developing strategies and methodologies to conduct detailed dimensional surveys at steel foundries. These methodologies have been piloted on a steel foundry and its dimensional data summarized in this report were from production steel castings produced at a particular foundry. Work is in progress at additional steel foundries to similarly characterize their dimensional capabilities. A complete list of foundries participating in year one are shown in Table 4. Table 5 summarizes the extent of the dimensional characteristics accomplished to date at these foundry locations. The foundry in this report used both green sand and shell sand for molding. Most of the castings produced are for truck and off-road equipment industries. The majority of the castings produced by this foundry weigh less than 150 pounds. Twenty-three different parts were selected and measured in this study; casting weight ranged from 2 to 118 pounds.

Castings were intercepted during their normal production cycle, measured for this study, and then returned to the production cycle. Some designed experiments were also conducted, using specially produced castings, to isolate the effects of certain process variables on dimensional variability. Procedures for collecting data from the production castings and descriptions of the designed experiments follow.

Production Casting Data Collection Procedures

Detailed procedures were established to select both parts and features for the study and to accurately measure them. The goal was to select parts and features that were representative of the castings produced at the various foundries.

Measurement System Analysis

The measurement system used to measure the castings must be sensitive enough to detect actual part variation. Gage repeatability and reproducibility (gage R & R) tests were used to measure the variability contributed by the measurement process. The measurement system had to be deemed acceptable before casting feature data were used. All of the gage R & R tests used were based on established measurement system analysis procedures.[3]

Table 4: List of participating steel foundries

COMPANY	LOCATION
Atchison Casting Corp.	Atchison KS
Falk Corp.	Milwaukee WI
Keokuk Steel Casting Inc.	Keokuk IA
Pelton Casteel Inc.	Milwaukee WI
Texas Foundries	Lufkin TX
Texas Steel Co.	Forth Worth TX

Table 5: Extent of accomplishments of participating steel foundries to date

57 different casting designs
1475 parts (individual castings)
498 features
12587 measurements

The variability of a measurement system is typically compared to either the designated feature tolerance of interest, or to the part variation, to determine acceptability. These general measurement system acceptability criteria were not sufficient for the purposes of this study. For the purpose of this project, a measurement system was considered acceptable if the measurement variability was less than 30% of the current SFSA T3 tolerance for the particular feature.[18] The SFSA T3 tolerance is defined for castings made by specialized molding processes, such as shell or no-bake. This grade was chosen as a comparison because it is believed that a new industry wide tolerance assessment would indicate tolerances tighter than the present standards.

It would have been infeasible to determine the gage R & R for each feature measured in this comprehensive study. Therefore, gage R & R tests were completed on a few representative features periodically during the study period. For example, if a caliper measurement was appropriate and capable for a certain feature, it was assumed that the caliper was also capable for similar features. Appendix C contains a summary of the specific gage R & R procedures developed and followed for this study. The complete data for one gage repeatability test is exhibited in Appendix D.

Selection of Castings and Features

Foundry personnel assisted in the selection of parts for this study. Parts were selected which represented a variety of production practices and geometry variables for the foundry.

Individual features for measurement on each part were chosen such that a full range of different features were represented. Features were chosen that were not affected by grinding or gating system removal, which are normal processing procedures. However, it should be pointed out that the customer will also be concerned about variability of such operations.

For each feature selected, a list of descriptors was compiled to describe the feature characteristics and associated molding variables, see Appendix E. All of the process and feature variables were entered into a database constructed in *Paradox* (registered trademark of Borland International) for subsequent analysis.

From the list of potential test parts, groups of castings were selected as they were produced. For most of the parts studied, approximately ten castings from a production run were randomly selected following shakeout and initial shot blasting. Risers and gates were removed as usual; and the castings were sent through heat treatment prior to any grinding. The castings were shot blasted, tie bars (if any) were removed, and then the castings were inspected prior to grinding. Attempts were made to capture a second group of ten castings for each part during the study period, but were not always successful.

For a few parts, castings were selected from more than one pattern cavity. Data from each cavity was analyzed individually.

In some instances, castings were selected for study after all of the finishing operations had been completed. For these castings, features which were not affected by any upgrading operations, such as grinding or pressing, were selected for dimensional characterization.

Measurement of Castings

The majority of the feature measurements were made using six inch digital calipers; other features were measured using twelve inch digital calipers or 0-1 inch micrometers. The only exception was that a Coordinate Measurement Machine (CMM) was used to measure all of the diameters. All of the measurement equipment used had been calibrated by an outside vendor within one year prior to its use in this study.

The castings measured on the CMM were set up on gage blocks, and then a surface on the casting was determined from four points. The diameter being measured was projected onto this surface. Diameter calculations were made using six points. If the diameter crossed a parting line, the diameter of the cope and drag halves of the features were determined separately, based on four points each. The CMM's internal algorithms were used to calculate the diameters.

For the feature measurements taken using hand instruments, specific instructions were recorded to assure that subsequent lots of castings would be measured in the same manner. Measurements on surfaces with draft were inherently the most difficult to obtain. Repeatability was insured by using one of a number of simple measurement techniques: laying out the measurement locations, using gage blocks to take the measurement a set distance from a casting surface, or measuring a feature at a set depth on the calipers. Measurements were always a cross sectional measurement made between two locations on a feature. The data collected for these features will be representative of the variability at a single location on a feature. The variability along the entire feature was not measured. This was done so that the casting feature measurements could be compared with the corresponding pattern measurement.

All of the data points were entered in the database with the corresponding casting descriptors, Appendix E. Figure 5 is a histogram of the data points collected for an example feature. The standard deviation was found for each feature in which ten or more observations were obtained, Appendix F. All feature variability described in this study is reported in terms of ± three standard deviations. For a normal distribution, ± three standard deviations will include 99.7% of all observations.

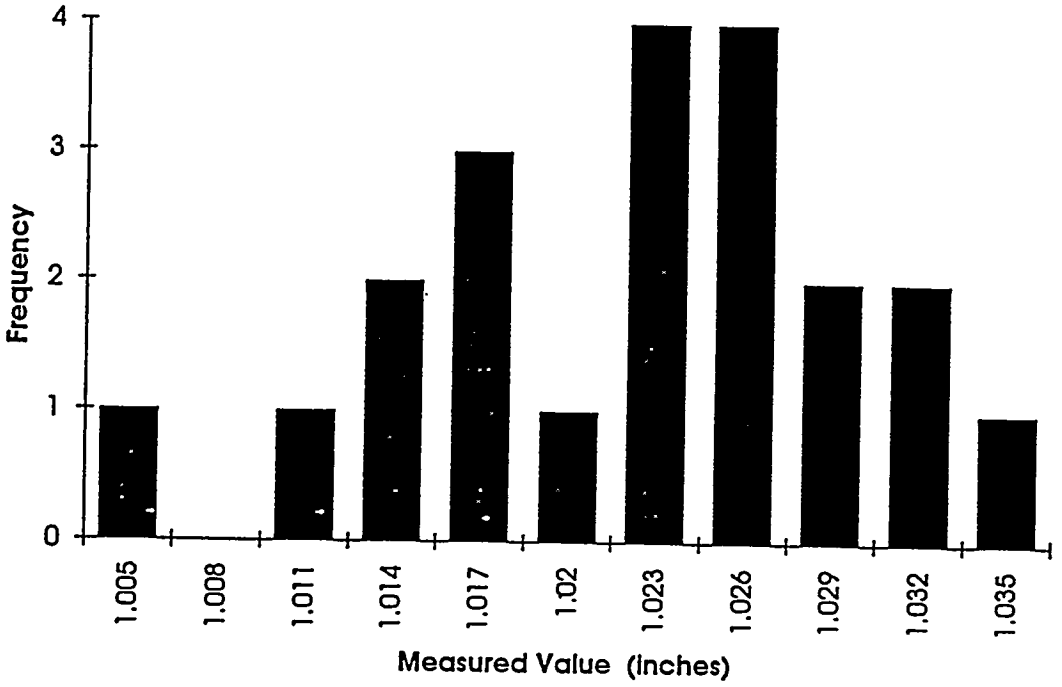

Figure 5: Histogram illustrating spread of measurements for one particular feature

Procedures for Designed Experiments

Two additional designed experiments were conducted to study the effects of specific casting variables on dimensional variability. One experiment studied the specific effects of core binder type and pouring temperature. The other experiment compared the dimensional variability of nearly identical castings made in green sand and shell molds. The dimensional information obtained from these designed experiments was not included in the overall database of dimensional capability of production castings because in some cases 'special practices' were used during the processing of these castings.

Core Binder Type and Pouring Temperature Experiment

This experiment was conducted to study the effects of core type and pouring temperature on the variability of several features for one particular part. The test castings used in this experiment were made using close to regular production procedures.

A 35 pound part was chosen which had two holes formed by a single core. A schematic representation of this part is shown in Figure 6. An oil sand binder was typically used to produce the core for this part. However, a sodium silicate - CO_2 binder was also used for half of the castings produced for this experiment.

All of the cores were produced from a single aluminum split core box. Measurement of the dimensional variability of the cores themselves was attempted using six inch digital calipers, but the method failed gage repeatability tests. Core hardness was also checked at several random locations. No significant hardness variations were observed among the cores for either of the binder systems.

The pattern for this part produced a mold that has two casting cavities with a single symmetric gating system feeding each of the cavities through a central sprue. Two identical castings were produced from each mold, and each contained a different core type. One particular core type was always placed in the same cavity to eliminate variability between the individual cavities. A pair of cope and drag, pin lift, jolt squeeze molding machines were used to produce the molds. Normal production methods were followed, including one shovel of facing sand for each mold half. Mold hardness readings were taken from each mold half. The AFS mold hardness number ranged from 80 to 89 along the parting line, with no consistent mold-to-mold variability. Two batches of six molds each were produced.

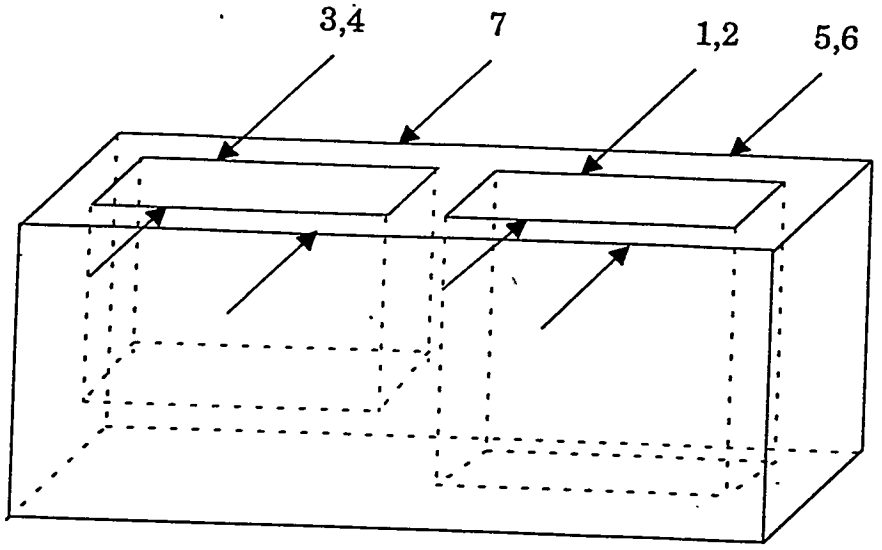

Dimension	Feature Type
3,4	Internal of Blind Hole
7	External of Blind Hole
1,2	Internal of Through Hole
5,6	External of Through Hole

Figure 6: Schematic diagram of casting used for core type and pouring temperature experiment

Approximately twenty molds were produced after the first batch and before the second batch. Each of the mold cavities was stamped with an identification number on the casting surface. Samples of the molding sand and facing sand were tested from each of the molding periods. The results are shown in Table 6.

The molds were made in two batches in order to effectively determine the influence of pouring temperature on dimensional variability. The first six molds were poured in the beginning of the day's pouring shift when the pouring equipment was relatively cold. Two ladles of metal were needed to pour the six molds. The initial ladle temperatures were 2885° F and 2864° F. The ladle temperatures for the second batch of castings were 2995° F and 2983° F. The pouring time was approximately 12-15 seconds for each of the molds. Hot topping was applied to the open after pouring. The castings were shaken out after approximately one hour of mold cooling. All of the open risers had well formed shrinkage pipes. After the risers were removed, the castings underwent a normalizing heat treatment and were then shot blasted.

Measurement procedures similar to those used for studies of production castings were employed. Seven measurement locations were identified on each casting. All of the measurements were made with six inch digital calipers. Each measurement was made twice by the same person and the two measurements were averaged.

Molding Sand Experiments

There were two part designs in use at the foundry for which pattern equipment existed to produce castings using either green sand or shell molding techniques. For each part, several castings were produced using both green sand and shell molding. The influence of mold type on the variability of casting features could be directly compared since the geometry was nearly identical.

The first part weighed approximately seventeen pounds and needed a core to form an external feature. The second part weighed three pounds, and had a cored internal cavity. The shell pattern for the second part had six separate cavities, while the green sand pattern had only a single cavity.

Due to production restrictions, the shell molded castings used in the comparison were randomly selected from a large production lot, while the green sand castings were produced sequentially. The green sand was sampled during the molding of each part to evaluate mold consistency, Table 6. Twenty and fifteen green sand castings were made for the first and second part, respectively.

All castings were measured using the techniques outlined for the inspection of production castings. On the seventeen pound part, four locations were measured on each of the green sand and shell castings. A single location was measured on the second part.

Table 6: Results of green sand sample tests

% moisture	permeability	green strength (psi)	% compactibility
pouring temperature and core binder experiment			
2.6	185	11.8	47
2.5	185	12.8	41
2.7	190	12.2	48
2.6	190	12.0	47
pouring temperature and core binder experiment -- facing sand			
2.5	180	6.5	54
molding sand experiment (casting #1)			
2.8	190	11.4	48
2.7	195	11.8	48
2.8	190	11.3	49
2.8	185	11.8	49
2.5	180	11.2	41
molding sand experiment (casting #2)			
2.4	175	13.2	39

Gage repeatability tests were conducted on the measurement system used to measure each of the parts. Acceptable repeatability values ranging from 10 to 14% of the measured part variation were found.

Chapter 4

RESULTS

Data were collected on the dimensional variability of 150 different features from production castings. The effect of casting geometry and production variables on the dimensional variability will be analyzed. The effect of specific variables on dimensional variability will also be discussed for the designed experiments previously described.

Results of Production Castings Data

Dimensional variability is reported in terms of three standard deviations. Each reported value of three standard deviations was determined from typically twenty but a minimum of ten measurements of a feature. Figure 7 is a plot of dimensional variability versus the feature length; the data from shell molding is identified. Figure 8 is a similar plot that identifies the features that cross the parting line.

Linear Regression Analysis

Linear regression analysis was used to develop an equation to predict the average dimensional variability (± three standard deviations) based on the casting geometry and process variables for the production castings measured. The following independent variables were initially chosen for use in the equation: feature length, casting weight, total pouring weight, dimension crosses mold parting line, dimension crosses core parting line, drafted surface, largest dimension on casting, height of cope, type of molding sand, mold-to-core dimension, and core-to-core dimension. Other independent variables were included in the database, but not used in the development of a regression model because there were not enough observations.

Step wise linear regression analysis was used to identify the best predictors of variability. The use of the logarithm of variability has been shown to sometimes fit better than variability.[9] Separate analyses were performed using three standard deviations and the logarithm of three standard deviations as the dependent variable. The final linear regression equation developed using the logarithm of three standard deviations is as follows:

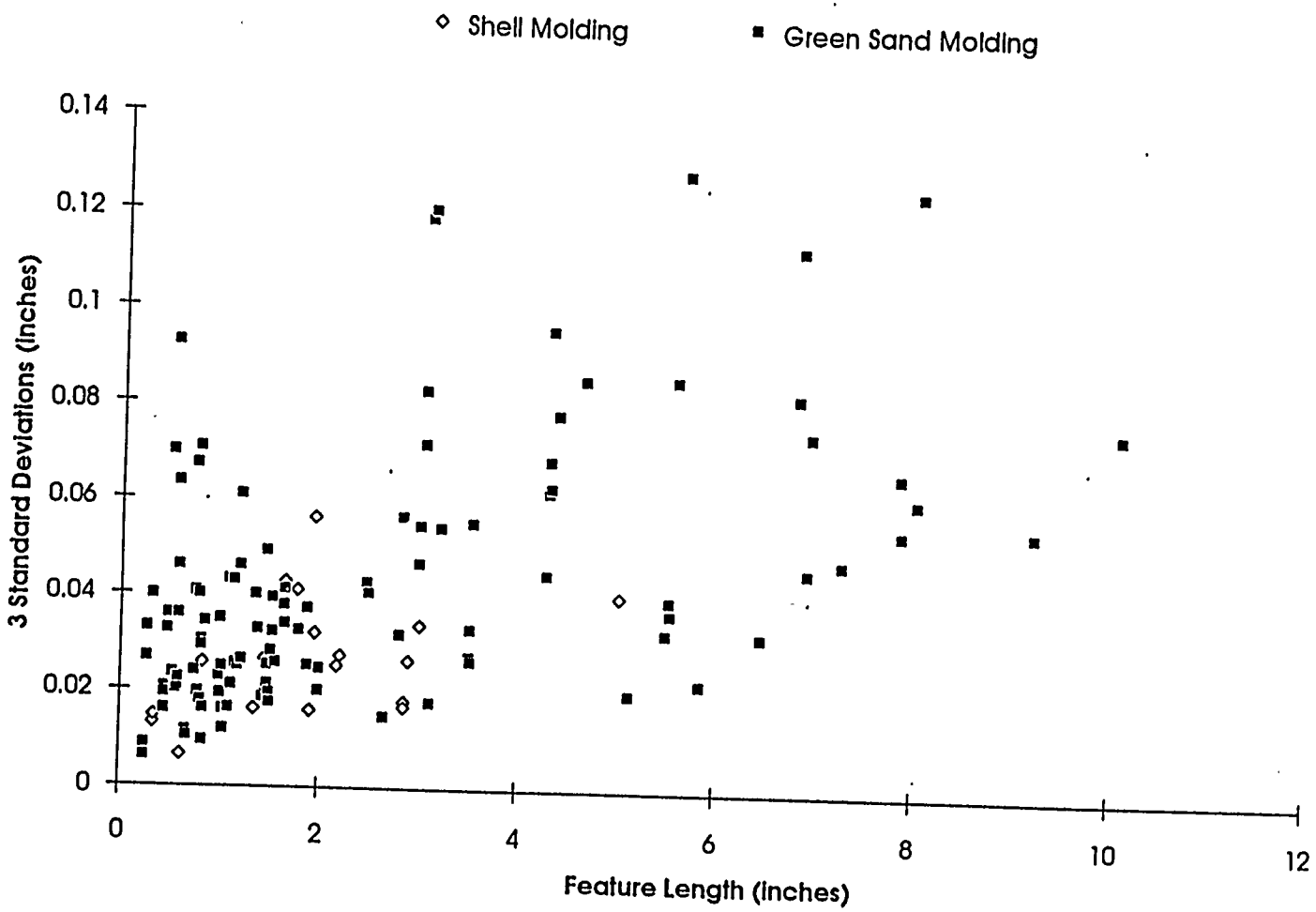

Figure 7: Dimensional variability as a function of feature length with features made with shell molding identified

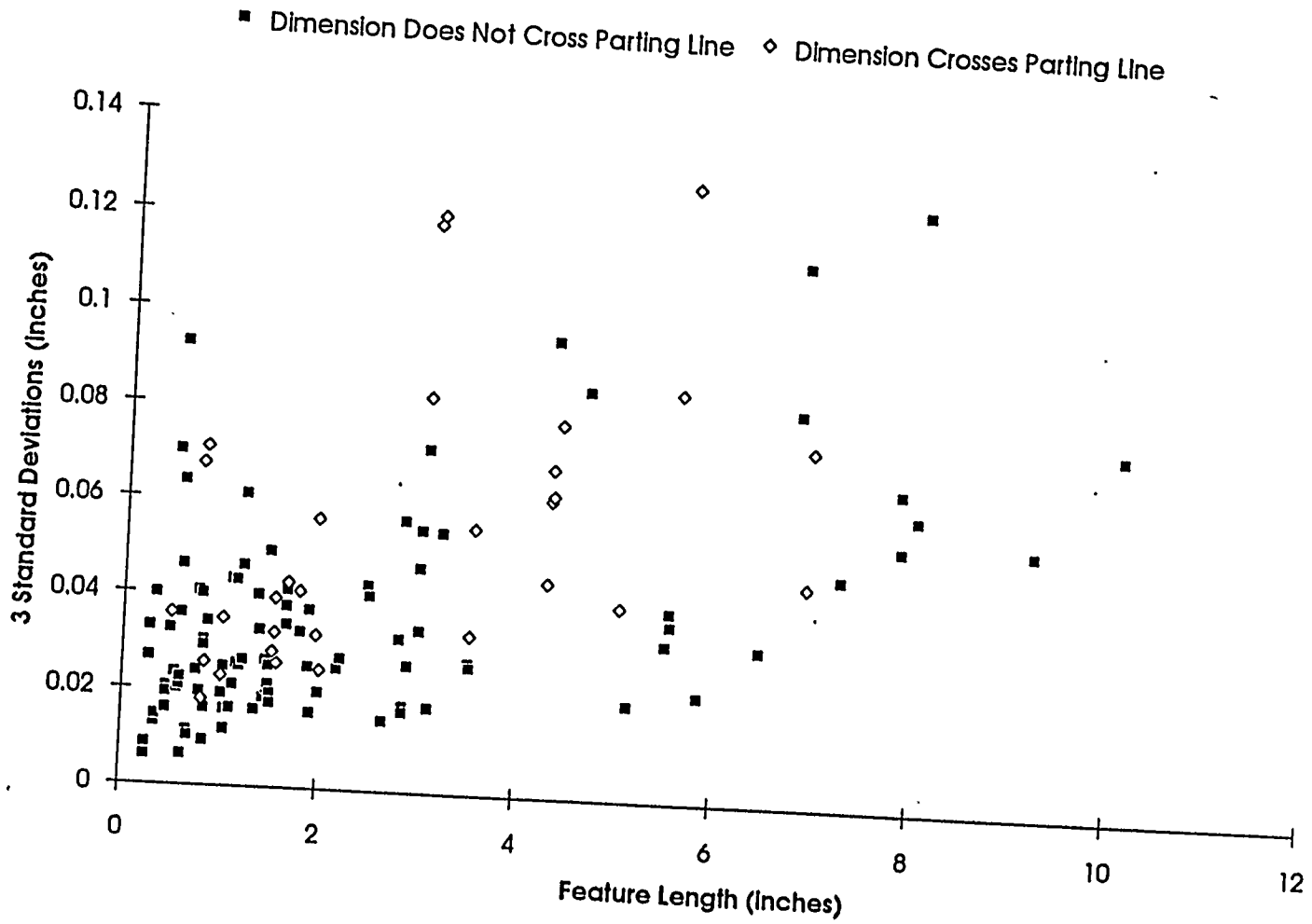

Figure 8: Dimensional variability as a function of feature length with features that cross the parting line identified

$$\log(3 \times \text{St.Dev.}) \text{ (inches)} = + 0.0655 \times \text{Feature length (inches)} + 0.0021 \times \text{Casting weight (pounds)} + 0.236 \text{ if the feature crosses mold parting line} - 0.094 \text{ if shell molded} + 0.149 \text{ if a mold-to-core feature} - 1.77$$

The coefficient of determination for this equation was 49.3 compared to 44.8 when the dependent variable was three standard deviations. Figure 9 is a normal plot of residuals for each of the two analyses. The plot for the analysis that used the logarithm of three standard deviations was more linear, which also indicates a better model.

Another important result of the linear regression analysis is the following variables that were not included in the equation because they were not significant: total pouring weight, dimensions crossing core parting lines, drafted surfaces, largest dimension on casting, height of cope, and core-to-core dimensions. These variables were initially suspected of being important to the dimensional variability, but were proven to be not significant for this particular data set. The reason that some of the variables were eliminated from consideration was that they were highly correlated with other variables. Any of the eliminated variables could be significant in future studies with more data.

Another linear regression analysis was conducted using the same dependent and independent variables as the equation used for the SFSA tolerances.[18] The new equation includes a correction factor. The equation is:

$$3 \text{ St. Dev. (inches)} = 0.032\ L^{1/3} + 0.006\ W^{1/3} - 0.0148$$

where L is the length of the feature (inches) and W is casting weight (pounds).

Results of Designed Experiments

Results of Core Type and Pouring Temperature Experiment

Castings were made with different core binder types and with steel at different pouring temperatures to study the effect of these variables. Specifically, sodium silicate and oil binder systems were studied. Data were collected from seven locations on the test part. For each measurement location, an analysis of variance was performed to see if there was any difference in the

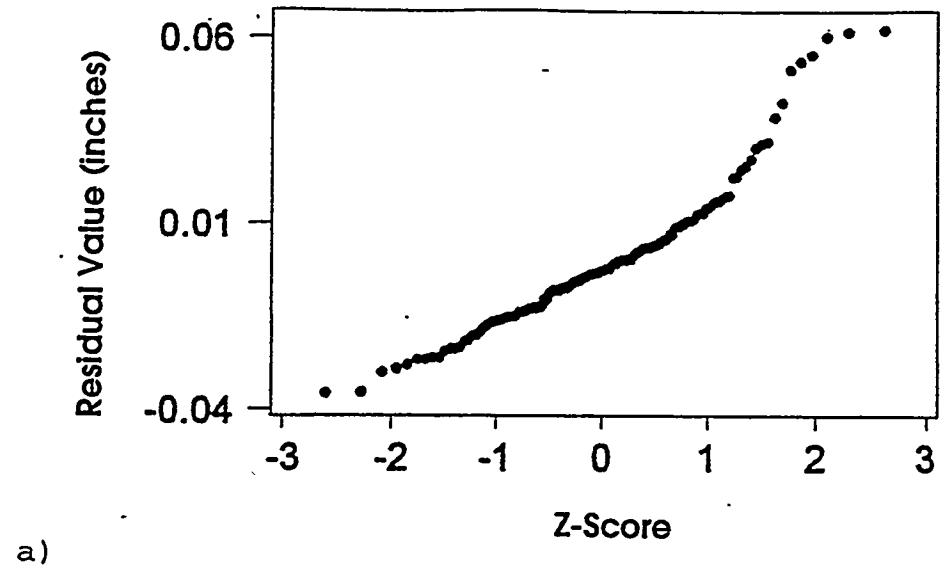

a)

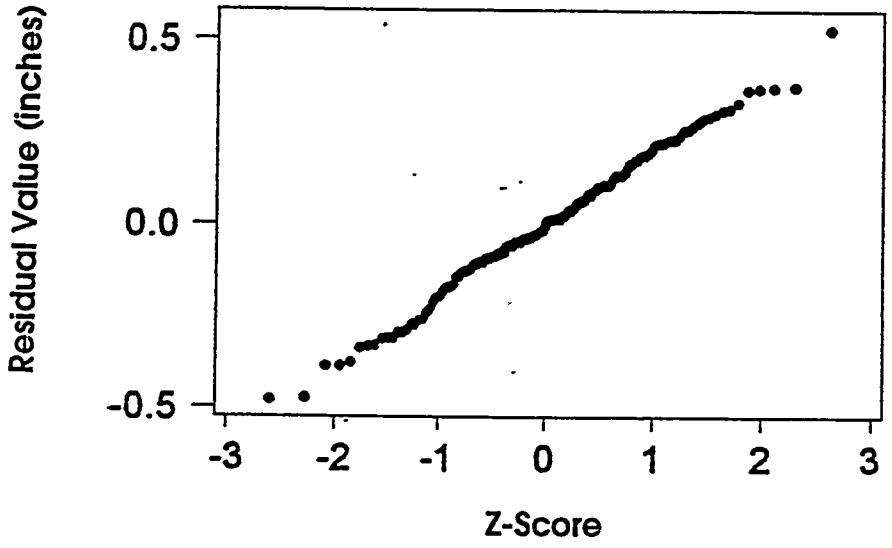

b)

Figure 9: Normal plots of the residual values from the linear regression models with the following dependent variable: a) three standard deviations b) logarithm of three standard deviations

mean of the dimensions. Due to omitted measurements and a core that broke prior to molding, there were several measurements missing. However, there were at least five data points for each set of test conditions. Because of the missing data, an analysis was performed twice, each time using five randomly selected data points. For each analysis, the conclusions were the same, therefore only the results of the first analysis were used, Table 7. Core type was found to be significant for all seven dimensions. Pouring temperatures of approximately 2890° F and 2990° F were used. The difference in pouring temperature was significant at the .05 significance level for all dimensions, except those dimensions that were internal of the blind hole.

Of notable interest is that core binder type significantly affected the mean of external dimensions. Core binder type also influenced the number of hot tears exhibited by the different core types. Magnetic particle inspection was used to inspect for defects. The average number of hot tears per casting in the corners of the open hole was 0.7 and 1.6 for the castings made with oil and sodium silicate cores, respectively. It can be expected that the sodium silicate binder was not effectively broken down by the heat from the casting during solidification and offered more restraint. Therefore, the external dimensions are larger and more hot tearing occurs when using the inorganic sodium silicate binder.

Further analysis was performed to study the effects of core type and pouring temperature on the variability of dimensions. The results of a Bartlett's Test for Equality of Variance test are summarized in Table 8. Binder type and pouring temperature were found to significantly effect the variability of only two of the seven dimensions. However, there was not a significant difference in variability for two other dimensions of the same types.

Results of the Molding Sand Experiments

Two parts were produced using green sand and shell molding to study the effect of the mold type on dimensional variability. A total of five features was measured on the two parts. Table 9 summarizes the type of feature and the three standard deviations measured for these features. Shell molding was less variable for one of two features that crossed the parting line. Of the other three features studied, shell molding was less variable for two features.

Table 7: Effect of core binder type and pouring temperature on the nominal dimension

DIMENSION NUMBER	DIMENSION TYPE	VARIABLE	P VALUE	RESULT
1	Internal	Core	.000	Sig.
1	Through hole	Temp.	.004	Sig.
1		Interaction	.960	Not Sig.
2	Internal	Core	.000	Sig.
2	Through hole	Temp.	.000	Sig.
2		Interaction	.760	Not Sig.
3	Internal	Core	.000	Sig.
3	Blind hole	Temp.	.161	Not Sig.
3		Interaction	.549	Not Sig.
4	Internal	Core	.000	Sig.
4	Blind hole	Temp.	.981	Not Sig.
4		Interaction	.079	Not Sig.
5	External	Core	.000	Sig.
5	Through hole	Temp.	.001	Sig.
5		Interaction	.589	Not Sig.
6	External	Core	.000	Sig.
6	Through hole	Temp.	.002	Sig.
6		Interaction	.049	Sig.
7	Internal	Core	.000	Sig.
7	Blind hole	Temp.	.001	Sig.
7		Interaction	.612	Not Sig.

Sig. - Statistically Significant
Not Sig. - Not Statistically Significant

Table 8: Effect of core binder type and pouring temperature on the variability of dimensions

DIMENSION NUMBER	SAMPLE STANDARD DEVIATION (INCHES) OIL LOW	OIL HIGH	CO_2 LOW	CO_2 HIGH	STATISTICAL VALUE	STATISTICAL RESULT
1	.013	.026	.005	.020	9.66	Sig.
2	.016	.020	.006	.013	5.15	Not Sig.
3	.008	.019	.006	.003	13.94	Sig.
4	.006	.006	.006	.005	.19	Not Sig.
5	.013	.020	.009	.023	4.05	Not Sig.
6	.012	.024	.010	.019	3.99	Not Sig.
7	.020	.009	.012	.010	3.78	Not Sig.

Test Statistic = $\chi^2_{.05,3} = 7.81$

Sig - Statistically Significant
Not Sig. - Not Statistically Significant

Table 9: Comparison of variability of the same features made using shell molding and green sand molding

FEATURE LENGTH	CASTING WEIGHT	3 STANDARD DEVIATIONS (INCHES) GREEN SAND	SHELL	CROSS PARTING LINE
.7	3	.009	.007	NO
5.2	17	.018	.027	NO
1.9	17	.063	.033	YES
1.9	17	.032	.056	YES
.8	17	.052	.026	YES

Chapter 5

DISCUSSION OF RESULTS

Influence of Casting Variables on Dimensional Variability

The following linear regression equation was developed from the data collected from production castings:

$$\log(3 \times \text{St. Dev.})\ (\text{inches}) = 0.0655 \times \text{Feature length (inches)} + 0.0021 \times \text{Casting weight (pounds)} + 0.236 \text{ if the feature crosses mold parting line} - 0.094 \text{ if shell molded} + 0.149 \text{ if a mold-to-core feature} - 1.77$$

The equation had a coefficient of determination of 49.3%, indicating a relatively poor fit. The variables included in the equation only account for approximately half of the variability. Similar linear regression equations developed in previous studies also had a relatively poor fit. The remainder of the variability is caused by unknown variables or variables which are too difficult to quantify for production castings. Such variables include the specific mold hardness and pouring temperature for a casting.

There were many variables which were eliminated from consideration because of insufficient data, high correlation with another variable, or lack of statistical significance. The problem of insufficient data was caused by the inherent difficulty and expense of collecting dimensional casting data. If more data were collected, the significance of these variables on dimensional variability could possibly be ascertained.

Regression analysis was also done using the same length and weight terms as the equation used for the current SFSA specifications.[18] Neither the coefficient of determination, 31.7, nor a plot of residual values versus the fitted values, Figure 10, indicate a good fit. The coefficient on the length term for the new equation is approximately twice that of the SFSA T5 equation. Weight was found to be less significant; the coefficient is one third that of the SFSA T5 equation. However, the data set used here is for castings under 120 pounds and the SFSA T5 equation is for castings up to 2000 pounds.

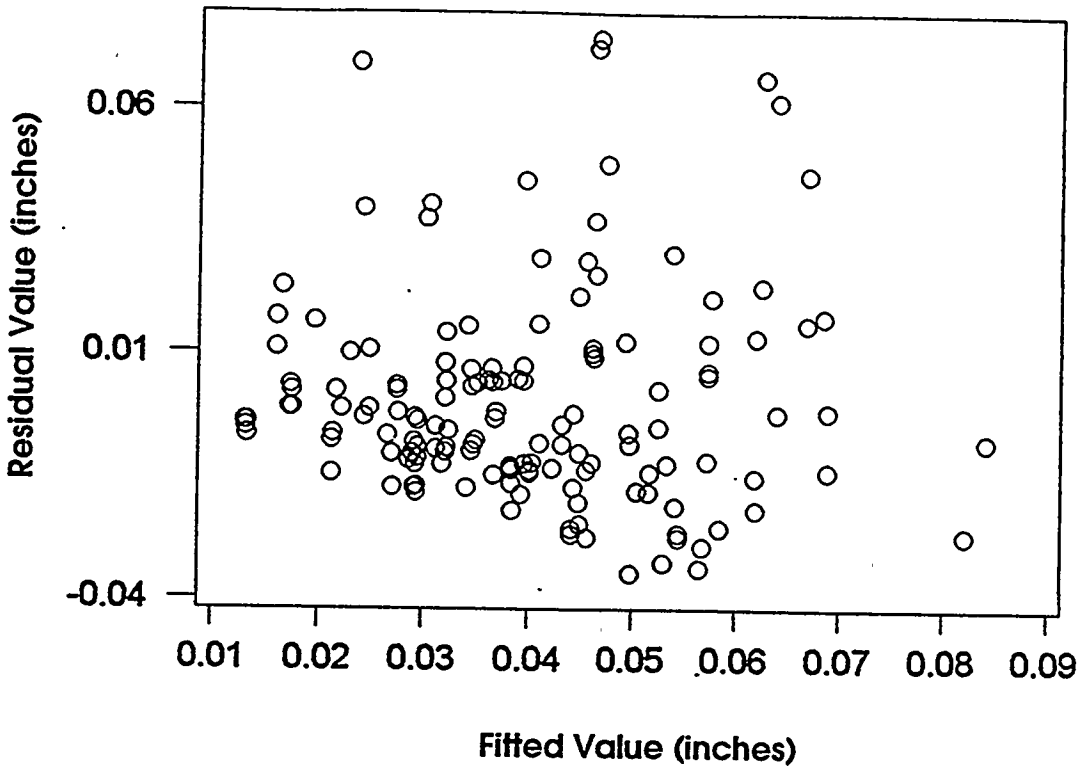

Figure 10: Fitted values versus residual values from the linear regression model that used the same variables as the current SFSA T5 tolerance equation

Comparison with Current Tolerance Standards

Figure 11 is a plot of the ISO CT8 through CT13 tolerance grades which are defined for long production series steel castings. Superimposed on the graph are the data collected for this project. Eighty-two percent of the data points are less than the ISO CT10 grade. CT8 through CT10 are for "sand cast, machine molded and shell molded castings." CT11 through CT13 are for "sand cast - hand molded steel castings." ISO CT13 through CT15 grades are for short production runs of steel castings made in green sand molds.

Another comparison was made between the sample variability measured in this study and the tolerances predicted by the 1977 SFSA tolerance guidelines,[18] the only published U.S. standards. For each feature, the SFSA T5 tolerance was calculated from the following equation:

$$T5 = 0.016\ L^{1/3} + 0.022\ W^{1/3}$$

where T5 = half tolerance (inches)
L = feature length (inches)
W = casting weight (pounds).

The half tolerance predicted by the T5 equation was subtracted from the measured three standard deviations for each feature.

X = (3 * Standard Dev.) - (predicted T5 half tolerance)

If the T5 equation was a perfect predictive model, all of the difference values would be zero. Instead, the result was a distribution of the difference values, as shown in Figure 12. There is a large grouping approximately centered at -0.035 inches. Based on the average of all the difference values, the T5 equation was modified to represent the majority of measured dimensional variabilities. The modified equation for the dimensional capabilities is:

Half tolerance = SFSA T5 - 0.027 (inches)

The modified equation predicted the half tolerance within ± 0.015 inches for 60% of the features.

This modified equation is intended to be used by the foundry as an indication of their dimensional capabilities compared with the SFSA T5 equation.

From Figure 12, there are seventeen features in which the difference was greater than zero; and they were investigated to determine probable causes. Nine of these features crossed the parting line, four were dependent on core placement, and four were subsequently straightened.

Some of the features in which the predicted tolerance was much greater than the observed variability were for small features on relatively heavy castings. The SFSA T5 equation has a large weight term, which does not fit well for such a feature.

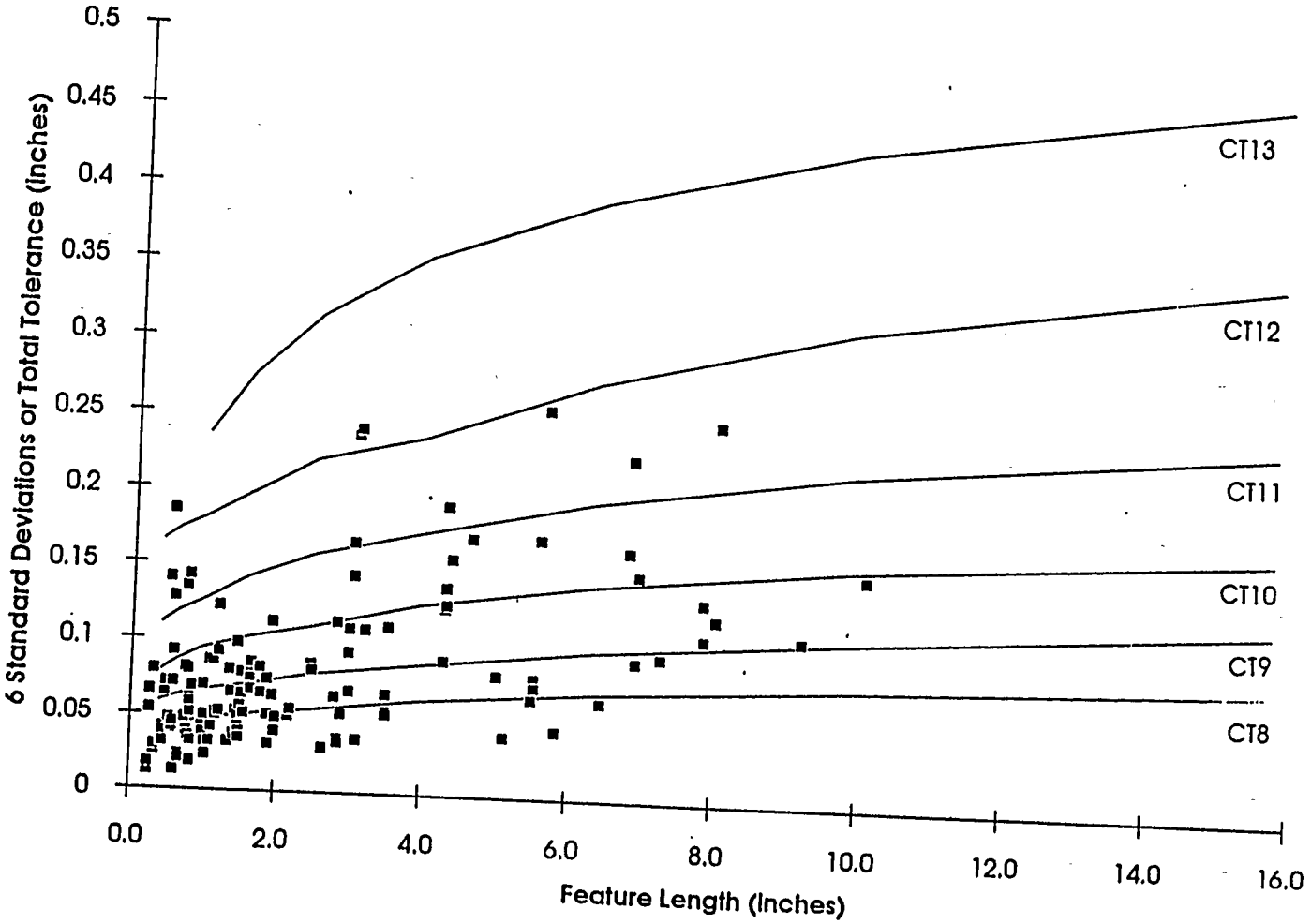

Figure 11: Comparison of the variability measured on the features studied and the ISO tolerance grades for steel castings. Note that six standard deviations or the total variability is plotted here to be consistent with the ISO standards.

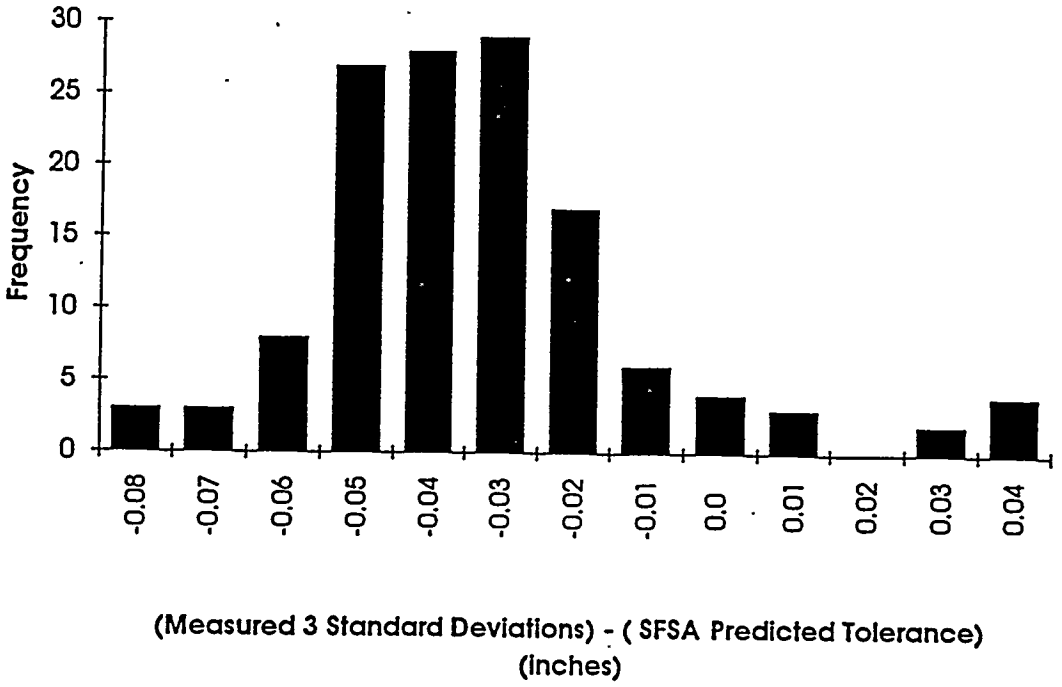

Figure 12: Comparison between the observed variability and the SFSA T5 grade.

Chapter 6

SUMMARY

Inspection techniques to conduct a dimensional capability assessment of steel castings have been described and carried out at a foundry. Modified measurement system analysis methods were developed for casting inspections that are being used to complete similar surveys at other participating foundry locations. Specific findings from the analysis of initial foundry data is as follows:

1 The total variability (six standard deviations) of eighty-two percent of the features studied was less than the ISO CT10 tolerance grade.

2 The half variability (three standard deviations) for the features measured were 0.027 inches less than the respective SFSA T5 tolerance, on average.

3 A linear regression model was developed to predict the dimensional variability of steel castings.

4 Pouring temperature and core binder type (oil sand and sodium silicate) did not significantly effect the variability of a cored hole. However, the core binder type significantly affected the mean dimensions of a cored hole.

Chapter 7

FUTURE WORK

Although this study collected a sizeable database of dimensional information for one foundry, more data are needed to better understand the effect of many process variables on dimensional variability throughout the industry. In order to maintain an accurate assessment of industry dimensional capabilities, additional data is being and will be collected at foundry sites across the country for a wide range of steel castings. This information would be helpful to track process improvements as well as provide up-to-date information for casting designers.

This initial effort has been concerned with the random error, or variability of casting dimensions, not systematic error caused by inaccurate patterns. Future work will investigate the accuracy of the pattern equipment. Specifically, research on casting contraction for different casting geometries is vital to design more accurate patterns.

Work is ongoing to develop a complete dimensional and casting descriptor database from which new dimensional tolerance guidelines, pattern shrinkage allowances and foundry dimensional control guidelines can be developed.

REFERENCES

1 American Foundrymen's Society; *Foundry Industry Research Plan - 1994,* Des Plaines, IL (1994).

2 Aubrey, L.S. et al.; *Dimensional Tolerances,* Steel Founders' Society of America, Report No. 84 (1977).

3 Automotive Industry Action Group; *Measurement Systems Analysis - Reference Manual* (1990).

4 Draper, A.B.; "Meeting the Dimensional Standards of Tomorrow," *AFS Transactions,* vol 85, p 577 (1977).

5 Institute of British Foundrymen Technical Subcommittee TS71; "First Report of Technical Sub-Committee TS 71 - Dimensional Tolerances in Castings," *The British Foundryman,* vol 62, part 5, p 179 (1969).

6 Institute of British Foundrymen Technical Subcommittee TS71; "Second Report of Technical Sub-Committee TS71 - Dimensional Tolerances in Castings," *The British Foundryman,* vol 64, part 10, p 364 (1971).

7 International Standards Organization; *Castings - System of Dimensional Tolerances,* ISO 8062 (1984).

8 Law, T.D.; "Aspects of Dimensional Control," *SCRATA Proceedings of the 1977 Annual Conference,* paper 13 (1977).

9 Montgomery, D.C.; *Design and Analysis of Experiments,* 3rd ed., John Wiley and Sons, New York (1991).

10 Peters, F.E. and R.C. Voigt; "Casting Inspection Strategies for Determining Dimensional Variability," *Proceedings of the Steel Founders' Society of America T & O Conference,* Chicago, IL (1993).

11 Reddy, D.C., S.S.N. Murty, and P.N. Chakraborty; "Development of a Tolerance System for Castings," *AFS Transactions,* vol 96, p 839 (1988).

12 Ross, P.J.; "Measurement System Capability Project," *Proceedings of the Steel Founders' Society of America T & O Conference,* Chicago, IL (1990).

13 Ross, P.J.; "Measurement System Capability Project - 1992 Update," *Proceedings of the Steel Founders' Society of America T & O Conference,* Chicago, IL (1992).

14 Steel Castings Development Committee; *Quality Standards for Steel Castings*, Sheffield, U.K. (1966).

15 Svensson I. and L. Villner; "Dimensional Accuracy of Castings," *The British Foundryman*, vol 67, part 10, p 277 (1974).

16 Villner, L.; "A General System of Dimensional Tolerances for Castings," *The British Foundryman*, vol 62, part 12, p 458 (1969).

17 Voigt, R.C. and F.E. Peters; "Dimensional Tolerances and Shrinkage Allowances for Steel Castings," *Proceedings of the Steel Founders' Society of America T & O Conference*, Chicago, IL (1992).

18 Wieser, P.F., ed.; *Steel Castings Handbook*, 5th ed., Steel Founders' Society of America, Des Plaines, IL (1980).

APPENDIX A

SFSA TOLERANCE SPECIFICATIONS

Source: Wieser, P.F.

Tolerances (±inches) for Tolerance Grade T3

	Casting Weight, lb																		
L*	2	5	10	20	50	75	100	150	200	250	500	750	1000	1250	1500	2000	3000	4000	5000
.5	.024	.026	.028	.031	.036	.039	.041	.044	.047	.049	.057	.063	.068	.071	.075	.081	.090	.097	.103
1.0	.028	.031	.033	.036	.041	.043	.045	.049	.051	.054	.062	.068	.072	.076	.079	.085	.094	.101	.108
2.0	.034	.036	.039	.041	.046	.049	.051	.054	.057	.059	.068	.073	.078	.082	.085	.091	.100	.107	.113
4.0	.041	.044	.046	.049	.054	.056	.058	.062	.064	.067	.075	.081	.085	.089	.092	.098	.107	.114	.121
6.0	.046	.049	.051	.054	.059	.061	.063	.067	.069	.072	.080	.086	.090	.094	.097	.103	.112	.120	.126
8.0	.050	.053	.055	.058	.063	.065	.067	.071	.073	.076	.084	.090	.094	.098	.101	.107	.116	.124	.130
10.0	.054	.056	.058	.061	.066	.069	.071	.074	.077	.079	.087	.093	.098	.101	.105	.111	.120	.127	.133
15.0	.061	.063	.065	.068	.073	.076	.078	.081	.084	.086	.094	.100	.105	.108	.112	.117	.127	.134	.140
20.0	.066	.069	.071	.074	.078	.081	.083	.087	.089	.091	.100	.105	.110	.114	.117	.123	.132	.139	.145
30.0	.075	.077	.079	.082	.087	.090	.092	.095	.098	.100	.108	.114	.119	.123	.126	.132	.141	.148	.154
40.0	.082	.084	.086	.089	.094	.097	.099	.102	.105	.107	.115	.121	.126	.129	.133	.139	.148	.155	.161
50.0	.088	.090	.092	.095	.100	.103	.105	.108	.111	.113	.121	.127	.131	.135	.139	.144	.154	.161	.167
60.0	.093	.095	.097	.100	.105	.108	.110	.113	.116	.118	.126	.132	.137	.140	.144	.150	.159	.166	.172

*Dimension length in inches

Tolerances (±inches) for Tolerance Grade T4

	Casting Weight, lb																		
L*	2	5	10	20	50	75	100	150	200	250	500	750	1000	1250	1500	2000	3000	4000	5000
.5	.030	.035	.039	.045	.054	.060	.064	.071	.076	.081	.097	.108	.118	.125	.132	.144	.162	.176	.189
1.0	.035	.039	.044	.049	.059	.064	.069	.075	.081	.085	.101	.113	.122	.130	.137	.148	.166	.181	.193
2.0	.040	.045	.049	.055	.065	.070	.074	.081	.086	.091	.107	.119	.128	.136	.142	.154	.172	.187	.199
4.0	.048	.052	.057	.062	.072	.077	.081	.088	.094	.098	.114	.126	.135	.143	.150	.161	.179	.194	.206
6.0	.053	.057	.062	.067	.077	.082	.087	.093	.099	.103	.120	.131	.140	.148	.155	.166	.184	.199	.211
8.0	.057	.061	.066	.071	.081	.086	.091	.097	.103	.107	.124	.135	.144	.152	.159	.170	.188	.203	.215
10.0	.060	.065	.069	.075	.084	.090	.094	.101	.106	.111	.127	.138	.148	.155	.162	.174	.192	.206	.219
15.0	.067	.072	.076	.082	.091	.097	.101	.108	.113	.117	.134	.145	.155	.162	.169	.180	.199	.213	.226
20.0	.073	.077	.082	.087	.097	.102	.106	.113	.118	.123	.139	.151	.160	.168	.174	.186	.204	.219	.231
30.0	.081	.086	.090	.096	.106	.111	.115	.122	.127	.132	.148	.160	.169	.176	.183	.195	.213	.227	.240
40.0	.088	.093	.097	.103	.112	.118	.122	.129	.134	.139	.155	.166	.176	.183	.190	.202	.220	.234	.247
50.0	.094	.099	.103	.109	.118	.124	.128	.135	.140	.144	.161	.172	.181	.189	.196	.207	.226	.240	.252
60.0	.099	.104	.108	.114	.123	.129	.133	.140	.145	.150	.166	.177	.187	.194	.201	.213	.231	.245	.258

*Dimension length in inches

Tolerances (±Inches) for Tolerance Grade T5

	Casting Weight, lb																		
L*	2	5	10	20	50	75	100	150	200	250	500	750	1000	1250	1500	2000	3000	4000	5000
.5	.038	.045	.052	.061	.076	.085	.092	.103	.111	.118	.145	.163	.178	.190	.201	.219	.248		
1.0	.042	.049	.057	.066	.081	.090	.096	.107	.116	.123	.149	.167	.182	.194	.205	.224	.253	.276	.296
2.0	.048	.055	.062	.071	.087	.095	.102	.113	.121	.129	.155	.173	.188	.200	.211	.229	.259	.282	.301
4.0	.055	.062	.070	.079	.094	.103	.109	.120	.129	.136	.162	.180	.195	.207	.218	.237	.266	.289	.309
6.0	.060	.068	.075	.084	.099	.108	.114	.125	.134	.141	.167	.186	.200	.213	.223	.242	.271	.294	.314
8.0	.064	.072	.079	.088	.103	.112	.118	.129	.138	.145	.171	.190	.204	.217	.227	.246	.275	.298	.318
10.0	.068	.075	.082	.091	.107	.115	.122	.133	.141	.148	.175	.193	.208	.220	.231	.249	.278	.302	.321
15.0	.075	.082	.089	.098	.113	.122	.129	.140	.148	.155	.181	.200	.215	.227	.238	.256	.285	.308	.328
20.0	.080	.087	.094	.103	.119	.127	.134	.145	.154	.161	.187	.205	.220	.232	.243	.262	.291	.314	.334
30.0	.089	.096	.103	.112	.128	.136	.143	.154	.162	.169	.196	.214	.229	.241	.252	.270	.299	.323	.342
40.0	.096	.103	.110	.119	.135	.143	.150	.161	.169	.176	.203	.221	.236	.248	.259	.277	.306	.330	.349
50.0	.102	.109	.116	.125	.140	.149	.156	.166	.175	.182	.208	.227	.241	.254	.265	.283	.312	.335	.355
60.0	.107	.114	.121	.130	.145	.154	.161	.172	.180	.187	.214	.232	.247	.259	.270	.288	.317	.341	.360

*Dimension length in inches

Tolerances (±Inches) for Tolerance Grade T6

	Casting Weight, lb																		
L*	2	5	10	20	50	75	100	150	200	250	500	750	1000	1250	1500	2000	3000	4000	5000
.5	.052	.064	.076	.091	.117	.131	.143	.161	.175	.188	.232								
1.0	.056	.068	.080	.095	.122	.136	.147	.166	.180	.192	.236	.267	.292	.313	.331	.362	.412	.451	.484
2.0	.062	.074	.086	.101	.127	.142	.153	.171	.186	.198	.242	.273	.298	.319	.337	.368	.417	.456	.490
4.0	.069	.081	.093	.108	.135	.149	.160	.179	.193	.205	.249	.280	.305	.326	.344	.375	.424	.464	.497
6.0	.074	.086	.098	.113	.140	.154	.165	.184	.198	.210	.254	.285	.310	.331	.349	.380	.430	.469	.502
8.0	.078	.090	.102	.117	.144	.158	.170	.188	.202	.214	.258	.290	.314	.335	.353	.384	.434	.473	.506
10.0	.082	.094	.106	.121	.147	.161	.173	.191	.206	.218	.262	.293	.318	.338	.357	.388	.437	.476	.509
15.0	.089	.101	.113	.128	.154	.168	.180	.198	.212	.225	.269	.300	.325	.345	.364	.395	.444	.483	.516
20.0	.094	.106	.118	.133	.159	.174	.185	.203	.218	.230	.274	.305	.330	.351	.369	.400	.449	.489	.522
30.0	.103	.115	.127	.142	.168	.183	.194	.212	.227	.239	.283	.314	.339	.360	.378	.409	.458	.497	.530
40.0	.110	.122	.134	.149	.175	.189	.201	.219	.233	.246	.290	.321	.346	.366	.385	.416	.465	.504	.537
50.0	.115	.128	.140	.155	.181	.195	.207	.225	.239	.252	.296	.327	.351	.372	.390	.422	.471	.510	.543
60.0	.121	.133	.145	.160	.186	.200	.212	.230	.244	.257	.301	.332	.357	.377	.396	.427	.476	.515	.548

*Dimension length in inches

Tolerances (±inches) for Tolerance Grade T7

	Casting Weight, lb																		
L*	2	5	10	20	50	75	100	150	200	250	500	750	1000	1250	1500	2000	3000	4000	5000
.5	.073	.093	.112	.137	.180	.203	.222												
1.0	.078	.097	.117	.142	.184	.208	.226	.256	.279	.299	.371	.422	.462						
2.0	.083	.103	.123	.147	.190	.213	.232	.262	.285	.305	.377	.428	.468	.502	.532	.582	.662		
4.0	.091	.110	.130	.155	.197	.221	.239	.269	.292	.312	.384	.435	.475	.509	.539	.589	.670	.734	.787
6.0	.096	.115	.135	.160	.202	.226	.244	.274	.297	.317	.389	.440	.480	.514	.544	.595	.675	.739	.793
8.0	.100	.119	.139	.164	.206	.230	.248	.278	.302	.321	.393	.444	.484	.518	.548	.599	.679	.743	.797
10.0	.103	.123	.142	.167	.210	.233	.252	.281	.305	.325	.397	.447	.488	.522	.551	.602	.682	.746	.800
15.0	.110	.130	.149	.174	.217	.240	.259	.288	.312	.332	.404	.454	.495	.528	.558	.609	.689	.753	.807
20.0	.115	.135	.155	.179	.222	.246	.264	.294	.317	.337	.409	.460	.500	.534	.564	.614	.695	.758	.812
30.0	.124	.144	.163	.188	.231	.254	.273	.302	.326	.346	.418	.468	.509	.543	.572	.623	.703	.767	.821
40.0	.131	.151	.170	.195	.238	.261	.280	.309	.333	.353	.425	.475	.516	.550	.579	.630	.710	.774	.828
50.0	.137	.157	.176	.201	.244	.267	.286	.315	.339	.359	.431	.481	.521	.555	.585	.636	.716	.780	.834
60.0	.142	.162	.181	.206	.249	.272	.291	.320	.344	.364	.436	.486	.527	.560	.590	.641	.721	.785	.839

*Dimension length in inches

APPENDIX B

ISO 8062 SYSTEM OF DIMENSIONAL TOLERANCES

Source: International Standards Organization

Raw casting basic dimension mm		Total casting tolerance[1] mm																
		Casting tolerance grade CT																
over	up to and including	1[2]	2[2]	3	4	5	6	7	8	9	10	11	12	13	14	15	16
–	10			0,18	0,26	0,36	0,52	0,74	1,0	1,5	2,0	2,8	4,2	–	–	–	–
10	16			0,20	0,28	0,38	0,54	0,78	1,1	1,6	2,2	3,0	4,4	–	–	–	–
16	25			0,22	0,30	0,42	0,58	0,82	1,2	1,7	2,4	3,2	4,6	6	8	10	12
25	40			0,24	0,32	0,46	0,64	0,90	1,3	1,8	2,6	3,6	5,0	7	9	11	14
40	63			0,26	0,36	0,50	0,70	1,0	1,4	2,0	2,8	4,0	5,6	8	10	12	16
63	100			0,28	0,40	0,56	0,78	1,1	1,6	2,2	3,2	4,4	6	9	11	14	18
100	160			0,30	0,44	0,62	0,88	1,2	1,8	2,5	3,6	5,0	7	10	12	16	20
160	250			0,34	0,50	0,70	1,0	1,4	2,0	2,8	4,0	5,6	8	11	14	18	22
250	400			0,40	0,56	0,78	1,1	1,6	2,2	3,2	4,4	6,2	9	12	16	20	25
400	630				0,64	0,90	1,2	1,8	2,6	3,6	5	7	10	14	18	22	28
630	1 000					1,0	1,4	2,0	2,8	4,0	6	8	11	16	20	25	32
1 000	1 600						1,6	2,2	3,2	4,6	7	9	13	18	23	29	37
1 600	2 500							2,6	3,8	5,4	8	10	15	21	26	33	42
2 500	4 000								4,4	6,2	9	12	17	24	30	38	49
4 000	6 300									7,0	10	14	20	28	35	44	56
6 300	10 000										11	16	23	32	40	50	64

Method	Tolerance grade CT								
	Steel	Grey iron	S.G. iron	Malleable iron	Copper alloys	Zinc alloys	Light metal alloys	Nickel-based alloys	Cobalt-based alloys
Sand cast, hand-moulded	11 to 13	11 to 13	11 to 13	11 to 13	10 to 12		9 to 11		
Sand cast, machine-moulded and shell moulding	8 to 10	8 to 10	8 to 10	8 to 10	8 to 10		7 to 9		
Metallic permanent mould (gravity and low pressure)		7 to 9	7 to 9	7 to 9	7 to 9	7 to 9	6 to 8		
Pressure die casting					6 to 8	4 to 6	5 to 7		
Investment casting	4 to 6	4 to 6	4 to 6		4 to 6		4 to 6	4 to 6	4 to 6

NOTE — The tolerances indicated are those which can normally be held for castings produced in long series and when production factors influencing the dimensional accuracy of the casting have been fully developed.

APPENDIX C

MEASUREMENT SYSTEM ANALYSIS PROCEDURES

An efficient and consistent method to test the measurement systems of all participating foundries is a critical aspect of the SFSA/Penn State Dimensional Capability Project. The procedures outlined below are not only important for this project, but also for any inspection completed by a foundry's inspection department.

Initially, Gage Repeatability and Reproducibility (Gage R & R) tests should be conducted on each of the measurement systems to be used by the foundry for the project, such as calipers, micrometers, Portage layout machines, or CMMs.

For calipers and other hand held instruments, the initial test will consist of at least two operators measuring the same feature on ten pieces two times each. The feature(s) measured should be representative of the features to be measured during the study. For example, the Gage R & R tests should not be limited to a 3 inch outside dimension if 12 inch internal diameters are to be measured.

The initial test for Portage machines or CMMs will require one (or more) operator(s) measuring the same feature on the same casting ten times. This casting should be retained for future measurement system checks. The casting will need to be set up and leveled on the machine between measurements, to capture all of the measurement process variations.

A calibration check should be periodically performed to insure the continued accuracy of all measurement instruments. These tests should be done each time castings are measured for the project, or weekly.

For calipers and other hand held instruments, this will involve checking a gage block or other part of known dimensions.

For Portage machines or CMMs, layout and check the standard casting, retained from the initial Gage R & R test, one time.

The initial Gage R & R test should be completed annually.

If the patterns are measured by different equipment and/or personnel, then similar tests will need to be performed on those measurement systems.

APPENDIX D

SAMPLE MEASUREMENT SYSTEM REPEATABILITY TEST

Units -- inches

Part	1	2	Range
1	2.866	2.867	0.001
2	2.865	2.864	0.001
3	2.861	2.861	0.000
4	2.860	2.864	0.004
5	2.861	2.861	0.000
6	2.866	2.863	0.003
7	2.868	2.863	0.005
8	2.876	2.871	0.005
9	2.856	2.862	0.006
10	2.865	2.868	0.003

$\overline{R} = 0.0028$

Repeatability = $\overline{R} \times K_1$

$K_1 = 6 / d_2$

$d_2 = 1.16$ for m = 2 and g = 10

Repeatability = $\overline{R} \times K_1$
= (0.0028) X (6 / 1.16)
= 0.0145

SFSA T3 tolerance for a 3 inch dimension on a 10 pound casting is 2 X 0.0425 = 0.0850

% Repeatability = (0.0145 / 0.0850) X 100
= .17 X 100
= 17%

Since only one inspector was involved, reproducibility error was 0. Therefore, the measurement error was 17%, which is acceptable

Sources: Automotive Industry Action Group
Wieser, P.F.

APPENDIX E

CASTING VARIABLE SURVEY FORM

SFSA/Penn State Dimensional Capability Project
Casting Variables Survey Form
General Variables

Please complete and return to:
Frank Peters, Industrial Engineering Dept.
207 Hammond Building, University Park, PA 16802

Please circle or fill in the most appropriate answer. Add additional comments wherever necessary. Thank You.

Foundry Name _____

Part Number _____

Approximate number of castings produced per year _____

Approximate number of castings produced per lot _____

Number of castings per mold _____

If more than one, what is the minimum between spacing _____

What is the casting used for (railroad, pump/valve, _____

Type of flask (tight, slip, flaskless, _____

Mold size (inch x inch) _____

Cope height _____ Drag height _____

Are jackets used during pouring _____

Alloy _____

Pouring temperature range specified High _____ Low _____

How are the molds weighted during pouring _____

Type of heat treatment _____

Is this casting typically upgraded by straightening _____

What is the total pour weight _____units?

What is the finished casting weight _____units?

What is the largest dimension on the casting _____units?

What is the wall thickness, if applicable, _____units?

How many and what type(s) of cores are used _____

How are cores made (blown, full box, split box, _____)

Are the cores lightened (hollow) _____

How are cores set in the mold _____

Are core assemblies used _____ Are they fixtured _____

What is the total volume of Internal coring (inch^3) _____
Rough estimate or I will figure it out

Is core wash used _____

If shell cores, what is the specified shell core thickness _____

Type(s) of core box(es) (Aluminum, epoxy, wood, iron, steel,
bronze, other _____)

Condition of core box(es) (excellent, very good, good, fair,poor)

How often are the pins and bushings on flasks checked _____

Molding method (jolt squeeze, squeeze, jolt, slinger, vibration,
hand rammed, other _____)

Is mold wash used _____

What type of chills used (none used, nails, block size _____)

Type(s) of pattern (Aluminum, epoxy, wood, iron, steel,
bronze, other _____)

Condition of pattern (excellent, very good, good, fair, poor)

How old is the pattern equipment (if known) _____

Type of pattern set-up (matchplate, separate cope & drag, loose
other _____)

Type of molding sand (green, no-bake, shell, other _____)

If no bake, what is the % binder _____

If green sand, what is the clay content _____

Is facing sand used _____ Is reclaimed sand used _____

What is the projected area of casting? _____ units

Bounding box that contains castings ? _____ units

Please add any comments about binders, additives, etc.:

SFSA/Penn State Dimensional Capability Project
Casting Variables Survey Form
Variables Specific to a Feature

feature number				
dimension location cope,drag,across PL				
dimension direction vert,horiz,neither				
does dimension cross core parting line				
does dimension cross core assbly joint				
type of core used for this feature				
do chills affect this feature				
does draft affect this feature				
does grinding affect this feature **				
does mold wash affect this feature				
does core wash affect this feature				
is this dimension upgraded by straightening **				
what is the nominal size and tolerance on the print				
choose one of the following mold/core relationships				

** NOTE: if this dimension is upgraded by straightening or grinding then the inspection should take place beforehand

A mold to mold across casting
B mold to mold across mold
C mold to mold across mold and casting
D mold to mold across casting/mold/casting
E mold to core across casting
F core to core across core
G mold to core across casting and core
H mold to mold across casting/core/casting
Other configurations ??

APPENDIX F

PRODUCTION CASTING VARIABILITY DATA

Three Standard Deviations (inches)	Feature Length (inches)	Casting Weight (pounds)	Does Dimension Cross Parting Line	Feature with Draft	Type of Molding Sand
0.160	6.528	2	No	Yes	GREEN
0.167	15.745	3	No	Yes	SHELL
0.197	6.382	2	No	Yes	GREEN
0.220	6.329	2	No	Yes	GREEN
0.225	6.528	2	No	Yes	GREEN
0.242	21.406	6.9	No	No	GREEN
0.268	17.262	17.7	No	Yes	GREEN
0.294	16.991	17.7	No	Yes	GREEN
0.306	26.649	6.9	No	Yes	GREEN
0.334	8.713	11	No	Yes	SHELL
0.372	8.776	11	No	Yes	SHELL
0.378	67.523	36.6	No	No	GREEN
0.400	11.278	2	No	Yes	GREEN
0.406	11.525	2	No	Yes	GREEN
0.408	48.581	11	No	Yes	SHELL
0.410	26.502	6.9	No	Yes	GREEN
0.414	21.370	6.9	No	No	GREEN
0.415	34.287	11	No	Yes	SHELL
0.416	27.827	5.1	No	No	GREEN
0.429	72.667	11	No	Yes	SHELL
0.452	38.168	2	No	Yes	GREEN
0.454	79.194	11.7	No	Yes	GREEN
0.458	72.633	11	No	Yes	SHELL
0.459	20.539	11.7	Yes	No	GREEN
0.476	36.543	5.1	No	No	GREEN
0.493	11.470	2	No	Yes	GREEN
0.495	25.622	3.6	No	No	GREEN
0.498	19.935	117.2	No	No	GREEN
0.503	38.140	2	No	Yes	GREEN
0.513	130.408	9.2	No	No	GREEN
0.514	50.544	11.7	No	Yes	GREEN
0.516	14.293	5.1	No	No	GREEN
0.521	11.386	2	No	Yes	GREEN
0.525	37.258	2	No	Yes	GREEN
0.531	14.753	8.4	No	Yes	GREEN
0.540	28.462	9.2	No	No	GREEN
0.543	56.005	6.9	No	No	GREEN
0.546	37.702	14.8	No	No	GREEN
0.547	14.649	35.8	No	No	GREEN
0.573	148.432	11.7	No	No	GREEN
0.574	14.808	35.8	No	No	GREEN
0.585	25.391	2	Yes	No	GREEN
0.598	13.492	5.1	No	No	GREEN
0.607	86.678	6.9	Yes	No	GREEN
0.610	19.017	35.8	No	No	GREEN

0.615	55.974	6.9	No	No	GREEN
0.631	50.790	9.2	Yes	No	GREEN
0.636	25.991	4.6	No	No	GREEN
0.640	29.981	5.1	No	No	GREEN
0.644	55.202	11	No	Yes	SHELL
0.647	37.584	2	No	Yes	GREEN
0.649	47.796	4.6	No	No	GREEN
0.653	29.468	41.7	No	No	GREEN
0.655	20.994	17.5	Yes	No	SHELL
0.660	39.636	4.6	Yes	No	GREEN
0.673	73.497	11	No	Yes	SHELL
0.674	31.001	35.8	No	Yes	GREEN
0.677	89.463	38.4	No	No	GREEN
0.678	36.929	11	No	No	SHELL
0.680	6.747	4.6	No	No	GREEN
0.693	135.386	17.5	No	Yes	SHELL
0.698	89.224	38.4	No	No	GREEN
0.699	55.975	11	No	Yes	SHELL
0.723	38.442	36.6	Yes	No	GREEN
0.748	20.794	8.3	No	No	GREEN
0.771	20.720	8.3	No	No	GREEN
0.790	103.960	3.6	No	No	GREEN
0.813	71.255	35.8	No	No	GREEN
0.816	49.492	17.5	Yes	No	SHELL
0.823	38.878	4.6	Yes	No	GREEN
0.828	164.052	11.7	No	Yes	GREEN
0.829	12.006	9.2	No	Yes	GREEN
0.832	45.534	117.2	No	Yes	GREEN
0.836	35.195	17.7	No	Yes	GREEN
0.836	139.691	4.6	No	No	GREEN
0.838	6.760	4.6	No	No	GREEN
0.844	89.258	8.4	Yes	No	GREEN
0.862	76.328	11	No	Yes	SHELL
0.866	41.899	35.8	No	Yes	GREEN
0.875	21.660	42	No	No	GREEN
0.890	25.552	2	Yes	No	GREEN
0.910	12.181	3.6	Yes	No	GREEN
0.913	14.858	35.8	No	No	GREEN
0.940	140.671	4.6	No	No	GREEN
0.950	47.681	4.6	No	No	GREEN
0.965	41.773	35.8	No	Yes	GREEN
0.976	52.650	3.6	No	No	GREEN
1.004	38.796	4.6	Yes	No	GREEN
1.010	140.349	36.6	No	Yes	GREEN
1.013	8.157	3.6	No	No	GREEN
1.019	20.098	42	No	No	GREEN
1.020	34.573	17.7	No	Yes	GREEN
1.027	127.560	11	Yes	No	SHELL
1.033	19.174	35.8	No	No	GREEN
1.035	63.202	41.7	No	No	GREEN

1.047	45.102	11	Yes	No	SHELL
1.052	41.899	42	No	No	GREEN
1.089	62.742	41.7	No	No	GREEN
1.091	41.942	11	Yes	No	SHELL
1.098	28.988	36.6	No	Yes	GREEN
1.098	27.702	42	No	Yes	GREEN
1.141	108.919	35.8	Yes	Yes	GREEN
1.168	14.795	35.8	No	No	GREEN
1.173	175.937	17.7	Yes	No	GREEN
1.174	30.513	35.8	No	Yes	GREEN
1.192	75.929	41.7	No	Yes	GREEN
1.221	184.724	118	No	Yes	GREEN
1.253	37.146	9.2	No	No	GREEN
1.384	81.475	35.8	No	No	GREEN
1.385	199.840	36.6	No	Yes	GREEN
1.391	76.138	14.8	No	No	GREEN
1.399	234.066	117.2	No	Yes	GREEN
1.411	89.601	8.4	Yes	Yes	GREEN
1.432	49.245	17.5	Yes	No	SHELL
1.440	71.628	17.5	No	Yes	GREEN
1.553	30.506	117.2	No	Yes	GREEN
1.555	203.783	14.8	No	Yes	GREEN
1.579	109.189	35.8	Yes	No	GREEN
1.603	109.691	35.8	Yes	Yes	GREEN
1.617	14.568	8.4	No	Yes	GREEN
1.677	86.593	6.9	Yes	No	GREEN
1.688	199.331	36.6	No	Yes	GREEN
1.713	19.104	17.5	Yes	No	GREEN
1.747	109.345	35.8	Yes	No	GREEN
1.780	13.003	117.2	No	No	GREEN
1.800	19.850	17.5	Yes	No	GREEN
1.827	77.160	14.8	No	No	GREEN
1.878	86.729	8.3	Yes	No	GREEN
1.896	176.390	17.7	Yes	No	GREEN
1.931	256.335	117.2	No	Yes	GREEN
1.989	111.105	35.8	Yes	No	GREEN
2.092	172.874	41.7	No	Yes	GREEN
2.106	76.886	14.8	Yes	No	GREEN
2.124	136.376	9.2	No	Yes	GREEN
2.148	57.839	8.3	Yes	No	GREEN
2.171	117.790	117.2	No	No	GREEN
2.176	141.546	38.4	Yes	No	GREEN
2.354	13.653	8.4	No	Yes	GREEN
2.434	109.240	5.1	No	Yes	GREEN
2.876	173.227	41.7	No	Yes	GREEN
3.014	77.468	14.8	Yes	No	GREEN
3.062	78.181	14.8	Yes	No	GREEN
3.180	203.450	14.8	No	Yes	GREEN
3.265	143.193	38.4	Yes	No	GREEN

Chapter 8

Development of a Data Base

During the past year, UMR has worked to develop a data base including properties of the mold, metal, and coating required for CAD/CAE model construction and development.

Literature review for material properties

The available literature concerning permanent mold coating materials, including their properties, applications, and methods for use, was reviewed; the results of the review were presented at the AFS Casting Congress in Hamilton, Ontario, in May, 1994 and will be a part of the 1994 AFS Transactions. The purposes of a mold coating were reviewed and the typical coating constituents (fillers, carrier liquids, suspension agents, and binders) were discussed. Procedures for applying coatings to permanent molds were summarized. Typical compositions for coating slurries were obtained and summarized in tabular form. Thermal properties, particularly for individual constituents in the coatings, were also summarized, and some data for the heat transfer coefficient of the gap between the coating and the mold was located. Although data was found for single-component coating materials, virtually no data is available for multi-component coatings, which are more typically used. The entire paper is attached to this report as Appendix I.

Much of the data used to characterize the properties of the mold and metal is available in the data base of ProCAST, the software package used for modeling. However, additional properties have been determined from the literature and have been used to update and modify the ProCAST data base. Thermophysical castability data for aluminum alloy 356 has been collected. Data on thermal conductivity, specific heat, density, high and low temperature strength, elastic properties (including Poisson's ratio and the modulus of elasticity), and fatigue properties has been compiled and is included as Appendix II.

A separate but extensive literature review has summarized the factors influencing thermal fatigue in cast iron permanent molds. Little information concerning thermal fatigue in permanent molds is available in the literature; instead, most prior research has concentrated on applications such as automotive and truck components, including diesel engines and brake parts. Based on the review, Mo and Cr alloyed gray cast iron is generally preferred for resistance to thermal fatigue in applications in the temperature range typically experienced in permanent mold casting, while other irons (such as ductile iron) may be preferable for more extreme thermal conditions, such as for producing ingot molds. This literature review has been written in the form of a paper, which is being considered for presentation at a Permanent Mold Conference in early 1995 and as a portion of the AFS Transactions in 1996. This paper is attached as Appendix III.

Experimental determination of material properties

Because of the dearth of literature pertaining to the thermal properties of mold coatings specifically for permanent molds, an preliminary experimental procedure was developed to estimate the thermal conductivity of both coating materials and mold materials. As will be pointed out in a later section, analysis of the results obtained by this procedure suggest errors and avenues for improving the experimental technique.

In this preliminary method, two 1-inch diameter metal (steel in preliminary tests) bars are simultaneously dipped into a molten aluminum bath held at 1292F (700C), Figure 13. The liquid aluminum acts as a constant heat source for the bar and closely approximates the conditions that would be encountered in a permanent mold casting operation. Normally, one bar is bare steel, while the second bar is coated on the end. Four thermocouples spaced 0.5-inch apart are located at the centerline of each bar. Thermal data is acquired from the thermocouples in both bars for 39 seconds. This provides heating curves for each thermocouple location as a function of time. Figure 14 shows a typical set of heat-up curves. In preliminary tests, two uncoated bars were immersed; the heat-up curves are shown in Figure 15 and indicate that, at least within a single run, the acquired data is quite consistent. Figure 16 shows the heat-up curves for a number of uncoated bars which were immersed in different runs. The repeatability between runs is not as good as that within a run. This might be attributed to somewhat different immersion depths, slightly different bath temperatures, and differences in the rate at which the bars were immersed.

The analysis is centered about the first thermocouple, located 0.5-inch from the surface. The first derivative of temperature with time (dT/dt) is calculated as a function of time at this first thermocouple. For example, if the temperature at this location is 90C at 9.9 seconds after dipping, and 95C at 10.0 seconds after dipping, then the dT/dt at 10.0 seconds is (95-90)/(10.0-9.9) = 50 C/s. Figure 17 shows a typical dT/dt curve as a function of time.

The second derivative of temperature with distance is determined at the 0.5-inch location as a function of time, using the approximation

$$d^2T/dx^2 = (1/6\Delta x^2)(12T_1 - 30T_2 + 24T_3 - 6T_4)$$

where the constants are for four-point one-dimensional heat flow. The Δx is 0.5 inch, the distance between the thermocouples. T_1 is the temperature of the bar at the first thermocouple location at a particular time, while T_2 to T_4 are temperatures at the other three locations at that same time. An example of this is shown in Figure 18. The d^2T/dx^2 is calculated as a function of time, and Figure 19 shows a typical result. The thermal diffusivity α of the system is then calculated from

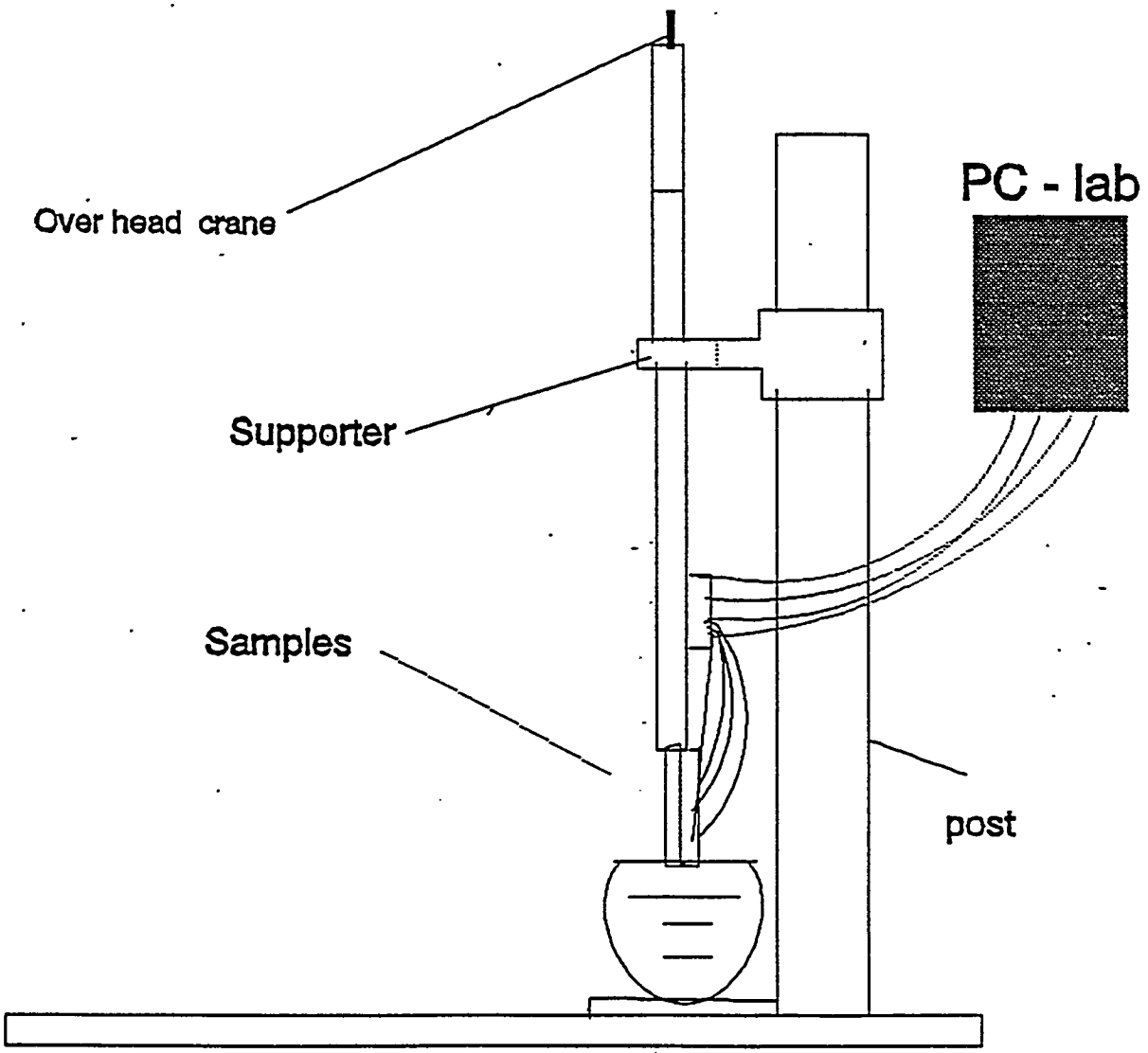

Figure 13: Experimental set-up for measuring the thermal conductivity of the mold and coating materials.

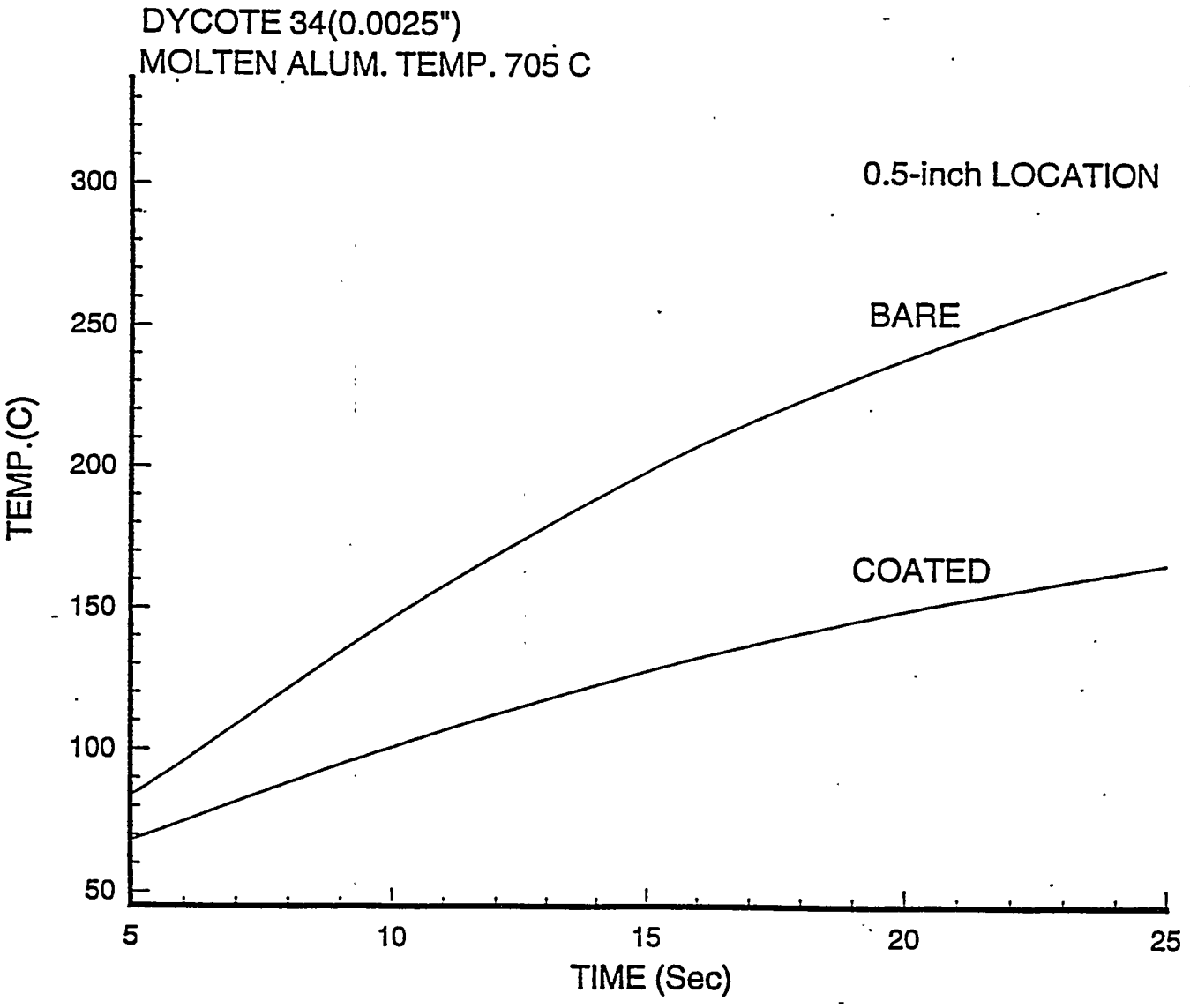

Figure 14: Example of heat-up curves in coated and uncoated bars from the same run. Curves are for the 0.5-inch location and for a 0.0025-in. Dycote 34 coating. The effect of even a thin insulating coating on the temperature distribution in the bar is evident.

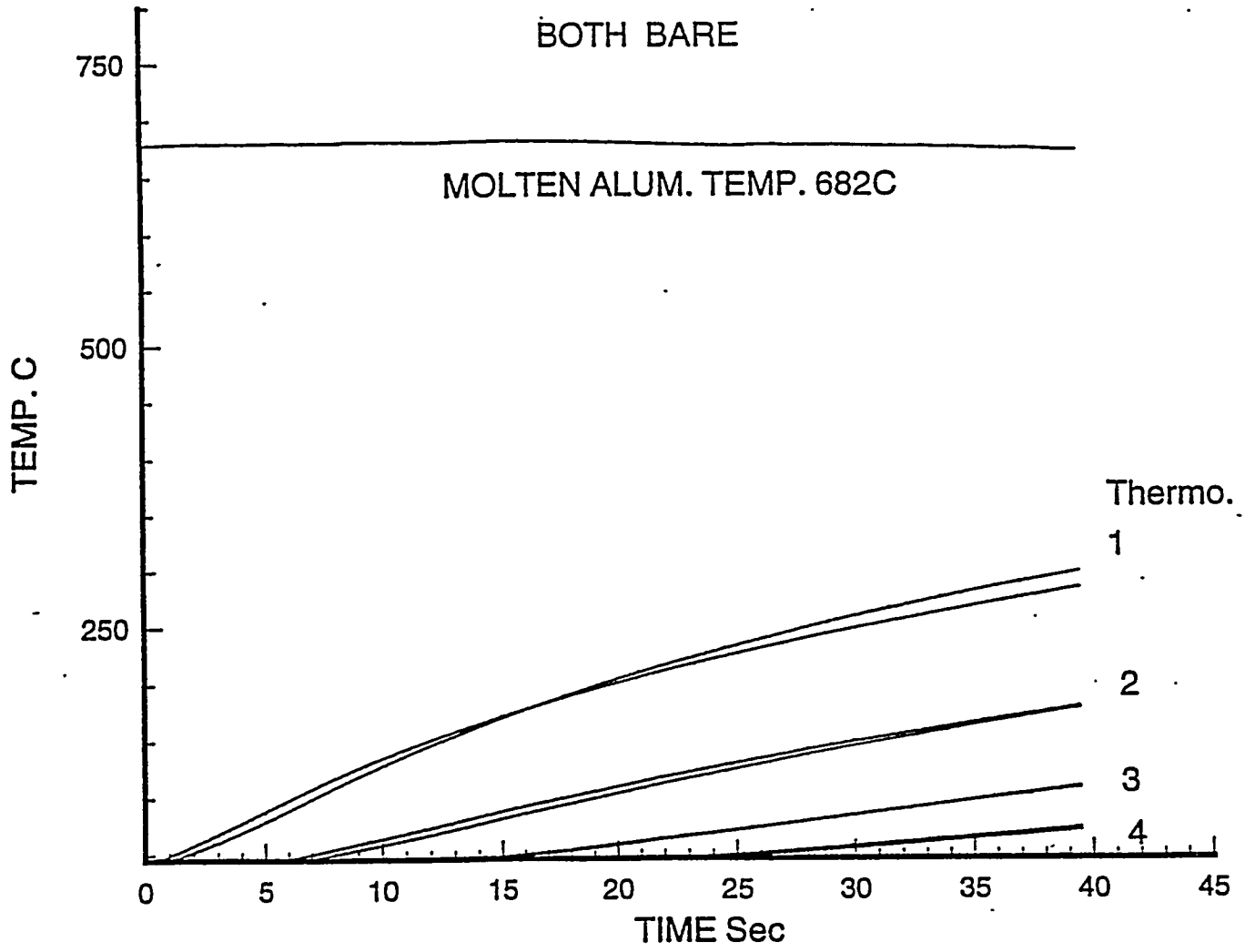

Figure 15: The heat-up curves for two uncoated bars from the same run nearly match. The reproducibility of acquiring data in the experimental system is considered to be reasonably good.

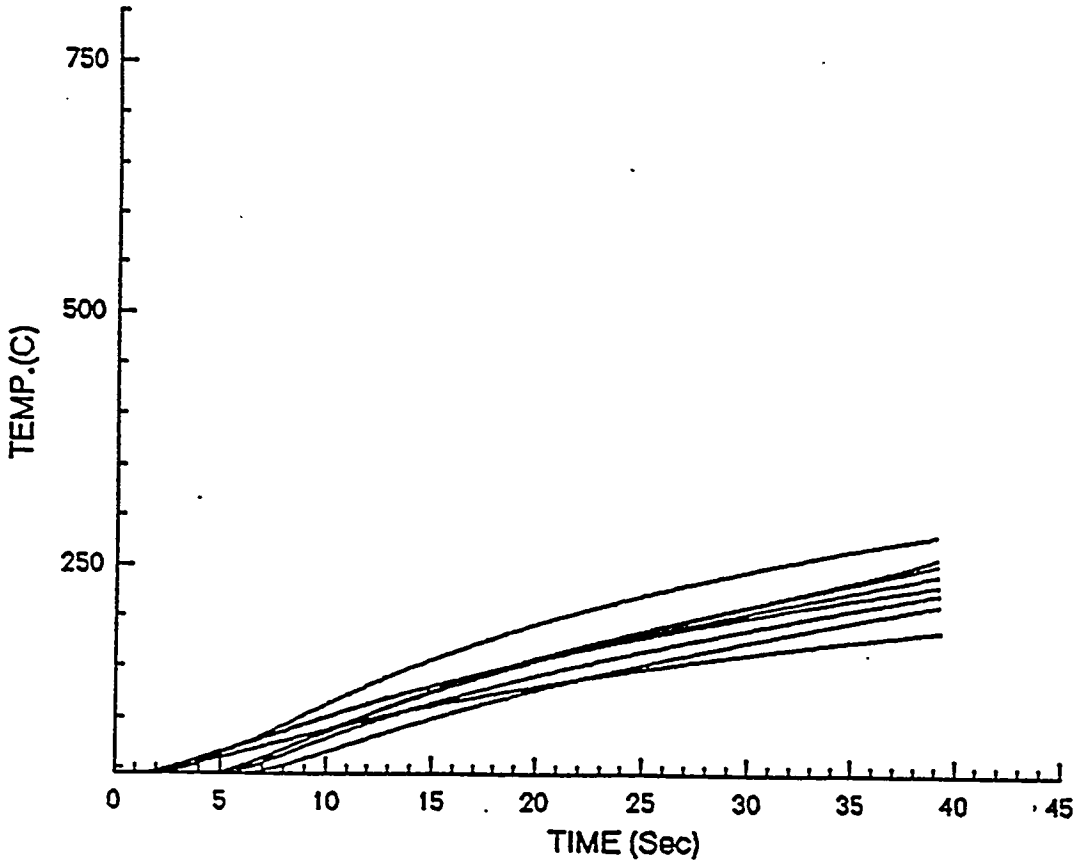

Figure 16: The heat-up curves for a number of uncoated bars from different runs generally fall within a narrow range; however the reproducibility from run to run is not as good as that within a single run.

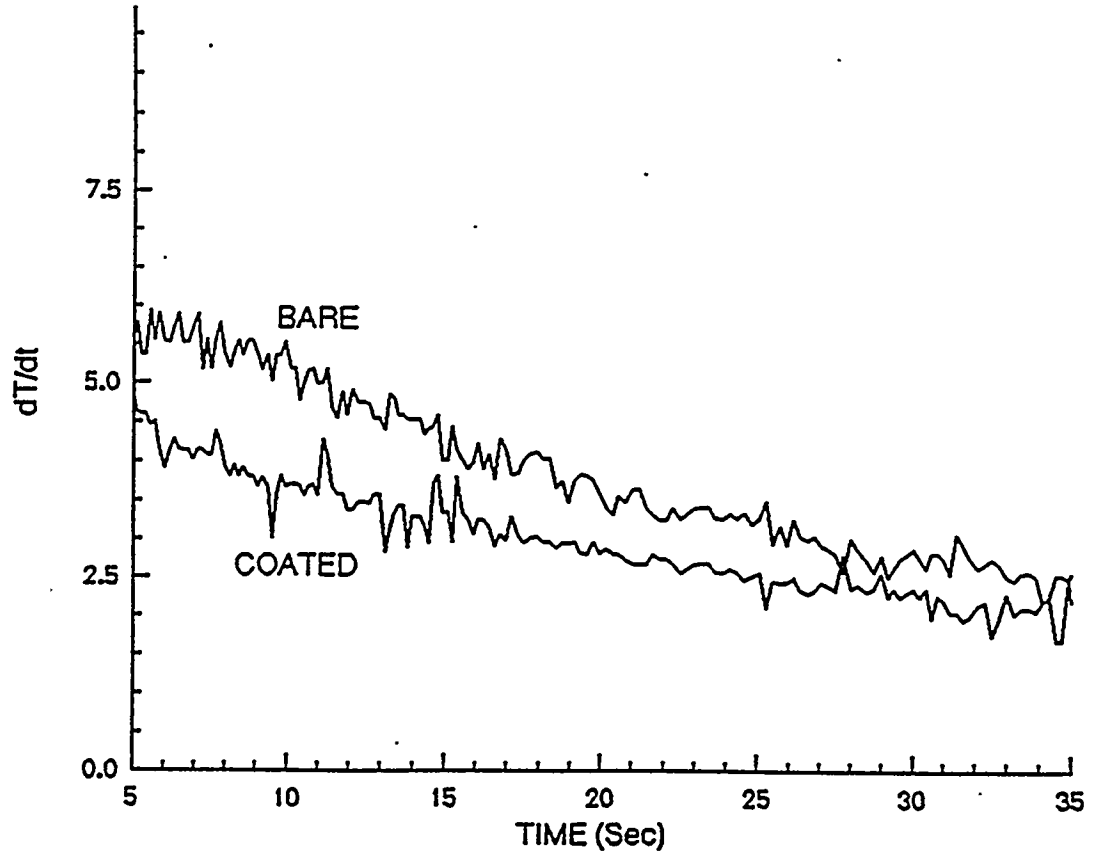

Figure 17: The first derivative dT/dt as a function of time after immersion of the bar for uncoated and coated bars. This data is used in calculation of the thermal conductivity of the steel and the steel/coating system.

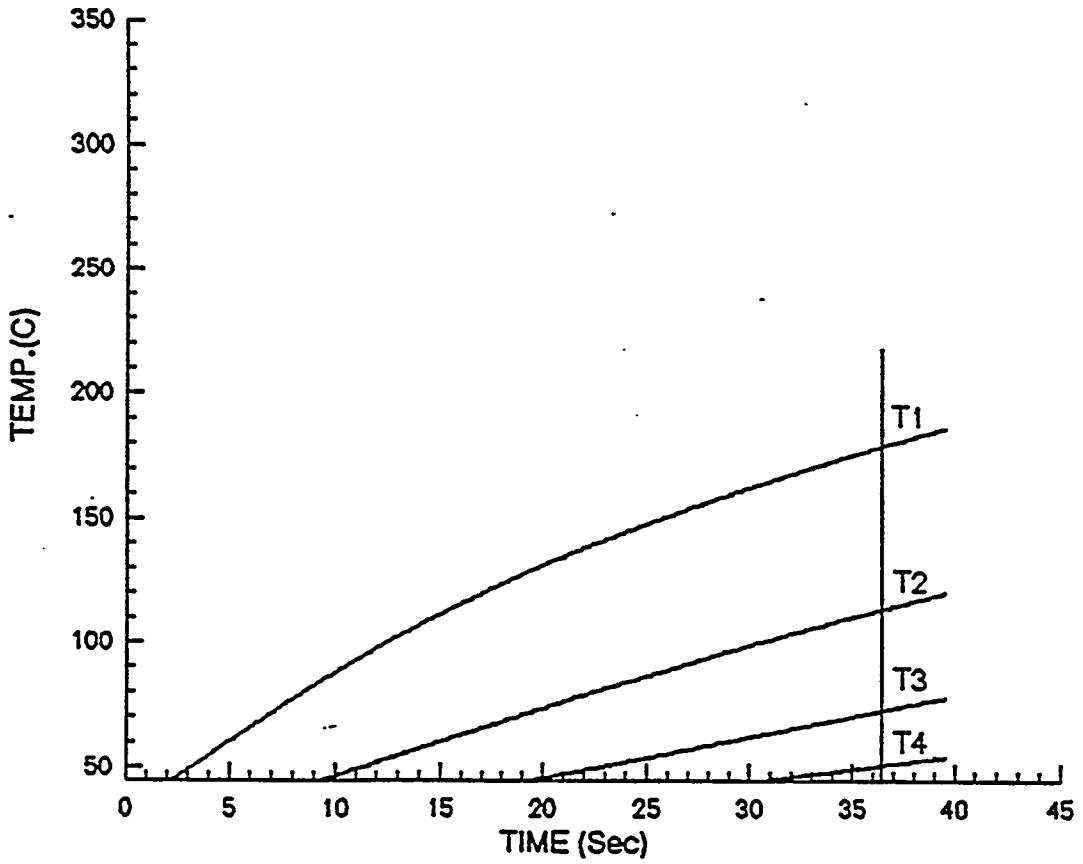

Figure 18: The temperatures of the bar at four locations for a particular time are determined from the acquired data and are then used to calculate the second derivative d^2T/dx^2.

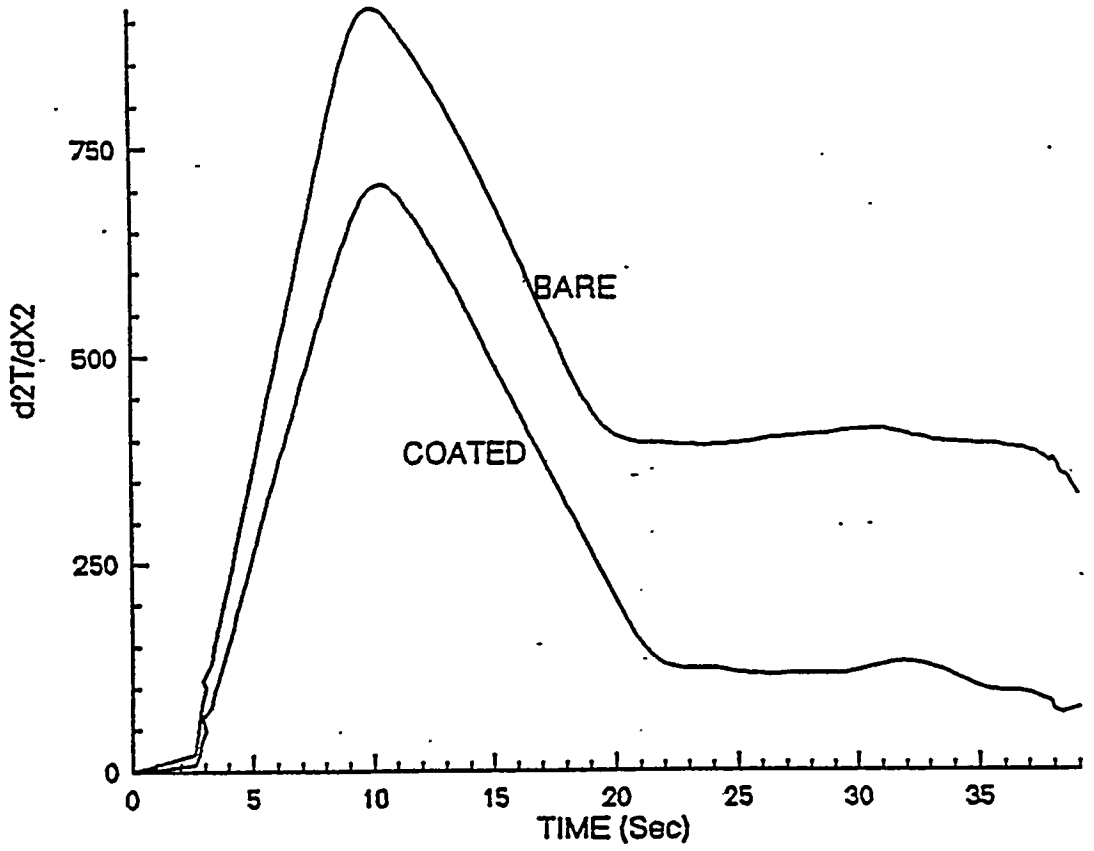

Figure 19: The second derivative d^2T/dx^2 is calculated as a function of time. These values, coupled with those for the first derivative dT/dt, are used to find the thermal diffusivity.

$$dT/dt = (\alpha) d^2T/dx^2$$

The thermal diffusivity is calculated as a function of time; Figure 20 shows a typical example.

For uncoated samples, the thermal conductivity can be determined from the thermal diffusivity by

$$K = \rho c \alpha$$

where ρ and c are the density and specific heat of the steel. The thermal conductivity of the steel bar can be calculated as a function of time (Figure 21) and, since the temperature of the steel is known as a function of time, the thermal conductivity of the steel is known as a function of temperature. Figure 22 compares the measured thermal conductivity of the steel bar with handbook values. Differences between the two may be attributed to use of a constant density and specific heat in calculating the thermal conductivity; of course density and specific heat are also dependent on temperature.

For coated samples, the thermal diffusivity of the coating/steel system was obtained from the differential equation. In the data presented here, a thermal conductivity for the system was then calculated using only the density and specific heat of the steel:

$$K_{system} = \rho_{steel} c_{steel} \alpha_{system}$$

The thermal conductivity of the coating was then calculated.

$$\frac{1.27 \text{ cm} + x_{coating}}{K_{system}} = \frac{1.27}{K_{steel}} + \frac{x_{coating}}{K_{coating}}$$

The thermal conductivity of the steel and the system are obtained from the experimental data so that the coating conductivity can be estimated for each coating thickness $x_{coating}$. In this experimental procedure, the temperature of the coating is assumed to be that of the molten aluminum with which it is in contact. Results from the theoretical model indicate that the coating temperature is within 40C of the molten metal, so this is a reasonable assumption. The coating conductivity can then be plotted as a function of time, Figure 23. There are transients in the calculation of the coating conductivity, but normally a constant value for the conductivity is present between the start of heating of the bar and later times when radiation might become excessive.

Table 10 shows the calculated values for the coating conductivity of Dycote 34. Dycote 34 is an insulating coating containing roughly 50% SiO_2, 25% Al_2O_3, 12.5% MgO, and 12.5% alkali oxides. By picking the best of the data and most reliable of the test runs, the thermal conductivity of the Dycote 34 coating is

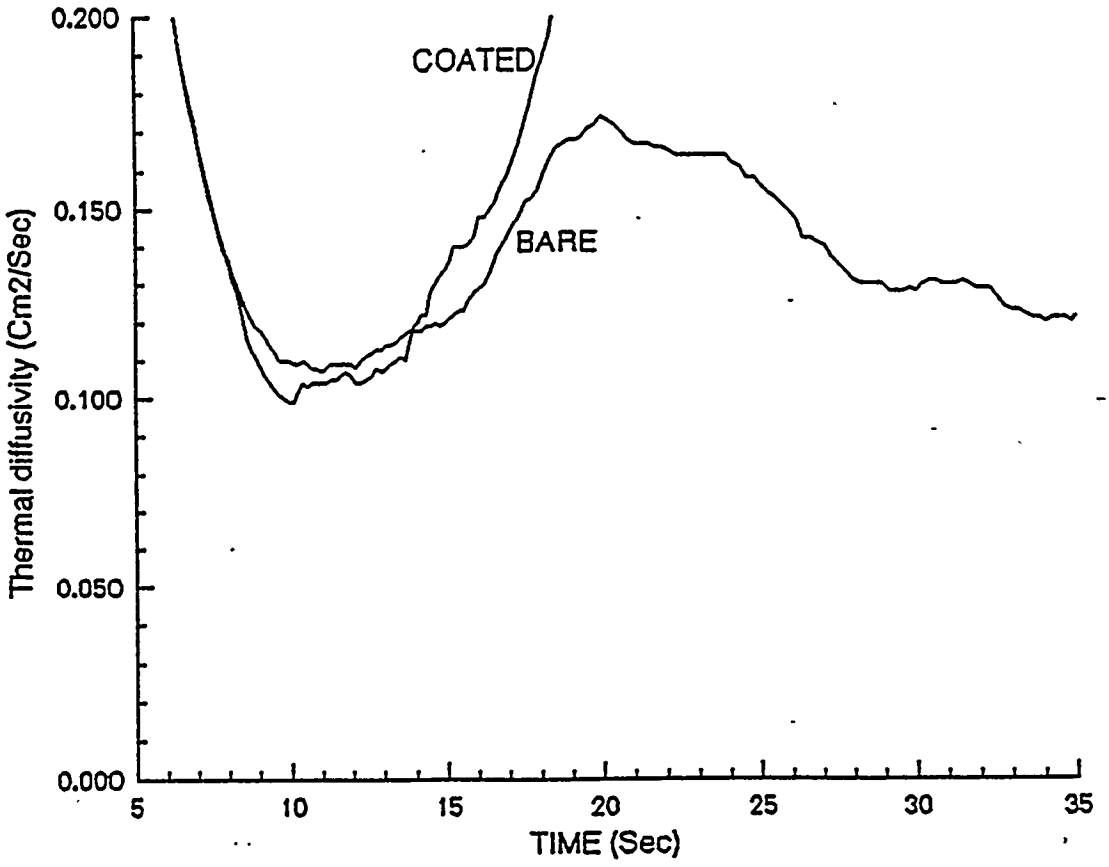

Figure 20: The thermal diffusivity calculated from the first and second derivatives as a function of time.

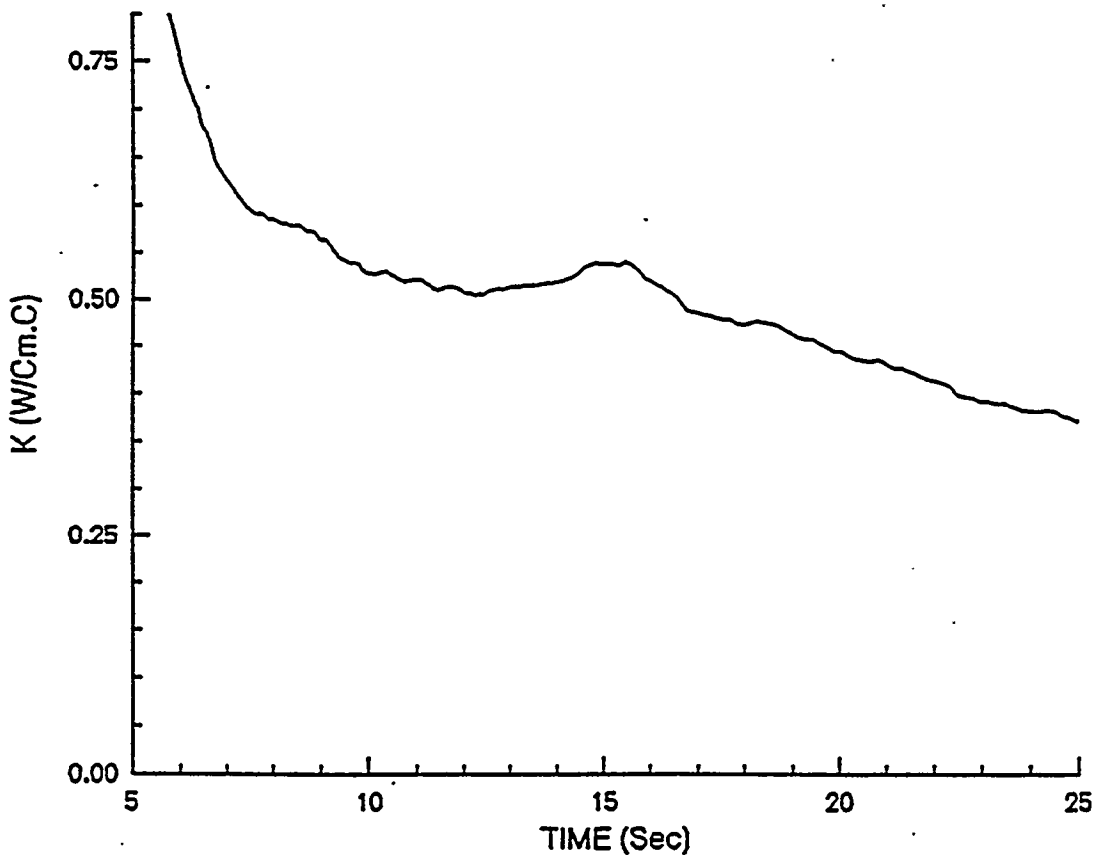

Figure 21: The thermal conductivity of the uncoated steel bar as a function of time; the conductivity is calculated from the thermal diffusivity.

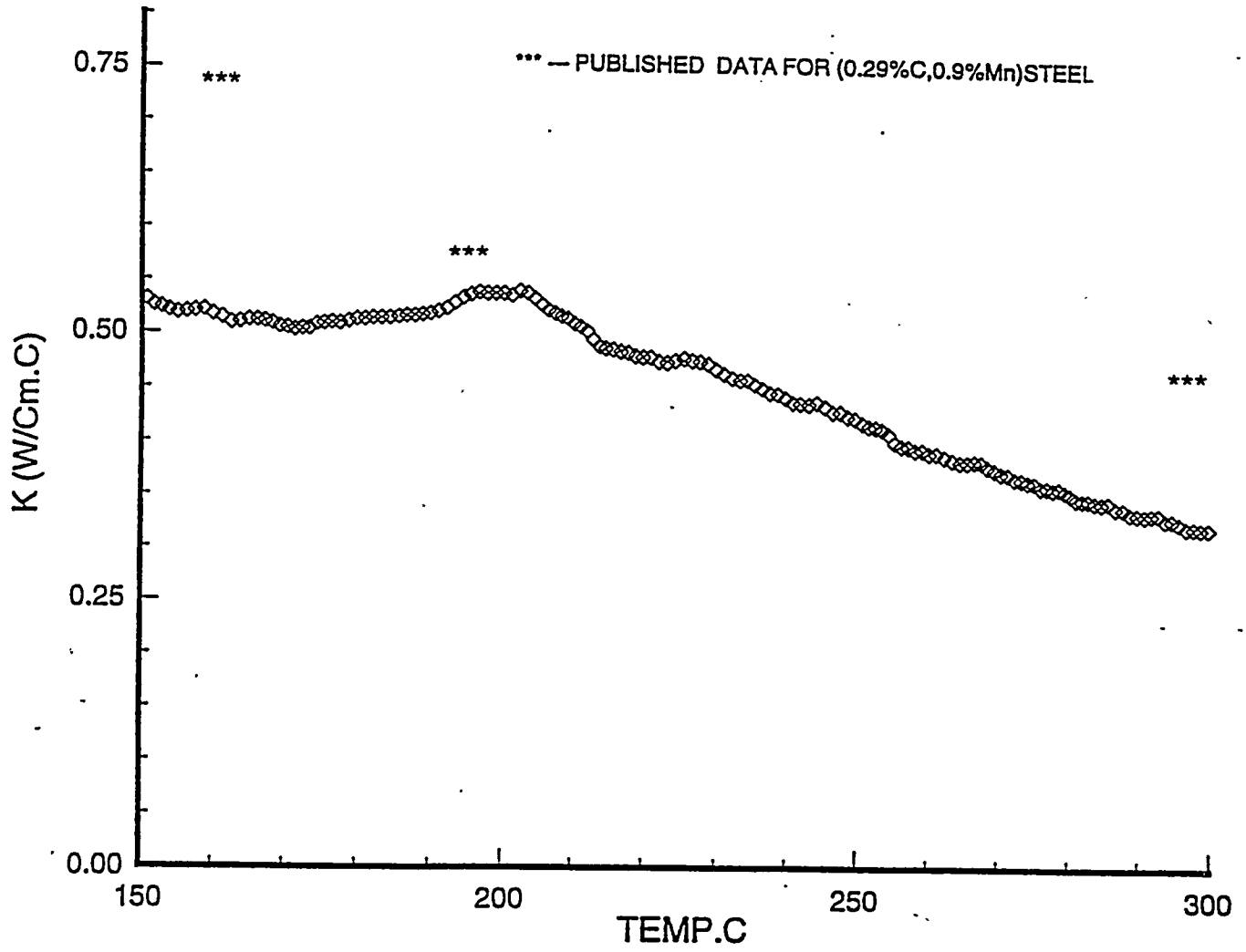

Figure 22: The thermal conductivity of the uncoated steel bar as a function of temperature. The thermal conductivity at a particular time was obtained from curves such as Figure 8 and the temperature of the bar at that same time was obtained from curves such as Figure 1 and 2. The handbook values for thermal conductivity of steel are included for comparison; experimental results are lower than accepted values for a similar steel.

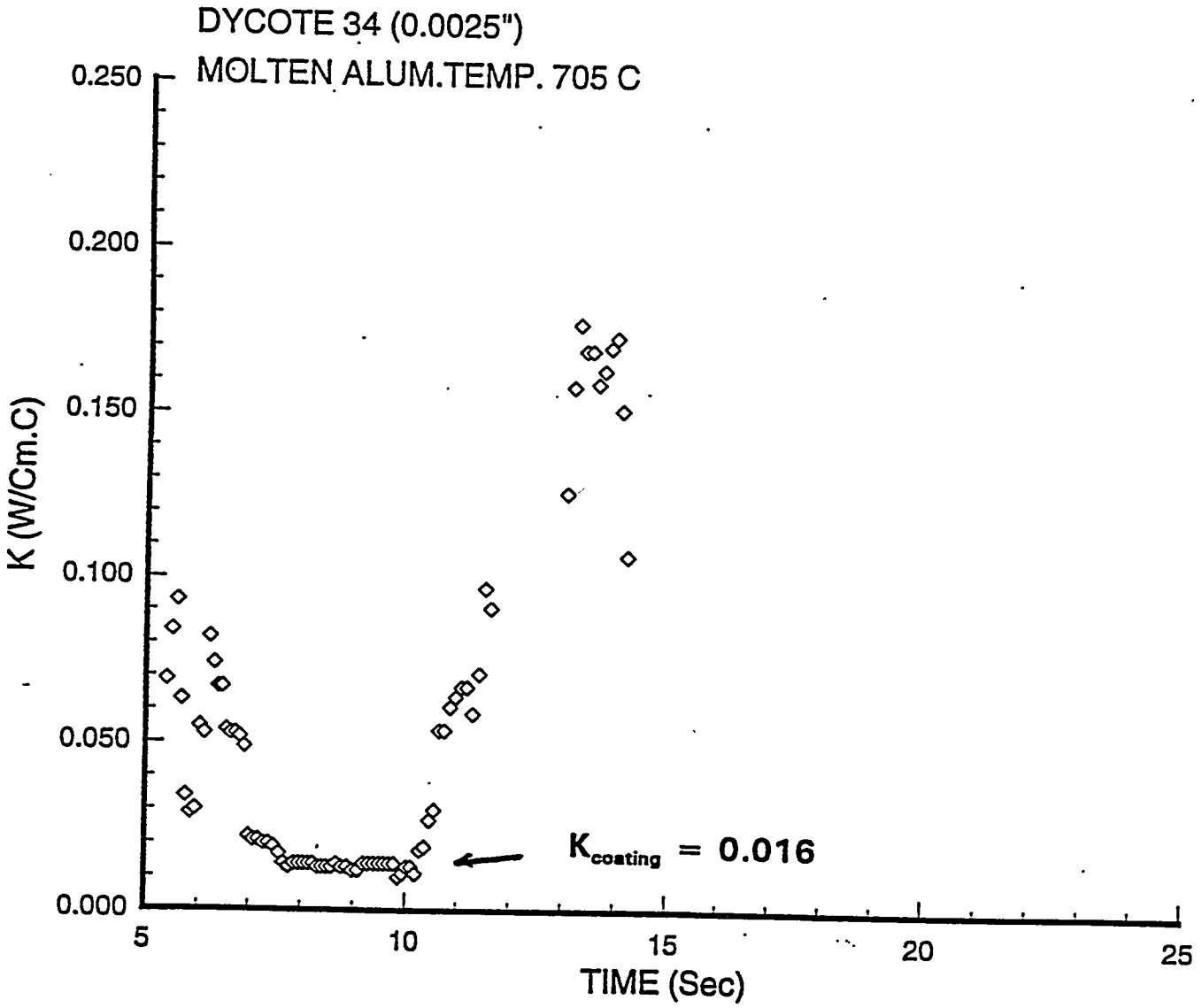

Figure 23: The thermal conductivity of a 0.0025-in. thick Dycote 34 coating at 700C. The calculated values appear to be erroneous when the bar first begins to heat, and later when more problems with radiation losses may occur. The thermal conductivity was taken to be the "steady-state" value shown in the figure.

estimated to be about 0.027 W/cm C or 2.7 W/m C.

Table 10: Calculated values for the thermal conductivity of the Dycote 34 coating at about 1292F (700C).

Coating Thickness (inch)	Thermal Conductivity (W/cm C)
0.0025	0.014, 0.016, 0.020
0.0035	0.024, 0.034, 0.037
0.0060	0.032, 0.041
0.0100	0.020, 0.028

The insulating coating does have a significant effect on the rate of heat transfer into the steel bars. One way of illustrating this is to plot the temperature difference at 0.5-inch from the surface between the coated and uncoated specimens in a particular run. Figure 24 shows this at 25 seconds as a function of coating thickness. The temperature difference varies from less than 20C to as high as 100C and, since these values are obtained within a run (where reproducibility is reasonably good), the values are expected to be reasonable as well. The temperature difference is quite large for the thinnest coating, small for intermediate thicknesses, and large again for the thicker coating. Differences in coating thickness were obtained by the number of layers of coating applied; this was done by heating the bar to at least 400F, this briefly immersing the steel bar in a small sample of the coating. For thicker coatings, the process was repeated.

0.0025 inch	1 coating layer
0.0035 inch	2 coating layers
0.0060 inch	4 coating layers
0.0100 inch	6 coating layers

The thickness of the coating was estimated by coating a thin steel strip at the same time as the steel bars, then measuring the change in thickness of the strip with a micrometer.

The higher temperature differences in Figure 24 point out the good insulation effect of the coating; the thinnest and thickest coatings appear to be better insulators. If we ignore the thinnest coating, the insulation effect increases with increasing coating thickness, as we would expect. The abnormally high insulation effect of the thinnest 0.0025-inch coating might be due to problems inherent in the experimental technique, or might be related to microstructure of the coating. For example, the first layer might contain a high percentage of porosity, which would improve insulation; the second coat might help to fill in the porosity, producing a denser and more conductive layer. Subsequent coats build up the coating thickness and provide better insulation.

Tests have been performed using a graphite coating (Dycote 11)

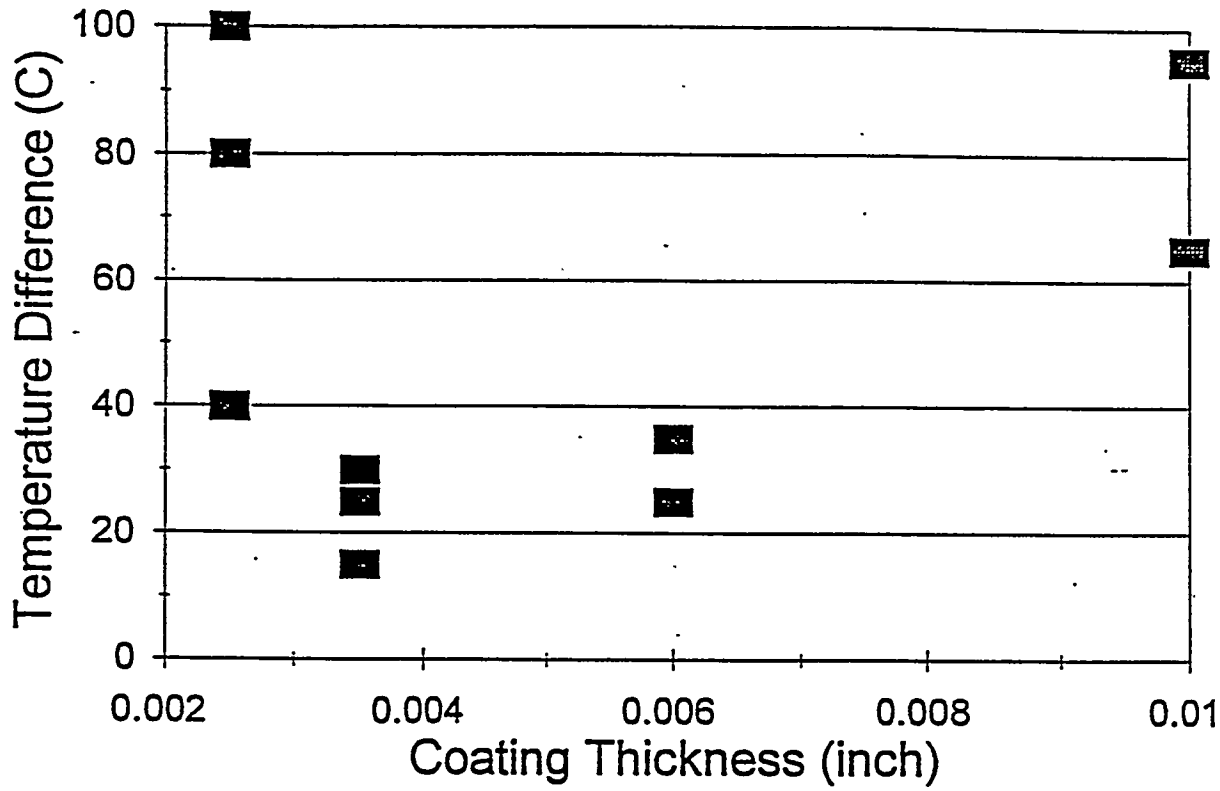

Figure 24: The effect of the Dycote 34 coating on the temperature difference at the 0.5-in. location between the coated and uncoated bars 25 seconds after immersion. Except for the thinnest coating, the thicker coatings provide a greater insulation effect.

of various thicknesses. Up to this point, the data has been difficult to analyze. Work is continuing in an effort to obtain appropriate data and to estimate a reasonable, working value for the conductivity of the graphite coatings. Even though the graphite is expected to have a high thermal conductivity, at least compared to that of the insulating coating, there is a significant effect on the rate of heating of the steel bar, Figure 25. This effect is not as great as that of the insulating coating, as we would expect.

Evaluation and suggested changes of the experimental procedure

Several deficiencies in the experimental method for obtaining the effective thermal conductivity of the coating were noted when the results were analyzed and compared to predictions based on simulation packages such as ProCAST.

The approximation for d^2T/dx^2 may not be accurate until the bar has heated at the location of the fourth thermocouple. This was partly compensated for by selecting as the thermal conductivity the value calculated near the end of the test, when the heat front did reach the fourth thermocouple. However, a second experimental approach, using ProCAST for analysis, will be used in the future.

ProCAST simulations suggest that there is an end effect that may affect the calculation of the coating's thermal conductivity. Other problems might include inadequate stirring of the molten aluminum bath, film and contact coefficients, gases and or solvents in the coating, and radiation effects from the bar. An alternate procedure will be designed in which two thermocouples will be mounted in a thick layer of the coating material to permit the temperature gradient in the coating to be measured. The steel rod will be insulated to eliminate any end loss effect and produce one-dimensional heat loss along the length of the specimen. The temperature gradient through this insulation will also be determined to verify that heat loss in the radial direction is negligible. The thermal conductivity of the coating will be determined from

$$m_c c_{pc} \Delta T/\Delta t = - k \Delta T/\Delta x$$

where

m_c = mass of the coating material
c_{pc} = specific heat of the coating material
$\Delta T/\Delta t$ = slope of the temperature versus time curve at the midpoint of the coating material
$\Delta T/\Delta x$ = temperature gradient in the coating material

The specific heat of the coating material will be determined by quenching a heated sample in water in an insulated container and measuring the equilibrium temperature reached in the water. The specific heat will then be calculated from

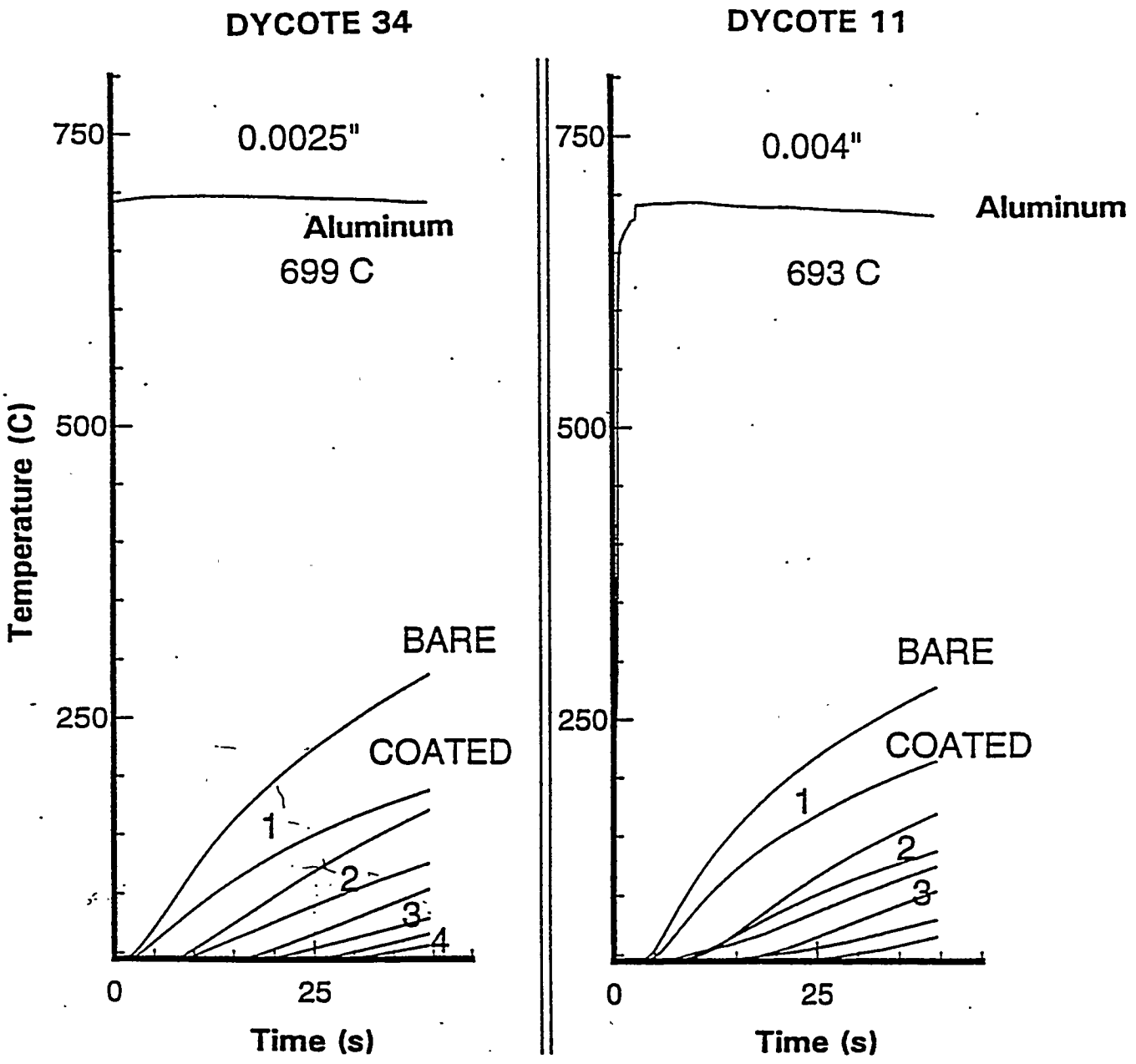

Figure 25: A comparison of the effects of the insulating and graphite coatings. Even though the graphite coating is thicker, it has less effect on the temperature in the bar.

$$m_c c_{pc}(T_{ic} - T_e) = m_{H2O} c_{pH2O}(T_e - T_{iH2O})$$

This will be done for several coating weights and temperatures to confirm the specific heat.

Using this experimental approach, difficulties with stirring of the aluminum bath, the film coefficient on the outside of the coating, and the contact coefficient between the coating and the steel should be eliminated. Any end effect will be minimized and radiation losses between the insulating sleeve and air should be minimized. The coating may also be baked to drive off any volatile materials prior to the actual test.

Finally, coating thicknesses will be measured directly from the specimen using verier calipers or a jig with a dial indicator.

Chapter 9

Construct Model

The heat transfer and thermal cycling within the mold were constructed using ProCAST, a sophisticated software package for modeling industrial casting processes. The capabilities of ProCAST include:

1. Efficient solution of the transient non-linear heat conduction equations in three dimensions by the finite element method
2. Efficient solution to the continuity and momentum equations, resulting in accurate modeling of transient mold filling
3. Turbulent flow modeling
4. Trapped gas modeling
5. Solidification modeling
6. Modeling of thermal cycling within a permanent mold
7. Modeling of cyclic thermal stresses and strains within a permanent mold

For this effort, only items 1, 5 and 6 were needed. Later, item 7 will be investigated.

The basic equation for the three dimensional transient heat conduction, with effect of latent heat, is given by:

$$\rho \, \partial H/\partial T \, \partial T/\partial t - \nabla \, (k \, \nabla T) - q(x) = 0$$

where:

$\nabla = \partial/\partial x + \partial/\partial y + \partial/\partial z$
ρ = density, constant or dependent on temperature
k = thermal conductivity, constant or dependent on temperature
T = temperature
H = enthalpy, dependent on temperature and includes the effect of latent heat of fusion
t = time.

The enthalpy function is given as:

$$H(T) = \int c_p \, dT + L[1-f_s(T)]$$

where c_p is the specific heat, L is the latent heat, and f_s is the fraction of liquid metal solidified.

Using both equations and appropriate boundary conditions, ProCAST will determine the following:

1. Temperature profiles as a function of time within the casting (including solidification analysis)

2. Temperature profiles as a function of time within the mold coating

3. Temperature profiles as a function of time within the mold geometry, including the inserts

Mold cycling is modeled by placing a heat flux boundary condition on the coincident node interface between the casting and the coating. When the metal begins to cool, a built-in time switch automatically sets itself to state 1, turning on the interface heat transfer or the boundary heat transfer. From this period to ejection time, the heat transfer proceeds from the metal to the mold. The time switch sets itself to state 0, at ejection time. From this time to the beginning of the next cycle, the interface heat transfer or the boundary heat transfer is turned on to conditions which represent the heat transfer between the coating and the air. Toggling between values 1 and 0 proceeds for the number of pouring cycles specified by the user. Depending on the cycle time, the user can adjust the time switch accordingly. The next section discusses construction of the geometric model and other modeling details in ProCAST.

Construction of Geometric Model ProCAST requires a geometric model as input information. In collaboration with the industrial monitoring committee, a test mold was designed and constructed for geometric modeling, heat transfer analysis, and model validation. The mold is designed to accept inserts with built-in stress raisers, typical of designs encountered in commercial molds, that will accelerate the crack initiation. Two sets of four types of inserts have been produced. Figure 26 shows the geometric models of sections through the male and female portions of the test mold, and Figure 27 shows a section through the entire mold. Figure 28 shows each of the mold inserts. Figure 29 shows the mold with insert and pouring cup. Note that the geometric model of a blank insert is used in the current model. Later, the models for the inserts including the stress raisers will be introduced to ProCAST.

Using IDEAS, a CAD software package, the geometric model of the test mold was designed. The model included the geometry of the insert and the coating. A graphite coating was initially selected. Later, an insulating coating material will be modeled. The casting thickness was about one inch. An initial coating thickness of 0.01 inch was chosen. Later, this thickness will be varied to match that used in the test. The finite element mesh was then constructed and the meshed geometry downloaded to ProCAST.

FEMALE MOLD

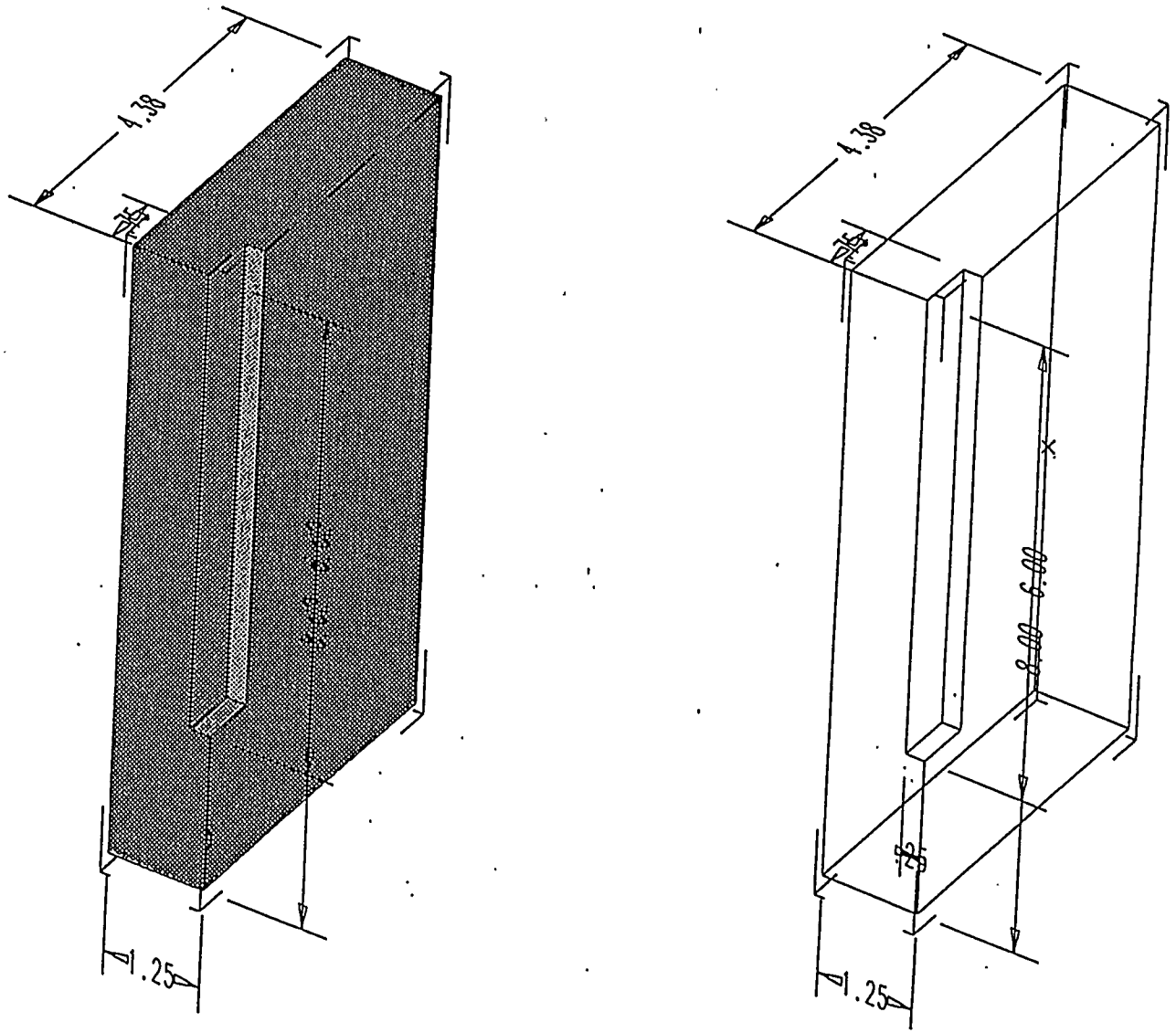

Figure 26 (a): Geometric model of the female portion of the permanent mold. Only half of the mold portion is shown.

MALE MOLD

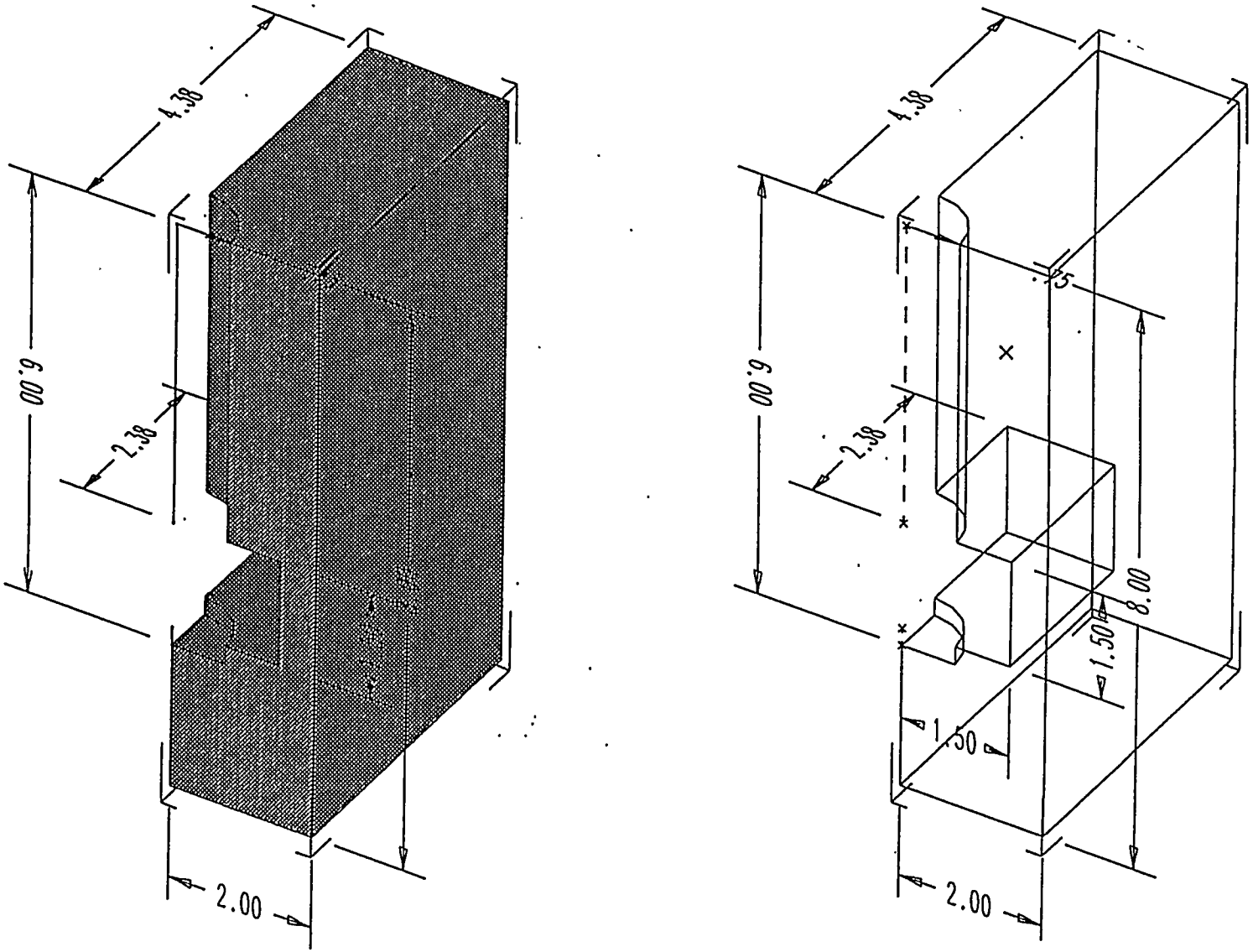

Figure 26 (b): Geometric model of the male portion of the permanent mold. Only half of the mold portion is shown.

FEMALE AND MALE MOLDS PLUS INSERT

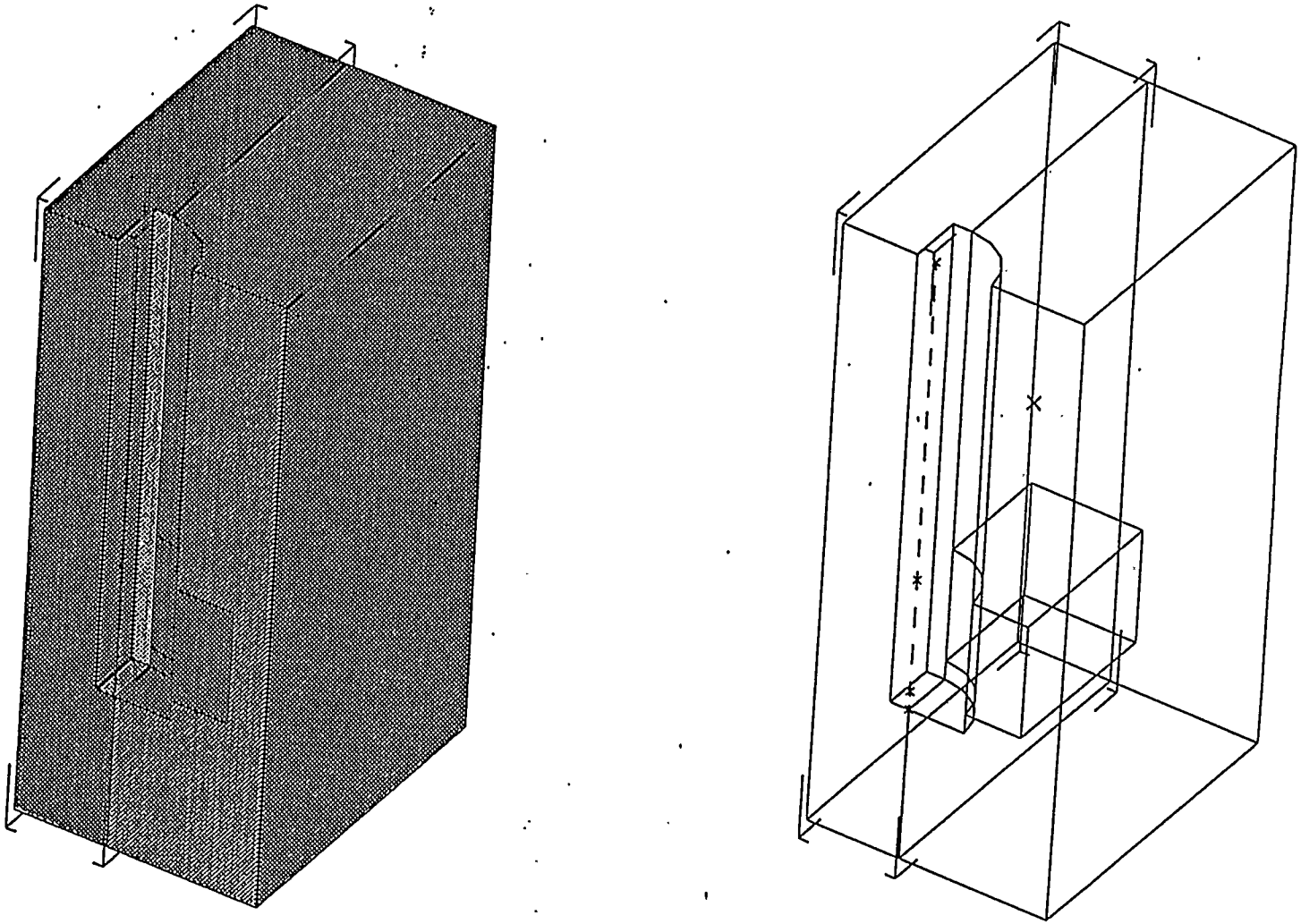

Figure 27: Geometric model of the permanent mold with the mold insert in place. Only half of the mold portions are shown.

INSERTS #1 AND #2

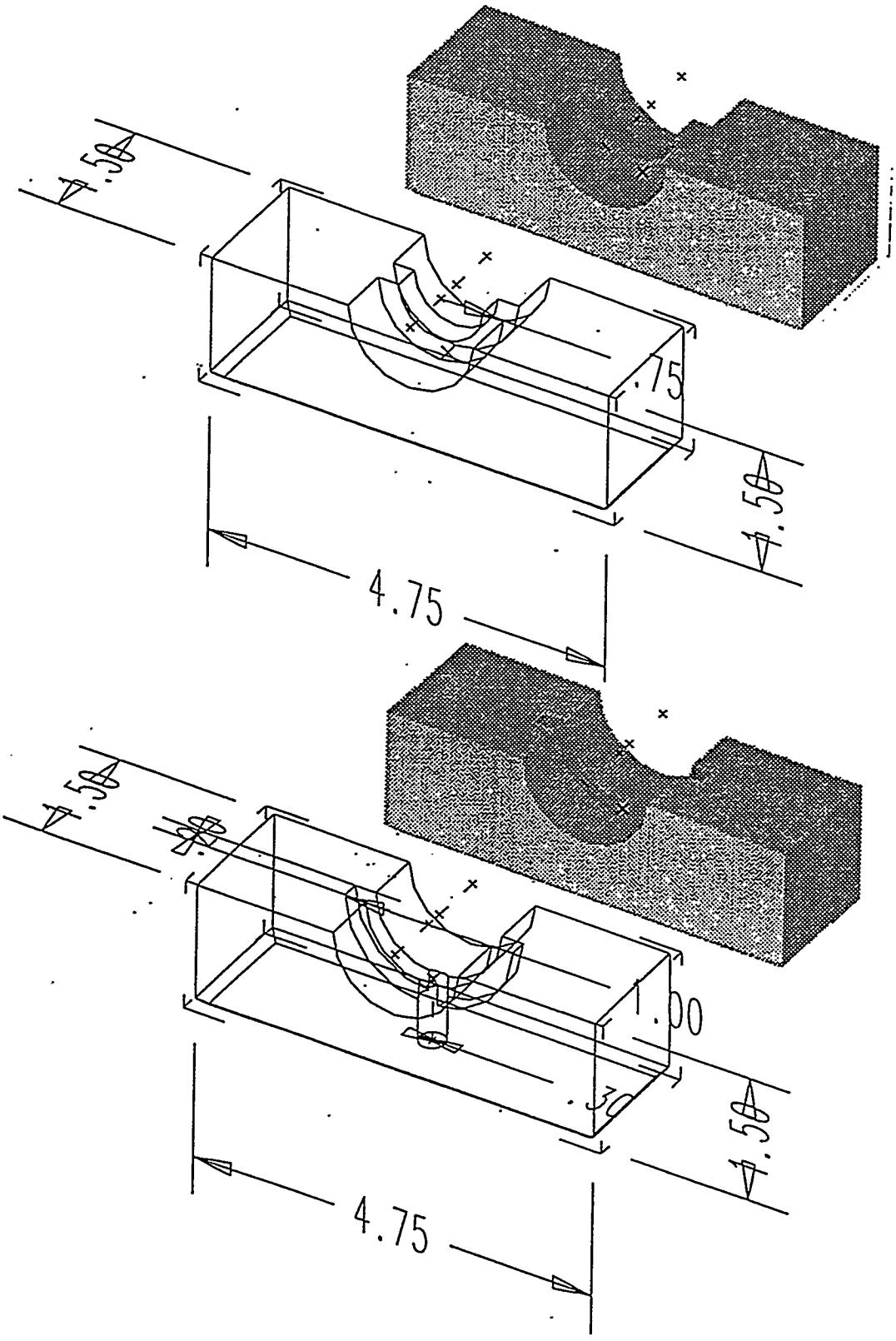

Figure 28: Geometric models of the mold inserts.

INSERT #3 INSERT#4

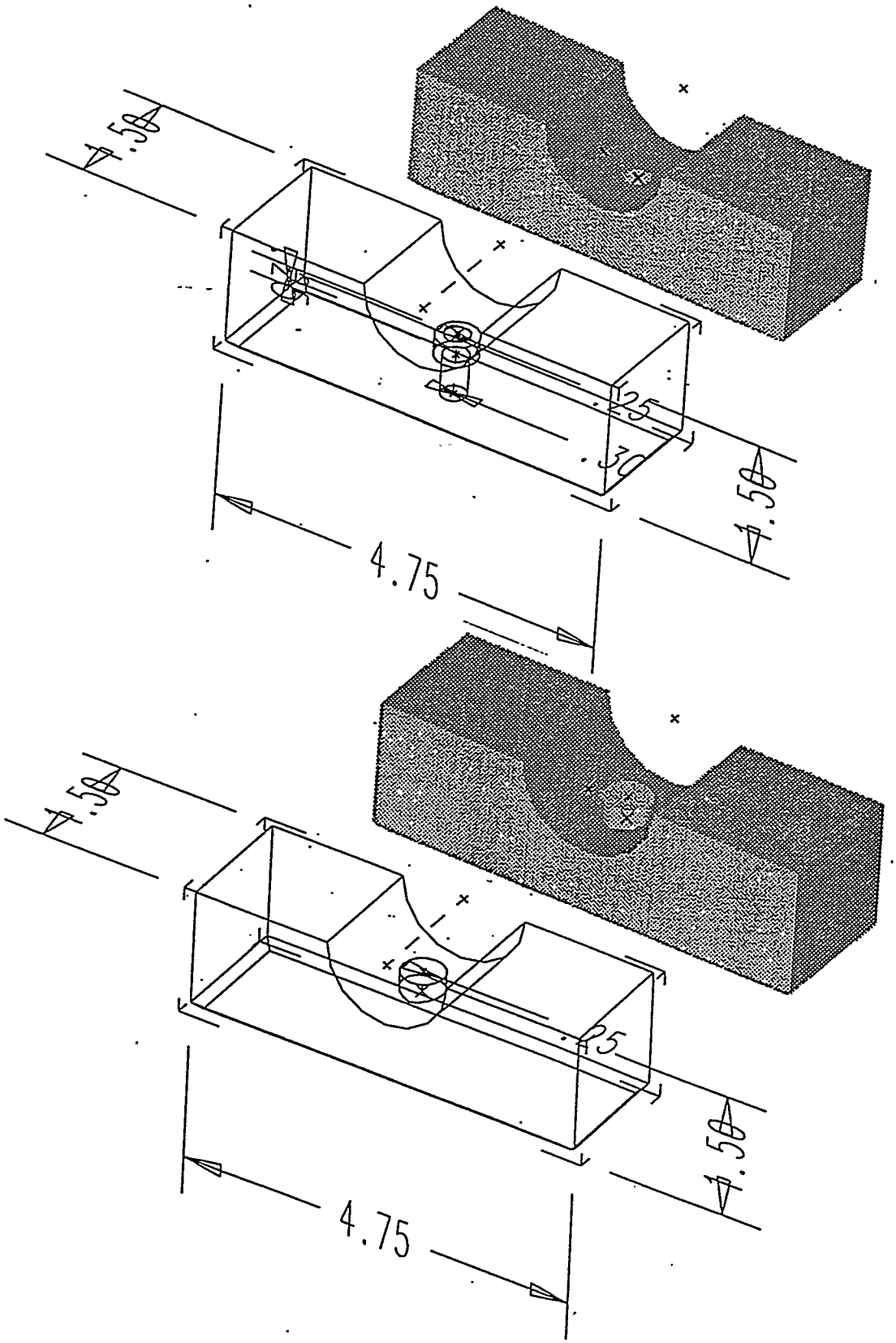

Figure 28: Geometric models of the mold inserts. (continued)

WHOLE MOLD PLUS POURING CUP

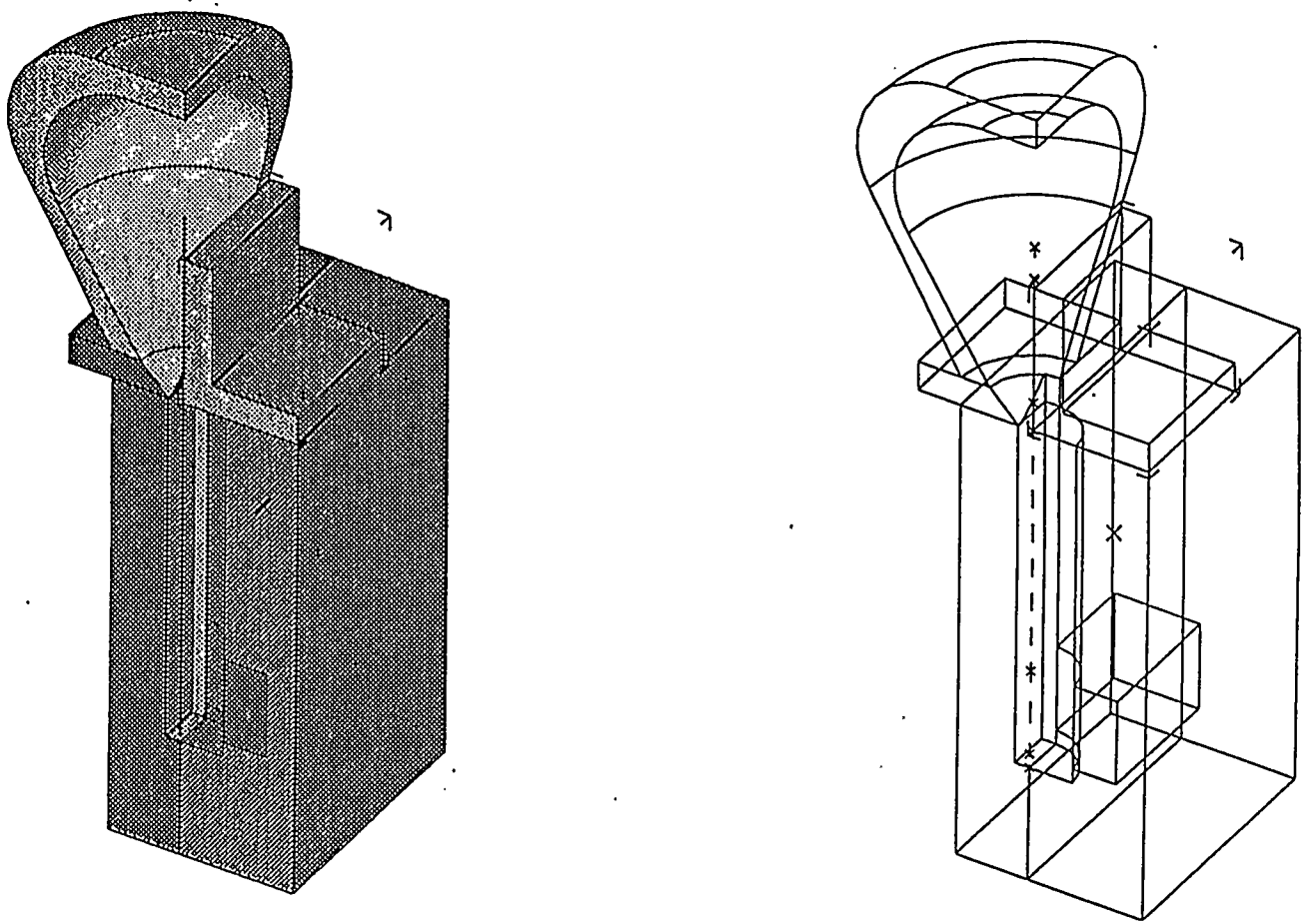

Figure 29: Geometric model of the mold, insert, and pouring cup. Only half of the mold and insert portions are shown.

Modeling Details in ProCAST

ProCAST requires five software packages for analysis. They are:

1. Mesh or geometric model
2. PreCAST
3. DataCAST
4. ProCAST
5. PostCAST

Except for the MESH, the others are all modules within ProCAST.

The Mesh represents the geometric model created by any of the 3D CAD packages such as IDEAS, PATRAN, ANVIL, ProEngineer, and so on. Because ProCAST accepts a finite element mesh created by brick, tetrahedral or wedge elements, the CAD package must also use these elements for constructing the mesh. Figure 30a shows the mesh used for the overall mold; the detailed mesh for the insert, which cannot be seen in Figure 30a, is shown separately in Figure 30b.

The PreCAST uses interactive menus to add more specific detailed information to the finite element model obtained from the MESH. With PreCAST, the user can

1. Specify node interface between the casting and the coating, the coating and the insert, and the insert and the mold
2. Assign interface heat transfer coefficient data
3. Specify material properties

The model must be completely defined in PreCAST before it is transferred to DataCAST.

The DataCAST reviews the model, checks for any errors and converts all units to the metric system. Also, it prepares the summary file of the complete model for documentation.

The ProCAST module performs the simulation analysis. It solves all the appropriate energy, momentum and mass balance equations. From these equations, the temperature profiles within the casting, the coating, the insert and the mold can be easily obtained. The thermal stresses and strains can also be obtained. Note that complete analysis from filling to ejection can be obtained. A hard copy of the simulation results can be obtained directly from this module. The results can also be obtained in postprocessing files. These files can be generated by PostCAST.

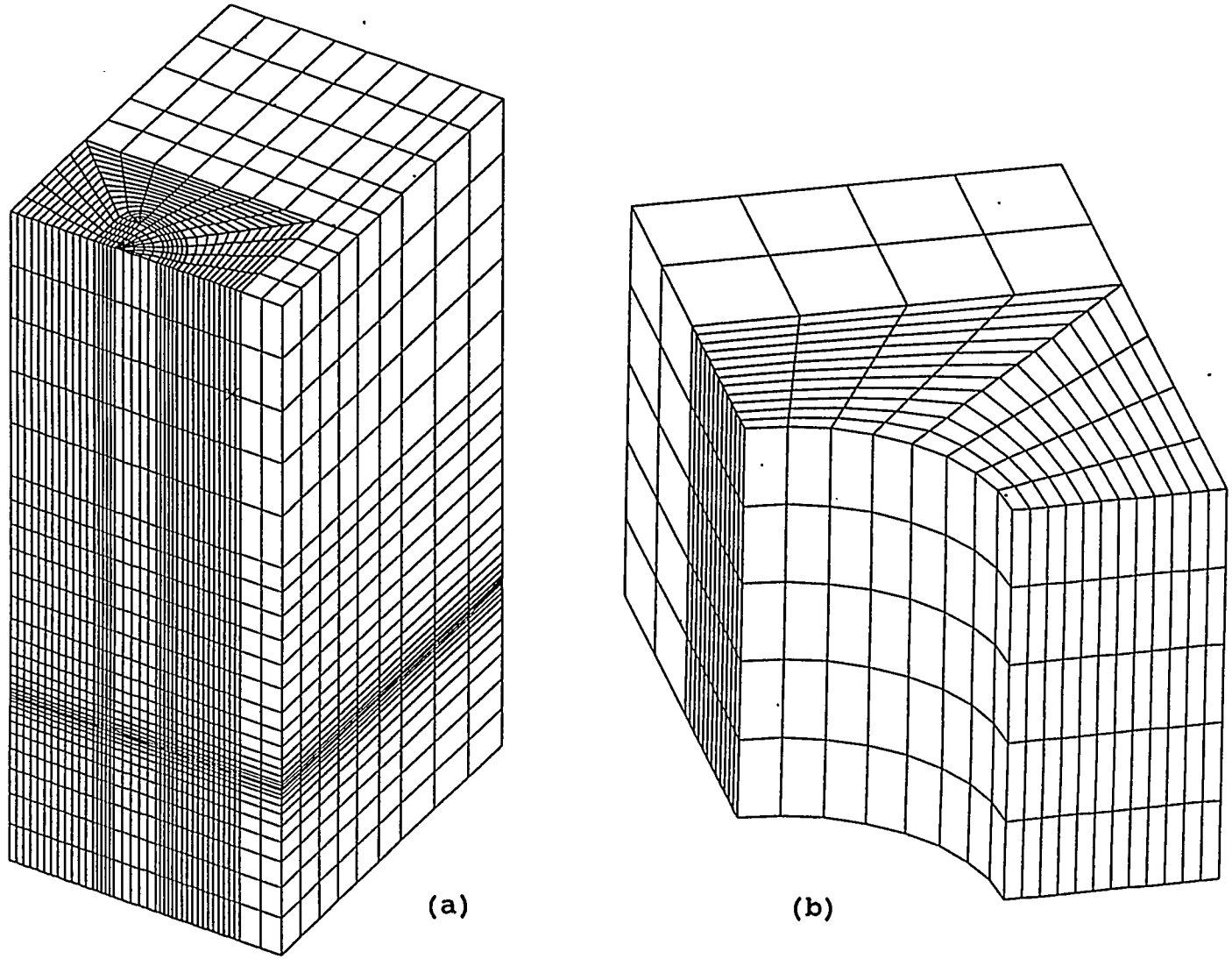

Figure 30: The mesh used in ProCAST modeling. (a) The mesh for the overall mold and (b) the mesh for the "blank" insert with no stress raisers. The details of the insert mesh cannot be seen in the mesh for the overall mold. Only half of the mold and insert are shown.

Examples of information provided by PostCAST are:

1. Temperature results at each time step
2. Pressure results at each time step
3. Velocity results at each time step
4. Turbulence quantities at each time step
5. Thermal stress and strain results at each time step
6. Temperature versus time results for various nodes
7. Solidification rate, cooling rate, and temperature gradients

Interfacial heat transfer coefficients

ProCAST permits the user to use either the data supplied in its database or any experimental data created by the user. The user can supply the heat transfer coefficient as a constant property or as a function of temperature. The interfacial heat transfer coefficients used in this model are included in Table 11 and include the natural convection (h_c), thermal radiation (h_r), and total (h_{total}) terms for external mold surfaces -- for a vertical wall, a downward-facing plate, and an upward-facing plate -- and the coefficient for various interfaces (h_g).

A remarkable feature about ProCAST is that it permits the user to simulate any interfacial heat transfer coefficient. That is, in the absence of any experimental data, the user can vary the heat transfer coefficient until the temperature results from the model agree with the experimental data. The model coefficient data must then be the correct data. Note that this data depends on the casting and mold materials, on the geometry, on the coating properties and thickness, and the deformation of the part and mold. So, the data must be generated again whenever any of these conditions changes.

Material properties

Like the interfacial heat transfer coefficient data, the user can supply his data or use those in the ProCAST database. The material properties used in ProCAST for thermal analysis are density, specific heat, and conductivity. Again, this data can be defined as constant or as a function of temperature. Table 12 shows the property data used in the model. Note that the experimental thermal conductivity data of the coating material will replace those in Table 12 in future modeling.

Boundary conditions

The boundary conditions can also be specified as constant or as a function of temperature. Table 11 shows the convection heat transfer coefficient between the mold outer surfaces and the air. The initial temperatures of the metal and mold are also shown in Table 12.

Table 11: The interfacial heat transfer coefficients used for the ProCAST model.

Vertical Wall

T (K)	$\bar{h}_c$ (W/m^2K)	h_r	h_{total}
300	0	5.51	5.51
350	5.269	7.05	12.32
400	6.097	8.93	15.03
450	6.577	11.19	17.77
500	6.899	13.88	20.78
550	7.131	17.02	24.15
600	7.305	20.67	27.98
650	7.441	24.84	32.28
700	7.553	29.60	37.15
750	7.648	34.96	42.61
800	7.734	40.97	48.70
850	7.815	47.68	55.50
900	7.896	55.11	63.01
950	7.959	63.31	71.27
1000	8.018	72.31	80.33
1050	8.073	82.15	90.22
1100	8.124	92.87	100.99
1150	8.173	104.51	112.68
1200	8.219	117.11	125.33

Plate facing down

T (K)	$\bar{h}_c$ (W/m^2K)	h_r	h_{total}
300	0	5.51	5.51
350	5.077	7.05	12.13
400	5.785	8.93	14.72
450	6.214	11.19	17.4
500	6.518	13.88	20.4
550	6.749	17.02	23.77
600	6.934	20.67	27.6
650	7.089	24.84	31.93
700	7.223	29.60	36.82
750	7.343	34.96	42.30
800	7.456	40.97	48.43
850	7.564	47.68	55.24
900	7.672	55.11	62.78
950	7.760	63.31	71.07
1000	7.844	72.31	80.15
1050	7.924	82.15	90.07
1100	8.002	92.87	100.87
1150	8.076	104.51	112.59
1200	8.148	117.11	125.26

Table 11: The interfacial heat transfer coefficients used for the ProCAST model (Continued).

Plate facing up

T (K)	$\bar{h}_c$ (W/m^2K)	h_r	h_{total}
300	0	5.51	5.51
350	6.827	7.05	13.88
400	7.912	8.93	16.84
450	8.540	11.19	19.73
500	8.958	13.88	22.84
550	9.256	17.02	26.28
600	9.480	20.67	30.15
650	9.653	24.84	34.49
700	9.794	29.60	39.39
750	9.914	34.96	44.87
800	10.02	40.97	50.99
850	10.12	47.68	57.80
900	10.22	55.11	65.33
950	10.30	63.31	73.61
1000	10.36	72.31	82.67
1050	10.43	82.15	92.58
1100	10.49	92.87	103.36
1150	10.54	104.51	115.05

Heat transfer coefficients for interfaces

Interfaces	h_g(Btu/hr.ft^2.°F)
Male -- female molds	70
Insert -- mold wall	70
Graphite coating -- mold	300
Casting -- mold (without coating)	
Before solidification	660
After solidification	70
Casting -- graphite coating	
Before solidification	660
After solidification	70

Table 12 Material properties used as input for ProCAST, assuming a eutectic gray iron mold and a 356 aluminum casting alloy.

Mold Material: Gray Cast Iron

Property	Value
Density	8.00 x 10^3 kg/m^3 for T = 298K
Solidus	1152C
Liquidus	1156C
Latent heat	241 kJ/kg
Specific heat	0.548 kJ/kg K for T = 373K
	0.561 kJ/kg K for T = 473K
	0.573 kJ/kg K for T = 573K
	0.586 kJ/kg K for T = 673K
	0.594 kJ/kg K for T = 773K
	0.619 kJ/kg K for T = 873K
	0.644 kJ/kg K for T = 973K
	0.703 kJ/kg K for T = 1073K
	0.720 kJ/kg K for T = 1173K
	0.732 kJ/kg K for T = 1273K
Conductivity	66.1 W/m K for T = 403K
	55.6 W/m K for T = 508K
	44.8 W/m K for T = 608K
	44.4 W/m K for T = 693K
	38.9 W/m K for T = 818K
	38.1 W/m K for T = 903K
	35.1 W/m K for T = 993K
	22.2 W/m K for T = 1173K

Table 12 (continued)

Casting Alloy: 356 Aluminum

Property	Value
Density	2.685 g/cm^3
Solidus	850K
Liquidus	891K
Latent heat	397.5 kJ/kg
Specific heat	0.963 kJ/kg K
Conductivity	0.35 cal/cm C s for T = 407K
	0.366 cal/cm C s for T = 420K
	0.370 cal/cm C s for T = 432K
	0.40 cal/cm C s for T = 590K
	0.397 cal/cm C s for T = 666K

Coating Material: Graphite

Property	Value
Density	26.0 lb/ft^3
Specific heat	0.201 Btu/lb F
Conductivity	2.7 Btu/ft h F

Initial Boundary Conditions

Property	Value
Initial mold temperature	300 to 450F
Initial casting temperature	1346F (730C)
Ambient air temperature	80F

Model results

Figure 31 shows the results at 1/16 inch from the outside surface of the insert (measured from the coating), at 1/16 inch from the outside surface of the insert (measured from the mold), and the outside surfaces of the mold. Note that the coating thickness was 0.01 inch. A cycle time of 100 seconds was selected -- 80 seconds for solidification, and the rest for mold opening, casting ejection, mold closure and filling. The initial temperature of the mold and the pouring temperature of molten aluminum were 620F and 1300F, respectively.

The temperatures reached steady state at about 5 cycles within the coating, the insert and the mold. The temperatures within the coating material were nearly identical to those within the casting. The steady state temperature at 1/16 inch from the outside surface of the insert (measured from the coating) was 750F. At 1/16 inch from the outside surface of the insert (measured from the mold), it was 730F.

Similar results were also observed for ANSYS, Figure 32. It should be noted that a coating thickness of 0.0025 inch was used for ANSYS analysis. It was initially believed that ANSYS would be required for the analysis of rate of crack growth; however since the rate of crack growth can be modeled analytically, only a high level language such as C^{++} is needed. Thus, an external program will be designed to capture the output data from PostCAST for predicting both the number of pouring cycles until the first crack appears in the mold and the rate of crack growth.

Some problems were encountered with the simulation. Because extensive computational time is required when the coating thickness is reduced below 0.01 inch, the current Sun Sparc workstations at UMR lack the computing speed for such analysis. This is also true for the cyclic thermal stress and strain analysis. Consequently, we could not predict the number of pouring cycles until the first crack appears in the mold. A new Sun Sparc workstation, being purchased, will remedy this problem.

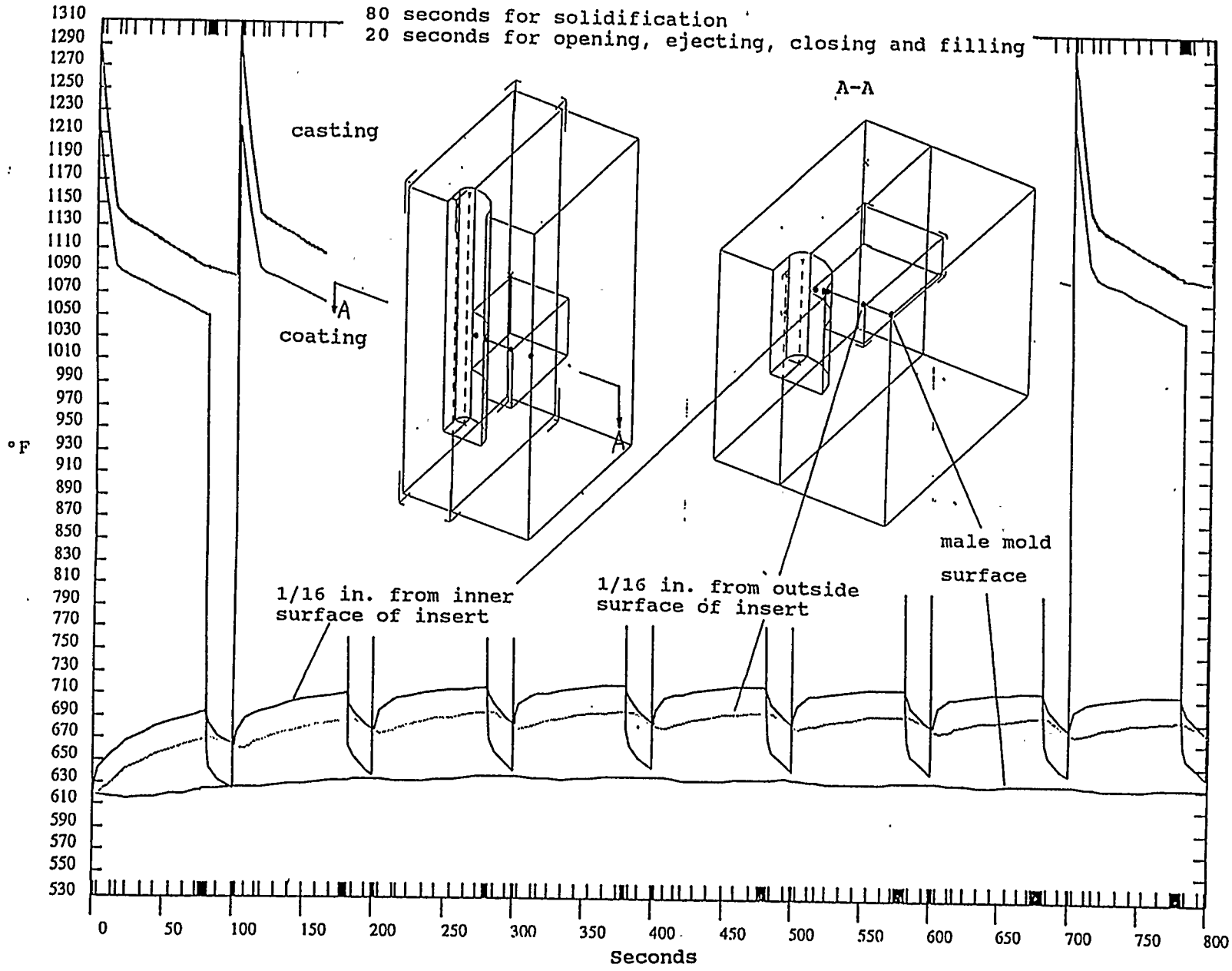

Figure 31: The theoretical results for the initial cycles of a casting run as predicted by ProCAST. In (a), the mold configuration is shown, while in (b), only the thermal history is included.

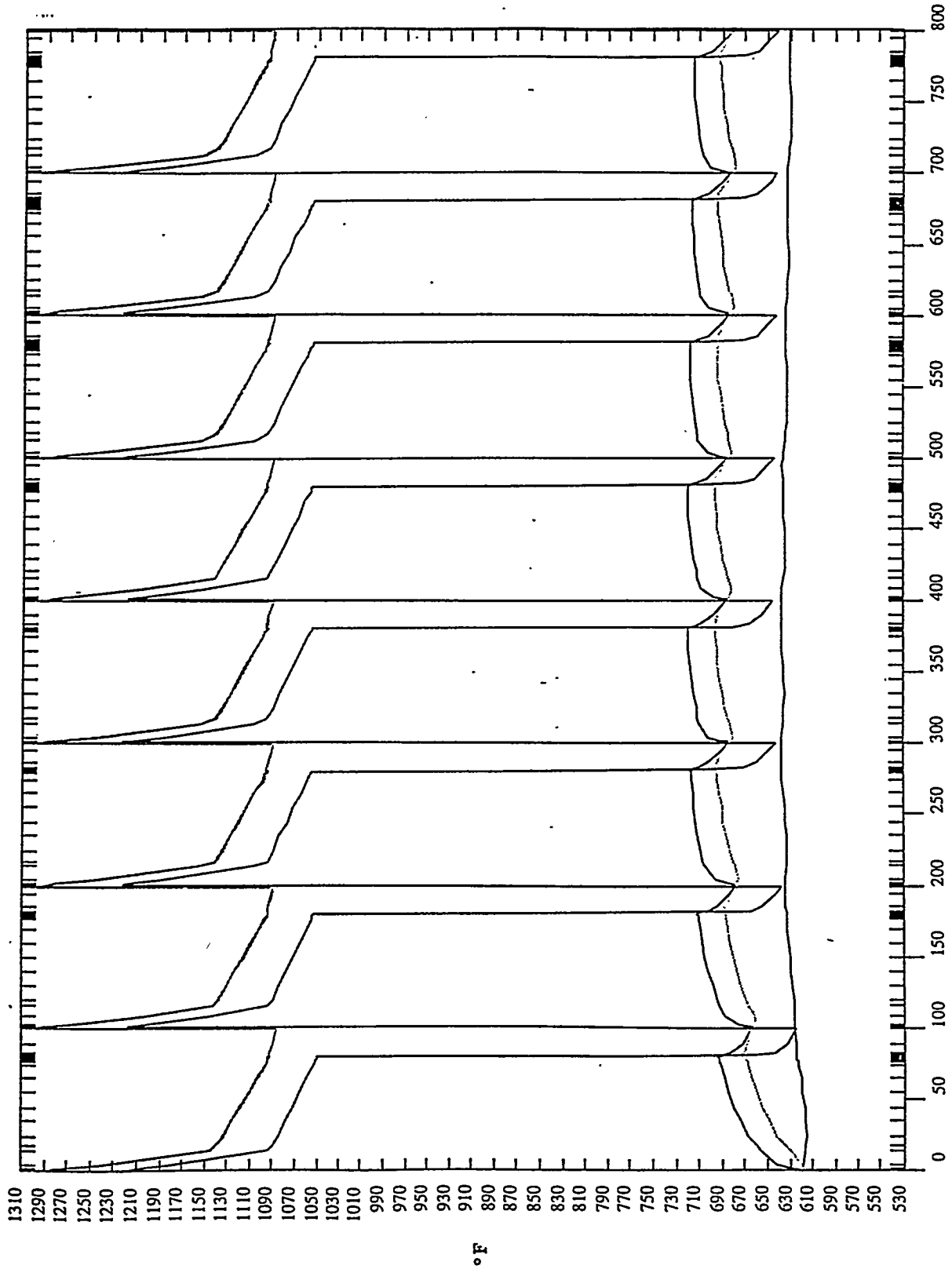

Figure 31: Continued.

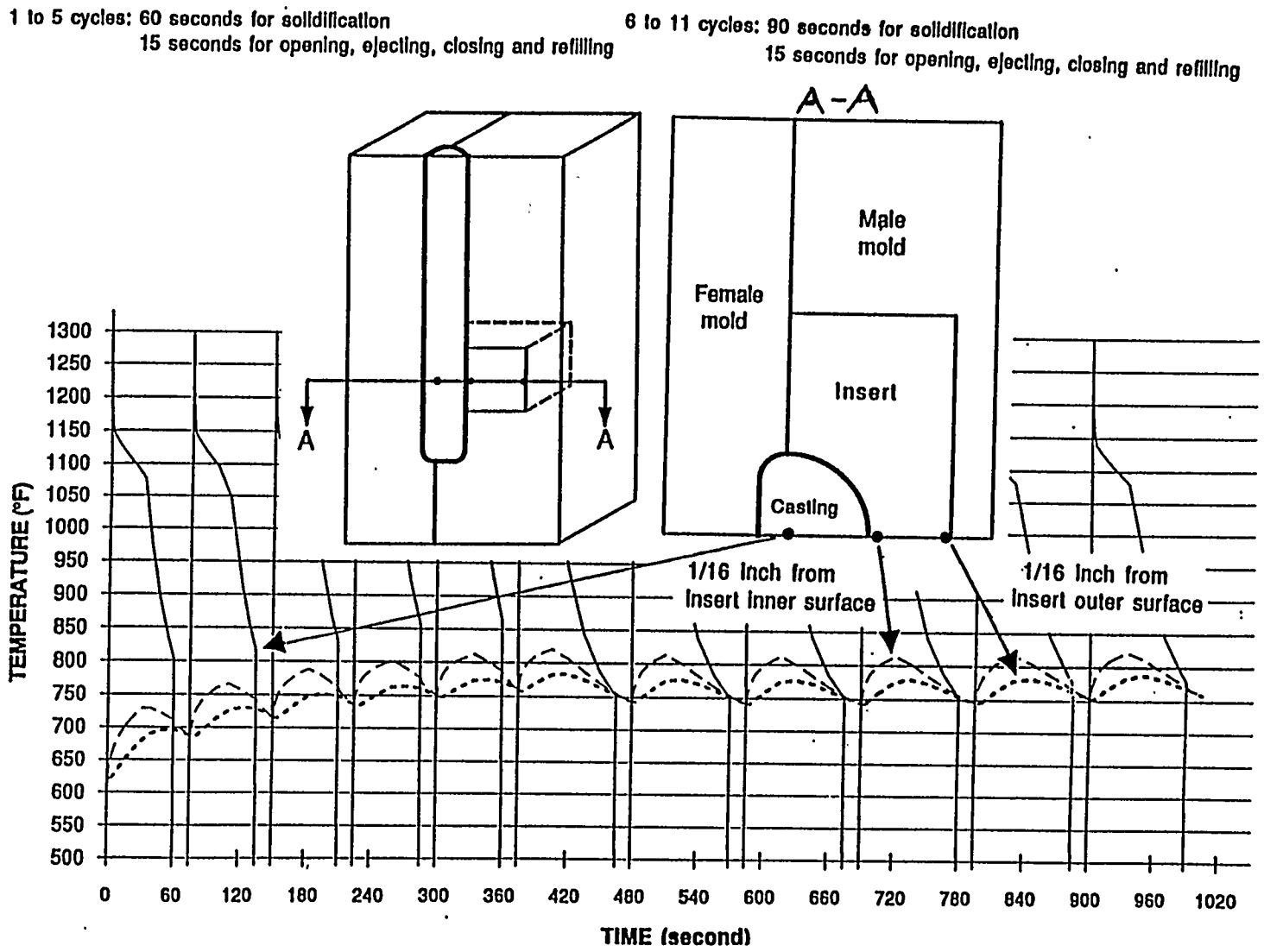

Figure 32: The theoretical results for the initial cycles of a casting run as predicted by ANSYS. In (a), the mold configuration is shown, while in (b), only the thermal history is included.

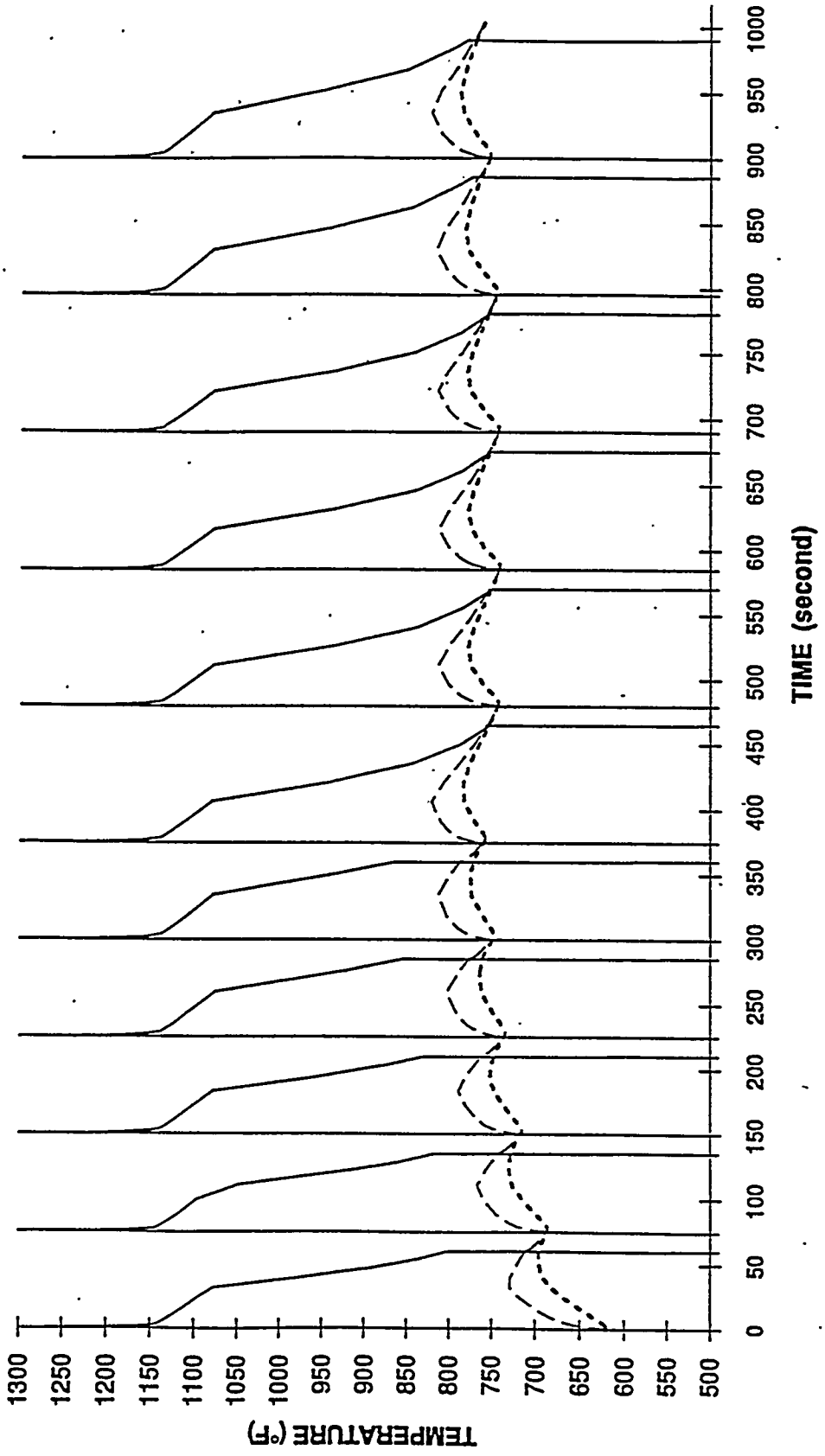

Figure 32: Continued.

Chapter 10

Validate Model

Controlled laboratory tests have been used to validate the CAD/CAE model's predictions of the solidification of the casting and the temperature of the mold during the course of a number of cycles, from start-up to the point where equilibrium is reached.

Case histories

In collaboration with industrial partners, information concerning the permanent mold process, including case-histories of permanent mold lives and failures, has been and continues to be obtained. Two of the graduate students have visited and worked in a permanent mold foundry to become acquainted with the operation of the equipment and the precautions and procedures required to produce permanent mold castings. In addition, one of the co-investigators has visited a number of permanent mold foundries and permanent mold suppliers; examples of failed permanent molds have been obtained and are currently being subjected to failure analysis.

3.3.2 Development of test mold

In collaboration with industrial partners, a test mold has been built that contains provision for inserts that are intended to encourage early crack nucleation and propagation. The overall mold configuration and the four designs for the inserts were shown in Figures 26-29. Each of the four inserts contains a stress raiser intended to nucleate cracks. Figure 33 shows the geometry of one of the castings produced from the mold and one of the inserts.

In addition, a small tilt-type permanent mold machine has been delivered, installed, and operated to provide validation of the model.

Instrumentation and operation of test mold

The inserts for the mold have been instrumented with thermocouples to permit thermal histories in the mold to be obtained. In preliminary tests, only two thermocouples have been used, with data acquired by a strip chart recorder. Further work in this subtask will utilize additional thermocouples and will use a computer data acquisition system and software. This equipment has been used to validate the thermal histories obtained from both the ProCAST and ANSYS models, as described below.

A test grid of castings was poured using two mold preheat temperatures and two mold coatings (an insulating coating, Dycote 34, and a graphite coating, Dycote 11). The metal was poured at a constant 1292F (700C) pouring temperature. The temperature in the mold insert was monitored continuously. Castings were poured until near equilibrium was obtained. This usually required approximately 40 castings. The insert used was a "blank", i.e. there was no

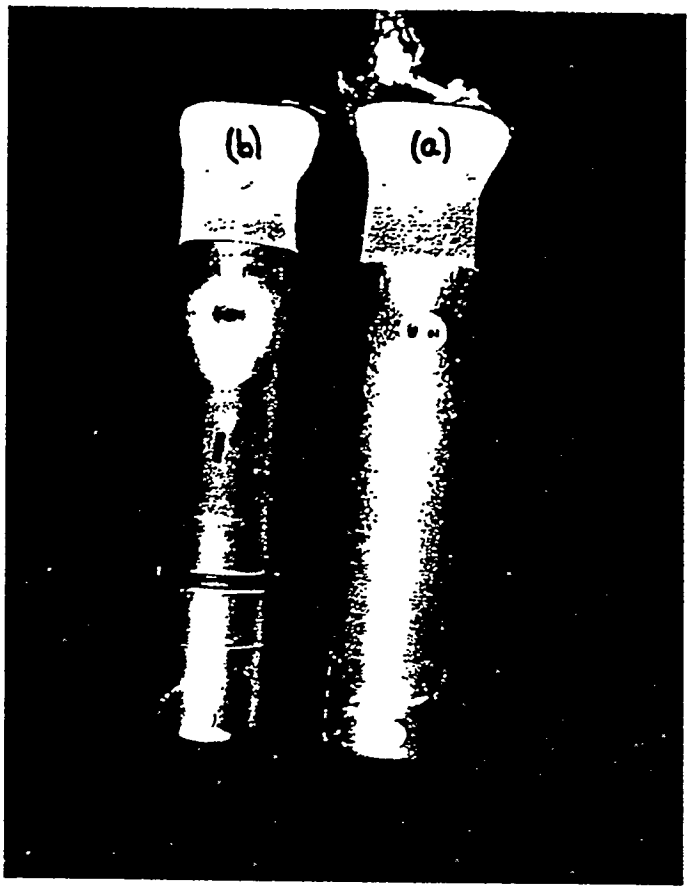

Figure 33: Typical castings produced with the mold. (a) With a "blank" insert and (b) with an insert containing a stress raiser.

stress-raising feature. This enabled the thermal analysis to be directly compared with the results from the model, which at this point still assumes an insert without a stress raiser.

Summary of the test grid

250F Mold Temperature Graphite Coating 1.5 min cycle Max: 880F Min: 745F ΔT: 135F	400F Mold Temperature Graphite Coating 1.0 min cycle Max: 970F Min: 870F ΔT: 100F
250F Mold Temperature Insulating Coating 1.5 min cycle Max: 870F Min: 738F ΔT: 132F	400F Mold Temperature Insulating Coating 1.5 min cycle Max: 740F Min: 675F ΔT: 65F

The graphite coating that was used was not thick enough to be measured. The insulating coating was sprayed on in several layers and was estimated to be about 0.0055 inch thick. The insulating coating covered the mold very effectively for the run in which the mold was preheated to 400F; for the run in which the mold was preheated to only 250F, the coating did not adhere well and was reapplied after several cycles when the mold had heated. In the future, this problem will be avoided.

In these tests, a thermocouple was located in the mold insert 1/16-in. from the interface with the casting. The data was

acquired using a strip chart recorder. Data acquisition is planned to be obtained via computer; however the computer system must not only record the data but must also display the data as it is being acquired in order to control the pouring process. A suitable system is being prepared.

A typical data set for a casting run is shown in Table 13. Several features were noted from the data, including the peak temperature reached in the mold insert during each cycle, the lowest temperature obtained in the mold insert during each cycle, and the temperature difference between the peak and lowest temperature during each cycle. The manner in which these temperatures and temperature differences changed during the run was observed, and differences in the shape of the temperature cycle in the mold insert were noted.

Graphical results are given in Figures 34 to 38. Observations include

a. Equilibrium temperatures (peak mold temperature, minimum mold temperature, and temperature difference) were obtained after 35 to 50 cycles. In the three runs with a 1.5 minute cycle, the equilibrium number of cycles was about 35, while in the run with a 1 minute cycle, the equilibrium occurred closer to 50 cycles.

b. For very low initial mold temperatures, the maximum and minimum insert temperatures and their temperature difference were nearly identical for both the graphite coating and the insulating coating.

c. The two runs using the graphite coating had quite different maximum and minimum insert temperatures, with much higher temperatures obtained for the 400F initial mold temperature. Unfortunately, this was the first of the runs and the cycle time was only 1 minute, rather than 1.5 minutes. Consequently we cannot at this point determine whether the difference in temperatures is due to the cycle time or the initial mold temperature.

d. The two runs using the insulating coating also had different maximum and minimum insert temperatures, with lower maximum temperatures for the higher initial mold temperature. In this case, the cycle time was the same, but the coatings may have been applied somewhat differently.

e. Relatively good control over metal temperature was achieved. The metal in the furnace was maintained at a high temperature and, each time one casting was poured, an old casting of the same size was added to the crucible. The metal was ladled from the crucible into the pouring cup and the temperature noted; the metal in the pouring cup was allowed to cool to 700C, at which time the tilt was begun. The metal entering the pouring cup varied somewhat in temperature from pour to pour; however with rare exceptions the temperature at the time of the tilt remained constant. With good control over the metal temperature in the

Table 13: Data obtained during a typical casting run. The columns labeled "mm" and "cm" refer to the chart paper and were converted to temperature and time.

Casting	Peak	Temp		Low	Temp		Delta Temp		Time			Tilt Temp		Metal Temp	
	mm	C	F	mm	C	F	C	F	cm	min	per cycle	C	F	C	F
1	56.00	209	408	3.00	104	220	104	188	0.45	0.23		700	1292	705	1301
2	83.50	263	505	24.70	147	297	116	208	4.20	2.10	1.88	700	1292	711	1312
3	96.00	287	549	34.50	166	331	121	218	7.90	3.95	1.85	700	1292	735	1355
4	107.00	309	588	42.70	182	360	126	228	11.40	5.70	1.75	700	1292	765	1409
5	114.30	323	614	48.00	193	379	130	235	15.45	7.73	2.02	700	1292	740	1364
6	120.00	335	634	56.00	209	408	126	227	19.25	9.63	1.90	700	1292	711	1312
7	123.20	341	645	58.70	214	417	127	228	23.70	11.85	2.23	700	1292	708	1306
8	131.00	356	673	69.50	235	455	121	218	27.35	13.68	1.83	700	1292		
9	137.20	368	695	77.70	251	484	117	211	31.00	15.50	1.82	700	1292	741	1366
10	143.70	381	718	85.50	267	512	114	206	34.60	17.30	1.80	700	1292	711	1312
11	148.00	390	733	93.00	281	539	108	195	38.10	19.05	1.75	695	1283	695	1283
12	149.00	392	737	95.70	287	548	105	189	41.90	20.95	1.90	700	1292	735	1355
13	155.00	403	758	101.50	298	569	105	189	45.50	22.75	1.80	691	1276	691	1276
14	158.20	410	769	106.50	308	586	102	183	49.25	24.63	1.88	700	1292	716	1321
15	159.00	411	772	108.00	311	592	100	181	53.20	26.60	1.98	700	1292		
16	163.00	419	786	111.50	318	604	101	182	56.90	28.45	1.85	692	1278	692	1278
17	165.00	423	793	117.00	329	623	94	170	60.80	30.40	1.95	700	1292		
18	168.50	430	806	118.70	332	629	98	176	64.50	32.25	1.85	700	1292	724	1335
19	171.00	435	815	123.50	341	646	93	168	68.25	34.13	1.88	700	1292	711	1312
20	173.00	439	822	126.50	347	657	91	165	72.10	36.05	1.92	685	1265	685	1265
21	175.00	443	829	128.50	351	664	91	165	75.80	37.90	1.85	700	1292	716	1321
22	176.70	446	835	131.00	356	673	90	162	79.60	39.80	1.90	700	1292	744	1371
23	177.00	447	836	135.00	364	687	83	149	83.30	41.65	1.85	700	1292	750	1382
24	177.20	447	837	137.00	368	694	79	142	87.00	43.50	1.85	700	1292	736	1357
25	179.00	451	843	137.00	368	694	83	149	90.80	45.40	1.90	700	1292	738	1360
26	181.00	454	850	138.70	371	700	83	150	94.60	47.30	1.90	700	1292	741	1366
27	181.50	455	852	140.50	375	707	81	145	98.30	49.15	1.85	700	1292	735	1355
28	182.00	456	854	142.00	378	712	79	142	102.10	51.05	1.90	700	1292	729	1344
29	182.00	456	854	142.70	379	714	77	139	105.90	52.95	1.90	700	1292	726	1339
30	184.00	460	861	144.00	382	719	79	142	109.70	54.85	1.90	700	1292	729	1344
31	184.00	460	861	145.50	385	724	76	136	113.50	56.75	1.90	700	1292	741	1366
32	184.50	461	862	145.50	385	724	77	138	117.30	58.65	1.90	700	1292	749	1380
33	185.50	463	866	146.00	386	726	78	140	121.00	60.50	1.85	700	1292	754	1389
34	186.50	465	869	148.00	390	733	76	136	124.70	62.35	1.85	700	1292	748	1378
35	187.00	466	871	148.70	391	736	75	136	128.50	64.25	1.90	700	1292	738	1360
36	187.00	466	871	149.50	393	739	74	133	132.20	66.10	1.85	700	1292	757	1395
37	188.00	468	875	150.50	394	742	74	133	135.90	67.95	1.85	700	1292	724	1335
38	184.00	460	861	146.50	387	728	74	133	140.10	70.05	2.10	700	1292	741	1366
39	188.00	468	875	149.00	392	737	77	138	143.90	71.95	1.90	700	1292	738	1360
40	189.00	470	878	151.00	395	744	75	135	147.70	73.85	1.90	700	1292	732	1350
41	189.50	471	880	150.70	395	743	76	137	151.60	75.80	1.95	700	1292	740	1364
42	189.00	470	878	151.50	396	746	74	133	155.40	77.70	1.90	700	1292	744	1371
43	187.00	466	871	151.20	396	745	70	127	159.30	79.65	1.95	700	1292	711	1312
44	190.00	472	882	151.70	397	746	75	136	163.00	81.50	1.85	700	1292	723	1333

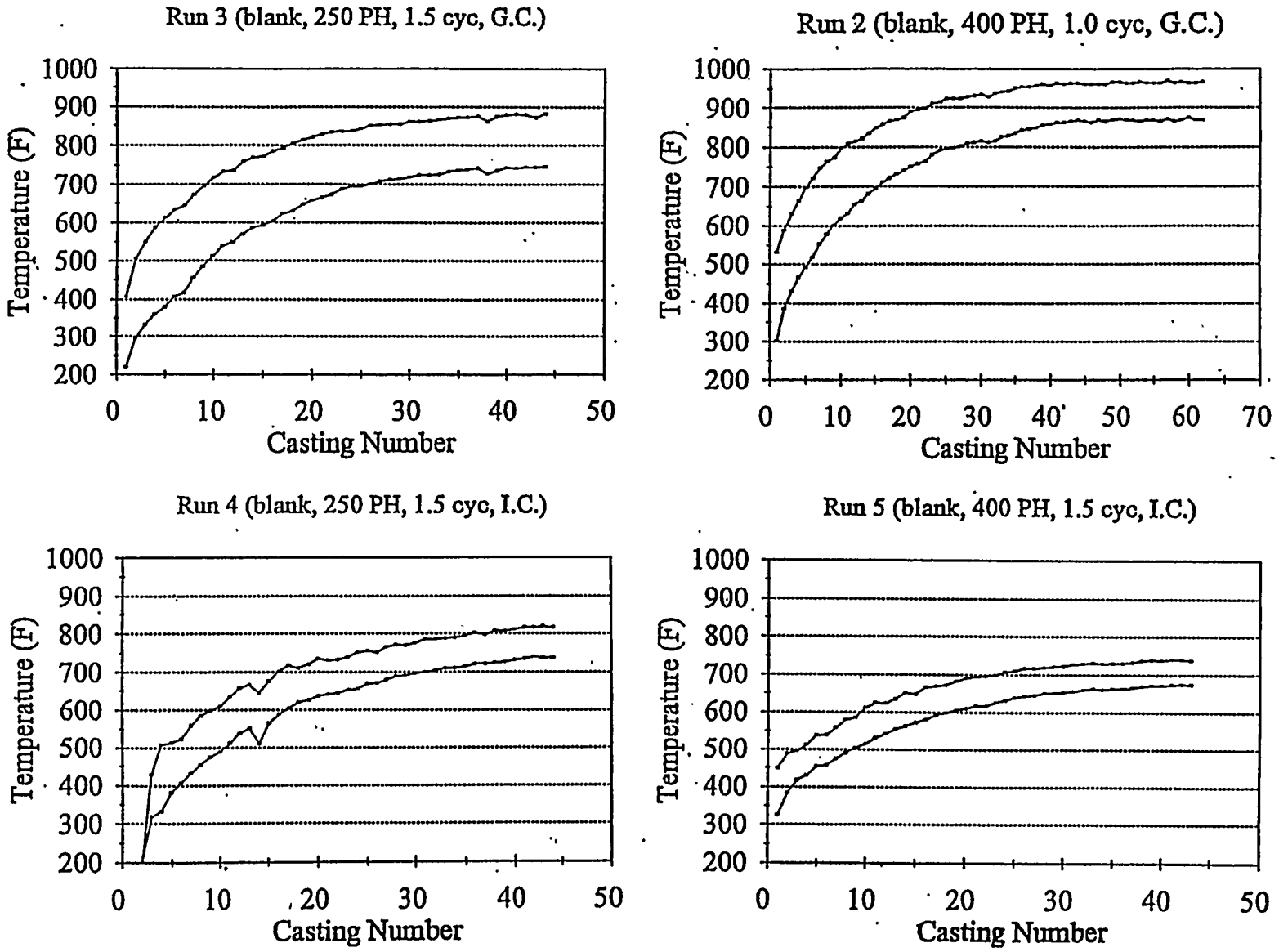

Figure 34: The peak temperatures and minimum temperatures in the mold insert, about 1/16-inch from the casting/mold interface, versus number of cycles. About forty castings are required to reach a steady-state mold temperature.

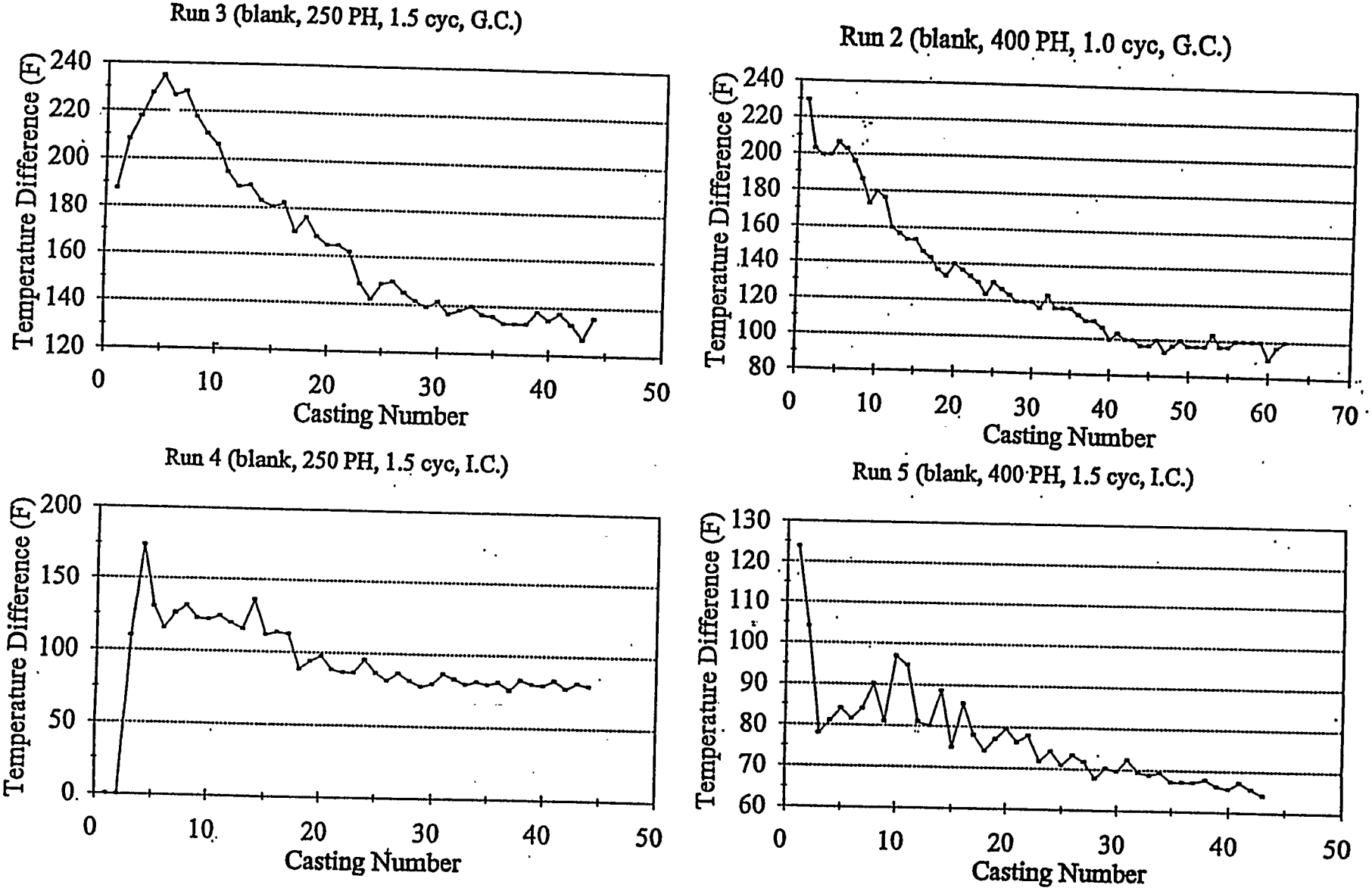

Figure 35: The temperature difference between the peak and minimum temperatures in the mold insert near the casting/mold interface versus number of cycles. The temperature difference decreases and reaches a steady-state value after about forty castings.

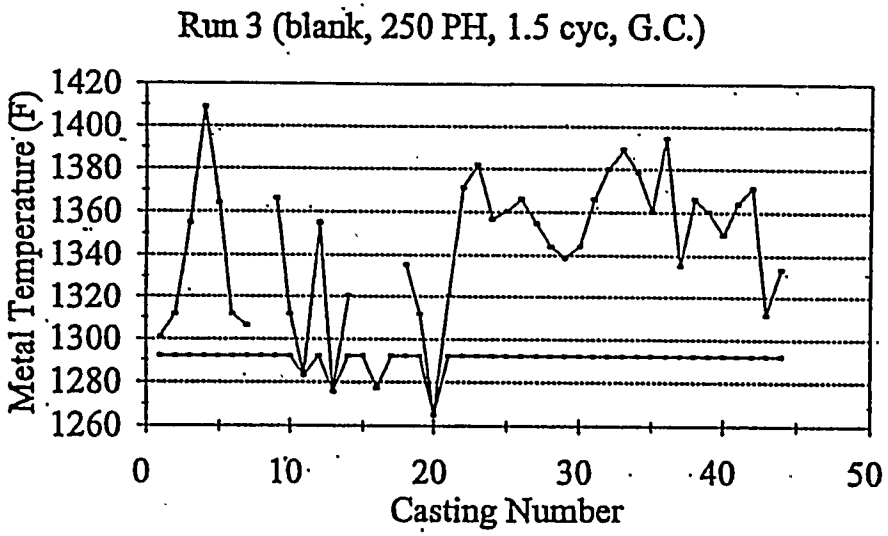

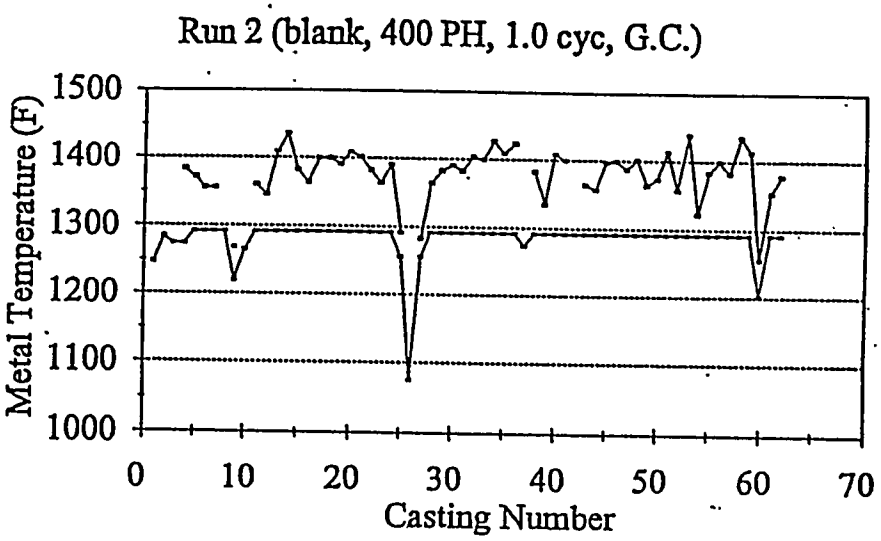

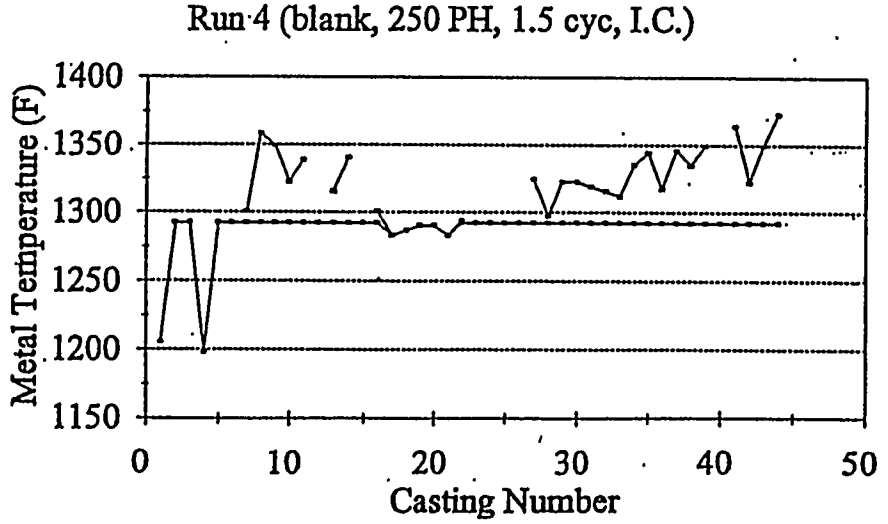

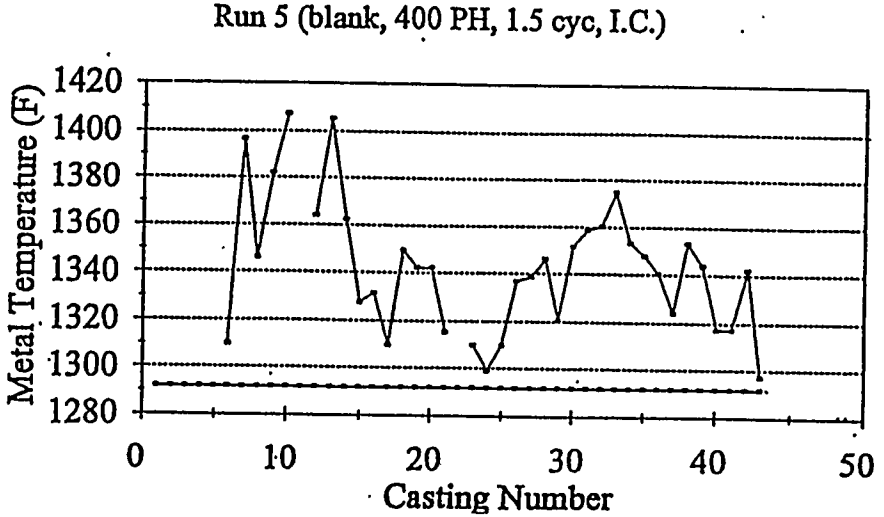

Figure 36: The temperature at which the metal is ladled into the pouring cup (upper curve) varies throughout an experimental run; however the temperature of the metal when the tilt begins (lower curve) is nearly constant.

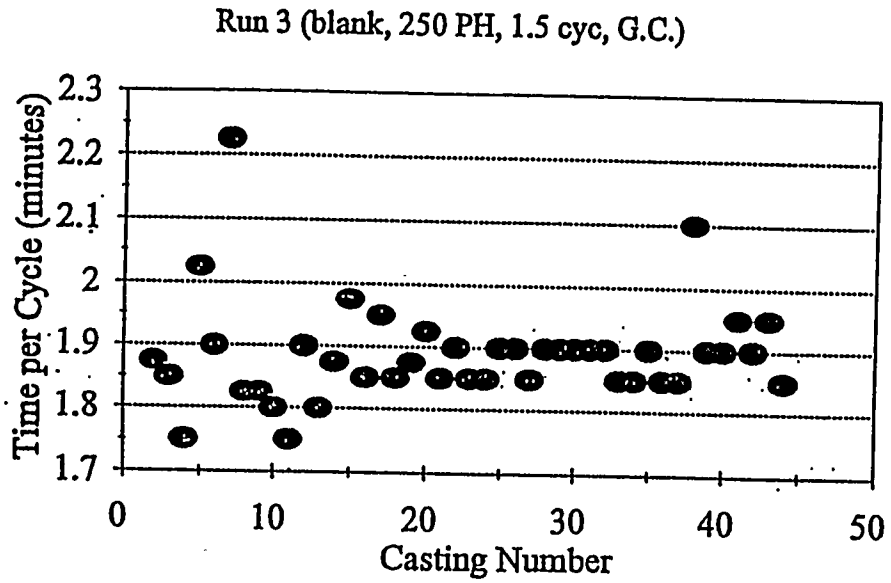

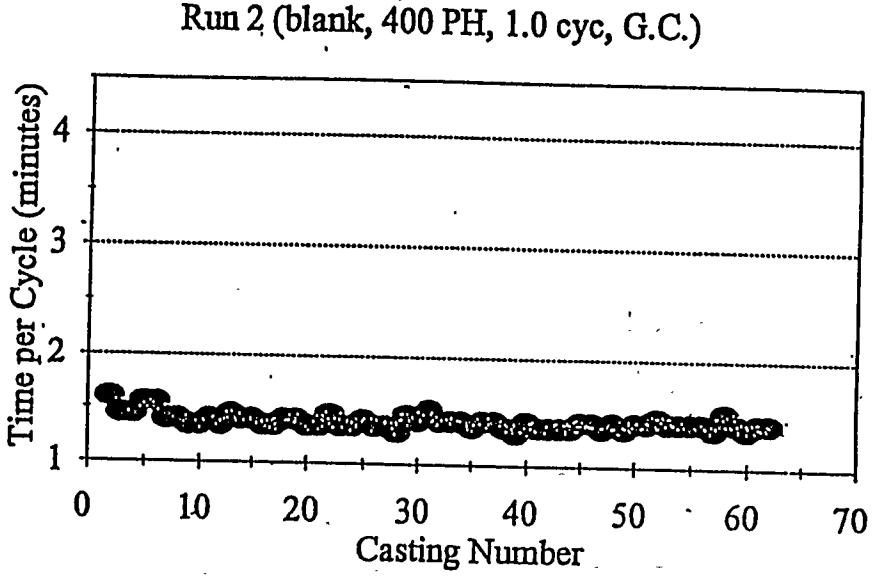

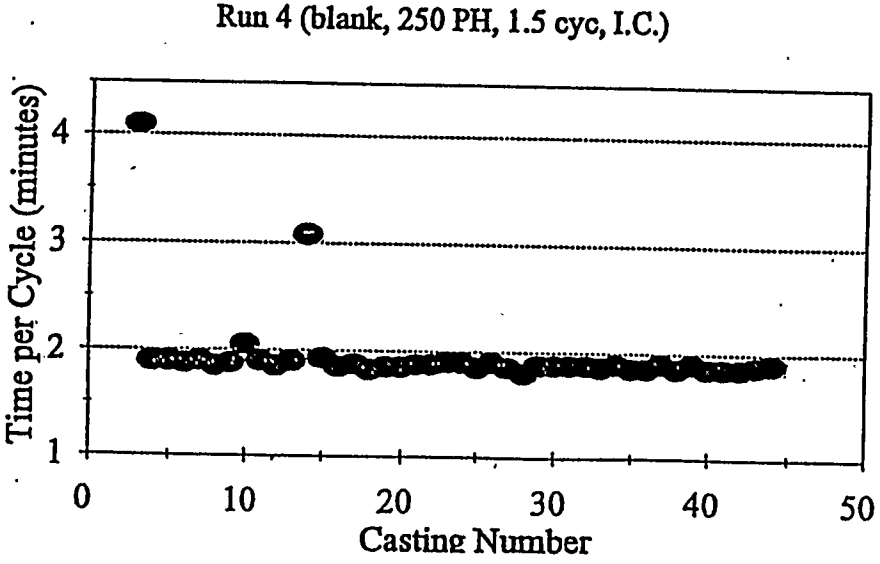

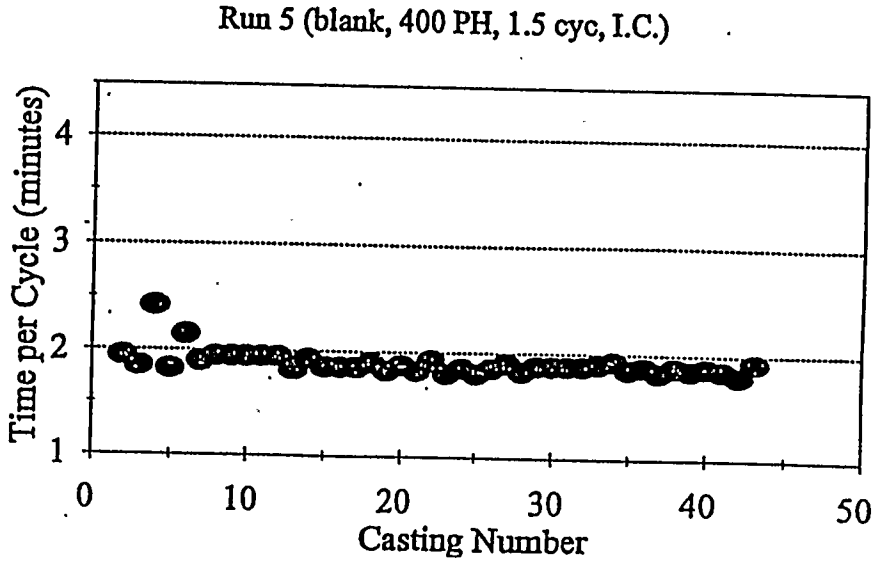

Figure 37: The time required for each cycle for producing castings. For the most part, the cycle time is very consistent.

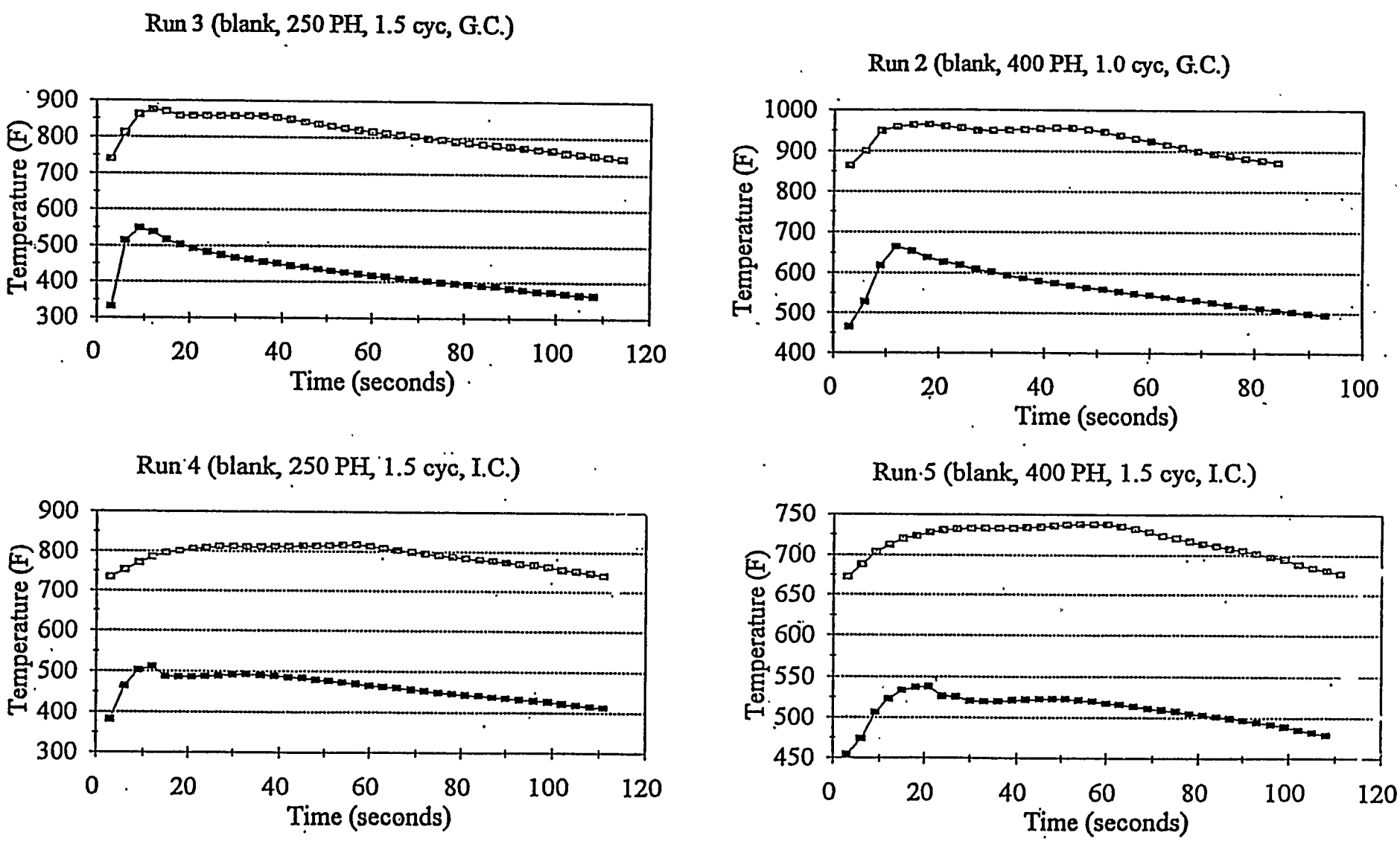

Figure 38: Typical temperature cycles in the mold insert near the casting/insert interface. The lower curve is from a casting poured near the beginning of the run, while the upper curve is for a casting poured near the end of a run. Data is average data obtained from strip chart recorder.

furnace, during ladling, and at the start of the tilt, the overall cycle times were quite constant.

f. In the first castings in each run, there was a large difference between the peak and minimum mold insert temperatures for the graphite coating. This temperature difference gradually was reduced during the run, as equilibrium was approached. These initial differences were much smaller when the insulating coating was used.

g. The shape of the temperature profile in the insert was unusual; examples are given in Figure 39. When a graphite coating was used, the first few cycles produced a temperature profile as one might expect, particularly when the initial mold temperature was low. However after a number of cycles (fewer for a higher initial mold temperature), the profile developed plateaus and eventually double peaks. Similar temperature profiles were observed when an insulating coating was used, for both initial mold temperatures, and the double peaks developed almost immediately.

A likely explanation for this behavior is related to the position of the thermocouple and the solidification behavior of the casting. When the casting solidifies, its latent heat of fusion must be released and transferred to the mold. When the mold is at a relatively low temperature, this extra thermal energy is transferred readily by the better "heat sink" capability of the mold material and only a single peak is observed in the thermal cycle. However as the mold heats, it is less capable of removing the latent heat of fusion and the mold may be reheated by the latent heat, producing a plateau or even a second peak. This effect was not observed further from the casting/insert interface because the latent heat surge was damped by the greater distance.

A greater effect was found for the insulating coating. The insulating coating led to a smaller difference between the maximum and minimum mold temperatures and to an almost immediate and pronounced double peak.

The difference in the shape of the temperature cycle near the casting surface and within the insert may introduce local stresses at the mold insert surface which is most subject to cracking. This may need to be considered when the model for thermal stresses is developed and tested.

The results obtained experimentally were compared to those predicted from the model.

a. Cooling Curves: A cooling curve was obtained from a casting near the early stages of a run and was then compared to similar cooling curves predicted by the ProCast and ANSYS models. The alloy cast was 356 aluminum, a hypoeutectic alloy that produces roughly 50% dendritic and 50% eutectic solidification. Thus both a liquidus arrest, near 1135F, and an eutectic arrest, near 1035F, are expected on the curve. The experiment produced the expected

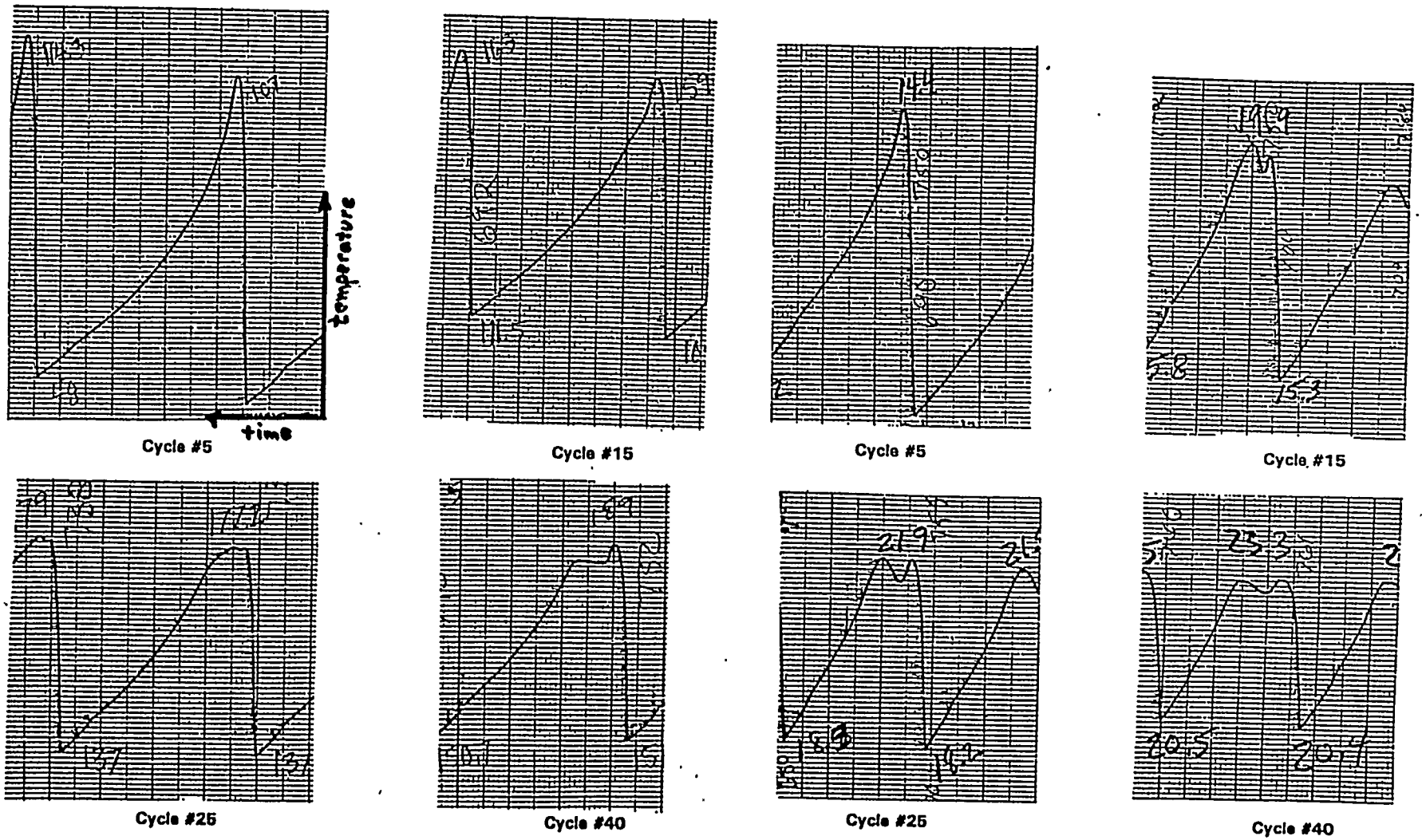

Figure 39: Actual strip chart recordings for the temperature cycle in the mold insert, showing the development of plateaus and double peaks in the mold insert near the casting/insert interface.

Insulating Coating - 250°F Mold Temperature

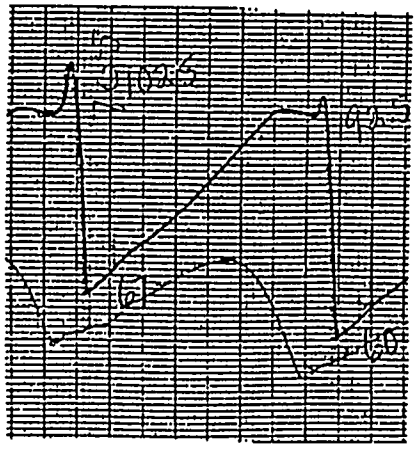

Cycle #5

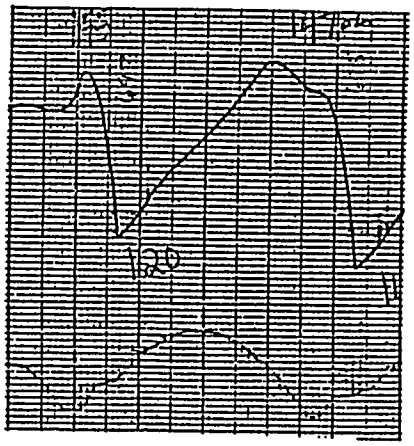

Cycle #15

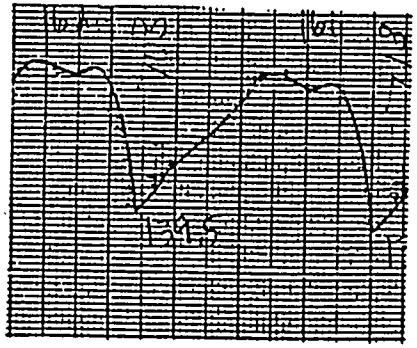

Cycle #25

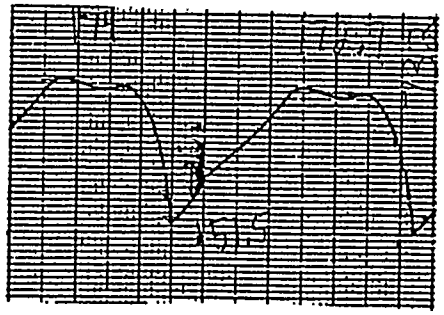

Cycle #40

Insulating Coating - 400°F Mold Temperature

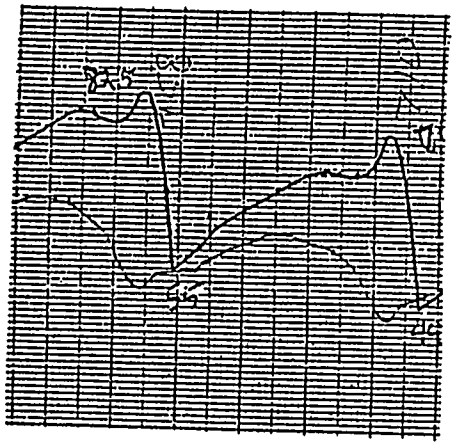

Cycle #5

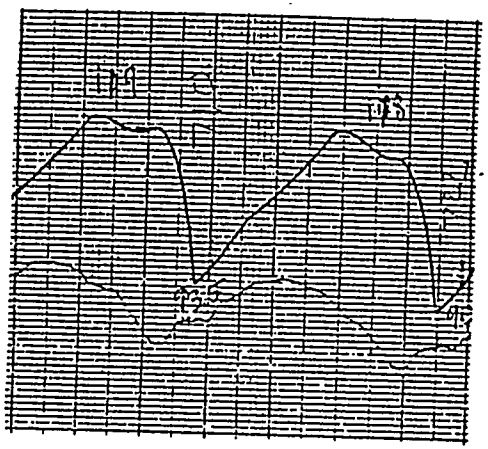

Cycle #15

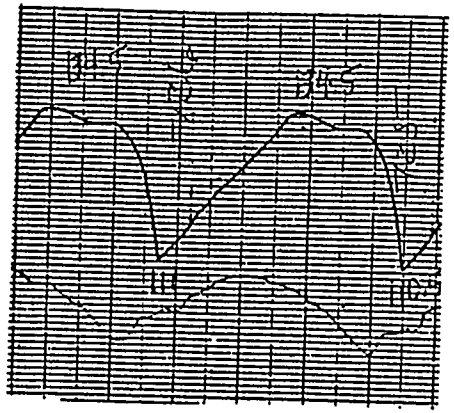

Cycle #25

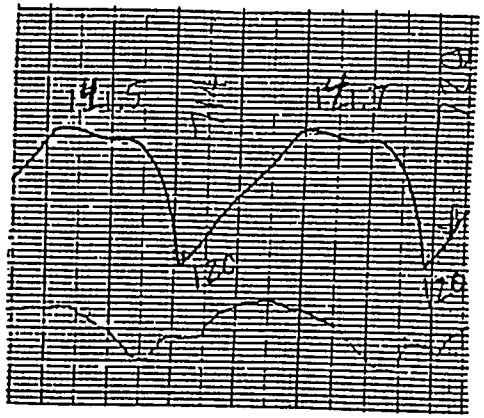

Cycle #40

Figure 39: (Continued)

cooling curve, with a total solidification time of about 30 seconds and well defined liquidus and eutectic arrests, Figure 40.

Initially, both models assume that the latent heat of fusion is evolved in a linear manner throughout the freezing range, which of course is not accurate. Consequently cooling curves from both models gave a cooling curve without an eutectic arrest. In spite of this, the Ansys model predicts a total solidification time of about 30 seconds, in good agreement with the experimental value. The ProCast model gave a similar shaped cooling curve, but predicted longer solidification times. It should be noted, however, that the casting conditions were not identical in all three cases -- different coating types, thicknesses, and initial mold temperatures were used in all three approaches. When the data base for the ANSYS model was adjusted to account for the latent heat evolution during the eutectic arrest, better agreement between the experimental and theoretical model results was obtained.

The initial cooling curves from the models also gave different solidus temperatures. The models used the data base in ProCast, which included a higher eutectic temperature than is normally observed. This adjustment has also been made to the model, providing better agreement with experiment. Future modeling will use thermal data that is consistent with that found experimentally.

b. Temperature Cycles: The thermal cycles in the mold insert near the beginning and end of a run were obtained experimentally and by both models. These were compared to determine the agreement, both in approximate temperatures and with respect to their shape. Again, it should be noted that the conditions (initial mold temperature, coating type, coating thickness) were not the same.

The temperatures predicted in the mold insert are quite different for the three approaches, Figure 41, which is expected since the initial conditions were not identical. The experiment and the two models used a graphite coating, but different coating thicknesses and initial mold temperatures. At the beginning of the run, the models both predict higher insert temperatures, since the model assumed a high initial mold temperature. However by the end of the run, the measured temperatures were higher than those from the model. The model also predicts that the insert temperatures reach a near steady state with about five cycles, while more than 25 cycles are observed experimentally. The shape of the temperature cycle also is different. In the early cycles, the temperature cycle is very steep and "pointed", with a large difference between maximum and minimum insert temperatures. Later, a double peak is observed. Both models predict comparatively flat temperature cycles with smaller differences in maximum and minimum temperatures.

c. Resolution of differences: The first year of the project has concentrated on understanding the processes (both experimental and theoretical) and developing expertise in their operation.

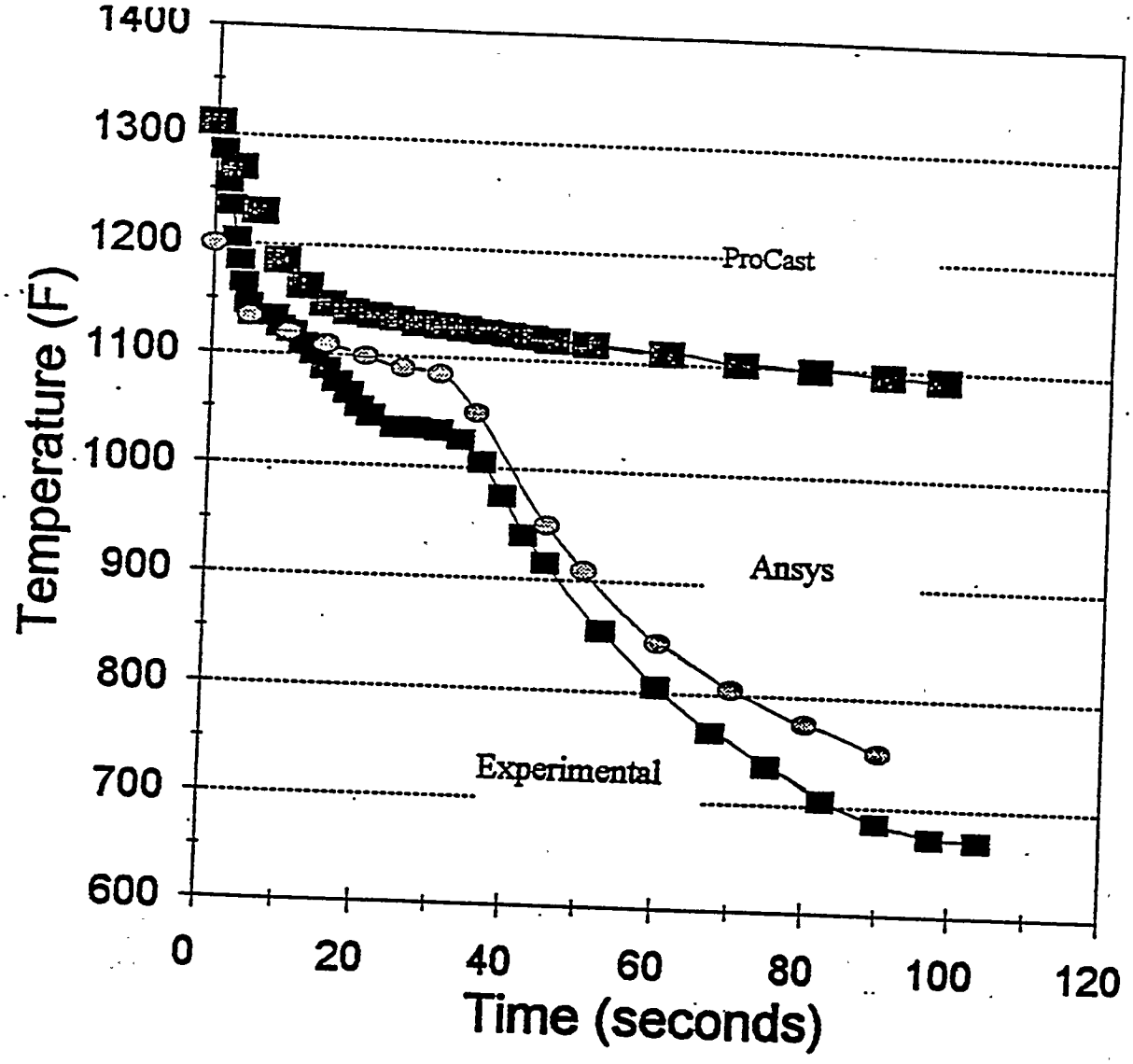

Figure 40: Comparison of experimental cooling curves in the casting with cooling curves from the ProCAST and ANSYS models.

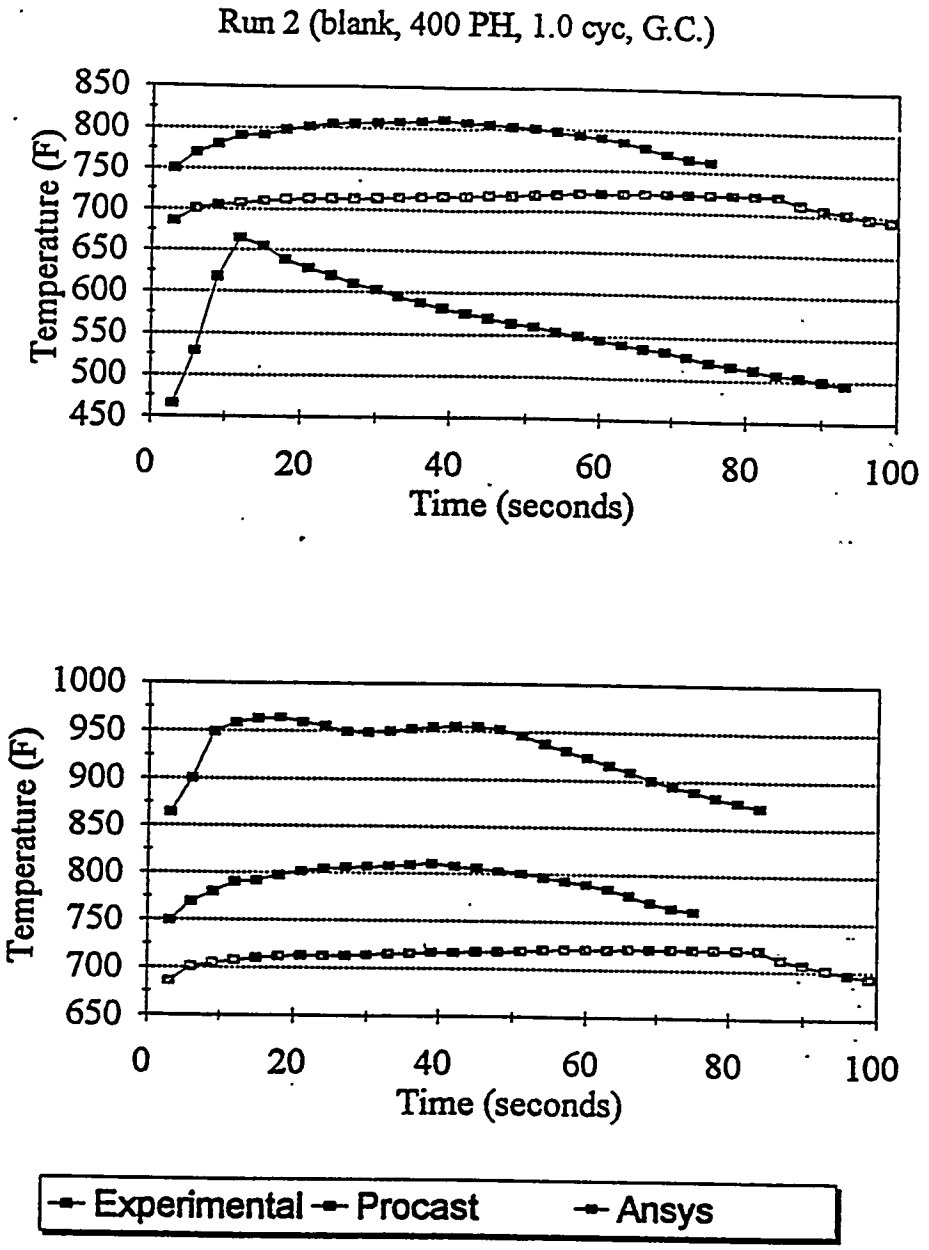

Figure 41: Comparison of the experimental temperature in the mold insert with that predicted by the ProCAST and ANSYS models.

During this period, casting parameters were selected that facilitated the work. For example, models have used data for the alloy and coating that were estimated from the literature. Experiments have used initial mold temperatures that were quickly obtained during preheating. Relatively little attention has been paid to the thickness of the coating, the properties of the coating, and other important parameters.

At this point, however, the required familiarity and background have been attained and future research will be orchestrated so that the modelers and experimentalists will be "producing castings" with the same casting parameters. In the future

- coating thicknesses for any particular run will be selected, by compromise, so that models can be run in a reasonable period of time yet the coatings actually applied to the mold will be possible. The models require a relatively thick coating in order to have a coarse enough mesh size to permit computations within a reasonable number of hours; however thick coatings are difficult to apply to an actual mold and, in the case of graphite, are virtually impossible to apply.

- models will begin to use experimentally obtained values for the coating properties. Currently, the model used data, obtained from the literature, which are not necessarily typical of permanent mold coatings. Data for graphite, in particular, are highly dependent on the type of graphite used. Data for insulating coatings will depend significantly on exact compositions as well as the amount of porosity. Reasonable estimates for the thermal conductivity of the insulating coating have been obtained and efforts are being made to obtain similar data for graphite, although the latter has presented a number of difficulties. Additional tests will be performed to continue characterization of the coatings, including estimates of the bulk density of the coating and the morphological aspects of the coating that might be significant.

- models will begin to use more appropriate physical data for the metal, in particular the liquidus and eutectic temperatures, which will be obtained directly from the metal poured. In addition, the input to the models will be modified to permit the latent heat to be evolved more realistically, producing cooling curves with the eutectic arrest. The models will also be examined to determine if the possible influence of latent heat on double peaks in the insert wall can be predicted.

- one of the purposes of the preliminary experimental tests has been to determine the number of cycles required to reach equilibrium temperatures in the mold insert. In these tests, this number of cycles was more than 25. This number of cycles takes an exceptionally large amount of computation time, at least with the current computing facilities and their availability. This will presumably be rectified with the acquisition of a dedicated work

station and larger numbers of cycles will be computed.

Summary

The significant accomplishments in the first phase of the research program are summarized below.

1. Literature reviews for mold coatings and thermal fatigue in iron molds were completed.

2. A data base for the thermomechanical properties of the metal, mold, and coating was compiled and is undergoing continuous up-dating.

3. Methods for estimating experimentally the thermal properties of the mold and coating have been developed and are being used to characterize coatings and mold materials.

4. A CAD/CAE model to predict the thermal behavior in the metal casting and mold has been developed.

5. A test mold, which included removable mold inserts, has been designed, built, delivered, and operated. The mold inserts have been instrumented to permit the thermal history of the mold to be followed.

6. The effects of mold preheat temperature and coating material on the thermal history have been determined experimentally.

7. Cooling curves for the casting have been obtained experimentally.

8. The results of modeling and experiment have been compared. Based on these results, procedures have been established to assure that experimental and theoretical conditions will be directly comparable in the next phases of the program, and deficiencies in both the model and experiment have been noted and addressed.

Acknowledgement

The support in the way of matching funds provided by the Missouri Research and Training Center (MRTC) is gratefully acknowledged.

APPENDIX I

A Review of Permanent Mold Coatings and Their Effect on Heat Transfer in the Mold

A Review of Permanent Mold Coatings and Their Effect on Heat Transfer in the Mold

by

Kofi Nyamekye
Associate Professor of Engineering Management
University of Missouri-Rolla, Rolla MO 65401

Sufei Wei
Graduate Student in Engineering Management
University of Missouri-Rolla, Rolla MO 65401

Don Askeland
Professor of Metallurgical Engineering
University of Missouri-Rolla, Rolla MO 65401

Bob Voigt
Associate Professor of Industrial Engineering and Management Systems
Penn State University, University Park PA 16802

Robert P. Pischel
Product Manager
Foseco, Inc., Cleveland, OH 44142

Wayne Rasmussen
Associate Technical Director
American Foundrymen's Society
Des Plaines, IL 60016

Chris Ramsay
Assistant Professor of Metallurgical Engineering
University of Missouri-Rolla, Rolla MO 65401

ABSTRACT

Relatively little information exists in the literature concerning mold coatings for the permanent mold process, and the published data lack technical detail about the properties of such materials. This information is important because it assists the foundryman in selecting an appropriate mold coating for a specific permanent mold casting application. Furthermore, the lack of thermal property data in the literature makes it extremely difficult to develop a good heat transfer model for this process. Consequently, a critical need exists in the permanent mold casting industry for a detailed summary of the properties of mold coating materials. This paper addresses this need.

First, the paper covers the basic constituents of coatings, their requirements, care and uses. Second, the thermal properties needed for modeling the effect of coating material on heat transfer through the casting and the mold are discussed for the permanent mold process. The paper also discusses the need for establishing a test procedure to obtain the thermal properties of permanent mold coatings that are typically used in the permanent mold foundry industry.

INTRODUCTION

Materials applied on interior surfaces of permanent molds or on surfaces of cores are known as mold coatings, washes, dressings or sprays. They are used on permanent molds for the casting of nonferrous alloys such as brass, bronze, aluminum, magnesium, and for the casting of iron. In all cases they act as barriers between the metal mold and the metal casting, providing the following beneficial results [1-6].

To prevent the molten metal from prematurely freezing. One of the first considerations of mold coatings is insulation. Because molds are made of a metal with a high thermal conductivity, it is necessary in many cases to use an insulating coating between the molten stream of metal and the mold itself. This is necessary to keep the molten metal from freezing before it reaches all areas of the cavity.

To control the rate and direction of solidification of the casting and therefore its soundness and structure. By varying the thickness of the insulation layer, solidification of the metal at different locations in the cavity can be controlled. This can help ensure a sound casting.

To minimize thermal shock to the mold material. Coatings can markedly reduce the temperature gradient at the metal-mold interface during the initial few seconds of casting, thus reducing thermal shock on the mold.

To prevent dissolution of the mold in the molten metal and soldering of molten metal to the mold (Isolation). Because metal in the molten state has a high affinity with most other metals, a barrier is necessary between the molten stream and the metal in the mold to prevent the former from picking up the latter. This action is often called erosion or washing. Without some means of preventing this, molds would not last long.

To vent air trapped in the mold cavity. Air in the cavity must be vented before complete filling can occur. A permanent mold has no permeability, that is air cannot pass through it. Sometime, grooves are made on the interior of a permanent mold to

help evacuate air. If the mold coating is applied on the interior of a mold, the textured surface of the mold coating material can also act as tiny channels to evacuate air between the casting and the mold itself.

To lubricate the mold. Since metal alloys shrink as they go through the solidification stage, a casting may grip tightly to certain areas in the mold where draft is minimal. A coating with lubricating properties will allow for release of the casting in these areas.

CONSTITUENTS OF A COATING

Permanent mold coatings may be divided into two general groups: insulating and lubricating[1,7]. Some coatings perform both functions. In any permanent mold coating, four basic constituents determine the usage, method of application, method of curing and performance when cast[8-9]. These include fillers, carrier liquids, suspension agents, and binders. Table 1 lists the composition of some typical coating slurries for permanent molds[1].

Fillers

The refractory filler determines the effectiveness of the coating in preventing erosion and metal mold reactions. It is selected according to the metal to be cast, the substrate (the mold wall), and possible defects.

The refractoriness and the sintering point of the material are extremely important. In addition, the filler must have the correct particle size, not react with the metal, and withstand wetting by molten metal. Certain fillers may contain compounds that evolve gases during casting and thus must be used with discretion. Properties of the most important fillers are listed in Table 2[9].

Thermal conductivity and thermal expansion of the filler affect heat expansion of the mold substrate. Thermal conductivity and thermal radiation (white vs. black

coating) also play an important part in the rate of substrate heating and in the rate of solidification of the casting.

The selected filler should not be too fine. Fine filler particles increase the risk of cracking in the fired coating and increase the proportion of binder required. Table 3[9] lists the suitability of various fillers for several metal casting alloys. Their behavior may be summarized as follows.

Ground coke - Coke is used mainly in coatings for casting of gray iron and nodular iron. Its properties may vary considerably due to salt contamination. The advantages of coke are high melting point, low reactivity and low wettability for almost all cast metals; its major disadvantage is its high porosity, which causes slow drying of the coating.

Graphite - Natural and electrode graphites serve as filler for many coatings. They are highly refractory and are not wetted by many metals. Pure graphite-based coatings are widely used in automotive and intricate iron casting production. As a refractory, graphite's high thermal conductivity and heat absorption by radiation make it unattractive for large castings, particularly when the mold substrate must be insulated.

Zircon - Along with graphite and talc, zircon is a major coating refractory. It is used alone or is combined with other refractories for copper, gray iron and nodular iron castings. Zircon has many favorable properties. The material bonds well and its sintering range begins at temperatures far below the melting point; this reduces the stresses in the coating, thus reducing spalling and minimizing defects.

Mica - Mica is a hydrated aluminum silicate with a flake-like structure. When it is heated, water is evolved and its structure is changed, causing the material to expand slightly. Due to mica's relatively low melting point, its early application was almost exclusively for copper alloys. Later, in the manufacture of automotive iron castings, mica was used as an insulating coating.

Talc - Talc is a complex hydrated magnesium silicate. Often found in conjunction with magnesium carbonate, it is used as the refractory in coatings for gray and nodular iron and for nonferrous metals. It has been found that talc additions improve the ability of metal to flow over a coating and reduce the risk of pinholing in gray iron[9]. Talc's insulating properties have proved useful in controlling the solidification rate in automotive castings[9].

Calcined magnesite - Due to its high melting point, magnesium oxide is useful for cast iron. It requires an anhydrous medium, since the formation of hydrated oxides in an aqueous phase leads to a hard-packed sediment, which makes application of the coating difficult.

Aluminum silicates - Pyrophyllite ($A_{12}Si_4O_{10}OH$), with its high melting point, is suitable for the casting of copper alloys and cast iron.

Chamotte - Chamotte is suitable as a refractory material for gray iron. However, pure chamotte-based coatings are not commonly used.

Carrier liquids

Filler is suspended in a carrier liquid, the choice of which is governed by operational conditions (such as drying and exhaust) and methods of application. Water is the most important carrier liquid due to its non-toxicity, low price and ease of adjustment of rheological properties.

For coatings that must be flame or air dried, alcohols (and less commonly petroleum-based solvents) are used. Occasionally rapid air-drying solvents are needed; these are normally of the chlorinated type. They are more costly and hazardous than alcohols, but may be used if adequate ventilation is present.

Suspension agents

Suspension agents are used to prevent settling of the refractory materials.

Addition of a suspension agent to a mold coating increases the risk of cracking.

Bentonites and clays are often used as suspension agents in aqueous systems. Their advantage lies in good thixotropic behavior and an ability to act as a high temperature binder. The long time needed to stabilize coatings that contain bentonite is, however, a drawback.

Celluloses and alginates are also used in aqueous systems. Risk of cracking of the dried coating is lower with alginates than with bentonite, while celluloses produce systems that tend to run and tear[9].

Binders

In aqueous systems, dextrins, sulfite lyes and partly unsaturated carbonic acid esters (such as linseed oil) are used as ambient temperature binders. With dextrins and those sulfite lyes sensitive to bacterial decomposition, anti-fermentation agents are necessary. All ambient temperature binders maximize their bonding strength at higher temperatures. However, abrasion resistance of the coatings decreases when the drying temperatures are too high.

Bentonites, other clays, phosphates and sodium silicate serve as high-temperature binders in aqueous systems. However, flocculation or peptisation may occur when using the phosphates or sodium silicate with bentonite. In addition to conventional water-soluble binders, dispersion binders similar to dye industry systems are employed. These binders dry irreversibly in air.

Alcohol-soluble synthetic resins such as novalacs, maleinates and ketones, together with natural resins and alcohol-soluble plastics, serve as binders in alcohol systems. The choice of binder is made according to its bonding relationship with a given individual refractory. For instance, binders with a good bonding capacity for graphite may not be suitable for zircon.

COATING PROCEDURES

To prolong mold life, a coating should be noncorrosive. It must adhere well to the mold and yet be easy to remove. Avoiding direct contact between molten metal and the mold surfaces is essential.

A mold coating must be inert to the cast metal and free of reactive or gas-producing materials. If insulation is needed to prevent thin sections, gates, and risers from solidifying too quickly, then fireclay, metal oxides, diatomaceous earth, whiting (chalk), soap stone, mica, vermiculite, or talc can be added to the mold coating. Graphite is added if accelerated cooling of the casting is needed. Lubricants, which facilitate removal of castings from molds, include soapstone, talc, mica, and graphite[1]. The various requirements of mold coatings are not always obtained with one coating formulation. These requirements are often met by applying different coatings to various locations in the mold cavity.

Mold Preparation and Prime Coats

The mold surface must be clean and free of oil and grease. Portions to be coated should be lightly sand blasted. If the coating is being applied with a spray, then the mold should be hot enough--400 °F (205 °C)[1]--to evaporate water immediately.

For optimum retention of the coating to the mold substrate, a primer coat, or water wash, should be applied before spraying the mold. Water wash is a highly dilute solution of mold coating. Dilute kaolin makes an excellent primer. An acceptable alternative is a 20 to 1 dilution of the coating to be sprayed[1]. By lightly oxidizing the mold surface, the water wash provides a substrate to which subsequent layers can stick. It should be sprayed until the mold's dark color starts to disappear. Lubricating materials or coatings cannot be used as primers. Though lubricants can be sprayed over insulating coatings, the latter will not adhere to the former.

Application Methods

The coating can be applied by brushing, dipping, swabbing or spraying. It must be thick enough to fill minor surface imperfections, such as scratches. How it dries is crucial: A smooth texture is desired on mold areas of light draft that form ribs and walls in the casting; a rough texture is preferred for large, flat areas of the mold to permit entrapped air to escape. Good cast surfaces are obtained when the coating has a matte or textured finish. Extremely smooth coatings increase the formation of oxide skins. Several application methods are employed:

Brushing - Brushing is the simplest method of applying the coating. However, it takes time and skill for the coating to have the desired uniformity.

Dipping - Dipping, the fastest method, is well adapted to mass production.

Swabbing - Swabbing is an extension of the brushing process with an emphasis on medium to large mold applications. Swabbing can be faster than brushing, provided the correct coating viscosity is achieved, and deep cavities can be coated relatively easily. Application through swabbing can also result in elimination of brush marks and, under certain circumstances, a thick coating can be achieved quickly.

Spraying - In practice for a long time, special equipment has been developed for this process. Pressure spraying units are preferred for viscous coatings. A coating with a matte or textured finish is best obtained by spraying.

Behavior of the coating during processing must fit the application method, and special properties of the process must be taken into account. Since each technique requires distinct rheological conditions, no universal coating suits all processes. For example, during brushing, potential brush marks should even out; flow should occur but without running. However such flow has a negative effect during dipping: fluctuations in coating thickness are severe and tearing occurs. A dip must therefore have a short flow-character; i.e., it must develop no flow movement or only a short movement in the resting state.

COATING LIFE

Coating life varies considerably with the temperature of the metal being cast, the size and complexity of the mold cavity, and the rate of pouring. Some molds require recoating at the beginning of each shift; others may run for several shifts with only spot repairs or touchups before recoating is needed. Light abrasive blasting is used to prepare the coating for touchup or to remove old coats.

MOLD COATINGS FOR SPECIAL CASTING ALLOYS.

The metal being cast has a major influence on the type of coating selected. Lubricating coatings are usually selected for the casting of aluminum and magnesium. Relatively complex mixtures are sometimes used. For the casting of copper alloys--with their high pouring temperatures and high thermal conductivities--an insulating type of mold coating is generally required. For small draft angles, lubricating mold coatings may also be required.

Mold coatings used in the production of gray iron castings are divided into two categories[1]: an initial coating, applied before the mold is placed in production, and a subsequent coating of soot (carbon), applied prior to each pour. The initial coating may consist of sodium silicate (water glass) and finely divided pipe clay, mixed in a volume ratio of 1 to 4 with enough water (usually about 15 parts by volume) to allow spraying or brushing. The secondary coating is a layer of soot deposited on the mold face and cavities for each pour. Acetylene gas is burned to form soot.

THERMAL PROPERTIES OF COATINGS

Mold coatings affect heat transfer differently for different metal casting processes. Coatings for permanent molds (good conductors) affect heat transfer rate significantly, while coatings for insulating molds, such as sand molds, don't. This is because the heat transfer resistance of the coating in the permanent mold process is a

large portion of the total heat transfer resistance within the mold and the casting, while the heat transfer resistance of the coating for the insulating molds is a very small portion of the total resistance. This can be shown as below.

The total heat transfer resistance, R, within a metal-mold system consists of the resistances of the mold wall, the coating, the air gap and the metal casting. It may be expressed as

$$R = \frac{L_m}{k_m} + \frac{L_c}{k_c} + \frac{1}{h_g} + \frac{L_{mt}}{k_{mt}} \qquad (1)$$

where L_m, L_C, L_{mt} represent the thicknesses of mold, coating and metal casting, respectively; k_m, k_C, k_{mt} are the thermal conductivities of mold, coating and metal casting, respectively; and h_g is the heat transfer coefficient across the air gap. Figure 1 shows this situation.

Thermal conductivity k_m of an insulating mold is only ~ 0.01 to 0.02 that of the metal[10] (k_C is on the same order of magnitude, but L_C is much smaller than L_m). Almost all the thermal resistance to the heat transfer is treated as within the mold itself. That is

$$R \approx \frac{L_m}{k_m} \qquad (2)$$

For a permanent mold, the thermal resistance of the coating and gap, L_C/k_C and $1/h_g$, cannot be neglected. They may be much greater than that of the metal casting, L_{mt}/k_{mt}, and that of the metal mold, L_m/k_m, and can therefore be used to change the casting's rate of solidification tenfold or more[11].

Almost all coatings are a mixture of one or more solid phases together with a pore phase. The conductivity of this mixture depends on the arrangement of the phases

present. The thermal conductivity of the coating, k_c, is different from the intrinsic thermal conductivity of the individual particles that make up the coating. On a microscopic level, the coating is porous so heat is actually transferred by intrinsic conduction through each particle, by point to point conduction among particles that are in contact, and by conduction and convection through the gas in the pores. In addition, radiation across the pores leads to heat transfer from particle to particle. The thermal conductivity, k_c, therefore, involves several factors: particle material, particle size, binder, volume fraction of pores, the gas in the pores, emissivity of the particles, and temperature. The calculation methods for the conductivity of coatings for different situations will be introduced as below.

Rules of Mixture

The rules of mixture are used for calculation of the thermal conductivity of two-solid phases that are in intimate contact. The idealized distributions of the two solid phases include a continuous major phase (the one with a larger proportion) with spherical inclusions of a secondary phase (Figure 2a) and nearly spherical particles of a discontinuous major phase with a continuous secondary phase (Figure 2b). The conductivity of the mixture is given by[13]

$$k_{mix} = k_{con} \frac{1+2V\dfrac{1-k_{con}/k_d}{1+2k_{con}/k_d}}{1-V_d\dfrac{1-k_{con}/k_d}{1+k_{con}/k_d}} \qquad (3)$$

where k_{con} and k_d are the thermal conductivities of the continuous phase and the dispersed phase, respectively. When k_{con} is much greater than k_d, then

$$k_{mix} \cong k_{con}\frac{1-V_d}{1+V_d/2} \tag{4}$$

If $k_{con} << k_d$, then

$$k_{mix} \cong k_{con}\frac{1+2V_d}{1-V_d} \tag{5}$$

A general empirical equation that can be used for a variety of mixtures is

$$k^n = \sum V_i k_i^n \tag{6}$$

where n is an exponent lying between -1 and +1 and V_i is the fraction of the volume occupied by phase i. Empirical correlations of experimental data are frequently made simpler by using Eq. 6 with the exponent obtained from statistical analysis of the experimental data.

Porosity

In addition to the solid phases present, almost all coatings contain a certain amount of porosity. Its effect on the thermal conductivity of the overall coating depends on the conductivity of the pores. At low temperatures, the gas in the pores has a lower thermal conductivity than any of the solid phases. It can be introduced into Eqs. 3 to 5 with an effective zero conductivity to obtain

$$k_c = k_{mix}(1-P) \tag{7}$$

as a good approximation for a continuous solid phase with isolated pores, where P is the fraction porosity. If the pore phase is continuous, as in a powder, the actual

conductivity of the pore must be considered.

In addition to the conductivity of the gas in the pores (convection is only important in pores larger than several millimeters in diameter[13]), radiation across the pores significantly contributes to heat transfer at high temperatures. Therefore, Eq. 7 is not valid for high temperatures.

The effect of radiation on effective conductivity of a pore phase can be calculated when the temperature gradient is small in the pore. Heat transfer between two parallel plates at different temperature when the intervening medium does not absorb any of the energy (for gas in the pores, it can treated as if it has zero absorbability since the gas layer is very thin) is given by

$$q = n^2 \sigma E_E A (T_1^4 - T_2^4) \qquad (8)$$

where n is the index of refraction, $E_E = E/2$, E is the effective emissivity with emission and reflection from both surfaces included, σ is the radiation constant, A is the surface area, and T_1 and T_2 are the surface temperatures. The term of $T_1^4 - T_2^4$ in Eq. (8) can be factored to $(T_1 - T_2)(T_1 + T_2)(T_1^2 + T_2^2)$; $T_1 + T_2$ nearly equals $2T_m$, and $T_1^2 + T_2^2$ nearly equals $2T_m^2$, where T_m is the mean temperature. Then Eq. (8) becomes

$$q = 4n^2 \sigma E_E A T_m^3 \Delta T \qquad (9)$$

If the heat transfer across a flat cavity is considered with parallel sides and a thickness d_p, an effective conductivity can be defined by the relationship[13]

$$q = -k_{eff} A \frac{\Delta T}{d_p} \qquad (10)$$

By comparing Eqs. (9) and (10), the effective thermal conductivity of the radiant heat

transfer in a pore is given by

$$k_{eff} = 4d_p n^2 \sigma E_E T_m^3 \qquad (11)$$

The effect of radiation on conductivity is directly proportional to pore size, emissivity, and the third power of the mean temperature. When the pore size is large, and the temperature and the emissivity are sufficiently high, the effective thermal conductivity of the porous material can be close to or even higher than that of the same material without pores. As a example, the conductivity of zirconia brick containing different-sized pores and different emissivities over a wide temperature range is illustrated in Figures 3a and 3b[13]. It can been seen that the conductivity of zirconia with large pore size increases significantly at high temperatures (Figure 3b), while the conductivity of zirconia with small pore size remains relatively low at high temperature compared to the solid zirconia (Figure 3a).

Therefore, the pore size is particularly important as a microstructure feature in determining heat transfer properties at high temperatures. For optimum thermal resistance, it is desirable to have the pore size small and the pore phase continuous. As mentioned previously, a pulverized material has much lower thermal conductivity than the same solid material. For instance, solid graphite has a very high conductivity, but when it is pulverized, the conductivity decreases significantly (see Table 4). If a material can maintain its small pore size at high temperature, it can be used as a good insulator even if it is a good heat conductor in the solid form (no pores in it). This is the reason why powdered mixtures of very fine materials (so, very small pore size) are the most effective kind of insulation. Even when graphite (normally assumed to be a chilling type of coating) is used in powder form, the coating will be more of an insulator, both because of the fine pore size (as indicated in Table 4) and because the graphite will not sinter during firing or use in the mold. This is also the reason why it is

difficult to make really satisfactory high-temperature insulating materials from fireclay compositions. The sintering of the fireclay particles makes the small pores disappear.

The effect of emissivity on the effective conductivity explains why it takes less time for a mold substrate with a black coating to reach a given temperature than for a mold substrate with a white coating[9]. This is because black coatings have higher emissivity than white coatings. The emissivity is in a range of 0.3 to 0.5 for most oxide materials, whereas for black coatings such as carbides and graphite it is 0.7 to 0.9.

Table 4 lists thermal properties of most basic fillers for the permanent mold casting process[11,15-18]. It can be seen that powdered materials have much lower thermal conductivity than those that are not pulverized. Therefore, thermal conductivity can be controlled by changing porosity. Tables 5 and 6[19] (their compositions are given in Table 7) list conductivity data for some single component and some multi-component coatings, respectively. These coatings have very low conductivities since they have very high porosity. High porosity was achieved by including finely comminuted sawdust or coke dust (0.25 mm diameters). After the first charge of metal this dust was burnt out, leaving pores that reduced the thermal conductivity.

The thermal properties for most raw single-component coating materials (binders are not added) are described in the literature. It is hard to obtain data for multi-component coatings (including single-component coatings with binder) for two reasons. First, the thermal properties of coatings are complicated. Second, little work has been done on them. If precise data are not required, thermal properties can be calculated by the methods mentioned previously. If accurate data are required, the conductivity must be obtained experimentally. Therefore a test procedure must be designed where a commonly used mold material of a given thickness and known thermal conductivity can be used as a coating substrate onto which is applied a predetermined, measurable and consistent coating. In this way, when the thermal conductivity is measured again,

the only change will be due to the nature of the coating material and not the mold substrate, coating thickness, or dilution of the coating. Of course, once this database is established, typical foundry variables such as coating thickness and dilution of the coating can be measured as to their effect on the thermal conductivity of the entire system. One of the subjects of a collaborative effort between the American Foundrymen's Society, University of Missouri-Rolla (UMR), and US Department of Energy is to conduct such experimental tests under The Penn State University - UMR Metal Casting Competitiveness Research Program.

Note that the coating has a strong effect only during the initial cooling period (removal of superheat, freezing of metal). At that point, the amount of heat lost from the casting to the mold is determined by the coating. But the coating has considerably less effect on the solid casting's rate of cooling at lower temperatures. This is because the coefficient of heat transfer through the coating layer is normally much greater than the coefficient of thermal diffusivity at the outside surface of the mold (with natural cooling from exposure to air). Consequently, the temperature difference between the casting and the mold rapidly disappears. Further cooling of the casting-mold system is then limited by convective and radiative heat transfer from the exterior of the mold.

HEAT TRANSFER COEFFICIENT OF THE GAP

Early in the solidification process, the resistance to heat transfer across the gap that forms at the mold-casting interface or mold-coating interface can also influence overall heat transfer.

Figure 4 shows schematically the formation of a gap during casting. This process occurs in the following steps[12].

(1) Liquid metal is in contact with the mold coating. Heat transfer is controlled by the thermal conductivity of the coating.

(2) Solidified metal is in contact with the mold coating. There is probably

some reduction in heat transfer, but the metal is still in good contact with the uneven mold coating, and heat transfer is still controlled by the thermal conductivity of the coating.

(3) The solidified shell contracts. There is no longer any intimate contact across the uneven interface, and heat transfer is reduced drastically.

If the characteristics of the gap are precisely known -- thickness variation with time, composition of the gas within the gap, and the emissivities of mold or coating (if a coating is used) and casting surfaces -- then the heat transfer across the gap can be estimated. Since such attempts usually fail, heat transfer associated with a gap is often treated empirically with a gap heat transfer coefficient (h_g), defined by the heat flux across the gap. The heat flux is

$$q = h_g \Delta T \qquad (12)$$

where ΔT is the temperature difference between the casting and the mold or coating. Because the characteristics of the gap are not precisely known, actual values of h_g can only be determined empirically. Table 8 lists some useful data for h_g[10].

ECONOMICS OF COATINGS

Costs of materials and coating processes are only a small percentage of the cost of the molds. Yet a suitable coating can substantially improve casting quality and prolong mold life. With greater realization of their benefits, the use of coatings in the permanent mold casting process is rapidly increasing, and the coatings play an increasingly important role in successful and profitable casting production.

CONCLUSION

A technical review of mold coatings for the permanent mold casting process has

been provided. Though data exist in the literature for the thermal properties of individual component of the coating materials, no studies have been conducted on thermal properties of multi-component coatings. Thus, there is a critical need for establishing a test procedure to obtain the thermal properties of permanent mold coatings that are typically used in the permanent mold foundry industry.

ACKNOWLEDGMENT

The authors wish to thank the U.S. Department of Energy, the Assistant Secretary for Energy Efficiency and Renewable Energy, under DOE Idaho Operations Office, Contract DE-FC07-93ID13235, for providing funds to support this research. Special thanks also goes to the Center for Technology Transfer and Economic Development at University of Missouri for providing matching fund for this research.

REFERENCES

1. *Metals Handbook* , ASM International, 9th edition, Vol. 15, pp 281.
2. F. Chiesa; "Measurement of the Thermal Conductance at the Mold/Metal Interface of Permanent Molds," *AFS Transactions*, 90-10, 1990, pp 193-200.
3. V. Mohan and R.N. Shenoy; "Prediction of Solidification Time of Iron Castings in Coated Cast Iron Molds," *AFS Transactions*, 82-80, 1982, pp 435-444.
4. Y. Ohtsuka etc.; "Application of a Computer Simulation System to Aluminum Permanent Mold Castings," *AFS Transactions*, 82-89, 1982, pp 635-646.
5. K.V.K. Nehru; "Influence of Insulating Mold Coatings on the Solidification of Copper Castings in Metallic Molds and Thermal Behavior of Molds," *AFS Cast Metals Research Journal*, Sept. 1974, Vol. 10, No. 3, pp 111-116.
6. Kenji Chijiiwa; "Research on the Behavior of Cast Metals in Mold Cavities by the Color Method," *Cast Metals Research Journal*, Sept. 1967, pp 113-119.
7. *AFS Mold Method and Materials*, First Edition, 1962
8. D.R. Bayliss etc.; "Mould and Core Coatings: first report of working group P8," *The British Foundryman*, Vol. 69, 1976, pp 25-38.
9. A.J. Broome; "Mould and Core Coatings and their Application," *The British Foundryman*, Vol. 73, 1980, pp 96-102.
10. D.R. Poirier and E.J. Poirier; *Heat Transfer Fundamentals for Metal Casting*, TMS, Warrendale, 1991.
11. A.I. Veiney; *Thermodynamics for the Foundryman*, Maclaren and Son's Ltd., London, 1968
12. V. de. L. Davies; "Heat Transfer in Gravity Die Castings," *The British Foundryman*, Vol. 73, 1980, pp 331-334.
13. W.D. Kingery; *Introduction to Ceramics*, John Wiley & Sons, Inc., New York, 1960, pp 502.

14. M. Isotani etc.; "Thermal Properties of Coatings in Metal Molds for Cast Iron," *AFS Cast Metal Research Journal*, June 1969, Vol. 5, No. 2, pp 90-92.

15. *Thermophysical Properties of Matter*, Vol. 2, IFI/Plenum·New York-Washington, 1970.

16. Kuzman Raznjevic; *Handbook of Thermodynamic Tables and Charts*, London, 1976, pp 37-40.

17. S.T. Hsu; *Engineering Heat Transfer*, D. Van Nostrand Company, Inc. New York, 1963.

18. E.J. Smoke; *Thermal Properties of Ceramics*, New Jersey, 1958.

19. A.I. Veynik; *Theory of Special Casting Methods*, The American Society of Mechanical Engineers, New York, 1962.

CAPTIONS TO TABLES

CAPTIONS TO FIGURES

FORMULAS

1. $$R = \frac{L_m}{k_m} + \frac{L_c}{k_c} + \frac{1}{h_g} + \frac{L_{mt}}{k_{mt}}$$

2. $$k_{mix} \cong k_{con}\frac{1 - V_d}{1 + V_d/2}$$

3. $$k_{mix} = k_{con}\frac{1 + 2V\dfrac{1 - k_{con}/k_d}{1 + 2\,k_{con}/k_d}}{1 - V_d\dfrac{1 - k_{con}/k_d}{1 + k_{con}/k_d}}$$

4. $$k_{mix} \cong k_{con}\frac{1 - V_d}{1 + V_d/2}$$

5. $$k_{mix} \cong k_{con}\frac{1 + 2V_d}{1 - V_d}$$

6. $$k_i^n = \sum V_i k_i^n$$

7. $$k_c = k_{mix}(1 - P)$$

8. $$q = n^2 \sigma E_E A(T_1^4 - T_2^4)$$

9. $$q = 4n^2 \sigma E_E A T_m^3 \Delta T$$

10. $$q = -k_{eff} A\frac{\Delta T}{d_p}$$

11. $k_{eff} = 4 d_p n^2 \sigma E_E T_m^3$

12. $q = h_z \Delta T$

Table 1 Typical composition of coating slurries for permanent molds, % by weight (remainder, water)[1]

Coating No.	Composition									
		Insulators				Lubricants				
	Sodium silicate	Whiting	Fireclay	Metal oxide	Diatoma-ceous earth	Soap stone	Talc	Mica	Graphite	Boric acid
1	2		4						1	
2	8		4							
3		7								7
4	12	9								
5	5	11		2			5			
6	9		4			14				
7	11			17						
8			4			23		5		
9	7		1			23		2		
10	23						20			
11	30				5		10			
12	18				41					
13	8			60						
14	7						62			
15	20	53								

Table 2 Properties of some refractory fillers[9]

Refractory	Chemical formula	Density (g/cc)	Melting point (°C)
Coke	C	1.6 - 1.8	-
Graphite	C	2.1 - 2.3	>3000
Silica	SiO_2	2.65	1800
Zircon	$ZrSiO_4$	4.0 - 4.8	2200
Mica	$KAl_2(OH,F)_2Si_3AlO_{10}$	2.3	750 - 1100
Calcined Magnesite	MgO	3.5 - 3.7	2800
Alumina silicate	$Al_2O_3SiO_2$	2.6 - 3.0	-
Chamotte	-	2.6	1700
Alumina	Al_2O_3	3.9	2050

Table 3 Suitability of fillers for common casting alloys[9]

Alloy	Coke	Graphite	Silica	Zircon	Mica	Talc	Calcined Alumina	Magne-site	Chamotte
Cast Steel	0	0	0	+	-	-	0	-	+
Alloy cast steel	0	0	0	-	-	-	+	-	+
Cast iron	-	+	-	+	0	+	-	0	-
Nodular Iron	-	+	+	+	0	+	-	0	-
Malleable iron	+	+	+	+	0	+	-	0	-
Copper Alloys	+	+	-	0	+	+	0	+	-
Al Alloys	-	+	-	+	+	+	-	0	-
Mg Alloys	0	0	-	-	-	-	+	-	-

+ Applicable
0 Possible under certain conditions
- Unsuitable or uncommon

Table 4 Thermal properties of raw materials for permanent mold coatings[11, 15-18]

Material	Temperature (°F)	Thermal conductivity k Btu/ft.hr.°F	Density at room temp. lb/ft^3	Specific heat C_p Btu/lb°F	Specific heat Mean temperature °F	Thermal diffusivity ($a=k/pc_p$) ft^2/hr
Coke pulverized	68	0.087	62.4	0.294	68-930	
Diatomaceous Sil-o-cel						
Kieselguhr	32	0.035	21.85		32	
calcined,dry	210	0.044	21.85			
	570	0.052	21.85			
Stirred with water and dried	300	0.056	36.2			
	660	0.083	36.2			
Graphite	122	26	131.6	0.20		1.10
powdered						
(40 mesh)	100	2.7	26.0	0.201	32-212	0.518
(20-40 mesh)	100	8.2	44.0			
(100 mesh)	104	0.104	30.0			
Magnesia powdered	116	0.35		0.222	32-212	
Mica	122	0.25				
Sawdust	98	0.040	12.48			
Silica finely ground	600	0.54	50.0			
	900	0.57				
	1200	0.62				
	1500	0.72				
Soapstone	1040	11.3	175.0			
Talc						
L-5 grade	100	1.08	152.35			
	200	1.85				
	300	1.92				
commercial	100	1.97	153.48			
	200	1.97				
	300	1.97				
Titanium oxide finely ground	1000	0.49	52.0			

Table 5 **Thermal conductivity of some single-component coatings with high porosity[14]**

Material	k, W/(m.°C)
Graphite	0.46
Marshalite (powdered quartz)	0.17
Calcined asbestos	0.17
Water glass	0.14
Powdered chamotte	0.14
Refractory clay	0.12

Table 6 Thermal conductivity of various coatings with high porosity[19]

Coating No.	k, W/(m.°C)
A	0.33
B	0.20
C	0.16
D	0.16
E	0.14
F	0.14
G	0.12
H	0.465
I	0.245
J	0.175
K	0.163
L	0.120

Table 7a **Composition of coating slurries in Table 6, % by weight[19]**

Coating No	Composition							
	Marshalite	Refractory clay	Graphite	Calcined asbetos	Sawdust	Potassium permanga-nate	Water glass	Water
A	4.4	12.5	25.0		0.6		7.5	50.0
B	19.4	12.5	10.0		0.6		7.5	50.0
C	32.0	6.2			1.3		10.5	50.0
D	32.0	6.15			1.2	0.15	10.15	50.0
E	26.9	12.5	2.5		0.6		7.5	50.0
F	7.5	10.0	4.0	20.0			8.5	50.0
G	6.9	25.0	10.0		0.6		7.5	50.0

Table 7b **Composition of coating slurries in Table 6, % by weight[19]**

Coating No	Composition											
	Finely gro-und chalk	Coll oidal gra-phite	Marsh alite	Calcined talc	Fire clay	Fine wood sha-vings	Pota-ssium perman-ganate	Pectic adhe-sive	Bento-nite	Soap stone	Water glass	Water
H		53.4						3.0	3.4	0.2		40.0
I			20.0	15.0							2.5	62.5
J	12.4	1.7									3.3	82.6
K			32.0		6.15	0.12	0.15				10.5	50.0
L	20.0										3.0	77.0

Table 8 **Heat transfer coefficients of the gap**[10]

Casting situation	h_g (Btu/hr.ft$^{2.\circ}$F)
Ductile iron in cast iron mold coated with amorphous carbon	300
Steel in cast iron mold	180
Aluminum alloy in small copper mold	300-450
Steel chilled by steel mold:	
before gap formation*	70-180
after gap formation	70
Aluminum die castings:	
before gap formation*	440-880
after gap formation	70

* With no gap, thermal contact between the casting and the mold is not perfect because of surface tension effects, oxide layers and mold coatings

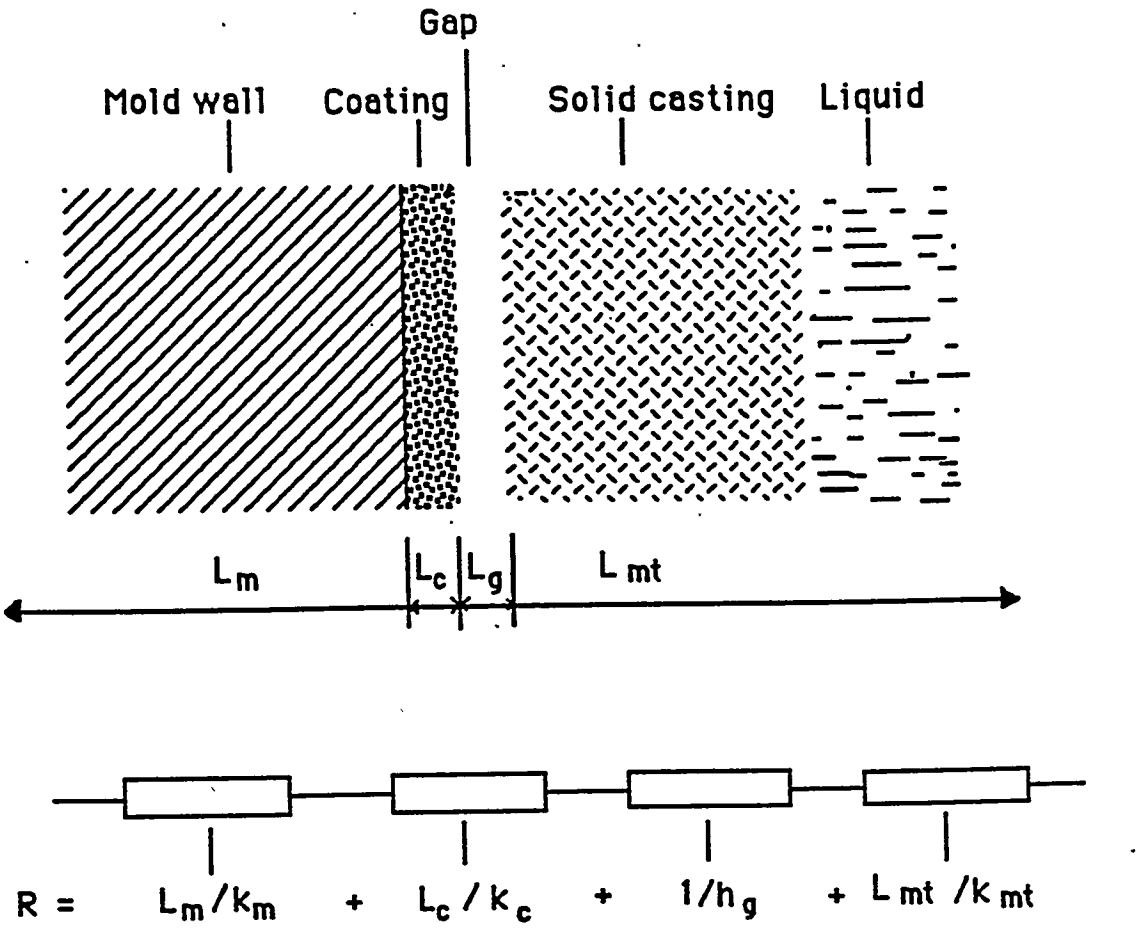

Figure 1 Heat transfer resistance includes contributions from the mold wall, the coating, the air gap, and the casting.

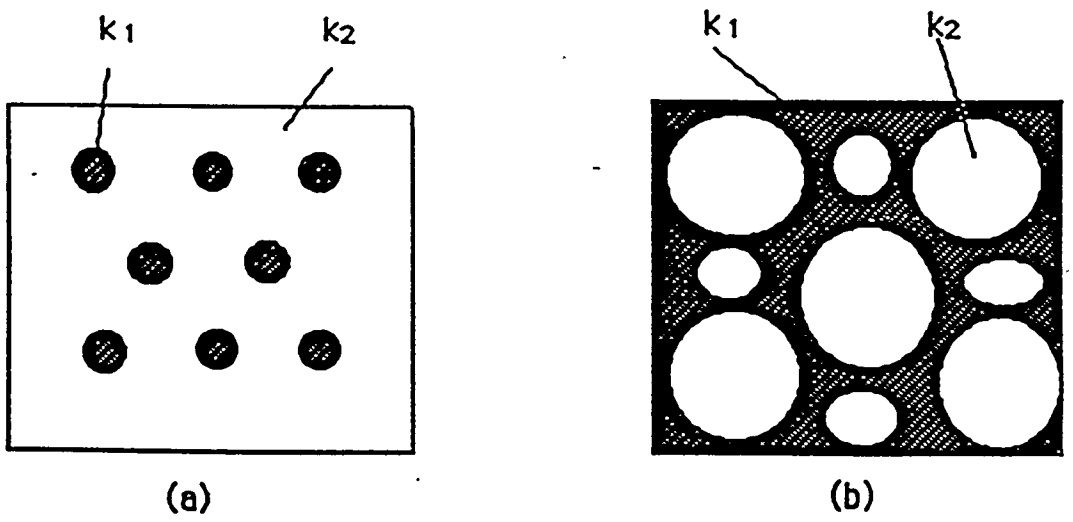

Fig. 2 Phase distributions with (a)continuous major phase and (b)continuous minor phase.

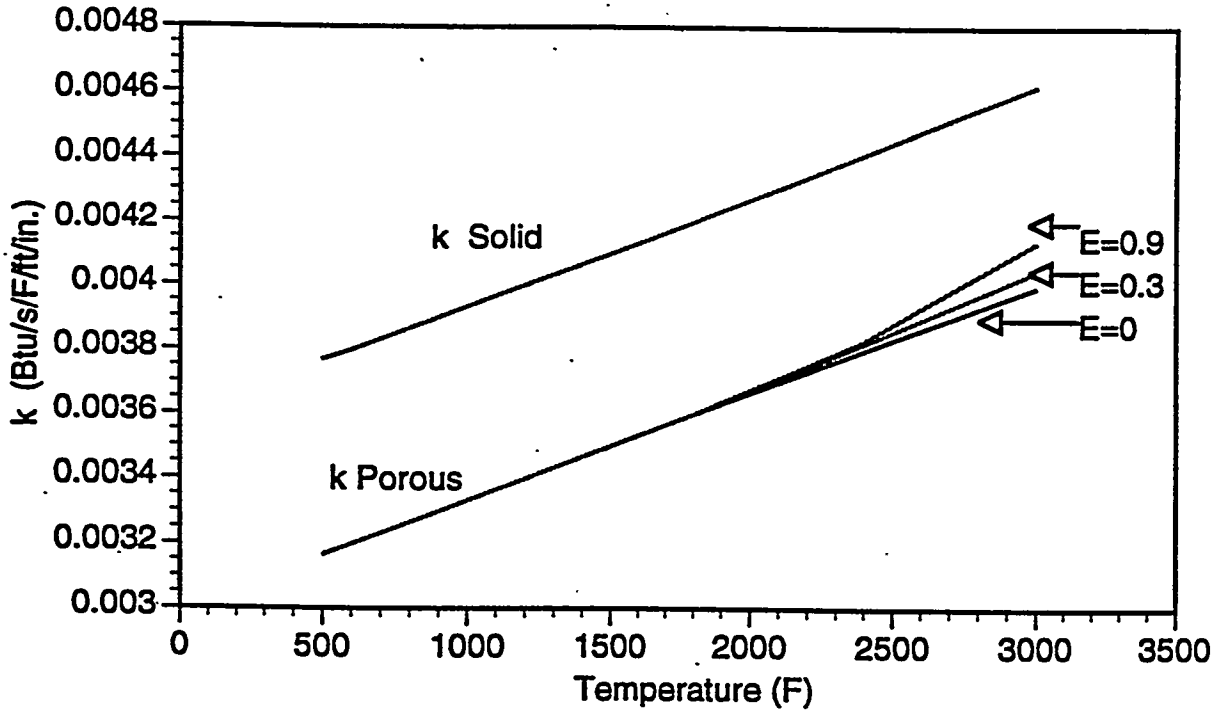

Fig. 3a Effect of small pores on the thermal conductivity of zirconia brick. Pore diameter - 0.004 in.[13]

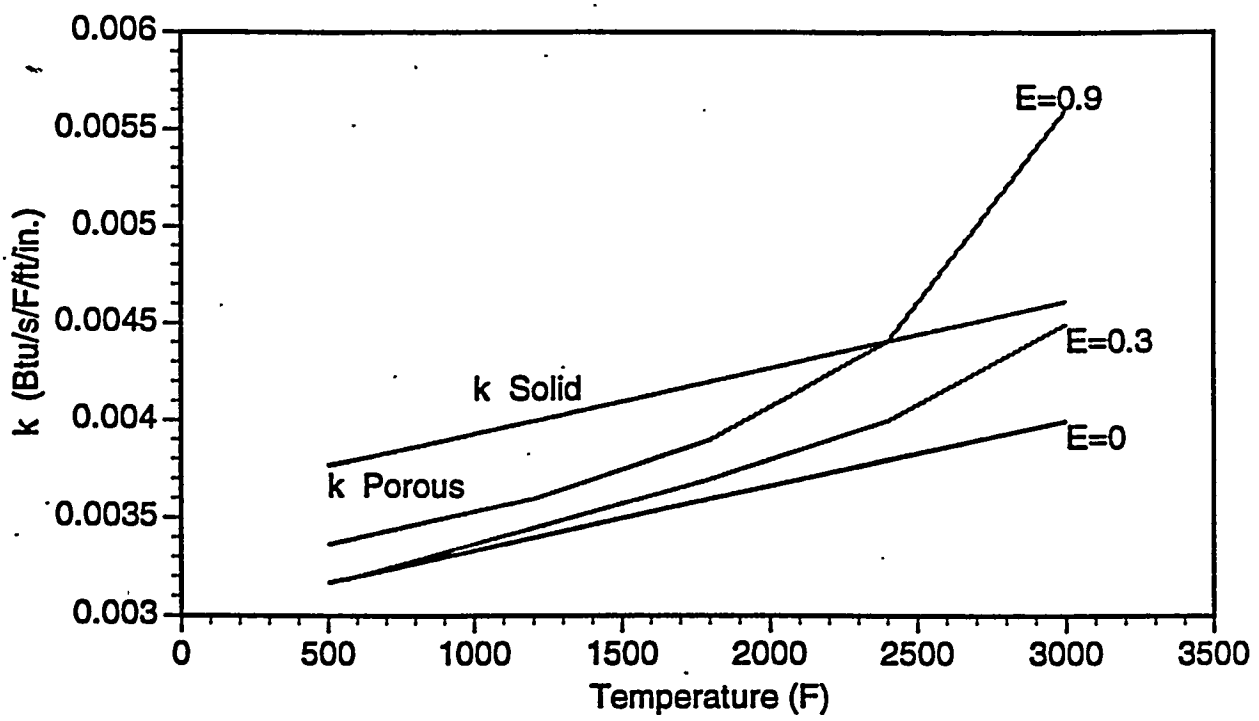

Fig. 3b Effect of large pores on the thermal conductivity of zirconia brick, pore diameter 0.1 in.[13]

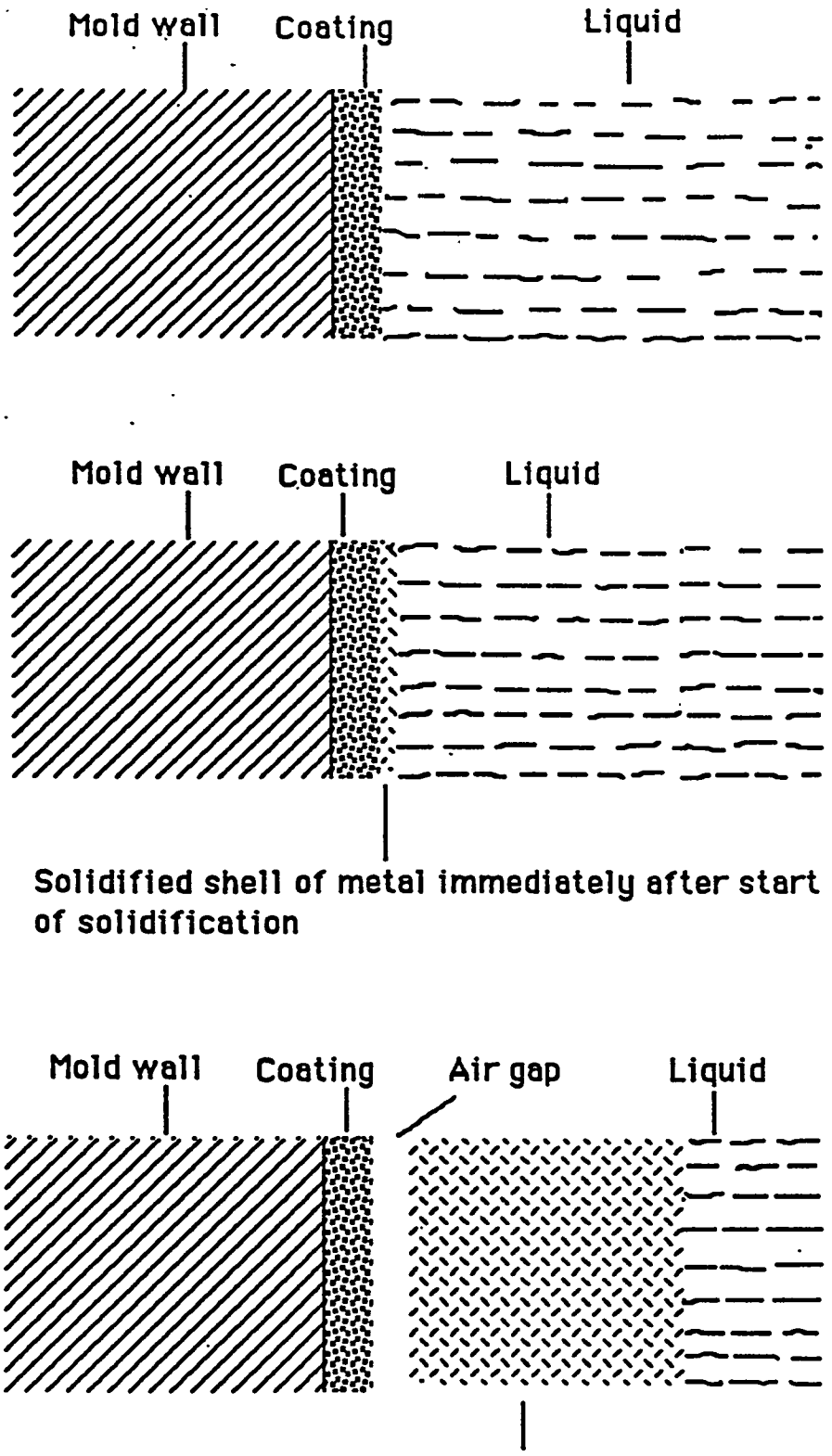

Fig. 4 Schematic describing the development of an air gap during solidification

APPENDIX II

Thermophysical and Mechanical Data for Gray Irons and Thermophysical Data for Aluminum Alloy 356

Thermophysical and Mechanical Data for Gray Irons and Thermophysical Data for Aluminum Alloy 356

Introduction

If a machine part undergoes cyclic temperature changes and if the natural expansions and contractions are either wholly or partially constrained, cyclic strains and stresses result. These cyclic strains produce thermal fatigue failure just as if the strains were produced by external mechanical loading, which arise from the static indeterminacy of the system under the following conditions:

1. Nonuniform heating of cooling of a body when it is not connected to any other bodies;
2. Uniform heating of cooling of a body which has external mechanical restraints to it;
3. Nonuniform heating or cooling of a body with external mechanical restrains.

The First condition is defined as thermal-stress fatigue, and the latter two conditions are defined as thermal-mechanical fatigue[1].

A permanent mold is subjected to cyclic temperature fields, which correspond to conditions 1 and 3 mentioned above. Thermal fatigue is the principle cause of mold failure.

Fatigue failure investigators over years have led to the observation that the fatigue process actually embraces two domains of cyclic stressing or straining that are significantly different in character, and in each of which failure is probably produced by different physical mechanisms. One domain of cyclic loading is that for which significant plastic strain occurs during each cycle. This domain is associated with high loads and short lives, or low numbers of cycles to produce fatigue failure, and is commonly referred to as low-cycle fatigue. The other domain of cyclic loading is that for which the strain cycles are largely confined to the elastic range. This domain is associated with lower loads and long lives, or high numbers of cycles to produce fatigue failure, and is commonly referred to as high-cycle fatigue. Low-cycle fatigue is typically associated with cycle lives from one up to about 10^4-10^5 cycles, and high-cycle fatigue for lives greater than about 10^4 or 10^5 cycles.

Thermal fatigue is in the low-cycle fatigue domain[1-9]. The relationship of thermal fatigue to

low-cycle fatigue is shown in figure 1[1]. It must be pointed out that, in some cases, such as thermal striping, it can occur at frequencies near 1 Hz and give rise to high-cycle fatigue cracking[9].

Obviously, to predict and prevent thermal fatigue problem of permanent molds some basic material data are needed. This includes:

1. Thermal properties of both casting and mold materials, which will be used to determine temperature fields;

2. Mechanical properties of mold materials, which will be used to determine the stress and strain distributions in the mold;

3. Fatigue properties of mold materials that link the stress and strains to fatigue life, including crack initiation, growth and fracture in the mold.

Since gray cast iron is the mold material most used (see Table 1[3]), This paper will concentrate on collecting the data for gray cast iron. Aluminum alloy 356 is used in our experiment, therefore, its data are also included.

The Thermophysical and Mechanical Data

The data for gray cast iron, which are all functions of temperature, are enough for calculations of heat transfer, temperature profile, stress, strain and fatigue life of a permanent mold. The data for aluminum alloy 356 are chosen for filling and solidification, since those are all needed. Some of the data are listed in tabular form, which are convenient to put into a database. Others are shown in graphic form, since the scattered data points make no sense unless they are regressed. The data on the regressive curves are therefore recommended to use. The data sources are listed in references #10-#15.

1. D.A. Spera, "What is Thermal Fatigue", *Thermal Fatigue of Materials and Components,* STP 621, ASTM, 1976 pp. 3-9

2. J.A. Collins, *Failure of Materials in Mechanical Design,* John Wiley & Son, 1981

3. ASM Committee on Production of Permanent Mold Castings, "Permanent Mold Casting", Metals Handbook, 8th edition, Vol. 5, 1961 pp. 265-284

4. S.S. Manson, "A method of Estimating High-temperature Low-cycle Fatigue Behavior of Materials", *Thermal and High-strain Fatigue,* The Metals and Metallurgy Trust, 1967 pp. 154-171

5. L.F. Coffin, "A Study of the Effect of Cyclic Thermal Stresses on a Ductile Metal", *ASME Trans.* Vol. 79, 1954 pp. 931-950

6. L.F. Coffin, "An Investigation of Thermal-Stress Fatigue as Related to High-temperature Piping Flexibility", *ASME Trans.* Vol. 79, 1957, pp.1637-1651

7. Ya.B. Fridman, *Strength and Deformation in Nonuniform Temperature Fields*, c/b Consultants Bureau, New York, 1964

8. S.S. Manson, *Thermal Stress and Low-Cycle Fatigue*, McGraw-Hill Book Company, New York, 1966.

9. R. Viswanathan, *Damage Mechanisms and Life Assessment of High-Temperature Components,* ASM International, Metals Park, Ohio, 1989.

10. H.T. Angus, *Cast Iron: Physical and Engineering Properties,* Butterworths, London-Boston, 1976

11. R.B. Grundlach, "The Effects of Alloying Elements on the Elevated Temperature Properties of Gray Irons", *AFS Transaction*, 1983, pp. 389-422

12. Charles Lipson, *Handbook of Stress and Strength,* The Macmillan Company, New York, 1963

13. TPRC, *Thermophysical Properties of High Temperature Solid Materials,* Vol. 3, 1967, The Macmillan Company, New York.

14. *Structural Alloys Handbook,* Vol. 1, 1985, Metals and Ceramics Information Center.

15. ProCAST database, which were obtained form National Technical Information Servece Handbook

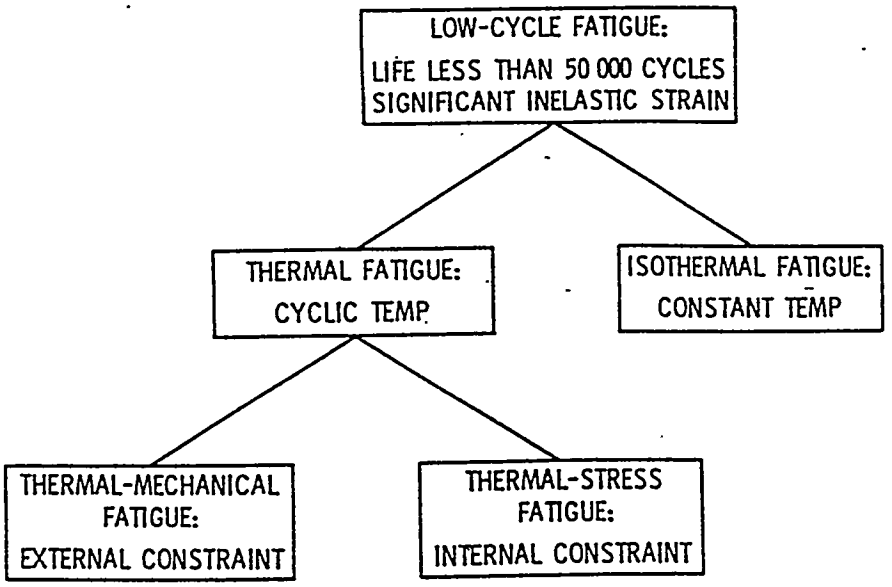

FIG. 1—*Proposed terminology for high temperature fatigue.*

Table 1. Recommended Materials for Permanent Molds

Alloy to be cast	Number of pours: 1,000	10,000	100,000
For Casting Small Parts, 1-In. Maximum Dimension			
Zinc	Gray iron, 1020 steel	Gray iron, 1020 steel	Gray iron, 1020 steel
Aluminum or magnesium	Gray iron, 1020 steel	Gray iron, 1020 steel, H11 die steel	Gray iron with H14 inserts, 1020 steel
Copper	Gray iron	Gray iron	Alloy cast iron
Gray iron	Gray iron(a)	Gray iron(a)	(This quantity not poured)
For Casting Medium and Large Parts, up to 36-In. Maximum Dimension			
Zinc	Gray iron, H11 die steel(b)	Gray iron, H11 die steel(b)	Gray iron, H11 die steel(b)
Aluminum or magnesium	Gray iron	Gray iron	Gray iron, H11, H14(c)
Copper	Alloy cast iron	Alloy cast iron	Alloy cast iron(d)
Gray iron	Gray iron	Gray iron	(This quantity not poured)

NOTE: Gray iron for permanent molds should be of controlled quality with respect to graphite size and soundness of the casting.

(a) Same composition as being poured. (b) Used where polish is required on parts of medium size. (c) Recommendations are for medium-size parts; for large parts, recommended materials are gray iron with H11 inserts or solid H11 die steel. (d) Large parts not poured in these quantities.

Thermophysical Properties for Aluminum Alloy 356*

Liquidus Temperature	615 °C
Solidus Temperature	555 °C
Latent Heat of Fusion	389 KJ/Kg (The volume fraction of eutectic is about 0.6)
Specific Heat	963 J/Kg.K
Thermal Conductivity	
°K	cal/cm/°Csec.
406.67	0.35
420.16	0.366
432.26	0.37
477.01	0.398
589.51	0.40
666.13	0.396
Viscosity	
°C	Centipoise
700	2.90
715	2.52
750	2.15
775	1.775
800	1.40

* Since aluminum alloy 356 has more than 10 kinds, which vary in impurity contents, especially iron content, the thermal property data may vary to some extent. The suppliers should be consulted if accurate data are desired

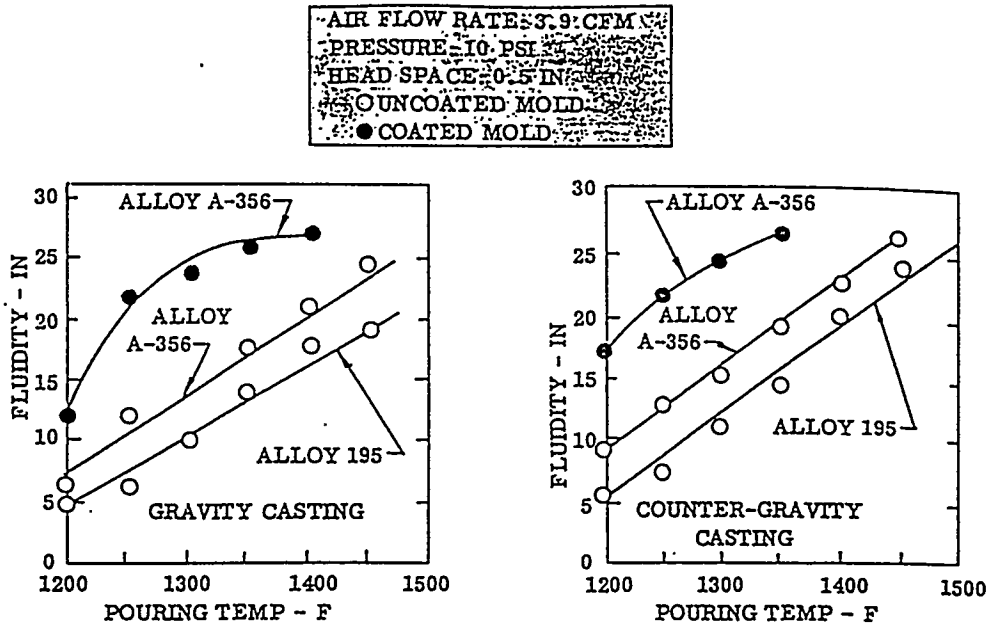

EFFECT OF POURING TEMPERATURE ON FLUIDITY COMPARISON FOR 195 AND A-356 ALUMINUM ALLOYS (12)

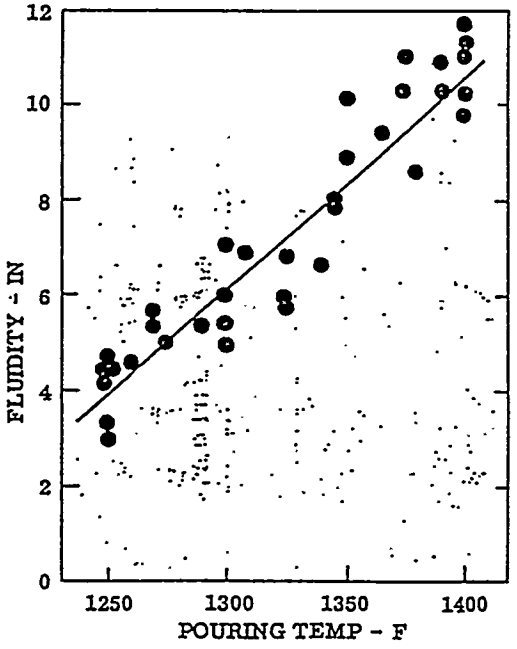

EFFECT OF POURING TEMPERATURE ON FLUIDITY FOR GRAIN REFINED ALUMINUM 195-T6 ALLOY (1)

IRON NO.	CHEMICAL ANALYSIS – % TC	Si	Mn	Cr	Cu	Mo
1	3.19	1.57	0.70	—	—	—
2	3.19	1.57	0.70	—	1.58	—
3	3.12	2.28	0.38	—	—	—
4	3.12	2.28	0.38	0.54	—	0.77

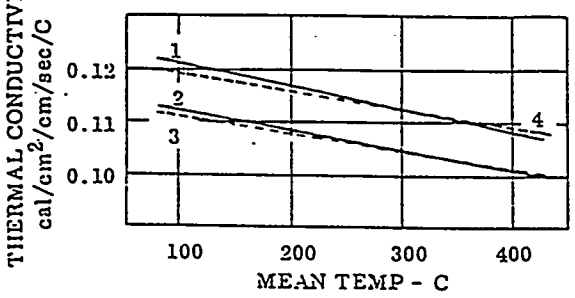

EFFECT OF TEMPERATURE ON THERMAL CONDUCTIVITY (1)

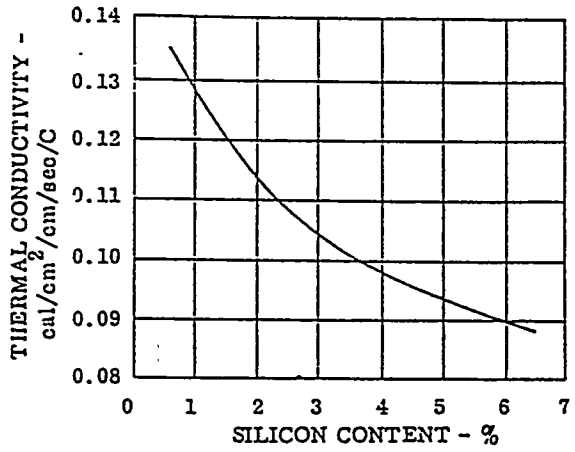

EFFECT OF SILICON ON THE THERMAL CONDUCTIVITY OF IRON (1)

IRON NO.	TC	Si	Mn	Ni	Cr	Mo	TENSILE STRENGTH (KSI)
1	2.56	2.20	0.63	—	—	0.58	56.9
2	3.41	1.03	0.65	1.49	0.54	—	48.2
3	2.61	2.46	0.45	—	—	—	50.8
4	3.10	2.51	3.11	1.00	—	—	55.3
5	2.80	2.51	0.68	1.71	0.54	—	56.0

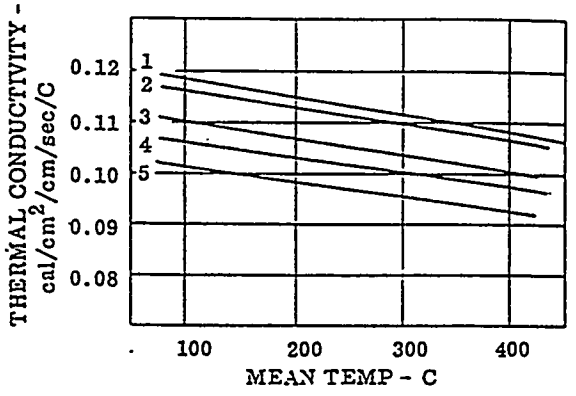

EFFECT OF TEMPERATURE ON THE THERMAL CONDUCTIVITY OF HIGH STRENGTH GRAY IRONS (1)

THERMAL CONDUCTIVITY OF SEVERAL GRAY IRONS (1)

Type of Gray Iron	Chemical Analysis TC	Si	Mn	Ni	Cr	Mo	Cu	W	Thermal Conductivity cal/cm²/cm/sec/C 100 C	400 C
Class 40 + low Si	3.35	0.65	0.85	—	—	—	—	—	0.135	0.114
Class 40 + Cr	3.17	1.40	0.97	—	0.392	—	—	—	0.131	0.115
Class 40 + Ni	3.16	1.56	0.94	0.746	—	—	—	—	0.108	0.101
Class 40 + W	3.02	1.89	0.76	—	—	—	—	0.475	0.118	0.105
Medium strength	3.20	1.56	0.72	—	—	—	—	—	0.121	0.108
Medium strength + Cu	3.18	1.58	0.69	—	—	—	1.58	—	0.112	0.101
Medium strength	3.11	2.26	0.39	—	—	—	—	—	0.111	0.101
Medium strength+Cr-Mo	3.12	2.31	0.39	—	0.54	0.77	—	—	0.119	0.109
Low carbon	2.61	2.46	0.45	—	—	—	—	—	0.110	0.100
Class 50 + NiCr	2.80	2.51	0.68	1.71	0.54	—	—	—	0.101	0.092
High Mn + Ni	3.10	2.51	3.11	1.00	—	—	—	—	0.106	0.097
Low carbon + Mo	2.56	2.20	0.63	—	—	0.58	—	—	0.118	0.108
Class 45 + NiCr	3.41	1.03	0.65	1.49	0.54	—	—	—	0.116	0.106

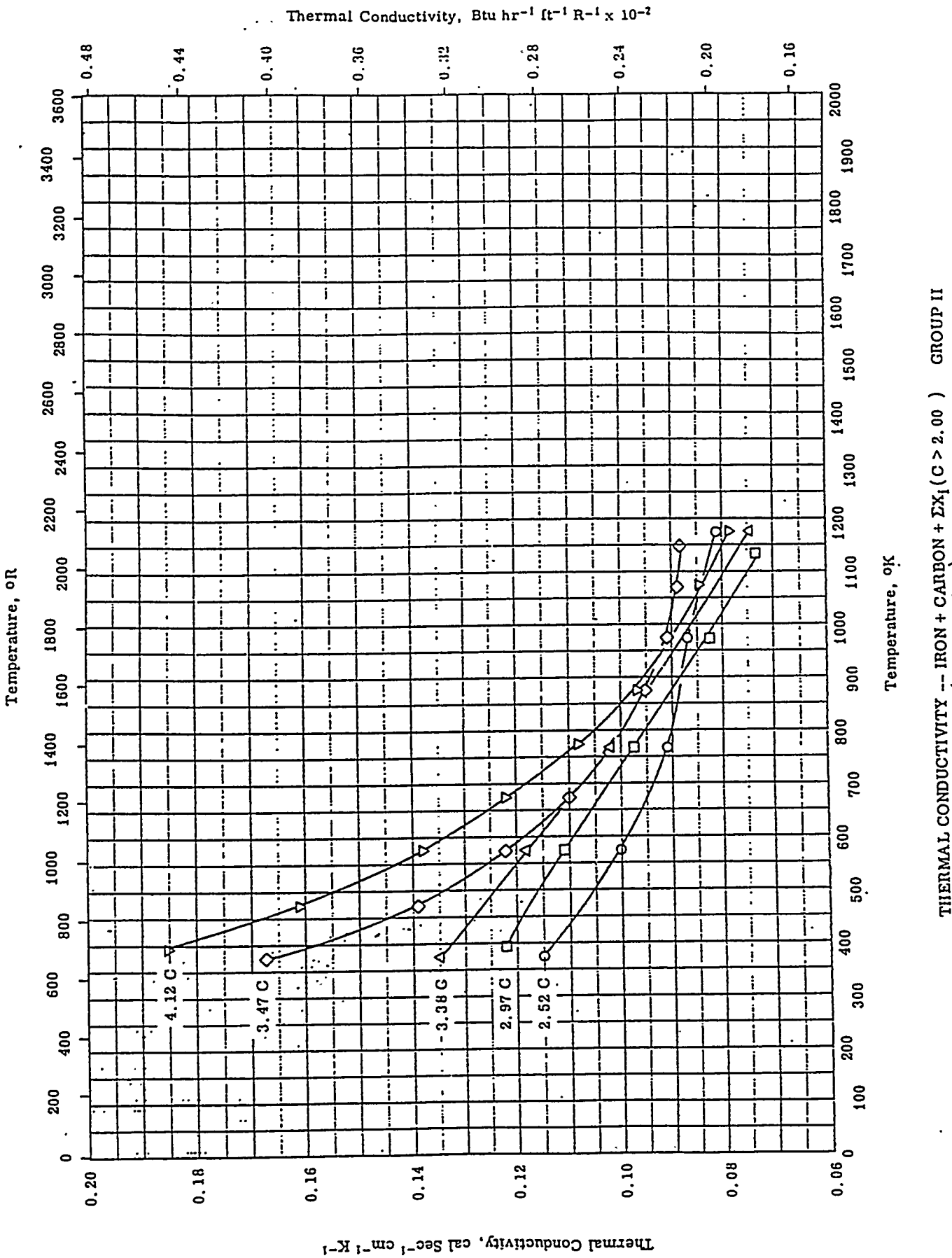

THERMAL CONDUCTIVITY -- IRON + CARBON + ΣX_i (C > 2.00) GROUP II
(Gray cast iron)

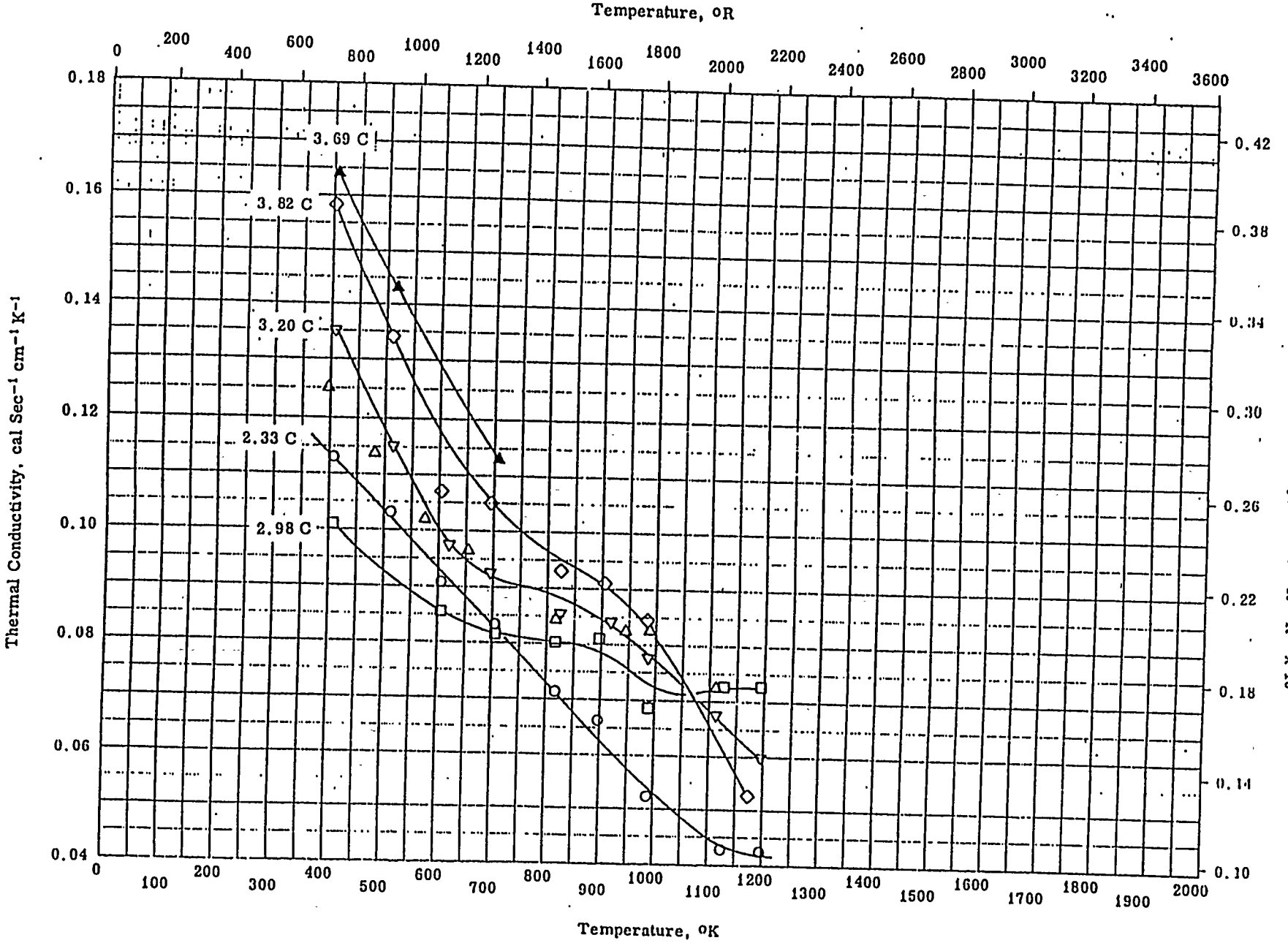

THERMAL CONDUCTIVITY -- IRON + CARBON + ΣX_i (C > 2.00) GROUP II
(Gray cast iron, pearlitic base)

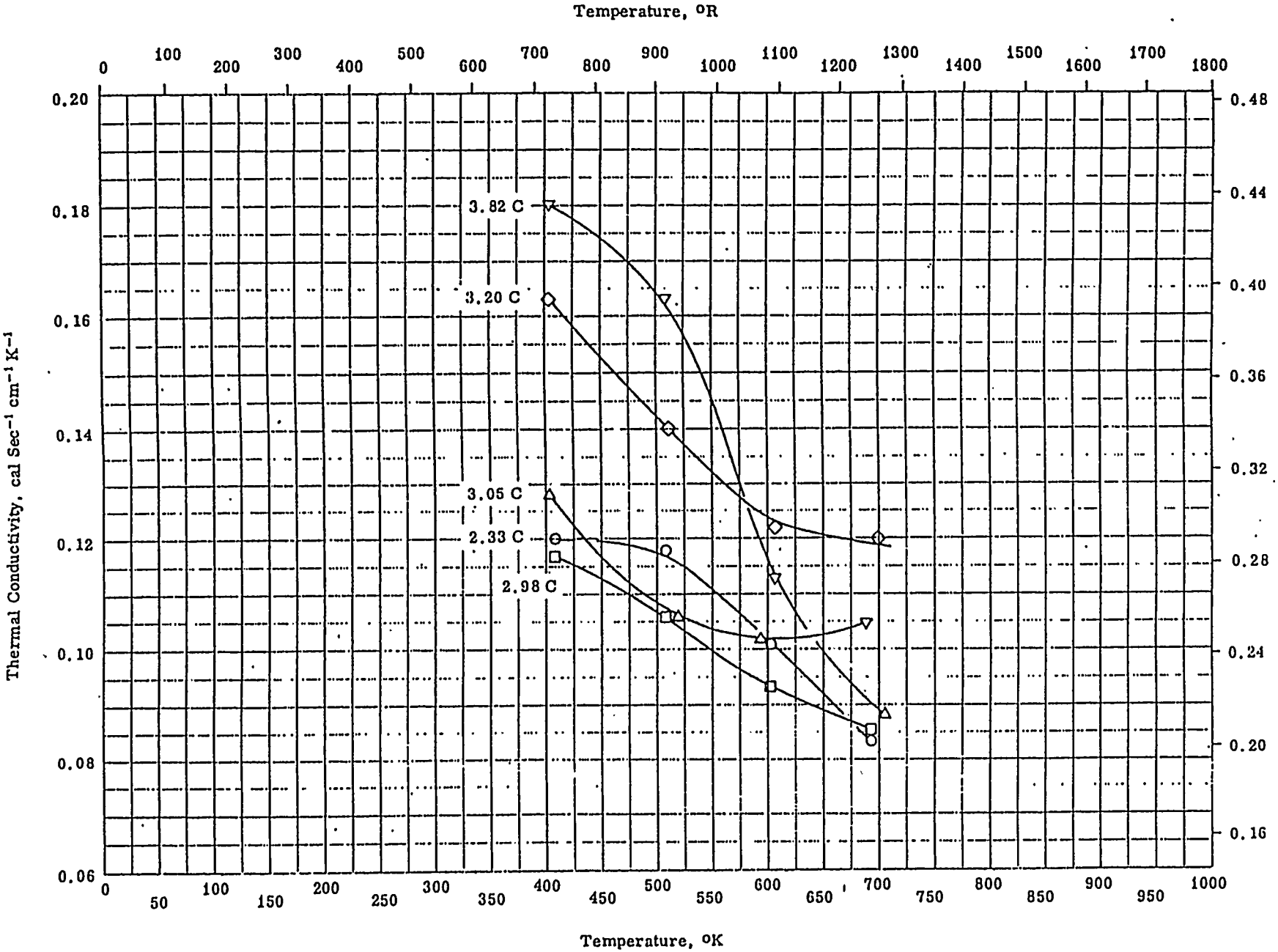

THERMAL CONDUCTIVITY -- IRON + CARBON + ΣX_i (C > 2.00) GROUP II
(Gray cast iron, ferritic base)

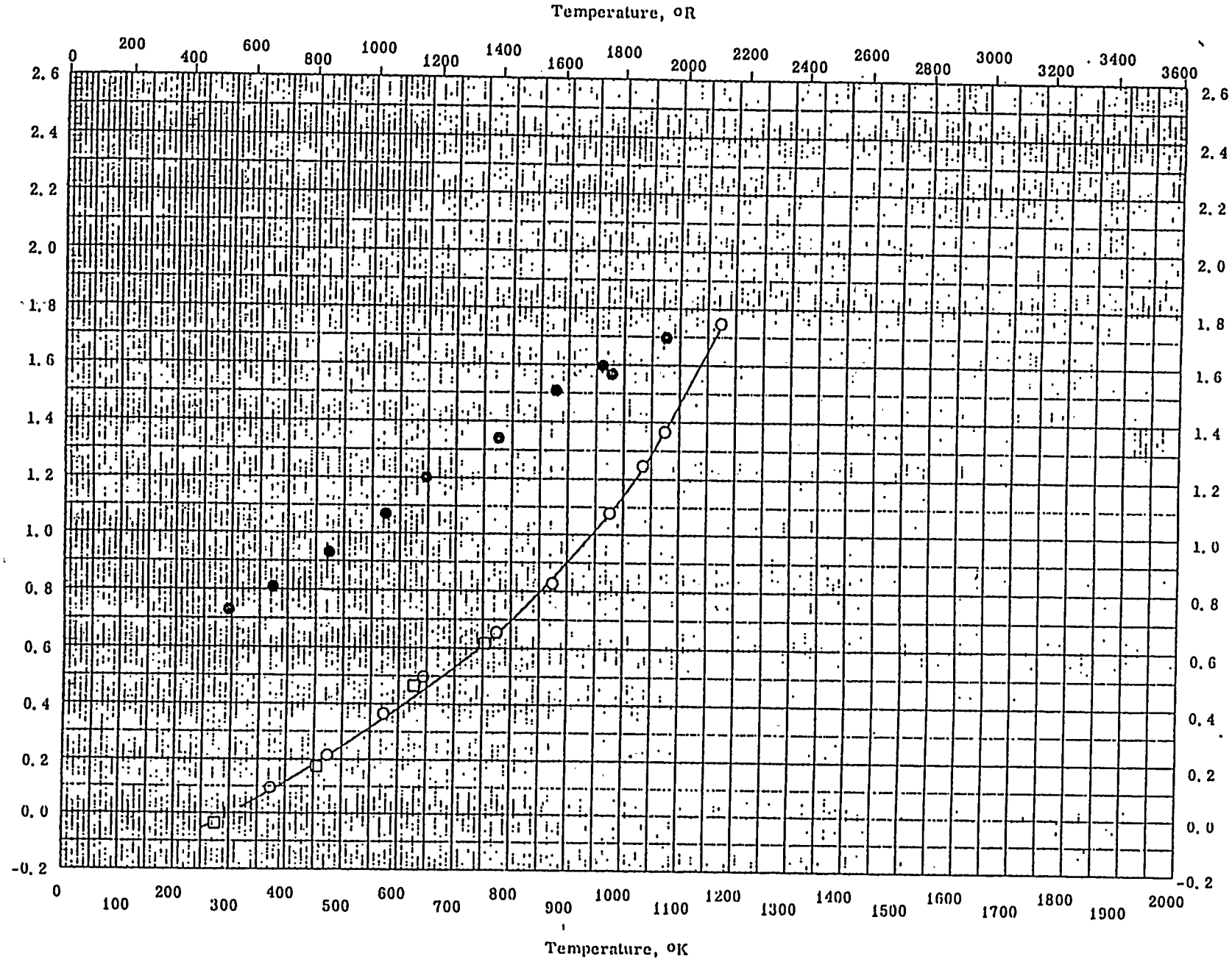

THERMAL LINEAR EXPANSION -- IRON + CARBON + ΣX_i (C > 2.00) GROUP II
(Gray cast iron)

CURVE NO.	TYPE IRON	%TC	%CC	%Si	%Mn	FTU (KSI)	(BHN)
1	CLASS 25	3.50	0.50	2.30	0.70	27.0	215
2	CLASS 40	3.00	0.05	2.00	0.75	43.0	235
3	NO. 2 ANNEALED					26.0	135
4	HIGH Si	2.60	0.80	3.40	0.40	45.0	
5	NO. 4 ANNEALED					30.0	
6	VERY LOW C	1.14		2.12	0.54		
7	SPECIAL	3.38	0.62	1.65	0.47	45.0	200

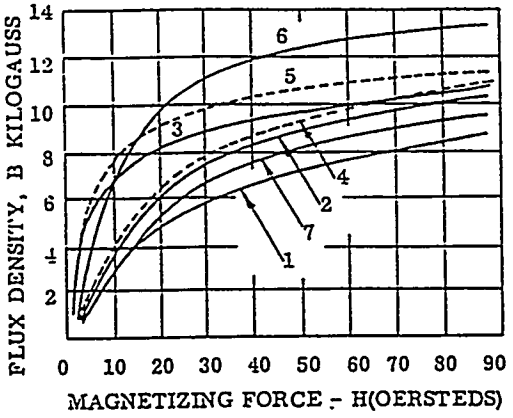

MAGNETIZATION CURVES FOR SEVERAL GRAY IRONS (1)

DENSITY OF CAST IRONS (16)

Iron Type	Density lbs/in^3
High carbon gray, ferritic	0.246
Medium carbon gray, ferrite & pearlite	0.255
Low carbon gray, pearlitic	0.263-0.267
White iron, unalloyed	0.275-0.282
High silicon, gray (Silal)	0.246-0.260
High chromium, white	0.264-0.271
High aluminum, gray	0.199-0.231
High nickel, gray, austenitic (Ni-Resist)	0.267-0.275
Nicrosilal, austenitic	0.260-0.267
Nickel-chromium, white (Ni-Hard)	0.275-0.282
High molybdenum, white	0.275-0.285
High carbon ductile, ferritic	0.257
High carbon ductile, pearlitic	0.258
High silicon, ductile, ferritic	0.257
High nickel, ductile, austenitic (Ni-Resist)	0.267

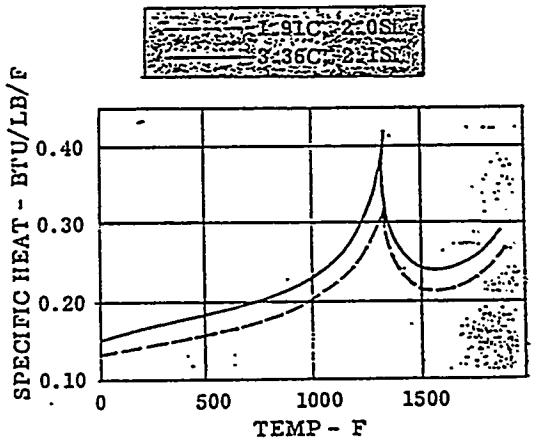

EFFECT OF TEMPERATURE ON THE SPECIFIC HEAT OF GRAY IRON (1)

DENSITY OF MICROCONSTITUENTS IN CAST IRON (16)

Constituent	Density (lbs/in^3)
Ferrite	0.284
Pearlite	0.281
Cementite	0.277
Graphite	0.081
Phosphide eutectic	0.264
Austenite	0.283
Martensite	0.276

EFFECT OF LOW TEMPERATURES ON GRAY IRON TENSILE STRENGTH (1)

Tensile strength (ksi)	Gray Iron Number				
	1	2	3	4	5
at 75F	20.5	31.1	21.8	18.0	21.8
at -4F	21.8	30.4	22.4	18.8	22.3
at -112F	-	-	24.2	-	24.1
at -150F	-	-	24.7	20.9	24.6
Brinell Hardness					
at 73F	134	180	151	142	164
at -4F	140	-	-	-	171
at -22F	140	-	-	-	-
at -40F	147	189	-	151	-
at -76F	-	195	-	153	-
at -292F	-	-	199	-	221
Chemical Analysis (%)					
Total carbon	3.56	3.42	3.64	3.78	3.42
Graphitic carbon	3.06	2.35	2.94	3.26	2.82
Silicon	1.80	1.24	1.81	2.03	2.17
Manganese	0.60	0.56	0.56	0.86	0.49
Sulphur	0.080	0.103	0.071	0.071	0.088
Phosphorus	0.527	0.326	0.509	0.095	1.084

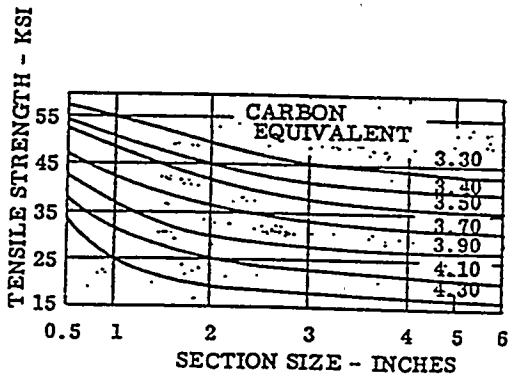

EFFECT OF SECTION SIZE ON THE TENSILE STRENGTH OF GRAY IRON (1)

IRON NO.	CARBON EQUIV.	TC	CC	Si	Mn	Ni	Cr	P	S
1	3.41	2.67	0.79	2.39	0.67	0.76	0.45	0.07	0.09
2	3.74	2.96	0.73	2.53	0.78	0.96	0.02	0.06	0.11
3	3.99	3.46	0.87	1.36	0.68	0.01	0.54	0.39	0.08
4	4.03	3.63	0.73	1.15	0.54	0.03	0.03	0.17	0.09

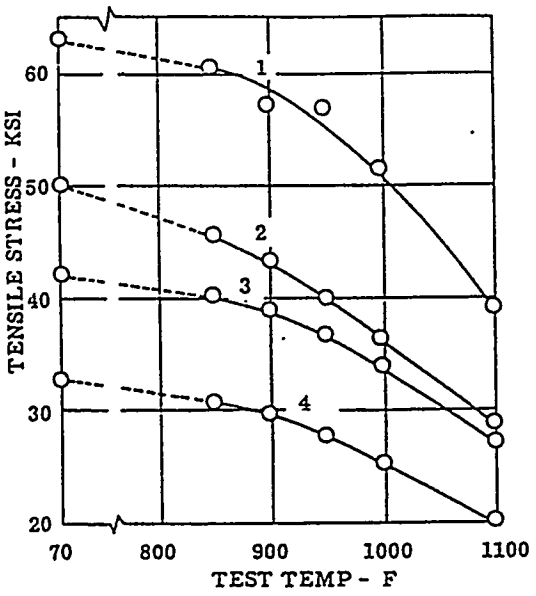

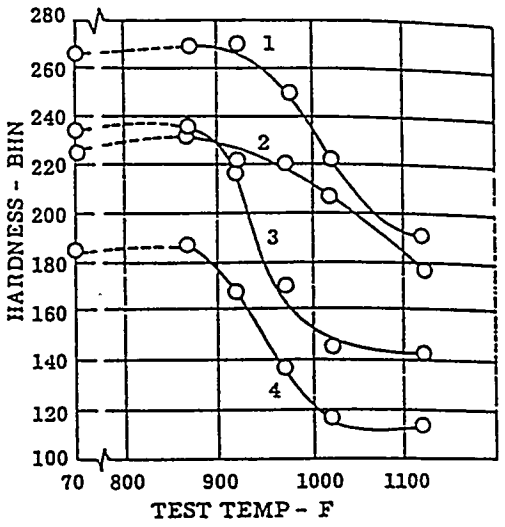

EFFECT OF TEST TEMPERATURE ON TENSILE STRENGTH AND HARDNESS OF GRAY IRON (1)

HIGH TEMPERATURE TENSILE PROPERTIES OF GRAY IRON (1)

Property		Testing Temperature: Room Temp.	750F	840F	930F
Tensile strength (ksi)		42.0	39.0	38.0	31.0
Elongation (%)		0.74	1.23	1.30	1.75
Modulus of elasticity (10^3 ksi)		18.5	18.0	16.0	15.5
Brinell hardness, determined at room temperature after testing at temperature indicated.	Edge	209	214	211	198
	Center	215	215	214	215

TC-3.19, CC-0.85, Si-1.66, Mn-0.91, P-0.077, S-0.089

ELEVATED TEMPERATURE PROPERTIES OF VARIOUS GRAY IRONS (16)

Iron No.	1	5	7	10	13	14
Type	Mo	NiMo	CrCu	NiMoCrV	Unalloyed	MoCr
Condition	Stress Relieved	Stress Relieved	Annealed	Stress Relieved	Stress Relieved	Annealed
Carbon	3.31	2.98	3.22	3.20	3.27	3.06
C E	3.83	3.46	3.85	3.82	3.87	3.61
Si	1.56	1.51	1.97	1.96	1.74	1.79
Mn	0.68	0.57	0.74	0.64	0.72	0.70
P	0.19	0.11	0.13	0.11	0.26	0.04
S	0.11	0.10	0.10	0.09	0.16	0.09
Cr	0.08	0.05	0.57	0.41	0.08	0.61
Ni	0.08	1.56	0.03	1.12	0.15	0.04
Mo	0.73	0.58	0.01	0.44	0.07	0.84
Cu	0.15	0.22	0.37	0.10	0.12	0.05
V	0.02	<0.01	0.02	0.12	0.02	<0.01

Alloy	Heat Treatment	Test Temp. (F)	Hardness (BHN)	Tensile Strength (ksi)	Elongation (%)
1	stress	80	225	47.7	1.0
1	relieved	800	-	45.0	1.5
1		1,000	-	33.1	0.5
5		80	258	58.8	1.0
5	stress	800	-	52.9	1.7
5	relieved	1,000	-	31.4	0.5
7	4 hr 1650F	80	192	37.4	1.5
7	furnace	800	-	33.2	1.0
7	cooled	1,000	-	20.6	1.0
10		80	255	54.8	1.5
10	stress	800	-	47.4	1.5
10	relieved	1,000	-	31.8	0.5
13		80	217	42.7	1.0
13	stress	800	-	36.5	1.2
13	relieved	1,000	-	24.7	0.5
14	4 hr 1650F	80	217	57.2	1.0
14	furnace	800	-	54.3	1.5
14	cooled	1,000	-	45.6	2.0

GRAY IRON SHORT-TIME TENSILE TESTS AT 750F (1)

Room Temp. Properties		Properties at 750F			
Tensile Strength (ksi)	Hardness (BHN)	Proportional Limit (ksi)	Modulus of Elasticity (ksi x 10^3)	Fracture Stress (ksi)	Elongation in 5 inches (%)
47.0	235	12.6	18.1	50.2	0.6
55.5	255	25.8	19.9	51.5	0.6
64.0	269	19.3	15.0	50.2	0.9
56.0	285	22.4	16.5	52.2	0.6
43.3	207	14.3	11.3	37.4	1.8

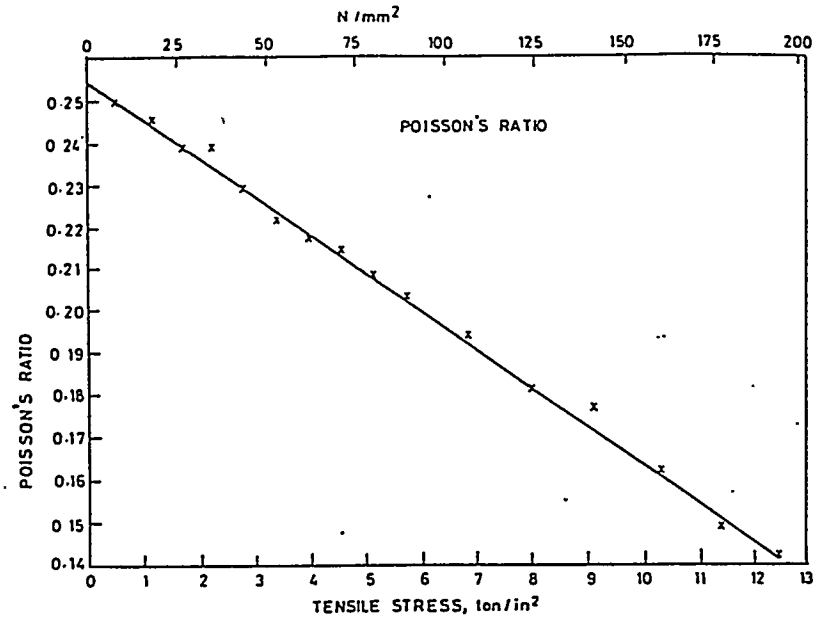

Figure 54(a)

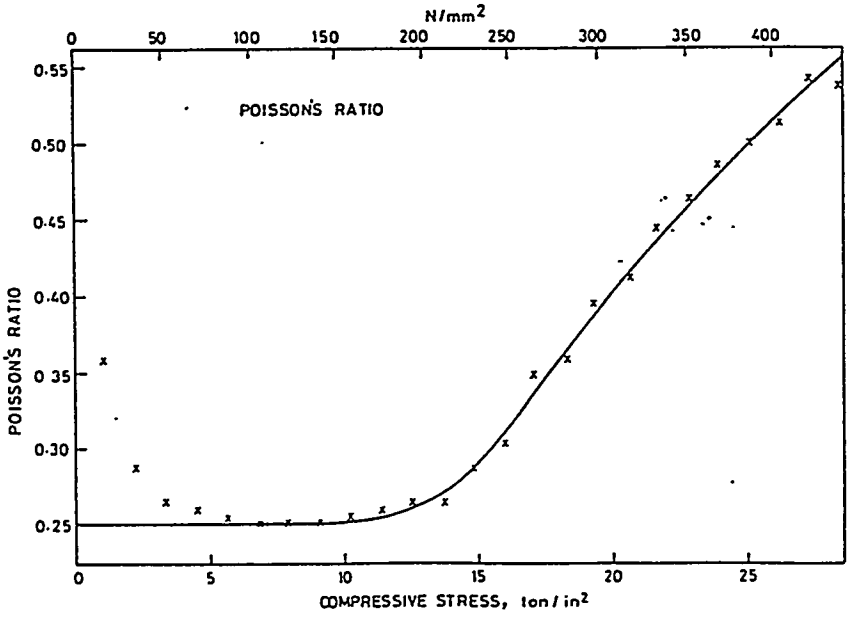

Figure 54(b)

Table 16 (THE MECHANICAL PROPERTIES OF THESE IRONS ARE SHOWN IN TABLE 17)

Sample no.	*TC* %	*Si* %	*Mn* %	*S* %	*P* %	*ASTM graphite size*	*Matrix*
3	3·52	1·32	0·61	0·082	0·066	2–3	Pearlitic
12	3·82	1·49	0·43	0·086	0·076	1–3	Mainly pearlitic
4	3·84	1·01	0·66	0·065	0·21	1	Mainly pearlitic
14	4·12	2·07	1·03	0·051	0·036	1	Mainly pearlitic

Table 17

Sample no.	*Tensile strength* ton/in² (N/mm²)		*Young's modulus (mean slope to 3 ton/in²)* lb/in² × 10⁶ (GN/m²)		*Applied load* ton/in² (N/mm²)		*Poisson's ratio at various temperatures*		
							Room temp.	450°C	650°C
3	10·3	(159)	13·1	(90)	1–4	(15–62)	0·21	0·14	0·25
12	7·7	(119)	10·5	(72)	1	(15)	0·25	0·14	0·18
					4	(62)	0·175	—	—
4	7·7	(119)	6·95	(48)	1	(15)	0·150	0·07	0·08
					4	(62)	0·125	—	—
14	5·7	(88)	5·2	(36)	1	(15)	0·12	0·05	0·09
					4	(62)	0·08	—	—

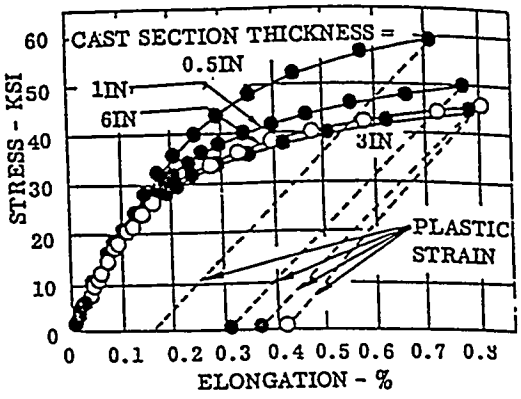

EFFECT OF SECTION SIZE ON STRESS-STRAIN CURVES FOR PEARLITIC GRAY IRON (1)

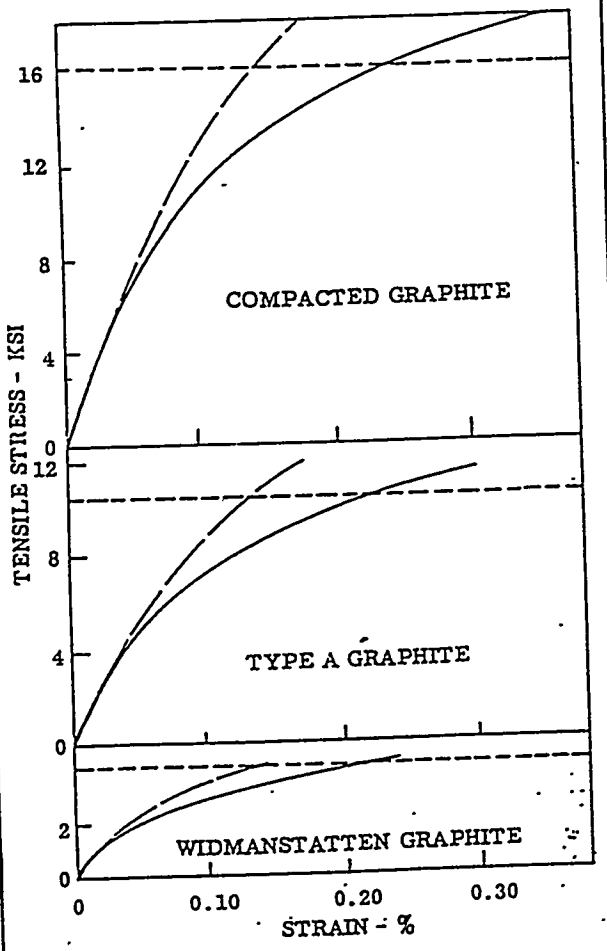

EFFECT OF GRAPHITE FORM ON THE STRESS-STRAIN PROPERTIES OF GRAY IRON (3)

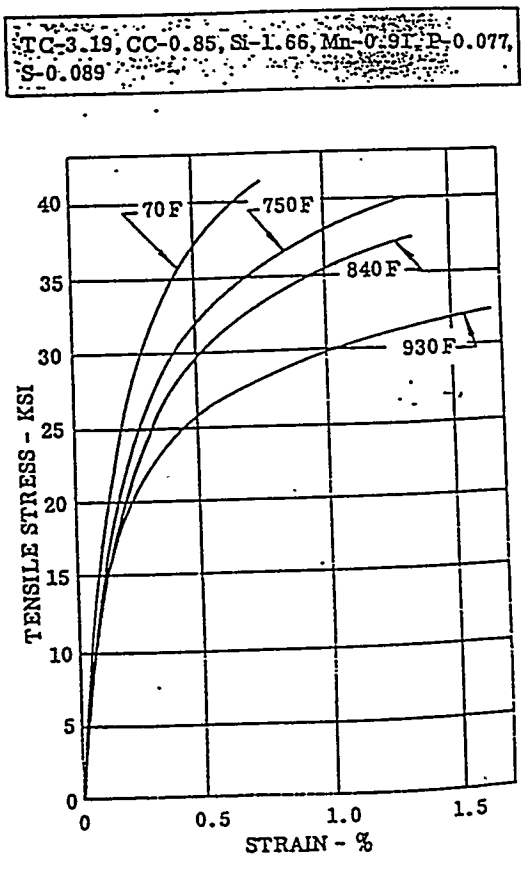

GRAY IRON STRESS-STRAIN CURVES TO FRACTURE (1)

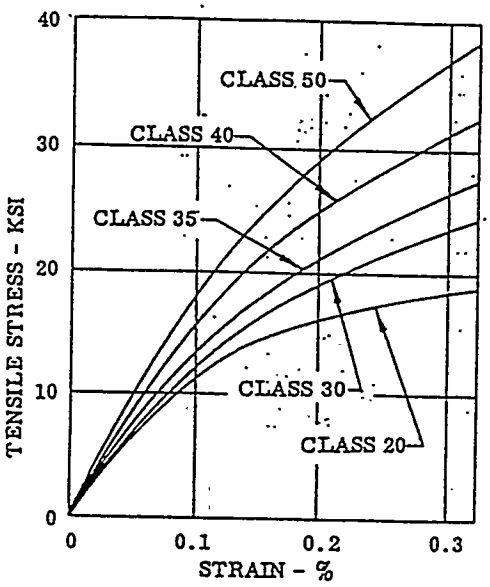

TYPICAL TENSILE STRESS-STRAIN CURVES FOR GRAY IRON (16)

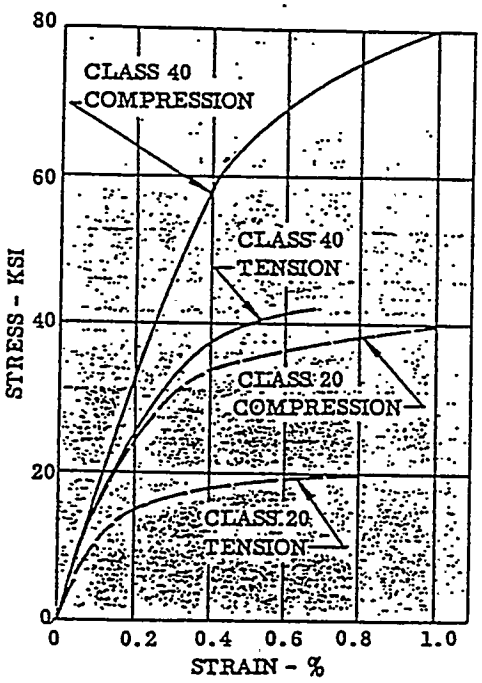

COMPARISON OF GRAY IRON STRESS-STRAIN CURVES IN TENSION AND COMPRESSION (16)

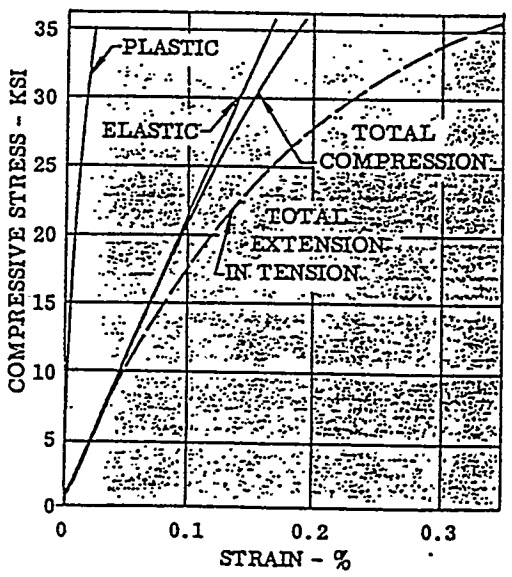

STRESS-STRAIN CURVES FOR GRAY IRON IN COMPRESSION (1)

FATIGUE ENDURANCE STRENGTHS OF SEVERAL GRAY IRONS (1)

Gray Iron No.	1	2	3	4	5
Tensile strength (ksi)	44.0	48.0	55.0	56.5	76.5
Endurance limit in complete reversed bending (ksi)	19.0	21.0	22.0	22.0	25.0
Endurance limit in half-cycle bending, O-max. (ksi)	23.0	32.0	27.0	33.0	38.0
Endurance limit in complete reversed torsion (ksi)	16.0	16.5	21.0	20.0	22.0
Endurance limit in half-cycle torsion, O-max. (ksi)	23.0	25.0	26.0	33.0	29.0

C-3.65, Si-2.46, Mn-0.73, P-0.26, S-0.13
TENSILE STRENGTH - 20.3 KSI
NOTCHED SPECIMEN
0.58 DIA AT ROOT OF 60° SHARP NOTCH

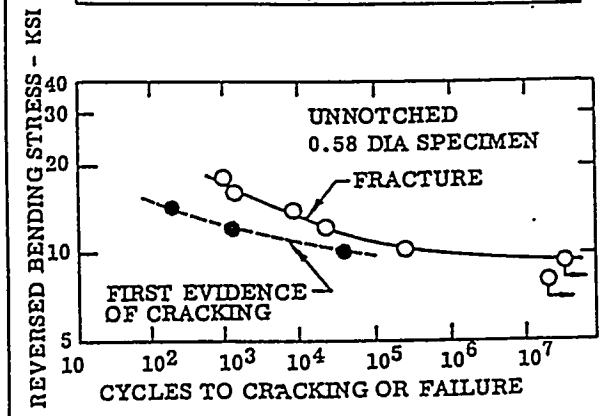

FATIGUE LIFE OF UNNOTCHED GRAY IRON MACHINED SPECIMENS (2)

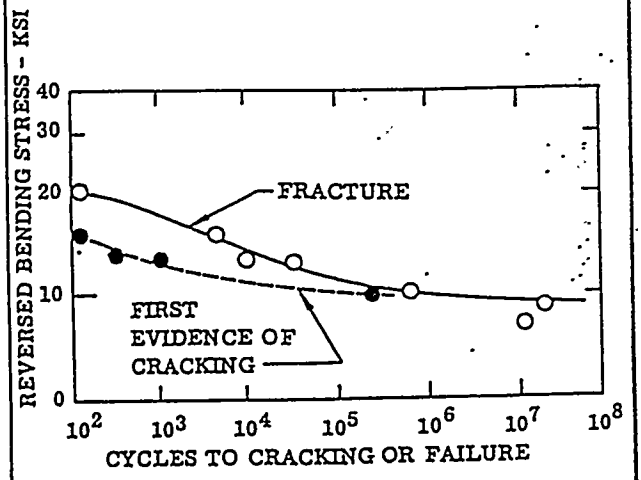

FATIGUE LIFE OF NOTCHED GRAY IRON MACHINED SPECIMENS (2)

REVERSE BENDING FATIGUE ENDURANCE LIMIT FOR GRAY IRON (16)

Class	Endurance Limit (ksi)
20	about 10.0
25	11.5
30	13.7-15.5
35	16.0-17.5
40	17.5-19.5
45	21.5-25.5
50	24.5-27.5
60	about 29.5

FATIGUE STRENGTH OF ACICULAR GRAY IRON (1)

Iron No.	1	2	3	4
Fatigue strength-(ksi)	24.6	24.6	25.8	25.8
Tensile strength-(ksi)	65.2	63.9	65.9	76.0
Hardness - (BHN)	312	343	283	331
Chemical analysis-%				
Total carbon	3.09	3.08	2.93	2.91
Silicon	2.19	2.00	2.11	2.16
Manganese	0.64	0.68	0.60	0.64
Nickel	1.58	2.21	1.25	1.92
Molybdenum	0.59	0.71	0.65	1.18
Phosphorus	0.04	0.04	0.03	0.04
Sulphur	0.05	0.05	0.02	0.06

FATIGUE

SYMBOL	GRAPHITE TYPE	GRAPHITE SIZE	BHN	CE	C	Si	P	F_{tu} (ksi)	e(% IN 1 IN)	E (10^3 ksi)	Ec (10^3 ksi)
○	A	4 1/2 -5	213	4.18	3.43	2.15	0.087	38	0.58	14.5	16.0
△	A	3 1/2 -4	172	4.40	3.49	2.49	0.24	21	0.52	8.0	10.0

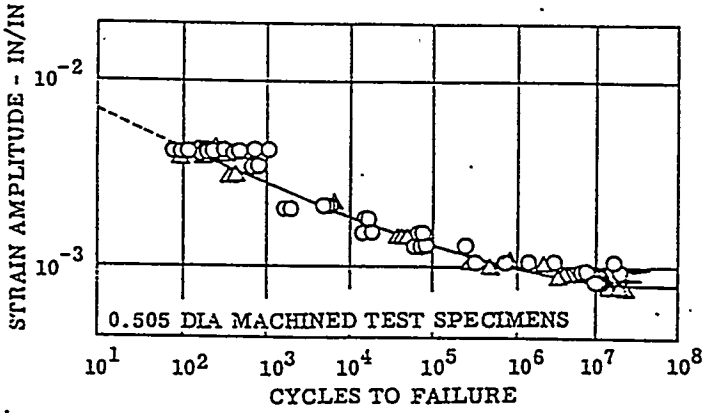

GRAY IRON AXIAL FATIGUE LIFE (13)

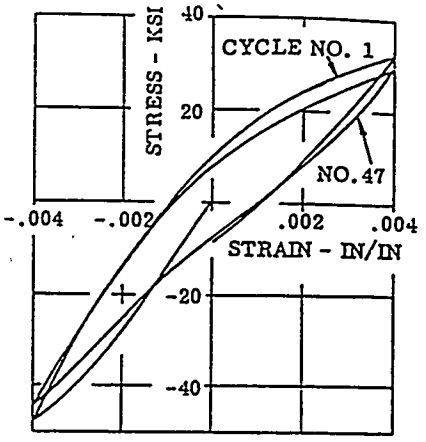

EFFECT OF CYCLE NUMBER ON AXIAL STRESS-STRAIN LOOPS OF GRAY CAST IRON (13)

EFFECT OF COPPER ON THE TENSILE AND FATIGUE PROPERTIES OF GRAY IRON (1)

Iron No.	Copper (%)	Tensile Strength (ksi)	Fatigue Endurance Limit (ksi)
1	0	48.5	23.0
2	0.53	47.5	19.0
3	0.99	50.0	22.0
4	1.45	53.0	24.0
5	1.98	54.5	24.0
6	3.10	56.0	23.0

C-3.15, Si-1.5

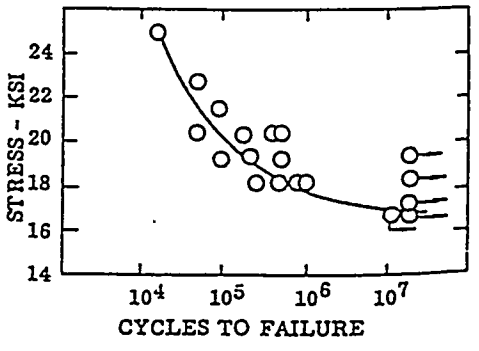

FATIGUE LIFE OF GRAY IRONS (16)

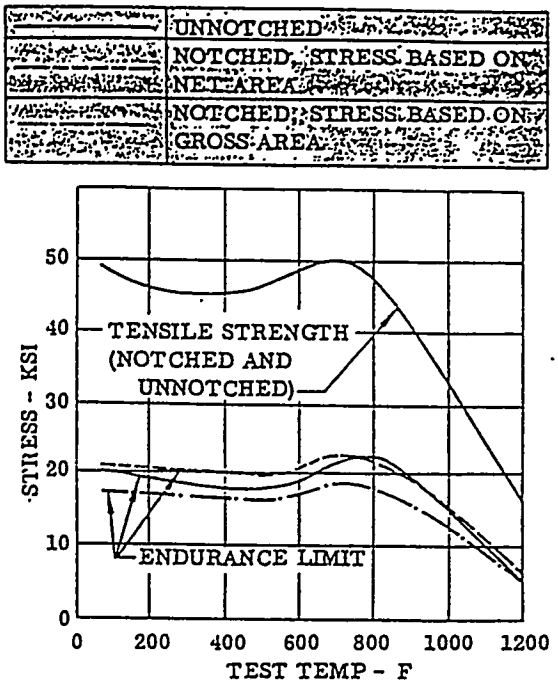

EFFECT OF TEMPERATURE ON TENSILE AND FATIGUE PROPERTIES OF GRAY IRON (1)

EFFECT OF NOTCHES ON THE GRAY IRON ENDURANCE STRENGTH (1)

Tensile Strength (ksi)	Endurance Limit	
	Unnotched (ksi)	Notched (ksi)
20.0	9.2	9.2
25.0	11.9	11.4
29.8	15.0	13.7
33.6	22.0	15.7
36.5	19.5	16.3
42.6	23.3	19.0

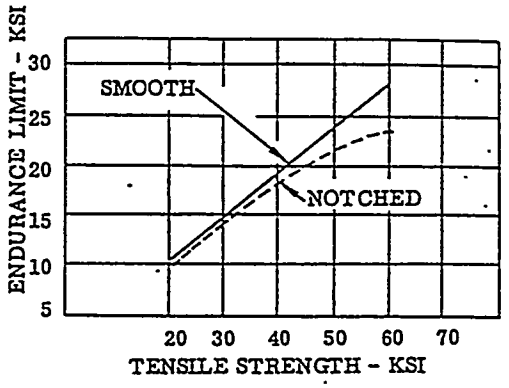

RELATIONSHIP BETWEEN TENSILE AND ENDURANCE STRENGTH OF GRAY IRONS (1)

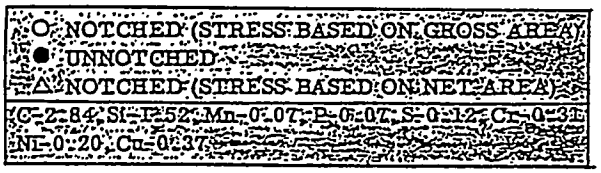

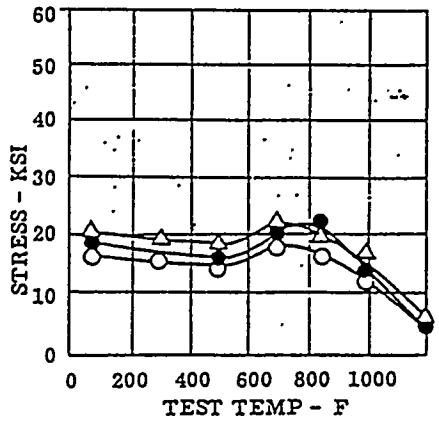

EFFECT OF TEMPERATURE ON FATIGUE ENDURANCE LIMIT OF GRAY IRON (15)

ROTATING BEAM FATIGUE ENDURANCE STRENGTH OF GRAY IRON (1)

Type of Matrix	Tensile Strength (ksi)	Endurance Limit (ksi)
Pearlitic	41.0	19.0
	42.1	19.0
	48.6	21.3
	52.9	23.5
Acicular	63.9	24.6
	65.5	24.6
	65.9	25.8
	76.0	25.8

MODULUS

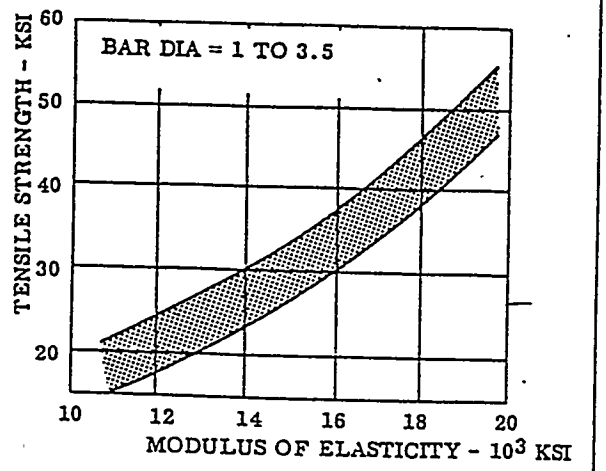

RELATIONSHIP BETWEEN TENSILE STRENGTH AND MODULUS OF GRAY IRON (1)

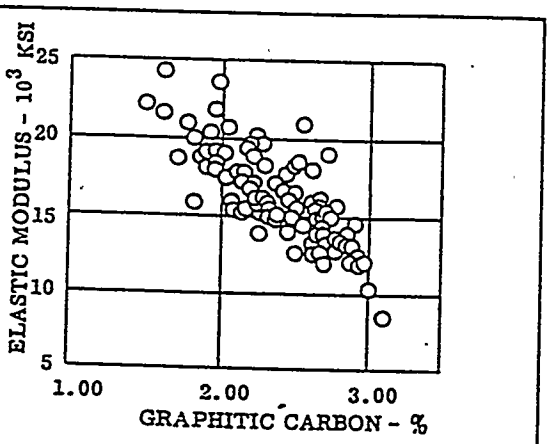

EFFECT OF GRAPHITE ON THE MODULUS OF ELASTICITY (7)

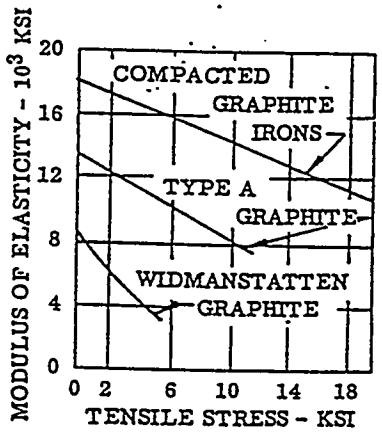

VARIATION OF MODULUS OF ELASTICITY WITH TENSILE STRESS (8)

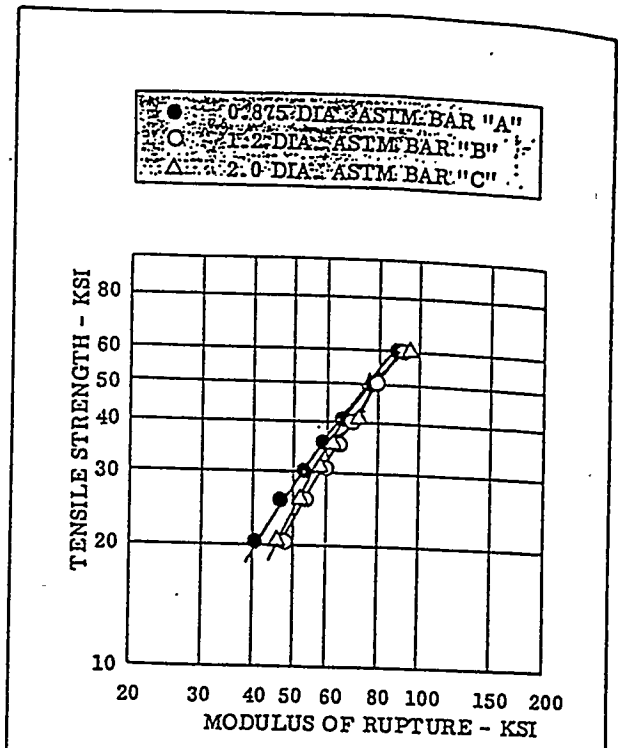

RELATIONSHIP BETWEEN GRAY IRON TENSILE STRENGTH AND MODULUS OF RUPTURE (1)

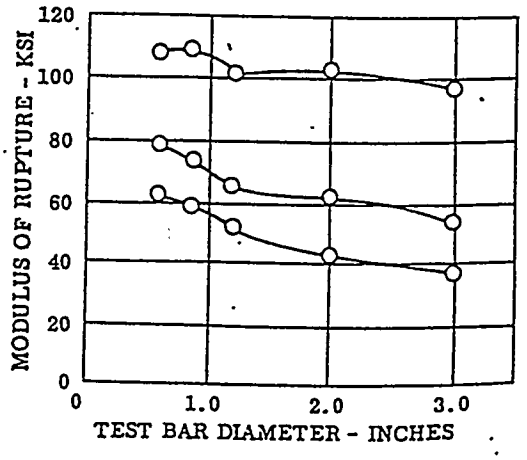

EFFECT OF TEST BAR SIZE ON MODULUS OF RUPTURE (1)

GRAY IRON TENSILE AND TRANSVERSE STRENGTH REQUIREMENTS PER ASTM SPECIFICATION A-438-62 (REAPPROVED 1968) (1)

Class	Minimum Tensile Strength (ksi)	Min. Transverse Strength Breaking Load, Lbs.		
		Test Bar "A" .875 in. dia. 12 in. span	Test Bar "B" 1.2 in. dia. 18 in. span	Test Bar "C" 2.0 in. dia. 24 in. span
20	20	900	1800	6000
25	25	1025	2000	6800
30	30	1150	2200	7600
35	35	1275	2400	8300
40	40	1400	2600	9100
45	45	1540	2800	9700
50	50	1675	3000	10300
60	60	1925	3400	12500

MINIMUM THICKNESS OF GRAY IRON CASTINGS (15)

ASTM Class	Minimum Section Thickness (inch)
20	1/8
25	1/4
30	3/8
35	3/8
40	5/8
50	3/4
60	1

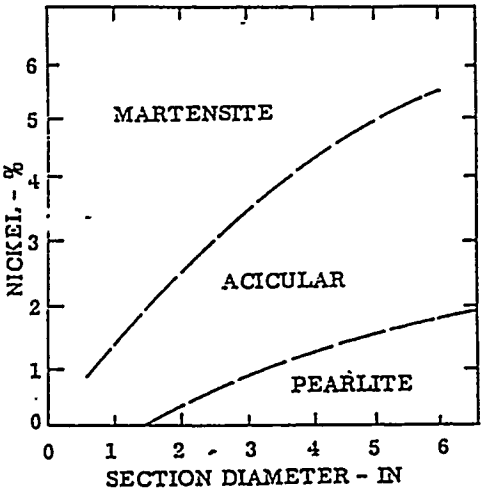

EFFECT OF SECTION SIZE ON AS-CAST MATRIX (11)

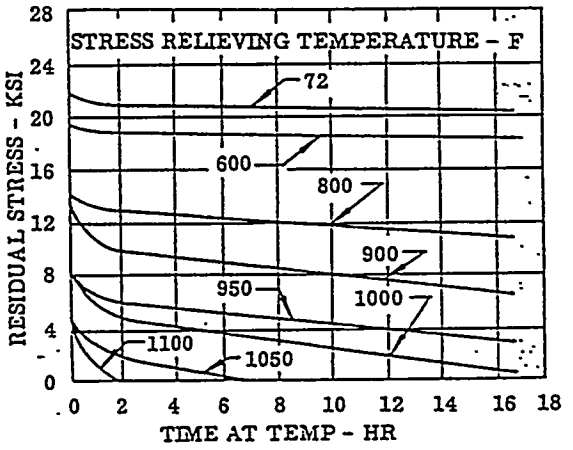

EFFECT OF STRESS RELIEF TEMPERATURE ON THE RESIDUAL STRESS IN GRAY IRON CASTINGS (15)

EFFECT OF THERMAL CYCLING ON GRAY IRON TENSILE STRENGTH (1)

Alloying Elements Additions (a) (%)	Original Tensile Strength (ksi)	Final Tensile Strength (ksi)
–	37.5	11.9 to 21.4
0.10 Vanadium	41.5	16.2 to 31.1
0.20 Zirconium	32.5	9.3 to 18.6
0.20 Zr, 0.10 V	34.0	16.4 to 25.5
1.50 Cu, 0.10 V	40.5	27.4 to 34.7
0.20 Ti, 0.10 V	37.5	12.0 to 30.5

Specimens heated 150 times to 1500F.

(a) Base composition: C-3.15, Si-1.80, Mn-0.60, S-0.12, P-0.14.

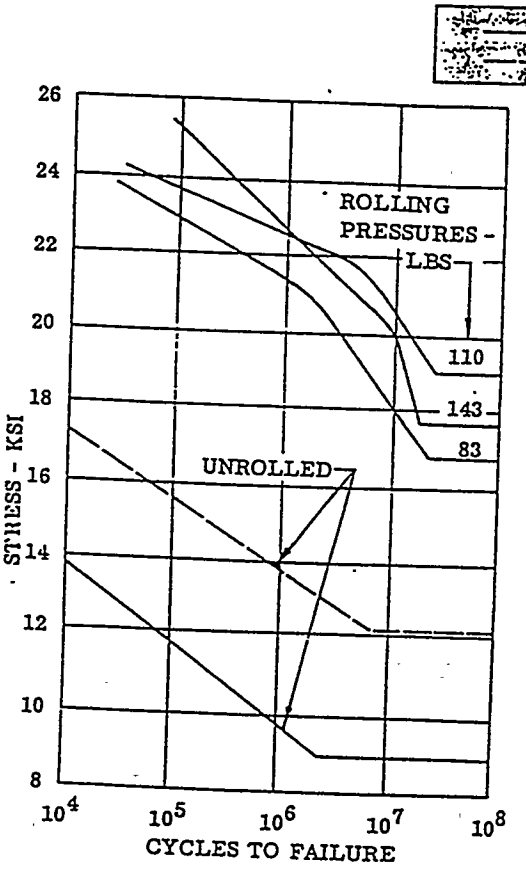

EFFECT OF SURFACE ROLLING ON FERRITIC GRAY IRON FATIGUE PROPERTIES (1)

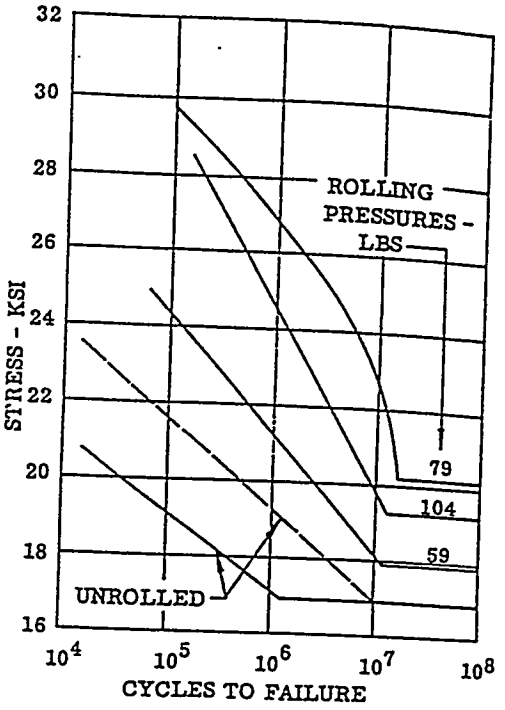

EFFECT OF SURFACE ROLLING ON PEARLITIC GRAY IRON FATIGUE PROPERTIES (1)

RUPTURE STRENGTH AND FATIGUE ENDURANCE OF GRAY IRONS (1)

Alloy	Tensile Strength (ksi)	Hardness (BHN)	10-Year Rupture Strength at 800F (ksi)	Fatigue Endurance Limit in Tension at 800F (ksi)
Chromium-molybdenum	63.0	269	30.0	17.5
Molybdenum	54.8	255	25.0	15.0
Cr-Ni-Mo-V	47.7	225	25.0	16.0
Unalloyed	42.7	217	15.0	12.5
Nickel-Molybdenum	58.8	258	25.0	18.0

COMPARISON OF SHEAR AND TENSILE PROPERTIES OF GRAY IRON (16)

Class of Iron Condition	25 As-Cast	30 As-Cast	30 Annealed	35 As-Cast	40 Alloyed
Hardness-BHN	187	207	137	212	235
Tensile Strength-ksi	29.9	33.7	20.6	34.8	41.9
Tangent Modulus-10^3 ksi	16.6	17.0	14.5	18.0	18.2
Shear Strength-ksi	44.0	49.0	29.4	51.1	61.0
Modulus of Rigidity-10^3 ksi	5.9	6.2	5.4	6.1	6.6

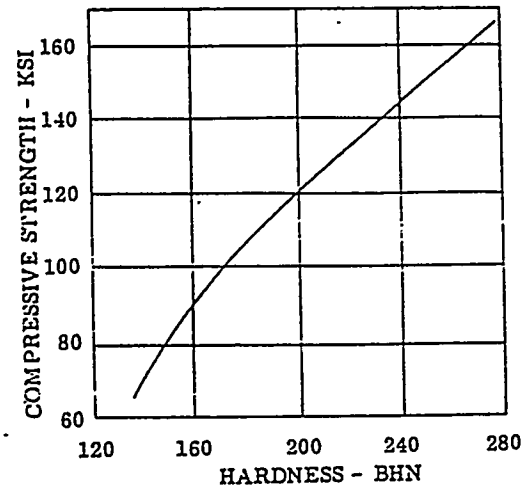

RELATION BETWEEN HARDNESS AND COMPRESSIVE STRENGTH OF GRAY IRON
(16)

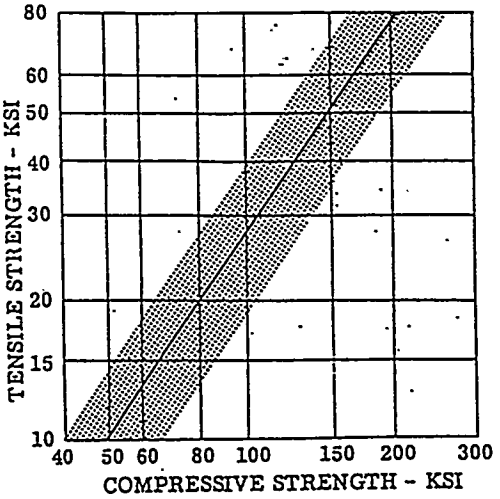

RELATIONSHIP BETWEEN THE TENSILE AND COMPRESSIVE STRENGTH OF GRAY IRON
(1)

EFFECT OF NOTCHES ON TENSILE AND COMPRESSIVE STRENGTHS OF GRAY IRON
(1)

Iron No.	Type of Specimen	Tensile Strength (ksi)	Compressive Strength (ksi)
1	Unnotched	19.3	80.0
	Notched	21.2	104.0
2	Unnotched	31.6	182.0
	Notched	32.1	327.0
3	Unnotched	46.0	140.0
	Notched	43.8	193.0
4	Unnotched	53.4	236.0
	Notched	51.6	270.0

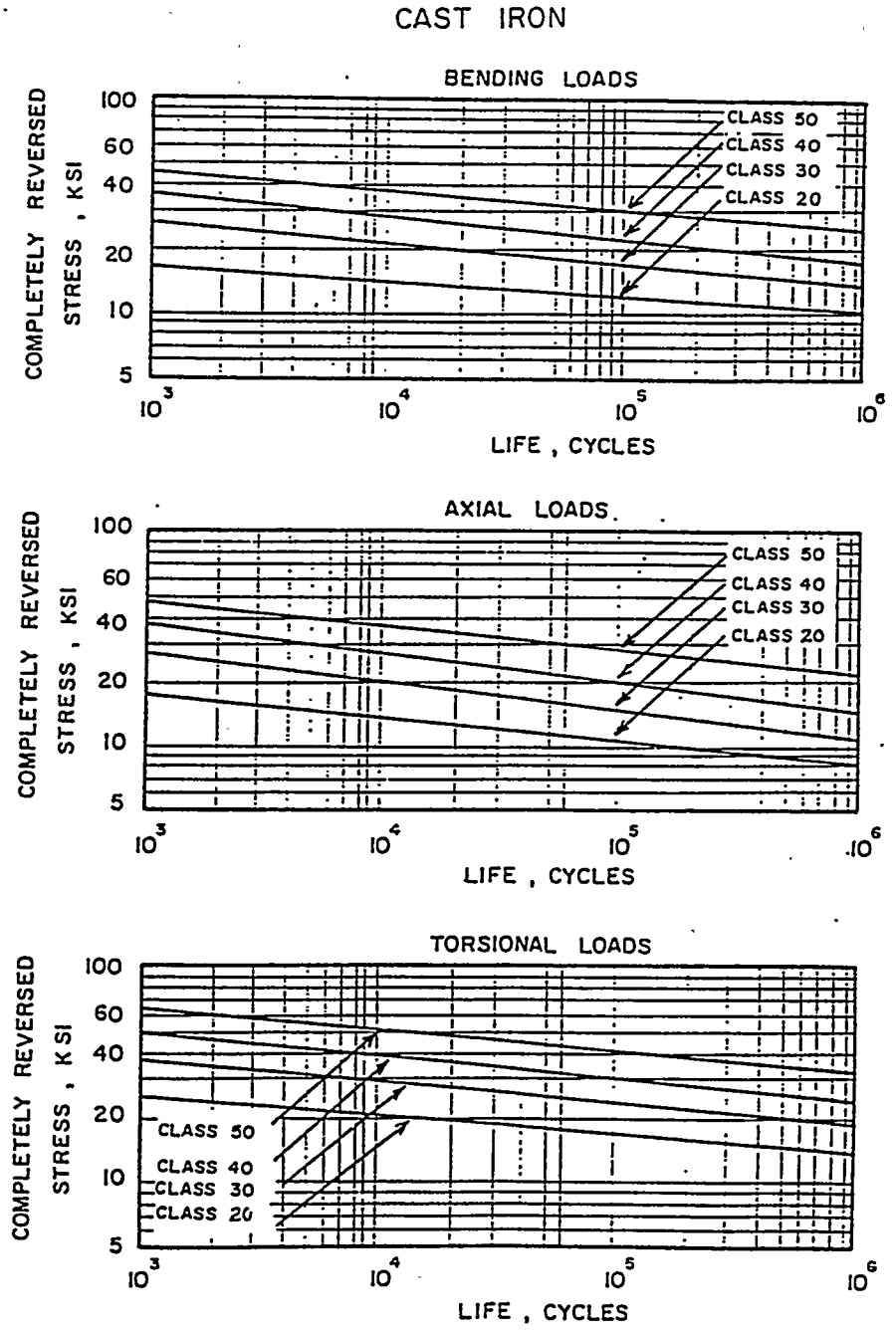
CAST IRON
BENDING LOADS
COMPLETELY REVERSED STRESS , KSI
100
60
40
20
10
5
CLASS 50
CLASS 40
CLASS 30
CLASS 20
10^3
10^4
10^5
10^6
LIFE , CYCLES
AXIAL LOADS.
COMPLETELY REVERSED STRESS , KSI
100
60
40
20
10
5
CLASS 50
CLASS 40
CLASS 30
CLASS 20
10^3
10^4
10^5
10^6
LIFE , CYCLES
TORSIONAL LOADS
COMPLETELY REVERSED STRESS , KSI
100
60
40
20
10
5
CLASS 50
CLASS 40
CLASS 30
CLASS 20
10^3
10^4
10^5
10^6
LIFE , CYCLES

Figure 21–19.

APPENDIX III

Thermal Fatigue in the Permanent Mold Process: A Literature Review

Thermal Fatigue in the Permanent Mold Process: A Literature Review

Introduction

While permanent molds may need to be repaired or replaced as a consequence of mechanical damage or wear/erosion, a particularly frequent cause for their failure is cracking or checking of the mold surface due to thermal fatigue. Penetration of molten metal into cracks may then lead to additional mechanical damage during ejection of the casting, causing accelerated deterioration of the mold and of the casting quality.

Molds for the permanent mold process are typically produced from cast irons, generally gray irons. A variety of other products, also produced from gray iron, are subject to operating conditions similar to permanent molds -- automotive and diesel engine blocks and heads, exhaust manifolds, brake components, glass molds, and ingot molds are common examples. Although the operating conditions for each may differ slightly, all experience temperature changes during use and all are subject to failure by thermal fatigue.

Thermal fatigue is caused by cyclical thermal stresses introduced by heating and cooling of the material. This can occur in a permanent mold, both due to start-up/shut-down of the casting process and to the temperature changes induced in the mold during pouring, solidification, and casting ejection. The stresses due to start-up/shut-down may be introduced relatively rapidly, resembling thermal shock; temperature changes during the normal casting production tend to be regular and repeatable, more typical of a fatigue situation. When considering the life expectancy of a permanent mold, both types of situations may have to be considered.

In addition, it should be noted that permanent molds often fail by a low-cycle fatigue, rather than the high-cycle mechanism often found in the mechanical fatigue failure of rotating, bending, or vibrating parts. Cracking may occur after thousands of cycles, after only a few cycles, and on some occasions during initial heating of the mold. In the low-cycle fatigue regime, factors such as creep resistance and oxidation are likely to be less important compared to high-cycle conditions.

Thermal stresses are induced by differential expansion and/or contraction in a statically indeterminate system[1-4]. Differential expansion can arise from temperature variations in the body or from differences in thermal expansion coefficients when the body temperature is changed uniformly[3]. During normal operation of a permanent mold, differences in thermal expansion are principally caused by different section sizes of the mold or by differences in casting thickness. However other factors, such as external heating or cooling of portions of the mold, can contribute to thermal stresses. The cyclical thermal stresses frequently result in the formation of cracks caused by the thermal fatigue of the metal[5].

Resistance to thermal fatigue depends on (a) the magnitude of thermal stresses induced and (b) the ability of the material to withstand those stresses. The magnitude of the thermal stresses can be estimated from the properties of the material and its environment by [6]

$$\sigma_{thermal} = [(\alpha E \Delta T) / (1-\nu)]F \qquad \text{Equation 1}$$

where α is the coefficient of thermal expansion, E is the modulus of elasticity, ν is Poisson's ratio, ΔT is the temperature difference that the material experiences during operation, and F is a geometry or form factor. This equation points out that materials having a low coefficient of thermal expansion and a low modulus of elasticity will develop lower thermal stresses. However this expression is difficult to use and correlate to fatigue because all of these factors change with temperature and, in some cases, (such as thermal conductivity) even with time and number of cycles. The equation also does not include the critical thermal stress (such as the tensile or yield strength of the material) for initiation or propagation of a thermal fatigue crack, nor does it include the thermal conductivity, which can influence the ΔT, temperature gradients, and maximum temperature. In addition, other factors can influence the thermal stresses; of special importance is the resistance of the material to stress relaxation, or creep, which may occur if the mold is exposed to elevated temperatures for a sufficient period of time. Creep will be influenced by both temperature and time. Changes in microstructure of the mold material may also influence these properties and, hence, influence the thermal stresses. In extreme cases, if the maximum temperature exceeds the transformation temperature of the iron, phase transformations can occur, causing additional stresses as well as cyclical changes in the microstructure. Growth of the iron may occur, both due to graphitization and oxidation, and can change the thermal stresses.

The ability of the material to resist the thermal stresses so introduced depends primarily on its strength, ductility, and creep resistance. Consequently the type of cast iron, the carbon content of the cast, the size and morphology of the graphite, the matrix structure, and the stability of the matrix structure are all important. A significant body of research has been conducted concerning the resistance of various cast irons to cracking by thermal fatigue and thermal shock. Much of this research has been directed toward transportation products, such as exhaust manifolds, brake components, and engine components. Some work concerning thermal fatigue of cast iron ingot molds used in the steel industry has also been reported. But relatively little work has been published concerning thermal fatigue in cast irons used as permanent molds. Because each general application may involve very different thermal cycles, the behavior of the cast irons in each is different and consequently different irons and different testing procedures might be more appropriate for each use.

Summary of Results for Permanent Molds

Based on the results of a number of tests described in the following literature review, an optimum material for producing permanent molds is a high-strength, creep-resistant pearlitic gray cast iron.

Thermal Fatigue Tests for Cast Irons

A large number of testing methods have been developed to study the fatigue properties of materials during thermal cycling. One method is to submit the actual fabricated part to cyclic thermal shock by repeated immersion in a bath of high temperature interspersed by immersions in a low temperature bath. After some critical number of cycles failure, as manifested by a fatigue crack, would occur at the point of severest stress reversal. In a similar manner, a test permanent mold could be cycled until failure. However this approach would give a number for the mold life applicable only to that particular part under specific test conditions. Testing of a variety of mold geometries, for example thick and thin sections, bosses, or fins, for both large and small castings,

would provide a useful set of experiences might be of valuable assistance in designing new molds or in developing methods for increasing mold lives; however this approach would be enormously expensive.

The usual method for evaluating the resistance of various materials to thermal fatigue is to develop a simplified test by which a large number of specimens can be tested in a more economical manner. However, design of the test specimens and testing procedures is critical in order to assure than the conditions of the test realistically represent the operating conditions. Consequently there is no standard test for thermal fatigue resistance; instead a wide variety of tests have been developed for this purpose and have been applied to gray, ductile, and compacted graphite cast irons. Special care must be exercised in selecting an appropriate test or in using the results of a test for design and materials selection; a particular test may be appropriate for one application (such as for ingot molds) but not for another (such as permanent molds for aluminum castings). In addition, one material may perform very well in one test (or application), but very poorly in another.

Because of the close relationship between experimental results and the type of test that is used to obtain those results, the literature will be reviewed below by describing many of the tests and the results together; this will lead to a number of contradictory observations concerning the thermal fatigue of cast irons. These contradictions, and an overall summary of the results, will be discussed in a later section.

Quenching (Thermal Shock) Tests

As reported by Roehrig, Friedrich[7] heated iron bars to various temperatures, then quenched the bars in water; this was repeated until cracking was observed. Figure 1 shows that increasing the maximum temperature increases the number of observed cracks and decreases the number of cycles required before cracking begins. Within each scatter band, irons containing Mo or Cr showed less cracking. Roehrig also described Namai's tests[8], in which bars were quenched into water from 450C, which showed that increasing the volume percent graphite in gray iron reduced the severity of cracking; however when type D graphite was present, the severity of cracking increased significantly, Figure 2. Others have also observed the deleterious effect of type D graphite and/or ferrite in gray irons.[9-12] Ductile and CG iron also fail at relatively low numbers of quenching cycles. In these types of direct quenching tests, the modulus of elasticity and the thermal conductivity appear to be of particular importance, while tensile strength is less important. Dinescu et. al.[13], who quenched various irons from 900C to room temperature, found that gray iron cracked most easily, CG iron performed better, and ductile iron survived the quenching process best; these conditions, which cause the iron to be heated above the critical temperature, are more typical of ingot molds than permanent molds.

Sukhodol'skaya and Zatolokin[14] compared the performance of various irons quenched with and without the application of an external load. The ferritic gray irons performed better when no external load was applied, while the pearlitic irons were much better when an external load was applied. Kattis and McPherson[15] also found that a pearlitic iron performed better than a ferritic iron when an external load was applied, and that thermal fatigue resistance correlated well with tensile strength.

Roehrig[6] suggested that for tests giving high cooling rates or high heating rates, the temperature differences and hence the thermal stresses become so high that a high strength, low

thermal conductivity iron is inferior to a high graphite gray iron. The temperature difference for the quench is also critical; for each 50C increase in peak temperature, the risk of cracking nearly doubles. Attempts to improve resistance by increasing the strength are offset by lower conductivity and higher modulus; only by adding Cr and/or Mo can strength be increased without changing conductivity or modulus. Increasing the carbon content, along with the alloying addition, can be even more beneficial.

Roehrig also noted that the optimum type of iron changes when the cooling rates decrease. For intermediate cooling rates, the good strength and ductility of ferritic ductile and CG irons compensates for their lower conductivity and higher modulus (although distortion is more likely). For very low cooling rates and constrained castings, high strength pearlitic ductile and high Si-Mo ferritic ductile iron may be best, but these irons are more subject to structural instability.

Mushroom test

Nechtelberger[12] used a mushroom-shaped test specimen (Figure 3) to simulate a cylinder head; the specimen was heated rapidly to 450C, water cooled to below 50C, and finally dried by an air blast. The process was repeated until cracking occurred; the depth of the cracks was then measured, Figure 4. High carbon irons performed much better than low carbon irons; Cr-Mo additions were required to make the low carbon irons survive. Ferritic ductile iron and CG irons also performed poorly under these conditions. His results using this approach are similar to those of others, such as Friedrich[7].

Constrained thermal fatigue test

In this test, a specimen similar to a normal tensile bar is placed in a rigid fixture, with only the test specimen heated by an induction coil[3,16-20]. A load cell embedded in the fixture provides a measure of the thermal stress. When the specimen is heated, compressive stresses are introduced into the specimen. If the heating cycle is sufficient long, some creep relaxation will occur, thus reducing the compressive stresses, and high tensile stresses will develop during cooling of the specimen. Eventually cracking may occur during the cooling, or tensile, portion of the thermal cycle. Cracking can be detected by a decrease in the thermal stress, as measured by the load cell.

In the constrained thermal fatigue test, the thermal conductivity and coefficient of expansion of the test material are relatively unimportant; instead, the test in particular measures the combined effect of resistance to mechanical fatigue caused by the thermal cycling and the resistance of the material to stress relaxation at high temperatures. The test also makes it relatively difficult to directly compare the thermal fatigue resistance of materials having a different modulus of elasticity. Consequently, this test is best suited to evaluating materials that are to be used in applications such as exhaust manifolds and engine components.

Trbizan[18] performed such tests using five gray irons and a ductile iron, Figure 5. He measured the residual tensile stress and the number of cycles to fracture as a function of the maximum temperature for bars, when the minimum temperature was 200C. As the modulus of the iron increased (and the tensile strength increased), the residual tensile stresses also increased; however the number of cycles to fracture also increased! The thermal stress increased, and the number of cycles to fracture decreased, for each iron as the maximum temperature increased; however there is an inflection point at the transformation temperature of the iron; just above this temperature, the

number of cycles to failure actually increased before again decreasing at higher maximum temperatures. The strongest iron had the longest life (even though the modulus of elasticity was high and the thermal stresses were highest.

Gundlach[17] performed tests on a series of alloyed gray irons, determining elastic modulus versus temperature, room temperature hardness, TS, and E, and stress-relaxation measurements, as well as structural stability and thermal fatigue. The experimental apparatus, intended to approximate conditions in a cylinder head, is shown in Figure 6, and the changes in thermal stress and temperature versus time is shown in Figure 7. He cycled irons between 540 and 100C; he also noted that much longer lives were obtained if he reduced the maximum temperature to 500C. Results are included for each of the 9 irons in Table 1. He found that there was a poor correlation between tensile strength and number of cycles to failure; by adding alloying elements, such as Mo, a large increase in life was obtained compared to the increase in strength. He attributes this to reduction of stress relaxation, similar to that noted by Bertodo[2]. He was able to derive a regression equation for the number of cycles to failure:

$$\ln N = 0.41 + 0.0903TS + 1.89\%V + 1.79\%\ Mo + 0.11\%\ Cr - 0.14(\%Ni+5Cu)$$

Equation 2

This closely correlated with the experimental results, Figure 8. The alloying elements have an effect beyond just increasing the tensile strength; this might be attributed to more resistance to stress relaxation, Figure 9. Mo and V were most effective, both by reducing creep and also by refining eutectic cell size, which in turn helps reduce fatigue cracking. Csontos[16] also found Mo to be important, with number of cycles to failure increasing with square of Mo; Gundlach found the exponent to be 1.8, Figure 10. Although alloying elements tended to increase modulus (or better retain high modulus at high T), better creep resistance offset these changes. Alloying also produced more stable structure; addition of Cr along with Mo was particularly effective. In summary, resistance to thermal fatigue is related to both tensile strength and creep resistance, with Mo and V very important in this regard.

In another series of studies comparing the thermal fatigue resistance of cast irons for use in diesel engines, Gundlach et. al.[19] used the constrained thermal fatigue test, allowing samples to cycle between 100C and 540C and also between 100C and 500C to compare gray and CG irons. Compositions and results are given in Tables 2 and 3. Specimens were held for about 4 minutes at the high temperature, permitting stress relaxation to occur; as this occurred, the compressive stress was reduced, which in turn led to higher tensile stresses during cooling. The thermal stresses could be followed as a function of the number of cycles; the results are similar to that of a tensile test, with the magnitude of the stresses increasing with number of cycles until fracture occurred, Figure 11. A number of observations were noted:

- increasing the tensile strength of the iron increases the resistance to mechanical fatigue, as illustrated in Figure 12.

- addition of molybdenum to the iron improves fatigue resistance both by providing a higher high temperature tensile strength and by reducing the magnitude of stress relaxation, Figures 12 and 13.

Table 1: Results from the constrained thermal fatigue test for thermal cycling between 100C and 540C.[17]

Iron Alloy	Number of Cycles to Failure		Thermal Stress, MPa (ksi)	
	Individual	Average	Thermal Stress Cycle	Max. Tensile Stress
Base Iron	42 59	51	306 (44.4)	182 (26.4)
Cr	32 48 63	48	317 (46.0)	181 (26.2)
Cr-Ni-Cu	61 82 91	78	339 (49.2)	194 (28.2)
0.4% Mo - Sn	137 154 242	178	353 (51.2)	182 (26.4)
V-Cu	104 127 142	124	348 (50.4)	177 (25.6)
Cr-Mo-Sn	215 312 338	288	370 (53.6)	190 (27.6)
Cr-Ni-Cu-Mo	113 114 191	139	356 (51.6)	190 (27.6)
Cr-Mo	218 221 223	221	374 (54.2)	193 (28.0)
0.8% Mo - Sn	483 539	511	388 (56.2)	203 (29.4)

- even relatively large changes in the ferrite content of the predominantly pearlitic gray irons did not appreciably affect the resistance to thermal fatigue, Figure 13.

- a change in the maximum temperature cycle of only 40C (100 to 540C versus 100 to 500C) caused a very large change in the number of cycles to failure, Figure 13.

- for equivalent molybdenum contents, compacted graphite iron provided better resistance to cracking than gray cast iron. However Mo-alloyed gray iron performed better than low-alloy compacted graphite iron, Figure 13.

The number of cycles required for failure to occur was found to be approximated by the following expression:

$$\log N = 0.934 + 0.026\,TS + 0.861\,\%Mo \qquad \text{Equation 3}$$

The effect of molybdenum is shown by this expression to be two-fold: Mo increases the tensile strength, but also has an additional benefit, presumably by reducing stress relaxation.

Table 2: Compositions of irons in thermal fatigue study.[19]

Sample	Iron	C	Si	Mn	Ni	Cr	Mo	Sn	Ti	Mg	P	S
1	Gray	3.30	2.07	0.54	0.11	0.19	0.03	0.012	0.016	0.001	0.03	0.09
2	Gray	3.28	2.36	0.52	1.10	0.27	0.30	0.011	0.027	0.001	0.04	0.10
3	CG	3.60	2.15	0.52	0.05	0.09	0.02	0.014	0.202	0.013	0.03	0.02
4	CG	3.58	2.14	0.54	0.07	0.15	0.58	0.013	0.187	0.020	0.05	0.01
5	CG	3.62	2.31	0.53	0.08	0.12	0.11	0.055	0.206	0.015	0.03	0.01
6	CG	3.61	2.27	0.53	0.08	0.13	0.51	0.056	0.212	0.023	0.03	0.02

Table 3: Results of constrained thermal fatigue tests.[19]

	Cycled between 100 and 540 C	Cycled between 100 and 500 C
unalloyed gray	58	214
Ni-Cu-Mo	199	1208
Cu-CG	274	650
Cu-Mo CG	1808	1665
Cu-Sn CG	852	425 (small specimen for equal strain)
Cu-Mo-Sn CG	1036	754 (small specimen for equal strain)

Gundlach et. al.[20] also determined the effect of Mo on thermal fatigue resistance of ductile and CG irons; one of the intents was to evaluate a 4%Si-Mo alloy that raises the temperature of

ferrite stability, provides oxidations resistance, and improves high-temperature strength and creep resistance. This permits exhaust manifolds to operate at higher temperatures. Samples were heated to 650C, held for two minutes, and cooled to 200C. Samples tended to bulge at the centerline because the high thermal stresses caused plastic deformation; eventually necking began near the bulge, with eventual failure. Results are included in Table 4.

Table 4: Comparison of the number of cycles to failure for a number of ductile and CG cast irons.[20]

Iron	Cycles to Failure
Ductile iron	
2.5Si-0Mo	75
2.5Si-0.4Mo	93
2.5Si-0.6Mo	195
4Si-0Mo	206
4Si-0.6Mo	274
CG iron	
0.5Cu	20
0.5Cu-0.6Mo	31
Ductile	
3Si-0Mo	98
3Si-0.5Mo	168
3.6Si-0Mo	173
3.6Si-1Mo	375
4.4Si-0.2Mo	209
4.4Si-0.5Mo	493
CG iron	
2Si (pearlite)	80
3.6Si-0.5Mo (ferrite)	248

Increasing silicon and Mo increased life, as also illustrated in Figure 14. However CG irons performed very poorly, which may have been caused by softening of the irons by annealing prior to testing. The beneficial effects of Mo and Si in ductile iron is partly due to increase in yield strength by the alloying elements -- Si is particularly effective at low temperatures and Mo at high temperatures. Higher yield strengths reduces the plastic deformation.

Constrained disc test

Shea[21] devised a test, simulating conditions observed on the surface of brake drums, for comparing six irons and steels, Table 5. His apparatus is shown in Figure 15 and consisted of a constrained disk heated by an induction coil on one surface, with the opposite surface continually maintained at 65C. The power input via the induction coil was intense and constant, but the heat-up rate of the specimen surface varied with the thermal conductivity of the specimen -- the surface of high conductivity gray iron heated slowly, nodular iron heated more rapidly, and a high carbon steel heated most rapidly. The heated surface was examined periodically until a crack 0.5 mm long at 60X was observed. His tests allowed the number of cycles required for cracking to be determined as a function of the maximum cycle temperature for each material. As the maximum cycle temperature increased, the number of cycles to failure decreased logrithmically; the steel was most resistant to failure, nodular iron provided intermediate life, and gray irons cracked in the shortest times, Figure 16. Gray irons containing the greatest amount of graphite and the coarsest graphite survived for a greater number of cycles. Although increasing the strength and hardness, alloying with Mo, Cu, and Al reduced the resistance to cracking by decreasing the volume of graphite in the structure. The ranking of the six materials was the same both above and below the eutectoid transformation temperature. However the curves for nodular iron and steel flattened out at temperatures (850C) above the transformation temperature; although the amount of martensite that formed as a result of the high temperature thermal cycle was the same for all six alloys, the graphite flakes dominated the cracking mechanism in gray iron, while the matrix dominated cracking in the ductile iron and steel. The tempered martensite structure obtained by the high temperature cycling was more resistant to thermal fatigue cracking than the original pearlitic structure when the flake graphite was absent.

Shea also correlated the total thermal strain, calculated from $\alpha\Delta T$, with the number of cycles to cracking; all of the materials fell on the same curve, Figure 17, and the data were represented by the expression

$$N^a\epsilon_t = B \qquad \text{Equation 4}$$

where $a = 0.097$, $B = 0.013$, and $\epsilon_t = \alpha\Delta T$. The thermal strain was higher for the irons containing less graphite, since the coefficient of thermal expansion for these irons was also higher; this in turn reduced the crack resistance of the high strength, low graphite irons.

In summary, Shea attributes crack resistance to amount and morphology of the graphite, with matrix and alloy content having no effect for equivalent graphite morphology. Shea reports that this observation is supported by References 22 and 23; when alloy content increases, the size and amount of flake graphite decrease, resulting in less accommodation of surface strains and shorter paths between graphite flakes. Large amounts of coarse graphite provide good accommodation of surface strains, minimizes the amount of thermal stresses and strains that develop, and because of the higher thermal conductivity[24] minimizes maximum surface temperatures, temperature cycles, and temperature gradients.

Table 5: Characteristics of thermal fatigue samples used by Shea[21]. More complete compositions for the samples are given in the original paper.

Alloy	BHN	%C	%Si	α	Type of Material
A	153	3.93	2.37	12×10^{-6}	Pearlitic gray iron, coarse Type A and C graphite
B	182	3.49	2.37	12.5×10^{-6}	Pearlitic gray iron, medium Type A graphite
C	232	3.48	0.60	13.0×10^{-6}	Pearlitic gray iron, fine Type A graphite
D	255	3.50	2.38	14.0×10^{-6}	Gray iron with pearlite/bainite matrix, coarse Type A graphite
E	187	3.62	2.64		Ductile iron, ferrite/pearlite matrix
F	277	0.84	2.06		Steel, pearlite matrix

Finned disc thermal shock test

In this case, a set of finned discs (0.125-in. fins on a 0.5-in. hub) mounted on a rod retainer are cycled between two fluidized beds maintained at different temperatures, Figure 18. This design was used by Rostoker[25-26]. The shape of the test specimen causes the fin to be heated and cooled more rapidly than the hub, causing the formation of compressive hoop stresses in the fin during heating and tensile stresses during cooling. Cycle times are generally short, causing the disk specimens to heat and cool rapidly. The testing is interrupted periodically to determine whether any cracking has occurred. In this test, thermal conductivity and thermal expansion are particularly important, while stress relaxation is relatively insignificant. This type of test might be particularly applicable to ingot molds used in the steel industry.

Gundlach[27] performed a variety of tests on five pearlitic gray cast irons, including creep and thermal fatigue, to evaluate materials for diesel engines. Compositions and results are given in Table 6.

Table 6: Compositions and results for several pearlitic gray irons using the finned disc thermal shock test.[27]

Iron	C	Si	Cr	Mo	Ni	Cu	Sn	TS (room)	TS (540)	E
1	3.43	1.65	0.11	0.004	0.11	0.11	na	38.7	21.5	15.2
2	3.45	1.74	0.49	0.004	0.60	0.59	na	43.8	26.7	15.4
3	3.45	1.68	0.30	0.30	0.97	0.87	na	47.0	30.0	15.5
4	3.44	1.69	0.21	0.38	0.10	0.30	0.077	44.4	29.6	16.5
5	3.43	1.66	0.50	0.39	0.10	0.12	na	48.0	32.3	17.1

Iron	N to first minor crack	N to first major crack	total cracks in 2000 cycles
1	475	925	28
2	800	1075	15
3	775	1475	11
4	925	1325	9
5	1100	1550	11

A stack of 14 specimens (four of which were dummies) in an alumina heat transfer medium was cycled between about 200 and 590C at the fin surface (beds were at 955 and 95C) Samples were held 5 s at the high temperature, then cooled for 120 s. Because the fin heats and cools faster than the hub, compressive hoop stresses are created in the fin during heating and tensile stresses during cooling. Cracks form on the outer diameter of the fin. Gundlach measured the number of cracks and total length of cracks versus number of cycles for each specimen, Figure 19.

Irons with Cr+Mo retained the highest percentage of tensile strength at high temperatures; irons containing Mo exhibited highest rupture strength and best creep resistance. Also alloyed irons resisted pearlite decomposition at long times. Alloying reduced the number of cracks and the length of the cracks compared to the unalloyed class 35 gray iron (#1); high Mo+Cr was best. All irons had similar thermal coefficient of expansion and similar thermal conductivity (since about same carbon level and thus same amount of graphite) and also similar modulus of elasticity. The number of cycles to the second minor crack correlated very well with tensile strength (both room T and 540C), Figure 20; tensile strength was the most dominant property influencing thermal fatigue resistance. In these tests, exposure times were very short -- creep not expected to be a factor.

Roehrig[6] also describes the results of Diesburg's (unpublished) results using the same conditions as Gundlach[27], showing the effect of crack length versus number of thermal cycles for gray iron containing various Mo levels when the fins were cycled between 650 and 290C, Figure 21. Additional tests were performed on a variety of irons, cycling between 720 and 290 C in one case and between 590 and 200C in a second case. Roehrig points out that Mo has a beneficial effect on the resistance of gray iron to thermal fatigue. On the other hand, even 5% free ferrite was detrimental

compared to a fully pearlitic matrix, Table 7. On comparing results from different sets of tests, Roehrig notes that increasing the temperature range of the thermal cycle is very significant; increasing the difference by 130C changed the number of cycles for first cracking by a factor of 3 to 4. In yet another set of tests, Roehrig compares the resistance to cracking of ductile and CG irons to gray iron for thermal cycling between 690 and 240C.

Table 7: Effect of ferrite on cracking in the finned disc thermal fatigue test for several irons.[6]

	N (first minor)	N (first major)
gray (10%F)	170	220
ductile (19%F)	360	370
(47%F)	700	800
(61%F)	700	800
CG (5%F)	340	380
(5%F+Mo)	350	380
(40%F)	430	460
(40%F+Mo)	430	510

Ferrite is beneficial in ductile and CG iron, just the opposite of that observed in gray iron; in addition, all of the ductile and CG irons performed better than the unalloyed gray iron containing ferrite, although not as well as most of the all-pearlitic irons noted by Gundlach. Ferritic ductile irons cycled between 590 and 200C compare favorably to gray irons. When too much silicon is added to encourage ferrite, the K and ductility decrease and their resistance to thermal fatigue suffers.

Gundlach[19] tested the same irons using the finned disc thermal shock test that he tested using the constrained bar method. The specimens were cycled between 95C and 955C, using zircon sand as the fluidized beds. The samples were heated for five seconds, then cooled for 120 seconds. In these tests, gray iron, particularly when alloyed with molybdenum, provided the best resistance to cracking; the molybdenum presumably provided better performance due to its effect on elevated temperature tensile strength, Table 8. The CG irons cracked rapidly, although increasing the amount of ferrite improved the performance. Molybdenum additions to the CG irons did not provide a beneficial effect.

Table 8: Effect of Mo on number of cycles to cracking for several irons using the finned disc method.[19]

unalloyed gray	775 cycles before first major crack
Ni-Cu-Mo gray	no cracks after 2000 cycles
Cu-CG	175
Cu-Mo CG	150
Cu-Sn CG	100
Cu-Mo-Sn CG	75

Bridge thermal fatigue test

Roehrig[6] reviewed a test specimen used by Buderus AG in which a flat disk containing holes is partially submerged in water, Figure 22, while the bridge between the holes is induction heated to 650C. Figure 23 shows the number of cycles to produce cracking in several irons. Higher strength irons produced better resistance to cracking, except when a ferritic matrix containing high Si-Mo was used; the highly alloyed iron had good strength and no problem, of course, with pearlite decomposition. The high strength pearlitic ductile and gray irons suffered from decomposition of the pearlite.

Cylinder test

In an effort to more closely duplicate the conditions found in permanent molds, Davis et. al.[28] designed a hollow cylindrical test specimen through which cooling water could be passed. An induction coil heated just a portion of the cylinder. Consequently large temperature gradients between the outer and inner surfaces as well as along the length of the cylinder were produced, eventually leading to cracks. In one approach, the power was adjusted to cause the water temperature to increase by 25C during the heating cycle (i.e. a constant input energy cycle test); the maximum temperature obtained in the sample was lower for high thermal conductivity metals in this approach. In a second approach, the power was adjusted to provide a 600C surface temperature for all specimens.

Using the cylinder test, Davis compared the resistance to thermal fatigue of gray, alloyed gray, CG, ductile, and austenitic ductile irons. For the simulated permanent mold application, they found that a high carbon equivalent gray iron performed best, with alloyed irons only slightly better than unalloyed irons. Compacted graphite iron behaved poorly in this situation, which utilized the constant input energy approach. Adding up to 0.5% Mo to the high carbon equivalent iron did not improve resistance to cracking. The presence of even 5% ferrite in gray iron reduces the resistance to cracking, although ferrite may be beneficial in CG and ductile irons; the reason may be related to the path that a crack takes. In gray iron, cracks follow graphite flakes as much as possible, then cross through pearlite in a zig-zag manner, following the lamellae until bridging must occur; additional energy is required for the bridging within the pearlite. In addition, ferrite will reduce the tensile strength of the iron, as well as its resistance to wear. They also found that the temperature and the maximum temperature cycle are both important. Increasing the temperature cycle by 50C may double the risk of cracking. In addition, there is a critical temperature above which cracking is particularly likely to occur; the critical temperature is between 500 and 600C for gray and CG iron, and about 600C for ductile iron. Finally, they note that a high conductivity material may be beneficial because the temperature of the mold surface remains low.

Contradictions

A number of contradictory results have been observed in the various studies, in some cases perhaps caused by the different types of test that are used. Some notable contradictions, as pointed out by Rukadikar and Reddy[29], include

- In a number of studies, resistance to thermal fatigue correlates closely with tensile strength, while in others, tensile strength is a poor predictor for thermal fatigue. Furthermore,

bainitic gray irons, having a high tensile strength, do not appear to provide good resistance to thermal fatigue.

- High carbon contents in gray irons often are found to provide good thermal fatigue resistance, but in some studies, the high carbon contents did not appear to be helpful.

- While a number of studies indicate that alloying additions, such as Mo, provide improvement in thermal fatigue resistance, others indicate no beneficial influence of Mo.

Prediction of Thermal Fatigue Resistance of Materials

In order to incorporate a number of properties that influence thermal fatigue resistance into an expression that might assist in the design or selection of materials, various quality factors have been proposed, such as those described by Eichelberger[30], Bertodo[2], and Nechtelberger[12]:

$$Q = (1-\nu)K / \alpha E \qquad \text{Equation 5}$$

$$Q = UTS\ F_r / \alpha HB \qquad \text{Equation 6}$$

$$Q = UTS\ K / \alpha E \qquad \text{Equation 7}$$

where ν is Poisson's ratio, K is the thermal conductivity, α is the coefficient of thermal expansion, E is the modulus of elasticity, UTS is the tensile strength, F_r is the precipitous relaxation stress, and HB is the Brinell hardness. These quality factors have been used in evaluating materials for use in combustion engine parts. Materials with a high thermal conductivity, low expansion and low stiffness, high strength but low hardness all give a high quality factor; gray cast iron with a pearlitic matrix, perhaps strengthened with alloying elements, ought to produce a high quality factor. A number of investigators have demonstrated that gray iron with a pearlite matrix does generally perform better in thermal fatigue and thermal shock in combustion and brake components. Alloy combinations of chromium and molybdenum appear to provide the best results – chromium helps stabilize the microstructure and improves resistance to growth and distortion, while molybdenum improves strength and creep resistance.

When the thermal strain produced by temperature changes is small (small maximum temperature change), then the tensile strength is particularly important. When larger strains (large temperature range) are encountered, the ductility of the material becomes more important; this is typical of severe braking of heavy duty vehicles. For the large strains, thermal fatigue can be reduced by minimizing the plastic strain range per cycle or by increasing the ductility of the material. The number of cycles required for failure by thermal fatigue can be estimated based on the properties of a ductile material by

$$N = (\epsilon_f/2)^2 / [\alpha\Delta T - (\sigma_{max} + \sigma_{min})/E]^2 \qquad \text{Equation 8}$$

where ϵ_f is the strain at fracture. This equation, which may help to explain the behavior of materials such as ferritic ductile iron and perhaps compacted graphite iron, is not applicable to gray iron. Instead, for brittle materials such as gray iron,

$$N^a \alpha \Delta T = B \qquad \text{Equation 9}$$

appears to provide better correlation with thermal fatigue.

Rukadikar and Reddy[29], in an effort to predict the thermal fatigue life of gray iron, proposed a thermal durability index (TDI) to take into account both mechanical and thermophysical properties of the material. The TDI is defined as

$$TDI = \frac{\text{Tensile strength at a temperature when } \sigma th \text{ occurs}}{\text{Maximum thermal stress, } \sigma th} \qquad \text{Equation 10}$$

A high tensile strength and thermal conductivity, and a low value of modulus of elasticity and coefficient of thermal expansion, give a high TDI and thus better fatigue life.

They studied 23 irons having various carbon, silicon, Mo, Cr, Ni, V, Sn, Sb, Cu, and Al levels, Table 9. All of the specimens were pearlitic; however the interlamellar spacing of the pearlite varied and the size and type of graphite also varied from coarse Type A to mixtures of Types B and D. The tensile strength, modulus of elasticity, and coefficient of thermal expansion were determined at temperatures up to 700C, and thermal conductivity measured up to 500C. The finned disc sample was modeled to obtain transient temperature distributions for several cycles and cooling rates: 700-40C with water cooling, 600-40C with water cooling, 500-40C with water cooling, and 720-290C with air cooling. The thermal stress distribution is then calculated from the temperature distribution, using the experimental values for modulus of elasticity and coefficient of thermal expansion. Finally, the TDI value is calculated, Table 9. The thermal fatigue resistance of each of the irons, for all four thermal cycles, were then measured experimentally: heating of the discs was done in a salt bath. The number of cycles to the first major crack (Table 9), the number of cracks after a selected number of cycles (Figure 24), and the propagation of the cracks (Figure 24) were all measured.

They found that the thermal fatigue life decreased with (a) increasing operating temperature, (b) increasing temperature gradient, (c) increase in heat transfer coefficient of the heating/cooling media, and (d) increasing component thickness. After defining several nondimensional parameters, the fatigue life N can be expressed as

$$N_f = \frac{R(TDI)}{(T_{avg}/T_{min})^A \, (\Delta T/T_{min})^B \, ((Bi)^C (Fo)^D} \qquad \text{Equation 11}$$

where $T_{avg} = (T_{max} + T_{min})/2$, $\Delta T = T_{max} - T_{min}$, Bi is Biot's number, Fo is Fourier's number, and A, B, C, D, and R are constants. Based on the experimental results for thermal fatigue, the five constants could be determined, giving an equation of

$$N_f = \frac{(21.06 \times 10^6)(TDI)}{(T_{avg}/T_{min})(\Delta T/T_{min})^{1.175}(Bi \; Fo)^{2.57}} \qquad \text{Equation 12}$$

Table 9: Alloys, TDI values, and number of cycles to produce cracking for various temperature cycles.[29]

S - 0.05%, P - 0.03%, Mn - 0.71% ; in all irons.

Iron No.	Carbon Percent	Silicon Percent	Alloy Content				TDI values for thermal cycle					Number of cycles to produce first major crack in cycle			
			Element	Percent	Element	Percent	700-40 C	600-40 C	500-40 C	720-290 C	Cumulative (+)	700-40 C	600-40 C	500-40 C	720-290 C
1	3.93	1.05	-	-	-	-	1.3930	1.8220	2.5099	3.871	9.5959	30	59	111	268
2	3.00	1.98	-	-	-	-	1.2610	1.4657	2.3378	2.844	7.9085	25	46	86	190
3	3.93	1.06	Mo	1.05	-	-	1.3280	2.2359	3.3585	6.730	13.8524	40	80	142	410
4	3.00	1.98	Mo	1.05	-	-	1.6640	3.2359	4.0148	5.137	14.0517	36	68	139	380
5	3.93	1.06	Mo	0.32	Cr	0.72	1.4540	1.9792	3.0131	5.764	12.1503	32	81	136	340
6	3.00	1.98	Mo	0.30	Cr	0.68	2.1570	2.2011	2.9623	3.9983	11.3187	40	72	143	363
7	3.93	1.22	Cu	1.02	Ni	1.08	1.4280	2.0359	2.0375	3.926	9.4274	23	52	97	220
8	3.00	1.98	Cu	1.02	Ni	1.04	1.3000	1.8429	2.7050	4.828	10.6759	24	55	100	259
9	3.93	1.40	Cu	1.04	-	-	1.4770	1.9107	2.8474	6.958	13.1931	32	73	125	286
10	3.00	1.98	Cu	0.98	-	-	1.3020	1.9489	2.6799	3.798	9.7288	28	62	104	272
11	3.93	1.40	Cu	0.28	V	0.69	1.1340	1.5345	2.4564	4.069	9.1939	19	57	90	210
12	3.00	1.98	Cu	0.32	V	0.72	1.00	1.5916	2.1549	3.337	8.0835	19	50	85	212
13	3.93	1.60	Cu	1.01	Sn	0.11	1.1500	1.4614	1.9920	3.374	7.9774	21	60	95	250
14	3.00	1.98	Cu	1.00	Sn	0.1	1.1800	1.6497	2.0266	2.385	7.2413	20	72	90	258
15	3.93	1.60	Cu	0.93	Sb	0.0...	0.6810	1.4273	2.0648	3.461	7.6181	12	39	78	168
16	3.00	1.98	Cu	1.00	Sb	0.005	0.9100	1.3209	2.1001	2.645	6.976	12	43	82	180
17	3.93	1.06	Cu	0.97	Al	2.11	1.0390	1.7144	2.7451	4.470	9.9685	28	55	110	280
18	3.00	1.93	Cu	0.94	Al	1.78	1.3290	1.4265	2.5363	3.307	8.5988	27	58	106	260
19	3.93	1.06	Cu	1.05	Al	3.10	1.6360	2.3255	3.3707	6.762	14.0972	39	72	140	362
20	3.00	1.98	Cu	1.04	Al	1.04	1.1980	1.7134	2.5560	3.743	8.8417	18	54	85	201
21	3.93	1.06	Ni	5.1	-	-	1.1270	1.6790	2.7185	3.728	10.2525	26	63	123	280
22	3.00	1.98	Ni	5.2	-	-	1.5960	1.6063	2.4626	3.339	9.0039	17	42	82	210
23	3.00	3.73	-	-	-	-	0.9810	1.3087	1.9626	2.364	6.6163	18	36	76	152

(+) Cumulative - Numerical addition of TDI values for all thermal cycles.

For each of the four thermal cycles that were tested, the equations become

$N_f = 19$ (TDI) ..... 700-40C cycle
$N_f = 31$ (TDI) ..... 600-40C cycle
$N_f = 41$ (TDI) ..... 500-40C cycle
$N_f = 65$ (TDI) ..... 720-290C cycle

Equation 13

Reasonably good correlation was observed between the actual and predicted fatigue lives, as illustrated in Figure 25. Unfortunately, no details on how TDI was calculated were provided in the paper. The results also predict that irons containing Mo, Mo+Cr, and Cr+Cu give high TDIs and thus good resistance to thermal fatigue. High Si irons and those containing Cr+Sb give low TDIs and poor resistance. Some of these predictions have been verified by other researchers.

Measurement of Thermal Stresses and Strains

Direct measurement of stresses and strains induced during thermal fatigue is not an easy task, particularly for complex geometries that might be found in an actual operating permanent mold. Gundlach used a load cell embedded in the grips of his apparatus and measured the stress exerted on the grips by the specimen.

Applications versus Materials

The conditions observed during operation of a component help to determine the optimum material that would best withstand thermal fatigue.

Ingot Molds: Because they reach T of 800 to 970C, phase transformations can occur and temperature differences exceed 300C[6]. Oxidation becomes a problem. A high C, low Si, material with low modulus and high K is beneficial; high Mn is used to reduce ferritization. However for small (less than 5T) molds, ductile iron may be better, although temperature gradients may be quite a bit higher and thermal stresses may be double; however tensile strength of ductile is about 4 times that of gray. Ductile restricted to small molds due to distortion problems. Gundlach[31] also notes that high C is desirable; matrix is not important but Cr-pearlitic iron with carbides does crack, while high P is helpful[32] – at high T (600C) high C is good but Ni, Cr, Mo, V, Zr, Sn, Al, are bad; for intermediate T (550C) high C is good as is Mo; for low T (500C) Mo is again good

Exhaust Manifolds: Operate near 500C and conditions similar to constrained bar test. Oxidation and ferritization are not important. Typically unalloyed or Cr-alloyed gray iron and with medium carbon are used.[6] Ferritic ductile irons have better thermal fatigue resistance than gray iron, but due to thin sections are more subject to distortion; addition of Mo helps prevent this problem.

Cylinder Heads: These typically operate below 450C, where oxidation is not a problem. Compositions are generally relatively low carbon equivalents for good strength. However higher carbon may be used to reduce thermal fatigue problems. Some very large engines, such as those in ships, may use ductile iron.

Brake drums and brake discs: Gundlach[31] notes that high graphitic carbon is desirable. Crosby and Timmons[33] found that Mo improved resistance to heat checking. Willer[34] found that a CE of 4-4.2% and all pearlite matrix is best and that carbide stabilizing elements should be low. Dunks and Turner[35] found that compacted graphite iron was free from thermal checking, while gray iron cracked severely.

Permanent molds: For permanent mold casting, however, cast iron molds are almost universally used. General practice is to use high carbon equivalent gray iron with relatively high (0.6 to 1.0) manganese; lower silicon contents might be typical for producing ferrous castings. Cast irons are also used for many other applications, including ingot molds, gasoline and diesel engine components, exhaust manifolds, brake components, and others that require resistance to temperature cycles. Ingot molds normally require high carbon equivalents gray irons (for high thermal conductivity) or often compacted graphite or ductile irons, while engine parts use lower carbon equivalent gray irons (for a better compromise of thermal conductivity and high strength). Research has therefore been directed towards fatigue crack growth in ductile, compacted graphite, gray, and malleable cast irons[2, 5, 6, 17, 27, 36].

Computer Simulations

The permanent mold process has been the subject of several computer simulations. With the popularity of high speed computers, combined with the availability of complex modeling software packages, the trial and error approach to problem solving can be minimized. These computer "models" take into account the mold material, the coating properties, coating thickness, solidification time of the casting, ejection time, cycle time, and other variables needed to predict the optimum pouring time and mold design. These models may eventually permit permanent mold foundries to cast high quality castings on the first run of a mold[37, 38].

Crack Nucleation, Growth, and Morphology

Nucleation and growth of the thermal fatigue cracks is somewhat different for the different types of cast irons. Initiation of cracks is associated with the graphite phase, often leading to multiple crack sites. Both Shea[21] and Roehrig[6] have examined the morphology of the cracks.

Gray iron

According to Shea[21], the rate controlling step in the thermal fatigue of gray iron is nucleation of the cracks in the graphite flake. Cracks initially propagate through the interior of the graphite flakes rather than by decohesion of the graphite-matrix interface. This represents fracture along basal planes of the graphite, known to have a low cohesion strength.

Crack propagation in gray iron is facilitated by the interconnected graphite and close spacing between graphite flakes. Cracks follow the shortest path from one flake to another, not necessarily from one tip to another tip. Growth through the flake is rapid and is not influenced by the matrix, grain boundaries, or pearlite orientation; Shea found that cracks propagated through pearlite both in interlamellar and translamellar modes.

Roehrig[6] found that both major and minor cracks form in gray iron and follow the graphite flakes. Many short cracks and crack branching occur in gray iron, perhaps because of the interconnected nature of the graphite. Oxidation along graphite flakes can weaken the gray iron, decrease thermal conductivity, and even cause growth. All of these will make it easier for a crack to propagate. Temperatures above about 550C may cause oxidation to be particularly severe.

Davis[28] also found that cracks follow the graphite flakes as much as possible, then propagate through a pearlite matrix when necessary. However he found that the cracks tend to be predominantly interlamellar, only following a translamellar path to provide bridging; this produces a zig-zag crack path.

Ductile and Compacted Graphite iron

In ductile iron, cracks initiate at the graphite-ferrite interface because the nodular graphite cannot accommodate large strains in the matrix and because the basal planes (with the lowest cohesion strength) are radial[21]. Cracks propagate radially through the ferrite ring and into any pearlite, heading for another nodule. Plastic deformation of ferrite may arrest crack; according to Shea, the rate controlling step may be renucleation of the crack in the matrix. Roehrig[6] points out that this different growth mechanism leads to only one major crack, rather than the multiple cracks observed in gray iron. The cracks eventually connect one nodule to another.

Because of the interconnected graphite in CG iron, crack initiation and growth is similar to that in gray iron.

Discussion

Very little information is provided in the literature concerning the resistance of permanent molds to thermal fatigue. Most of the work concerning the thermal behavior of cast irons is directed more towards automotive and diesel engine components, including cylinder blocks, exhaust manifolds, and brake parts. In some applications, compacted graphite and ductile cast irons are considered to be optimum materials, at least in comparison to gray iron; these applications include those in which the iron is heated above the transition temperature, and hence the thermal stresses introduced due to the phase transformations must be accommodated.

For applications (including permanent molds) in which subcritical peak temperatures are achieved, gray cast iron appears to generally behave best. High surface strain leads to high stresses and more rapid failure[21]; consequently a large volume of graphite should result in lower surface strains due to the ability of the graphite to accommodate expansion of the matrix. A large amount of graphite also improves the thermal conductivity. An iron with a low modulus of elasticity and high resistance to plastic deformation can minimize thermal stresses and a high thermal conductivity will minimize temperature differences; again, this is typical of high carbon gray irons. On the other hand, a high tensile strength and fatigue strength to withstand the thermal stresses requires that the gray iron have a pearlitic matrix. The material must resist oxidation and structural changes, including creep; alloying a gray iron, particularly with molybdenum and/or chromium, helps meet these requirements. While higher tensile and fatigue strengths can be achieved using ductile iron, ductile iron also has a high modulus and low conductivity.

Virtually nothing in the literature is provided concerning the effect of mold design, including geometry, and other processing variables, in particular the mold coating. A mold coating would be expected to improve resistance to thermal fatigue by minimizing the surface temperature, and therefore the magnitude of thermal stresses and strains.

Several aspects related to thermal fatigue have been studied. Mathematical modeling is one of the important topics; however as cracks form and interact, the models become very complex. Other studies show that the temperature range of the thermal cycle has a crucial impact on the life of a material. By decreasing the maximum temperature of a cycle by as little as 40C, the life of the material can increase by as much as four times. Smaller sections fail more quickly because of the larger stress cycles created by rapid heating and cooling.

Future research should be directed towards testing of actual mold materials and a variety of mold configurations, permitting the creation of a data base that could be used for the design of permanent molds. Furthermore, the effect of the operating cycle, particularly the effect of stresses introduced during start-up/shut-down operations versus continuous running, must be studied. Development of effective and validated computer simulations may represent an important and cost-effective step in understanding failure of the molds and for improving mold life.

References

1. L. F. Coffin, N. Y. Schenectady, "A Study of the Effects of Cyclic Thermal Stresses on a Ductile Metal", Transactions of the ASME, August, 1954, pp. 931-950.

2. R. Bertodo, "Grey Cast Irons for Thermal Stress Applications", Journal of Strain Analysis, Vol. 5, No. 2, 1970.

3. L. F. Coffin, R. P. Wesley, N. Y. Schenectady, "Apparatus for Study of Effects of Cyclic Thermal Stresses on Ductile Metals", Transactions of the ASME, August, 1954.

4. A. Gierek, T. Lamber, V. Shladek, "Estimation of the Resistance to Thermal Shocks of Materials for Permanent Metallic Moulds", Russian Metallurgy, No. 1, 1981.

5. I. A. Vorob'ev, et. al., "Modeling of the Process of Thermal Crack Nucleation in Pressure Die Casting and Permanent Molds", Equipment-Manufacturing Technology, No. 11, November, 1987.

6. K. Roehrig, "Thermal Fatigue of Gray and Ductile Irons", AFS Transactions, Vol. 86, 1978, pp. 75-88.

7. W. Friedrich, Werkstatt und Betrieb, v 100, p583-589, 1976.

8. Namai, Giesserei Praxis, no 4, p49-59, 1977.

9. H. Terada, Imono, vol 41, no4, p237-238, 1969

10. P. I. Talanov et al, Metallovedenie i termiceskaja obrabotka metallov, no 12, p50-52, 1970.

11. K. Prasse, Aus Wissenschaft und Praxis des Diessereiwesens, Giessereiverlag, Duesseldorf, p314-326, 1955.

12. E. Nechtelberger, "Systematic investigations to improve the quality of cylinder head cast irons with special reference to the tendency of crack formation, part 2- Results of thermal shock testing.

13. I. Dinescu, C. Craciunescu, K. Haltrich, and F. Constantin, "Thermal Fatigue in Cast Irons with Modified or Non-Modified, Vermicular and Nodular Graphite, Metallurgia, v37, p90-93 (1985).

14. E. A. Sukhodol'skaya and E. A. Zatolokin, "Influence of Load on Thermal Durability of Cast Iron," Russian Castings Production, vol 10, p420 (1972).

15. J. R. Kattus and B. McPherson, "Properties of Cast Iron at Elevated Temperatures," ASTM Publication STP no. 248 (1959).

16. Csontos, Czako, and Bollobas

17. R. B. Gundlach, "Thermal Fatigue Resistance of Alloyed Gray Irons for Diesel Engine Components, AFS Transactions, Vol 87, 1979, pp. 551-560.

18. M. Trbizan "Thermal Shock Behavior of Gray Cast Iron"Berg-und Huttenmannische Monatshefte v120no2 p174-184 1975.

19. Y. J. Park, R. B. Gundlach, R. G. Thomas, J. F. Janowak., "Thermal Fatigue Resistance of Gray and Compacted Graphite Irons", AFS Transactions, Vol 86, 1985, pp. 415-422.

20. J. Park, R. B. Gundlach and J. F. Janowak, "Effects of Mo on Thermal Fatigue Resistance of Ductile and Compacted Graphite Irons, AFS, v95,p267-272, 1987.

21. M. M. Shea "Influence of Composition and Microstructure on Thermal Cracking of Gray Cast Iron", AFS, 1978, p23-30.

22. T. Namai, "Observation on Crazing Formation Process in Gray Cast Iron", National Research Institute for Metals, Transactions, v 16, p 21 1974.

23. P. I. Talanova et al, "The Resistance of Cast Iron Brake Drums to Heat Checks", Metal Science and Heat Treatment, 11-12, p1045, 1970.

24. E. C. Toghill, H. T. Angus, "Cast Iron Brake Drums", Automobile Engineer, p 409, Oct 1953.

25. W. Rostoker "Thermal Fatigue Resistance of Martensitic Steel Materials", JMLSA, v4, no 1, p117-144, Mar 1969.

26. W. Rostoker, "Thermal Fatigue Resistance of Gray Cast Iron Materials", JMLSA, v4, no 4, p909-923, Dec 1969.

27. Gundlach, Elevated-Temperature Properties of Alloyed Gray Irons for Diesel Engine Components, AFS, p55-64, (1978).

28. K. G. Davis, D. A. Brown, J-G Magny, and D. Hui, "Choice of Permanent Mold Materials for Iron Castings", AFS, p85-104 (1989).

29. M. C. Rukadikar and G. P. Reddy "Prediction of Thermal Fatigue Life of Flake Graphite Cast Irons", AFS, v95, pp575-586 (1987).

30. Eichelberg, "Some New Investigations of Old Combustion Engine Problems", Engineering, v 148, p 463, (1939).

31. Gundlach, "The Effects of Alloying Elements on the Elevated Temperature Properties of Gray Irons", AFS, p389-422 (1983).

32. M. DeCrop, J. Coppolani and J. C. Margerie, "Experimental Investigation of Thermal Shock Behavior in Cast Irons,", AFS Cast Metals Research Journal, vol 2, pp118-138, (1966).

33. Crosby and Timmons

34. Willer

35. Dunks and Turner AFS, 1981

36. B. Ostensson, "Fracture Toughness and Fatigue Crack Growth in Nodular Cast Iron", Scandinavian Journal of Metallurgy, Vol 2, pp. 194-196 (1973).

37. A. J. Kearns, et. al., "Computer Simulation of the Permanent Mold Process", Modern Casting, Vol. 76, October, 1986.

38. Y. Ohtsuka, et. al., "Application of a Computer Simulation of Aluminum Permanent Mold Castings", AFS Transactions, 1982, pp. 635-642.

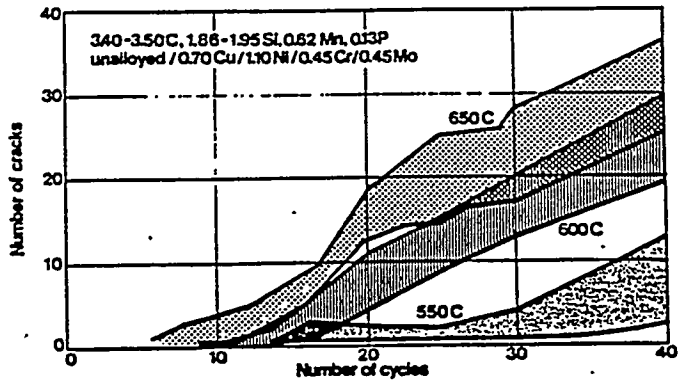

Figure 1: The effect of the maximum temperature of the thermal cycle on thermal fatigue in gray iron. Irons containing Cr or Mo are near the bottom of the band.[7]

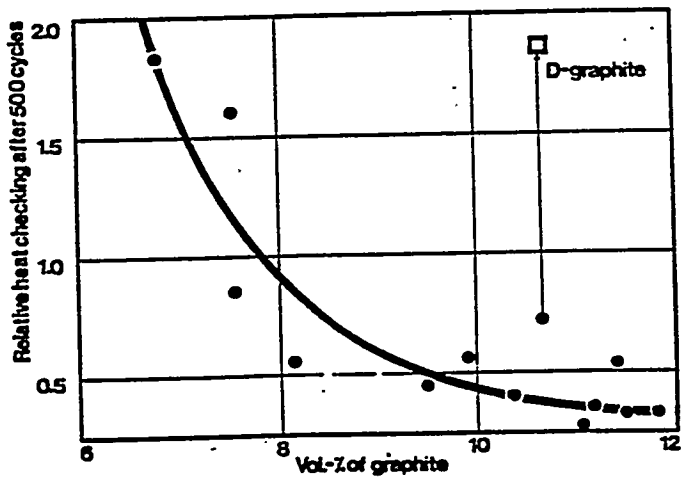

Figure 2: The effect of volume percent graphite on the relative severity of cracking in gray cast irons. Specimens were held at 450C for 2 s, then quenched to room temperature. The deleterious effect of Type D graphite is illustrated.[8]

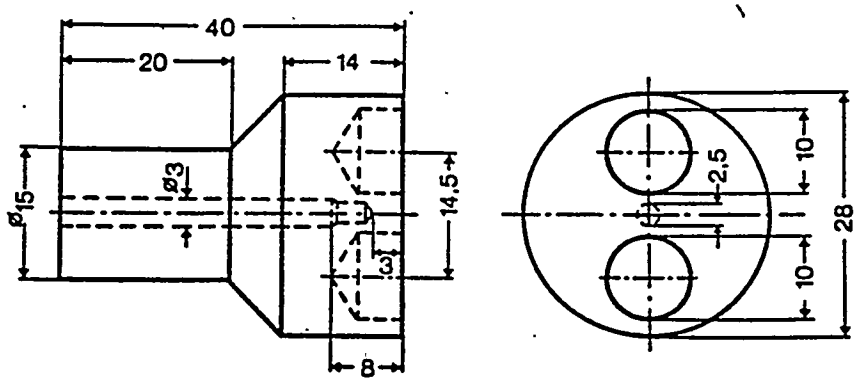

Figure 3: The "mushroom" thermal fatigue specimen used to simulate conditions found in a diesel cylinder head. Dimensions are given in millimeters.[12]

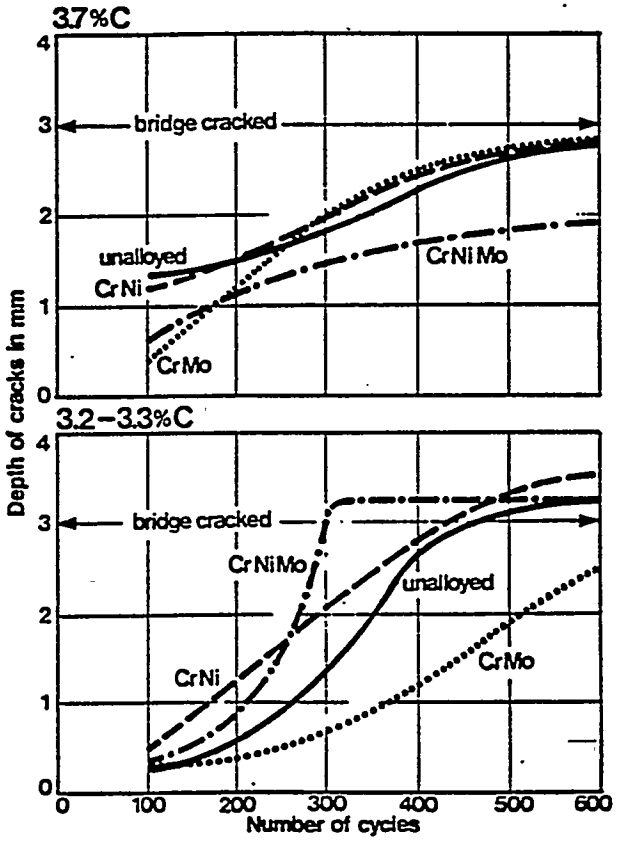

Figure 4: Effect of composition and number of cycles on the depth of cracks in the "mushroom" thermal fatigue specimens. The specimens were cycled between 460C and room temperature.[12]

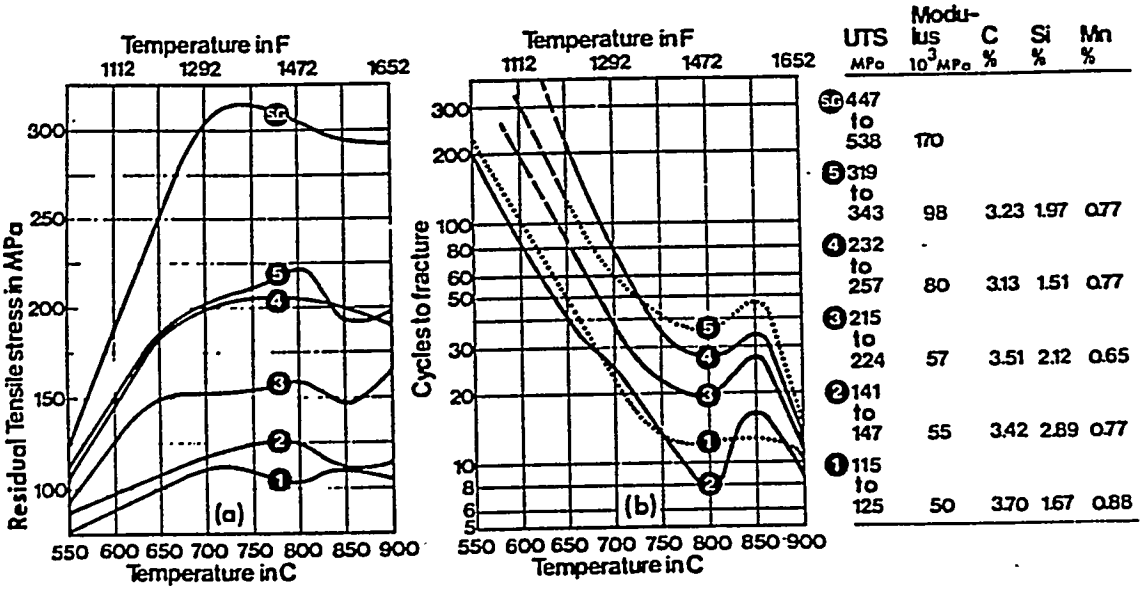

Figure 5: The effect of maximum temperature on the thermal stresses and cycles to fracture for several gray irons using the constrained thermal fatigue test. High strength, high modulus irons developed the highest stresses but also displayed the best resistance to fatigue.[17]

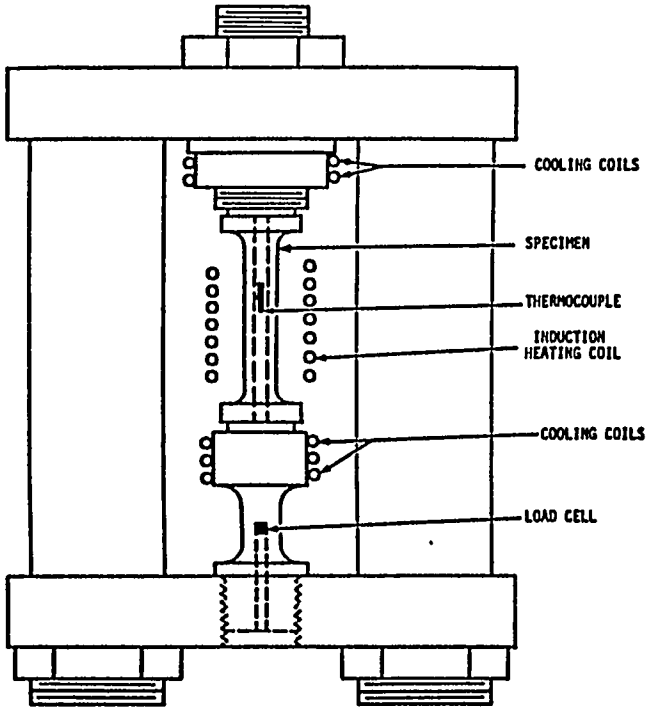

Fig. 9. Thermal fatigue test apparatus.

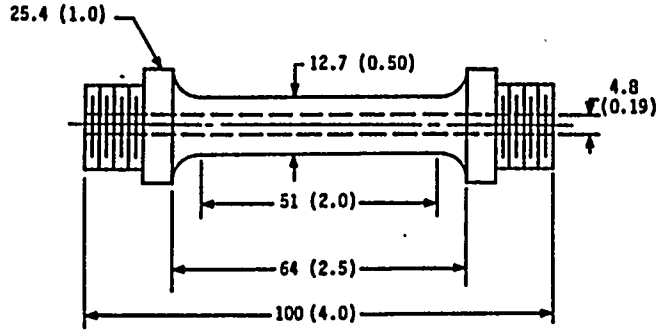

Figure 6: Test apparatus and specimen (in mm) for the constrained thermal fatigue test.[17]

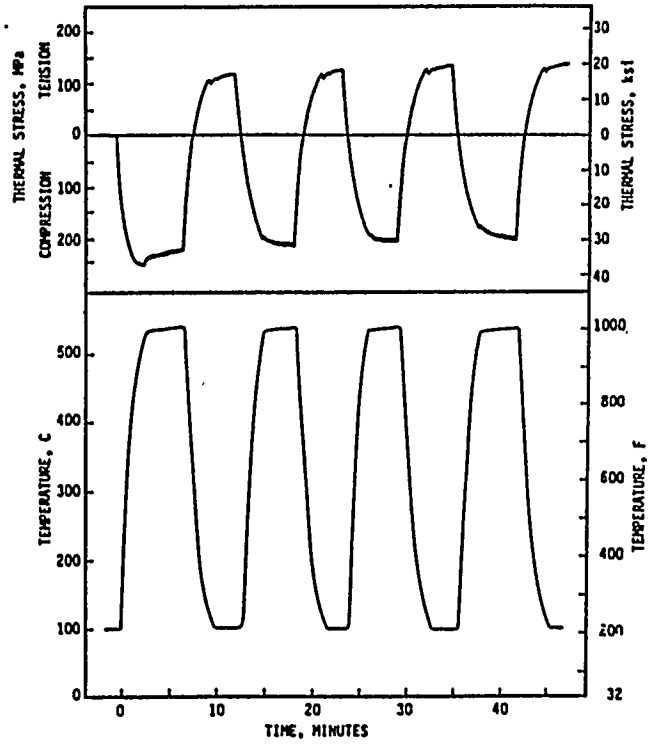

Figure 7: The specimen temperature and thermal stresses produced in the constrained thermal fatigue test specimen.[17]

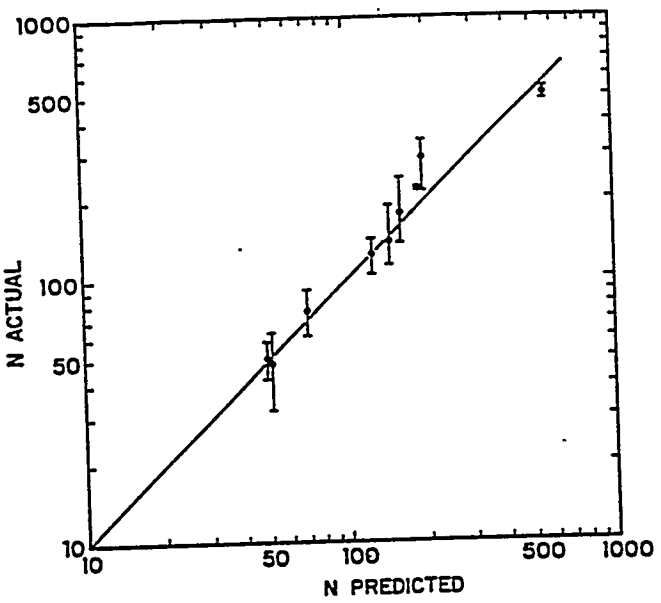

Figure 8: Corelation of thermal fatigue life with that predicted from the regression equation (Equation 2).[17]

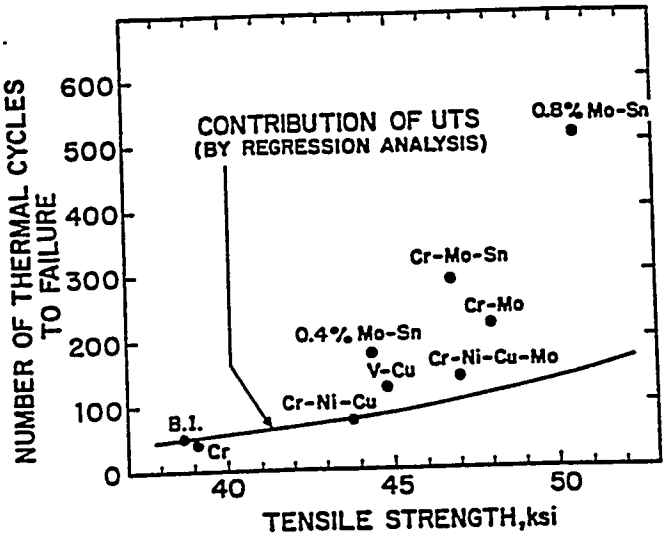

Figure 9: The effect of tensile strength on number of cycles to failure in the constrained thermal fatigue test. The solid curve shows the effect of tensile strength of the gray iron, while the points above the curve indicate the contribution from improved creep resistance.[17]

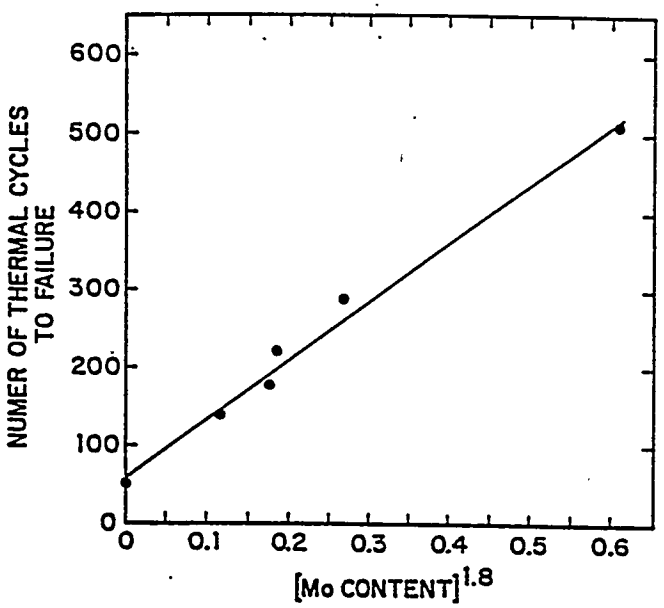

Figure 10: The effect of molybdenum in gray iron on the number of cycles to failure in the constrained thermal fatigue test.[17]

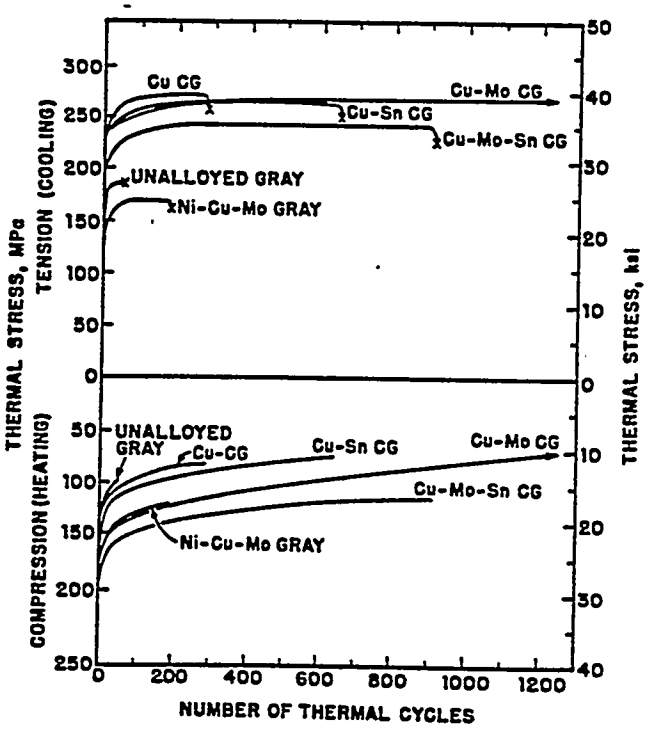

Figure 11: The effect of number of cycles on the thermal stresses produced in the constrained thermal fatigue test. The thermal stresses increased with increasing cycles until fracture occurred.[19]

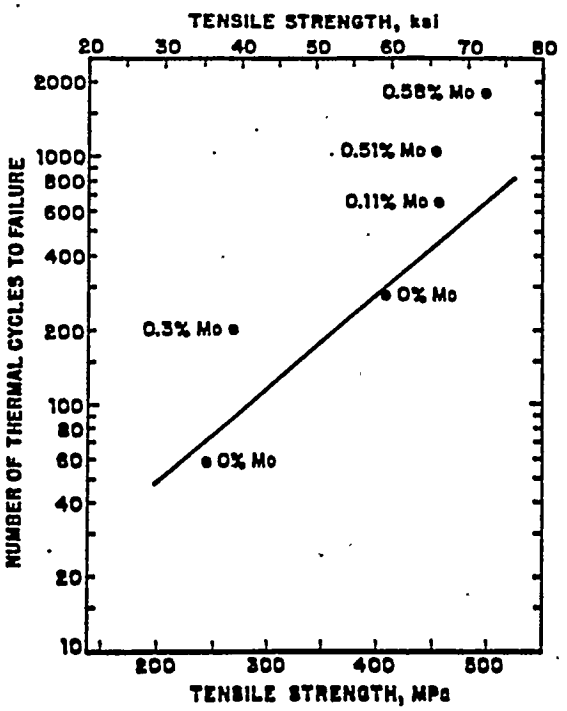

Figure 12: The effect of tensile strength and molybdenum content on the cycles to failure for gray irons in the constrained thermal fatigue test. Molybdenum additions provide an effect above that of tensile strength by improving creep resistance.[19]

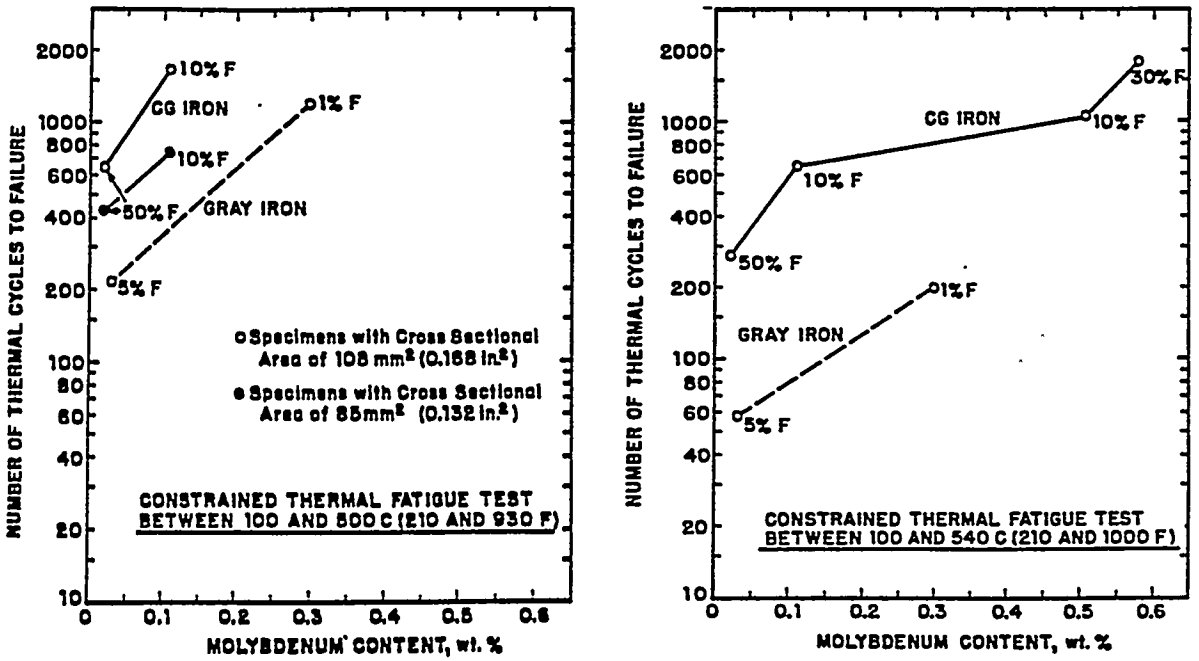

Figure 13: Effect of molybdenum and ferrite content for several gray and CG irons in the constrained thermal fatigue test.[19]

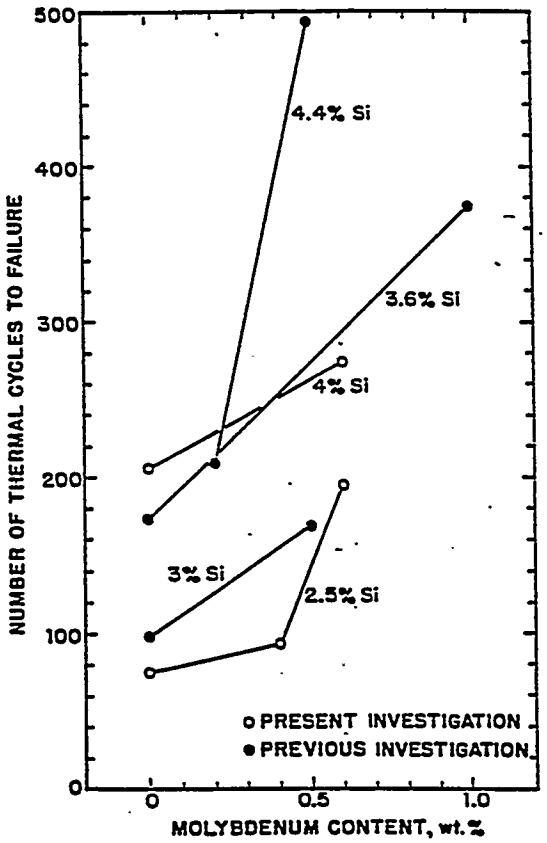

Fiigure 14: Effect of molybdenum and silicon on the cycles to failure in the constrained thermal fatigue test[20].

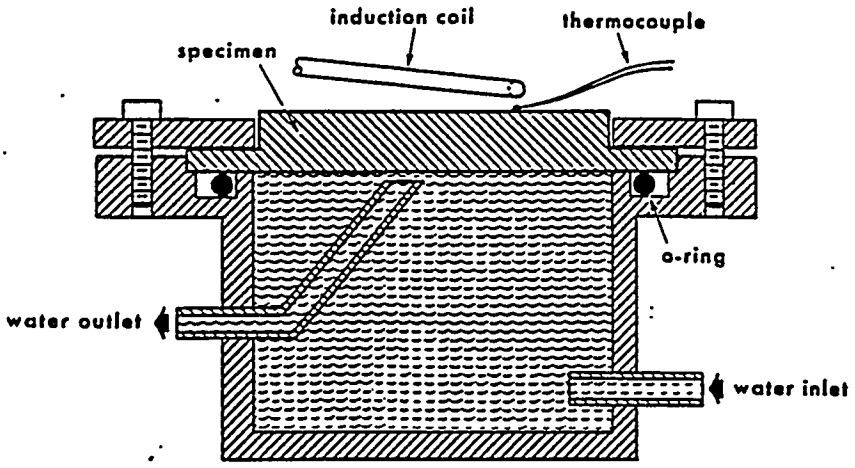

Figure 15: Test apparatus used to produce temperature gradients in the constrained disc thermal fatigue test.[21]

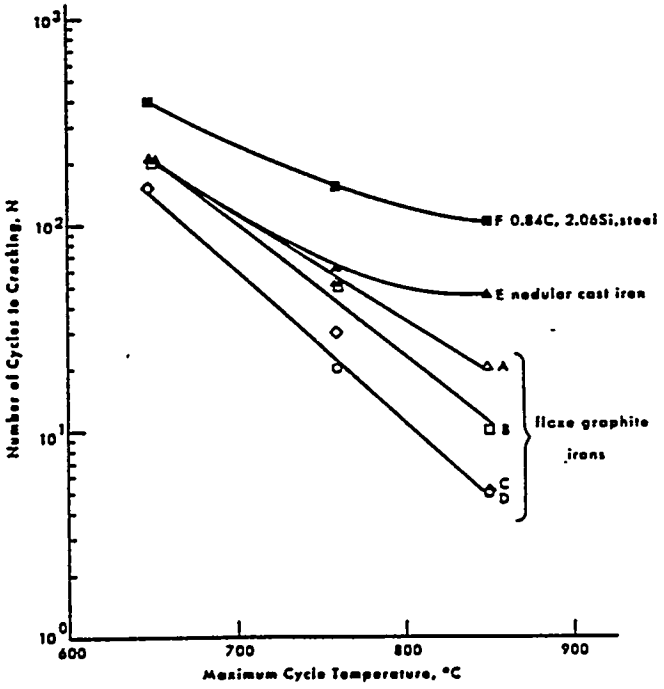

Figure 16: The effect of maximum temperature on the number of cycles to failure for several irons, using the constrained disc method.[21]

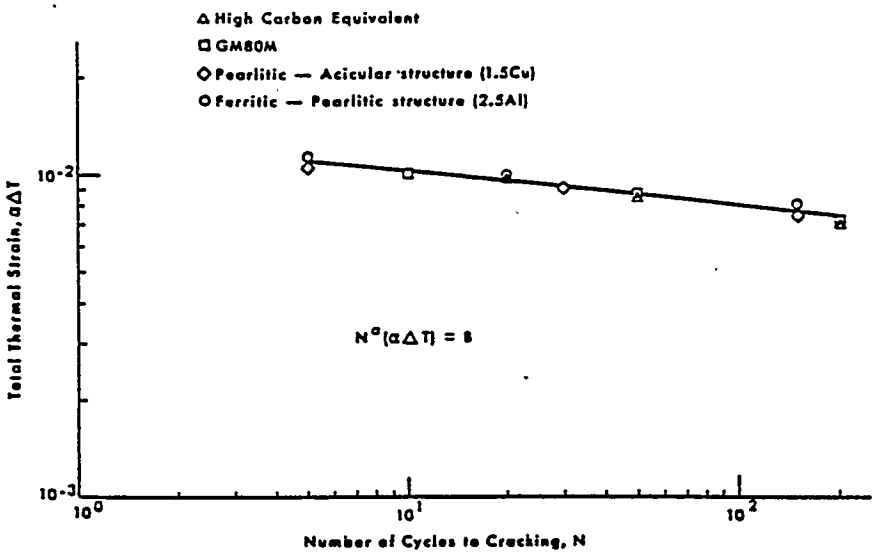

Figure 17: The number of cycles to failure in the constrained disc thermal fatigue test is related to the total thermal stress produced during the cycle.[21]

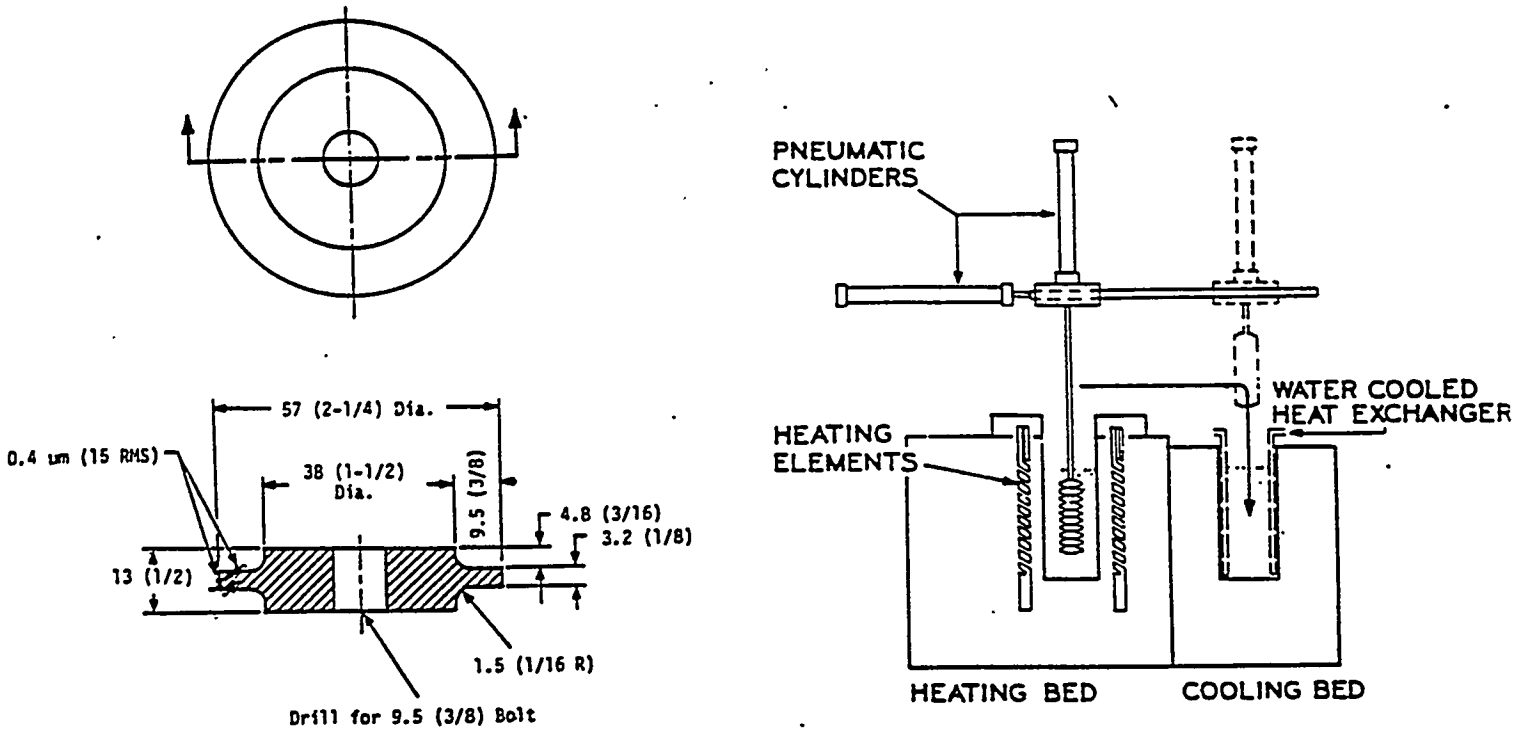

Figure 18: Test specimen and apparatus for the finned disc thermal fatigue test.[27]

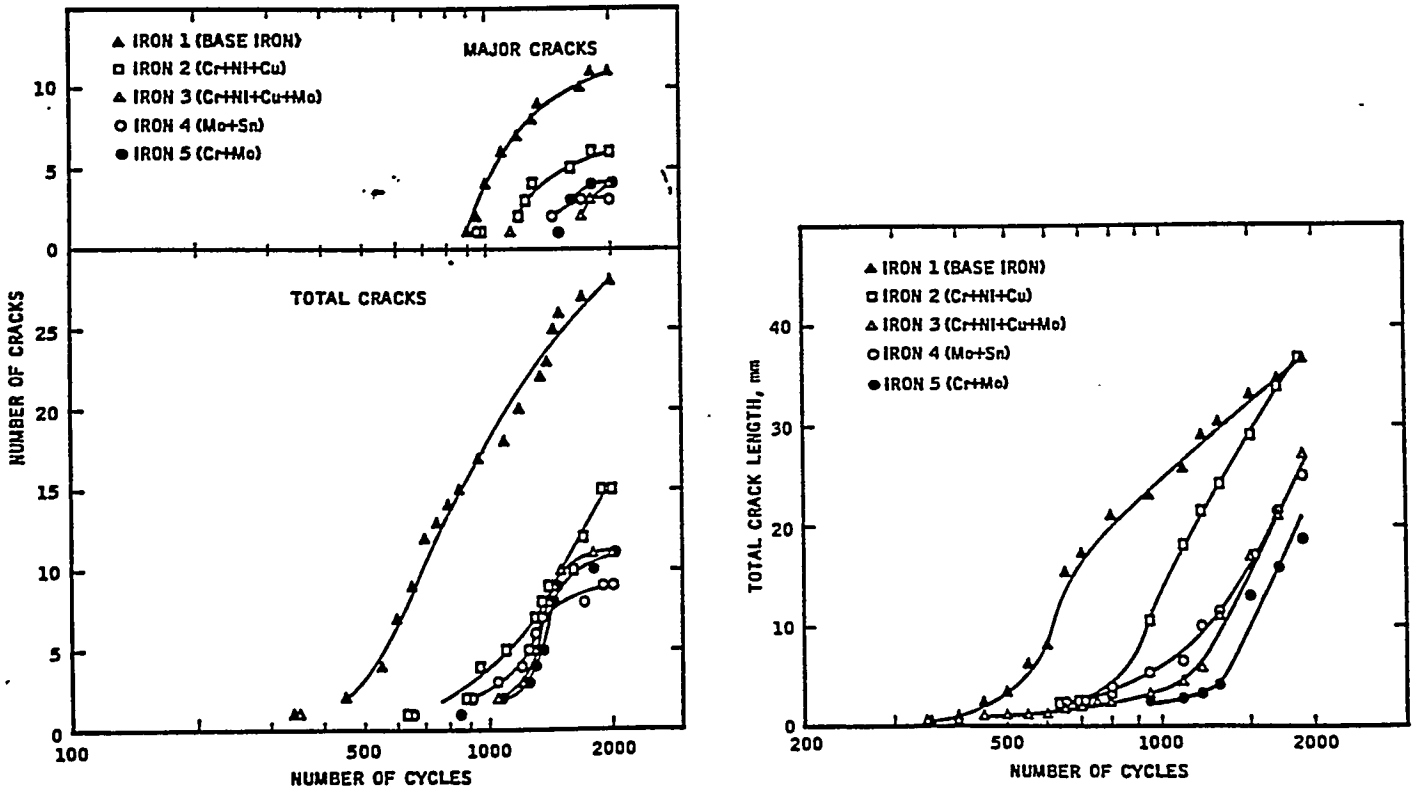

Figure 19: Total number of cracks, number of major cracks, and total length of cracks versus number of cycles for several gray irons, using the finned disc thermal fatigue test.[27]

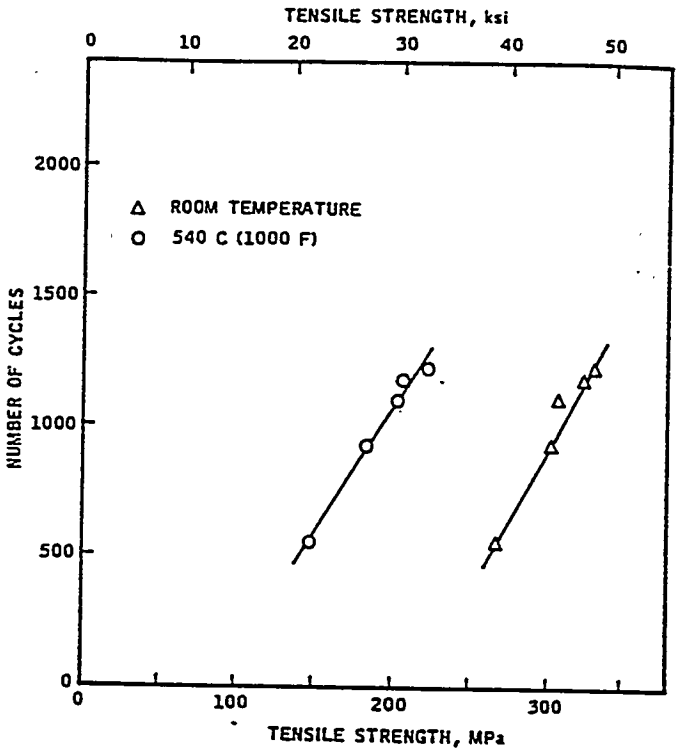

Figure 20: The number of cycles required before the second crack is observed in the finned disc thermal fatigue test correlates with the tensile strength of the iron.[27]

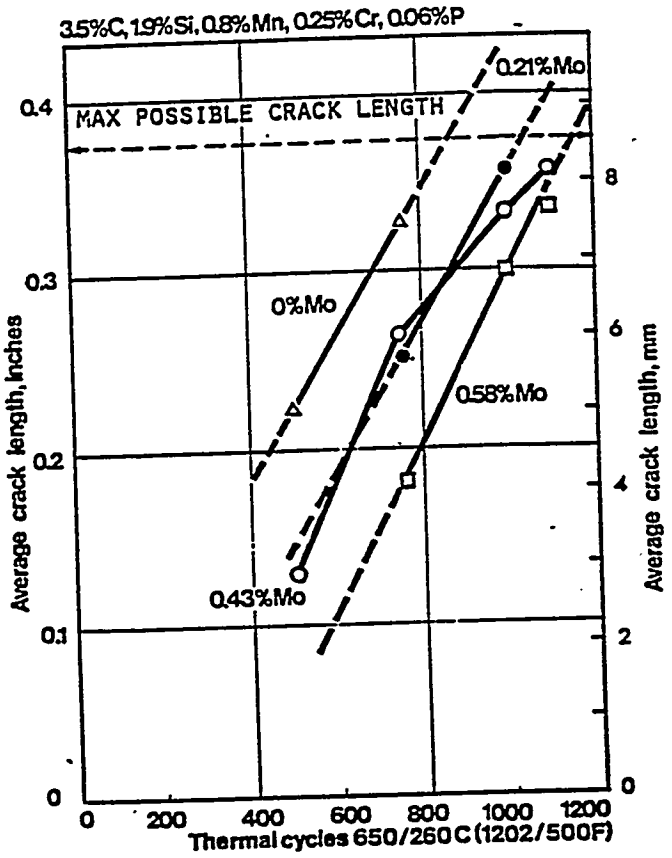

Figure 21: The average length of the first crack as a function of the number of cycles and the molybdenum content for gray iron cycled between 650 and 260C.[6]

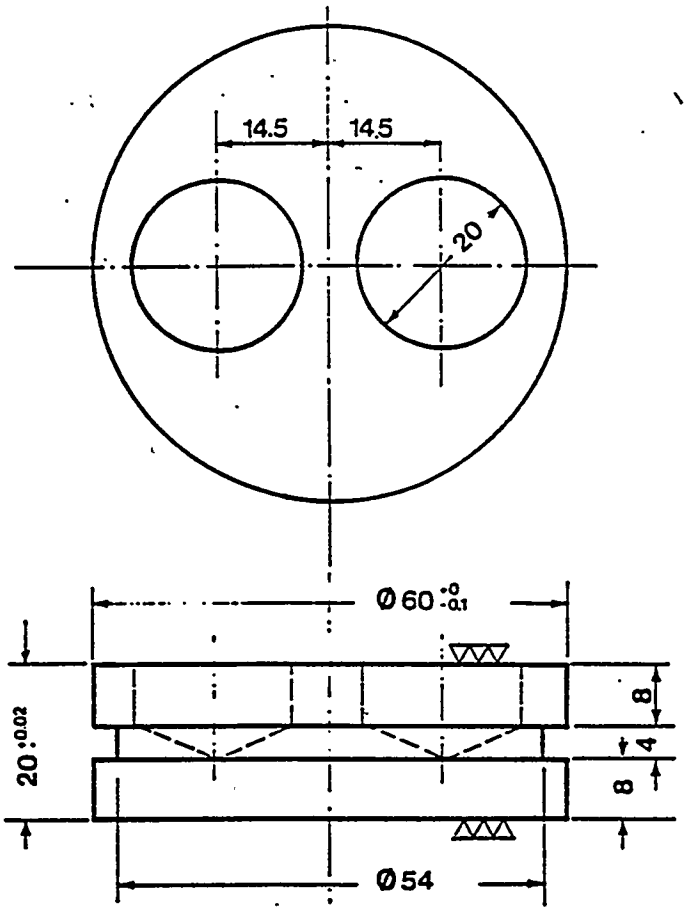

Figure 22: Specimen for the "bridge" thermal fatigue test, with dimensions in millimeters.[6]

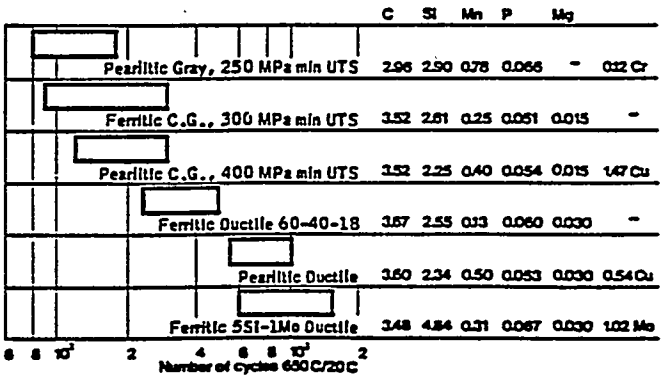

Figure 23: Number of thermal cycles required to produce cracks in the bridge thermal fatigue specimens for a number of cast irons.[6]

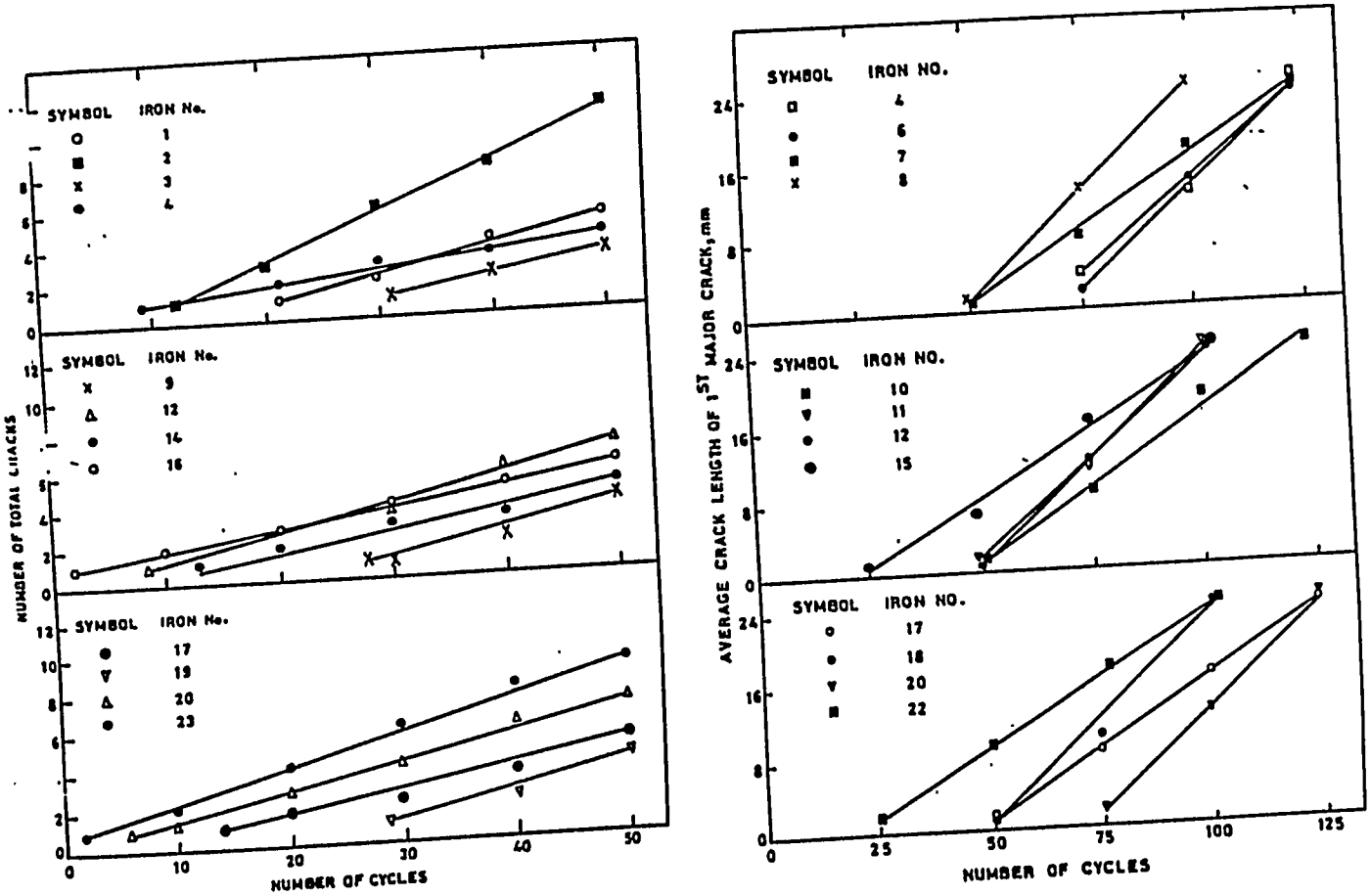

Figure 24: Number of total cracks and average length of first major crack versus number of cycles.[29]

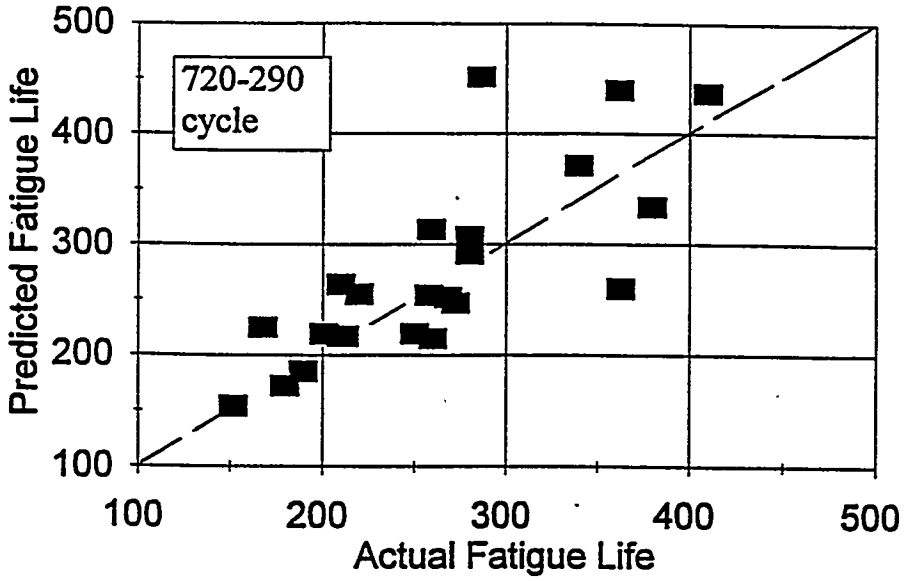

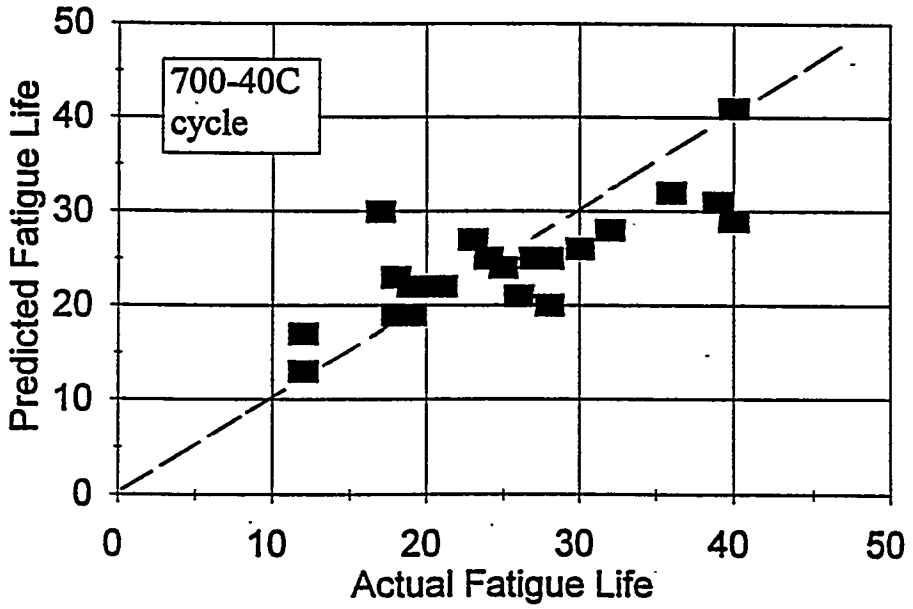

Figure 25: Comparison of actual and predicted thermal fatigue lives.[29]

UNIVERSITY PARTICIPANTS:

THE PENNSYLVANIA STATE UNIVERSITY

Dr. Robert C. Voigt, Associate Professor
Dr. Edward C. DeMeter, Assistant Director
Corey L. Jarvis, Program Manager
Frank E. Peters, Research Assistant
Wayne G. Vaupel, Research Assistant
John W. Ristey, Research Assistant
Chad L. Hafer, Research Assistant

UNIVERSITY OF MISSOURI-ROLLA

Kofi Nyameke, Associate Professor
Sufei-Wei, Research Assistant
Donald R. Askeland, Distinguished Teaching Professor
Christopher W. Ramsay, Assistant Professor
Marlin Jiranek, Research Assistant
John Dillingham, Research Assistant
Mohamed Reza Banki, Research Assistant